Image Cover Sheet

CLASSIFICATION	SYSTEM NUMBER 509935
UNCLASSIFIED	

TITLE

DETONATION OF 100-GRAM ANTI-PERSONNEL MINE SURROGATE CHARGES IN SAND - A TEST CASE FOR COMPUTER CODE VALIDATION

System Number:

Patron Number:

Requester:

Notes:

DSIS Use only:

Deliver to:

DRES

DEFENCE RESEARCH ESTABLISHMENT SUFFIELD

SR 668

UNCLASSIFIED

Detonation of 100-Gram Anti-Personnel Mine Surrogate Charges in Sand
A Test Case for Computer Code Validation

By:

Denis Bergeron, Robert Walker and Clay Coffey*

* Amtech Aeronautical Engineering Ltd.

October 1998

CRAD

National Defence Défense nationale

Canada

DEFENCE RESEARCH ESTABLISHMENT SUFFIELD
RALSTON, ALBERTA
CANADA

SUFFIELD REPORT No. 668

DETONATION OF 100-GRAM ANTI-PERSONNEL MINE SURROGATE CHARGES IN SAND

A TEST CASE FOR COMPUTER CODE VALIDATION

by

Denis Bergeron*
Robert Walker*
and
Clay Coffey†

* Defence Research Establishment Suffield
† Amtech Aeronautical Engineering Ltd.

Abstract

This report presents the results from a series of 20 experiments in which 100-gram charges of C4 explosive were buried at various depths in Silica 20 sand and detonated. These experiments were conducted with the goal of studying the basic explosion physics of shallow-buried charges, representative of land mines, and to generate a high-quality data set for the validation of computer codes. The data recorded includes overpressures and shock wave time of arrivals in air and in soil. Above ground gauges 30, 70, 110, 150, and 190 cm above the surface of the sand recorded side-on pressure. In-ground gauges at 7.5, 10.0 and 12.5 cm from the bottom of the charge recorded the passage of the shock in that medium. Flash x-ray exposures captured the early soil deformation while a high-speed camera captured the expansion of the detonation products and late ejecta motion. The data is presented in a format suitable for code validation.

Résumé

Ce rapport présente les résultats de 20 tirs durant lesquels des charges de 100 grammes de C4 furent enterrées à différentes profondeurs dans du sable Silica 20 puis détonnées. Les but premier de ces expériences était d'étudier la physique associée avec l'explosion de petites charges représentant des mines terrestres. Les données résultantes peuvent aussi être utilisées pour la validation de simulations numériques. Les données receuillies incluent la surpression et le temps d'arrivée des ondes de choc dans l'air ainsi que dans le sol. La pression incidente a été enregistrée avec des capteurs placés 30, 70, 110, 150 et 190 cm au-dessus de la surface du sol. Des capteurs placés 7.5, 10 et 12.5 cm sous la charge ont enregistré la surpression dans le sable. La déformation initiale de la surface du sol a été capturée avec rayons-x tandis que l'expansion des produits de détonation et l'éjection du sable a été filmée avec une caméra haute vitesse. Les données sont présentées de façon quelles puissent être utilisées directement pour la validation de résultats de logiciel.

Executive Summary

From January 1991 to December 1995, the Canadian Forces (CF) suffered 44 mine strikes while deployed on UN peacekeeping missions in Somalia and the Former Republic of Yugoslavia. Roughly, 2 out of 3 mine strikes were against vehicles, and the remainder against dismounted personnel. These casualties made it clear that mine protection is important to the CF and other Western armies.

The acquisition of mine-protected equipment is a challenging task. The Army normally states its requirements in terms of threat, e.g., "vehicle protection against a 6.5 kg TNT anti-tank mine" or "personnel protection against a 100-gram TNT anti-personnel mine". Although these statements clearly identify the interest of the Army, they are difficult to translate to technical specifications for design and engineering purposes, i.e., loading functions and material response. Usually, requirement officers in charge of contracts cannot provide this technical information to industry. This presents the inherent danger that the CF can -and have been- put in a position where they are forced to waive the statements on mine protection and accept whatever industry can deliver. From contacts with scientists in other countries, it appears that the CF are not alone to face this kind of situation.

The Defence Research community is addressing this problem by conducting research into mine blast output. Early in this project, it became apparent from a review of the literature that detailed quantitative information on mine blast output is not available. This is further compounded by the fact that the blast output of the same mine is greatly influenced by how it is buried, what the soil conditions are, etc. Results from previous mine blast work are typically presented in terms of time-independent integral quantities, i.e., total impulse imparted to free-flying plugs or total deflection of floor plates. Integral quantities are useful for vehicle design purposes, but not sufficient to check the accuracy of computer codes. It is the time variation of physical variables (pressure, density, velocity, etc.) that is required to ensure that the relevant physics of the mine explosion and its interaction with the soil and target are properly accounted for in computer codes.

It was therefore decided to commission small-scale experiments with 100-gram explosive charges, about the size of an anti-personnel mine, to further the understanding of the physics of mine explosions and to generate a high quality data set that could be used to calibrate and validate computer codes. The quantitative results produced herein are directly applicable to the anti-personnel mine problem. The physics apply equally well to anti-tank mines, but further work is required to scale the results. Some of the important conclusions to be retained from this work are outlined below.

One key characteristic of mine explosions is the strong directionality of the resulting flow field. The soil constrains the hot detonation products to expand along the path of least resistance, i.e., upwards. The explosion happens very quickly, within 1 to 100 thousandths of a second, this time being proportional to the mass of explosive. Three distinct phases exist. The first phase encompasses the detonation of the explosive and its early interaction with the soil. When the hot gases break through the soil surface, it marks the beginning of the gas expansion phase. Later on, soil material flows within an annulus surrounding the core of gaseous products. This third phase is called late ejecta flow.

The principal parameter varied during the present small-scale experiments is Depth of Burial (DoB). This parameter has a strong influence on mine output, as quantified by physical variables such as the ejection velocity of the soil cap, the propagation speed of the air shock, the incident pressure behind the air shock and the expansion velocity of the hot detonation products. The table below summarises some of the important flow variables observed during these experiments.

Description	DoB	Value/Range
Soil cap maximum ejection velocity (m/sec)	3	1690
	8	425
Initial propagation speed of air shock (m/sec)	0	3730
	3	1200
	8	440
Average incident pressure of air shock 30 cm above surface (psi)	0	437
	3	257
	8	21.3
Average incident pressure of air shock 190 cm above surface (psi)	0	20.1
	3	13.1
	8	3.0
Initial expansion speed of detonation products (m/sec)	0	2660
	3	940
	8	400

These experiments have shown that the physical processes taking place in the near-field of an explosion are highly stochastic. Each experiment was repeated at least three times. In spite of the tight control over the experimental geometry and procedures, the variance of the results is between 20% and 80%. Variables such as the explosive charge geometry, the location of the initiation point and the size of detonator are important.

As with any research project, one learns as events unfold. Some important information is missing from the data set. For new experiments, it is recommended that:

- A camera be positioned directly above the charge to observe the processes in the cloud of expanding detonation products;
- Additional in-soil pressure transducers be used to establish the final wave propagation velocity in the soil medium. These new transducers should be located near the bottom of the soil container; and that
- Total or pitot pressure measurements be attempted within the region of strong vertical flow.

New experiments should investigate the effect of soil variations. Important variables are soil particle size, bulk density, compaction, water content and cohesion. Two or three combinations should be selected to bracket a wide range of conditions encountered in real life situations. Possibilities include gravel, silty sand and clay. Fully dry and water saturated conditions should be investigated.

New experiments may also be needed to quantify the effect of explosive mass and chemical composition. It is known that the fuel-to-oxidiser ratio varies from one explosive to another. It is possible that this factor plays a significant role on target loads in the near-field.

Acknowledgements

A successful project requires contributions from many individuals, be it from government or from industry. These contributions are what makes or breaks the project. Unfortunately, only a few names appear on a report such as this one and, too often, the contributions from individuals working in the background are forgotten soon after the project is over. Here, the authors would like to list the personnel that contributed to this project, from start to finish, both to thank these people, but also to stress the importance of a team effort to achieve a successful outcome in a project of this type. We are indebted to (not in any particular order):

- *Bruce Isbister* and *Jim Roseveare* from Amtech Aeronautical for their every day efforts at organising and running the experiments;
- *Gurdev Boghal*, *Arnold Ross* and *Wilfred Pudwell* of the DRES Experimental Model Shop for manufacturing most of the test apparatus;
- *Barrie Boulter* for machining the C4 containers and the wedges;
- *Russ Fall*, *Ron Bengston* and *Rob Matheson* for their help during setup;
- *Dave Schmaltz* for help with the CRG setup;
- *Ken Torrance*, *Randy Lynde*, *Shelley Ewing* and *Doreen Hicken* for their help during report preparation and reproduction;
- *Fan Zhang* and *Bob Herring* for their careful review of the document;
- *Linda Beaupre* of HF Research for on-site help during the experiments;
- *Tom Storrie* for running the x-ray system;
- *Scott Trebble* of DRES Photo Instrumentation for running the high-speed camera;
- *Darrell Boechler* for running the electronic instrumentation;
- *W. Smith* from Sabatini Geotechnical Services for the soil analysis;
- *Dave Ulriksen* and *M/cpl P. Fewer* for medical support during the experiments;
- *Steve Kirvan*, *Garth Woolf*, *Ken Kihn* and *Ken Pirie* for preparing and handling the explosives;
- *Bob Martin* and *Paul Mast*, the FTOs for looking after everyone's safety.

This long list clearly shows that even a simple project such as this one requires a full team to succeed. Many thanks to all. We hope that we did not forget anyone. If we did, please accept our sincere apologies.

Table of Contents

List of Figures

List of Tables

1. Introduction

During summer 1996, the Defence Research Establishment Suffield (DRES) carried out two series of small-scale experiments where 100-gram explosive charges were shallow-buried in sand and detonated. The goal of these experiments was (i) to provide further understanding of the physics of a mine explosion, and (ii) to generate a high quality data set suitable for the validation of computer codes. With respect to the latter point, it became apparent after a survey of the unclassified literature that the need for such data existed. Although mine blast output has been measured before, the results are typically presented in terms of time-independent integral quantities, i.e., total impulse imparted to free-flying plugs or total deflection of floor plates. Integral quantities are useful for the validation of computer codes, but it is the time variation of physical variables like pressure, density and velocity, which is required to ensure that the relevant physics of the mine explosion and its interaction with the soil and target are properly taken into account.

Before proceeding further, it is useful for the reader to understand how DRES got involved in the measurement of the blast output of land mines. The request to undertake this work came from the Canadian Forces (CF) following a series of mine-related accidents. Over a period of 5 years, from January 1991 to December 1995, the CF suffered 44 mines strikes[1] while deployed on UN peace keeping missions in Somalia and the Former Republic of Yugoslavia. It was apparent that land mines posed a serious threat to both personnel and equipment. This significantly raised the level of awareness to this problem throughout the CF and more emphasis is now placed on mine protection when generating requirement documents for new equipment. Recent examples include the acquisition of mine protection kits for B fleet vehicles and Armoured Personnel Carriers, the acquisition of the Heavy Engineer Support Vehicle, and the proposed acquisitions of new Light Utility Wheeled Vehicles and a new mine detection system.

As a general rule, requirement documents state the CF mine protection needs in terms of threat, e.g., "protection against a 6.5 kg TNT anti-tank mine". While this kind of statement clearly identifies the interest of the CF, industry often finds it difficult to translate such requirements into technical specifications for design and engineering purposes, i.e., loading functions and material response. Usually, requirement officers in charge of contracts cannot provide this technical information to industry. This presents the inherent danger that the CF can -and have been- put in a position where they are forced to waive the statements on mine protection and accept whatever industry can deliver. From contacts with scientists in other countries, it appears that the CF are not alone to face this kind of situation. This is further compounded, as will be shown, by the fact that the blast output of the same mine is greatly influenced by how it is buried, what the soil conditions are, the geometry and construction of the vehicle, etc.

The overall project on mine protection is quite broad in scope, ranging from the protection of dismounted soldiers to the protection of personnel riding in soft-skinned and light armoured vehicles. The military engineering community is also interested in protecting mine detection and mine neutralisation equipment. The project involves two research establishments of the Defence Research and Development Branch (DRDB), namely DRES and DREV (Valcartier). The goals are to:

- measure the blast output of live anti-personnel and anti-tank mines;
- quantify the effect of soil characteristics and depth of burial; and
- develop a numerical capability to predict mine blast loads on nearby personnel and equipment.

The present work is one small step towards achieving these goals.

1.1 Physics of a Mine Explosion

Explosions in or on the earth's surface transmit energy to its surroundings, i.e., to the ground, the air and nearby structures. This energy release takes many forms, including heat, air and soil kinetic energy, soil deformation and work done by expanding gaseous products. Several factors affect the energy partition and the interest of the current report lies with the energy transmitted to a nearby structure. Consider the following limiting cases. On one end, if an explosion occurs deep into the soil, the energy is totally absorbed by soil compression and deformation. The detonation products are contained and no air shock is generated. This is called a *camouflet* and is of no interest to the present work. At the other extreme, surface detonation of a mine on frozen soil transmits very little energy to the ground and most of the work on a nearby structure is done by the expansion of the detonation products and the air shock. In between these limiting cases, there exists a broad range of conditions where a substantial portion of the available energy is transmitted to soil kinetic energy, thereby generating ejecta. Under the right conditions, the ejecta carries considerable momentum which is available to damage a nearby structure.

Hence, from a mine protection point-of-view, the interest is to predict and protect against the loads imparted by shallow-buried explosives, say down to 1-meter depth. The total amount of energy released by the explosion is finite and well defined by the type and quantity of explosive used. To analyse an explosion, it is then necessary to track how this energy is transferred to the soil, the air shock and the detonation products. In the time domain, the complete event may be divided into three distinct phases. The first phase is concerned with the detonation of the explosive and the immediate interaction with the soil. The second phase includes the formation and propagation of an air shock and the expansion of the detonation products. Finally, the third phase, which happens relatively late in the event, is concerned with soil ejecta.

1.1.1 Phase I - Early interaction with the soil

When the mine explosion is initiated, a detonation wave transforms the (usually) solid explosive into detonation products, a mass of hot, high-pressure gas. At the explosive/soil interface, the energy transfer results in three modes of soil dynamics response. Very near the explosion centre, there is a *zone of crushing* where pressure and temperature are so high that shock wave transmission is independent of the physical structure of the soil. Everything is simply crushed or vaporised. Bangash[2] found that this zone extends from $2R_w$ to $3R_w$, where R_w is the charge radius. Further away, from $3R_w$ to $6R_w$, Drake and Little[3] report a *zone of plastic deformation* where irreversible crushing and collapsing of the soil matrix void volume takes place. They used a relative density in granular soils, and the air void volume in cohesive soils, as key attenuation indices. Further out, there exists an *elastic zone* where shock transmission results in reversible deformation of the soil.

The early interaction phase is important because it determines the amount of energy available to impart work on the target. Many parameters influence this phase, including depth of burial, distance from the explosion centre, soil physical properties, and soil moisture content. The effect of depth of burial are bounded by the extreme cases of complete energy containment within the soil, and complete reflection to the atmosphere for an explosion on a rigid soil surface. For the case of shallow-buried explosive, a depth of burial is selected to provide soil confinement and produce preferential venting to the atmosphere. This redirects the force of the explosion in the upward direction.

The explosion generates various stress waves[4-8] that travel away from the centre of explosion. Three types of stress waves are observed: compression (P), shear (S) and Rayleigh (R) waves. These waves are subject to geometrical damping as the shock expands away from the source. The P and S waves depend on the source geometry and distance. They expand in a spherical manner and their

amplitude decreases proportionally with $1/r^2$, where r is the distance from the source. The Rayleigh waves expand on a cylindrical front and decay proportionally with $1/\sqrt{r}$.

The rate of decay is a strong function of the physical properties of the soil. For example, ground shock intensity from identical source explosions can vary up to two orders of magnitude whether propagation occurs in dry soil with low density, or in saturated clay. Moisture also has a significant effect. At high saturation levels, the water adds to the soil stiffness and strength and increases the soil's ability to transmit a shock.

1.1.2 Phase II - Gas expansion

When the compressive stress wave reaches the density discontinuity at the soil-air interface, it is partly transmitted to the air as a shock wave and partly reflected back towards the centre of explosion as a tensile stress wave. The latter stress wave combines with the push by the high-pressure detonation products to fragment and eject material into the air. Early motion of the soil and the eventual breakthrough of the detonation products act like a piston to form and sustain the air shock. As the soil cap is ejected, it leaves a cavity that acts like a pressure vessel venting to atmosphere.

The whole process described above takes a finite amount of time, micro to milliseconds, during which a complex system of shocks and rarefaction waves is established within the cavity and in the air. The detonation products undergo adiabatic expansion, resulting in a rapid temperature and pressure drop. They and the associated air shock can impart significant work on any object in their path.

1.1.3 Phase III - Soil ejecta

During the early stages of the explosion, the high-pressure gases cause hemispherical swelling of the ground, followed by ejection at supersonic velocity. The volume of this soil cap, however, is relatively small. The high-pressure gas in the soil continues to do work on the cavity walls long after this initial phase. Soil material continues to be eroded and ejected at high speed for tens, sometimes hundreds of milliseconds. The final volume ejected can be as much as one or two cubic meters for an anti-tank mine buried in a sandy soil. The trajectory of the ejecta is generally in the upward direction, within an inverse cone with an included angle between 60° to 90°. As a general rule, the included angle increases with decreasing depth of burial and looser soil.

1.2 Previous Mine Characterisation Work

Literature surveys of in-ground and mine explosion reveals that a large body of work looked at in-soil shock transmission for the purposes of design and protection of underground structures. Explosive excavation is also a subject that was studied extensively, and the reader is referred to Reference [9] for a particularly good explanation of the physical processes at work during the early stages of an in-soil explosion. The above studies are interesting and sometimes useful, but they fall outside the current scope of work. From the point-of-view of mine protection, the interest lies with understanding the loads imparted by shallow-buried explosives to nearby aboveground structures. Some authors, e.g. [10], suggest that the soil dominates the event as it contains lateral soil expansion and redirects momentum in the upward direction. The ejecta thereby generated imparts a large impulse to floor plates and other objects in its path. The claim is that ejecta loading is an order of magnitude more severe than any loads from explosively driven shock in air. This clearly depends on depth of burial and local soil characteristics.

Westine *et al.*[11] used a rigid plate with plug inserts to measure the total impulse resulting from the explosion of sub-scale charges buried in soil. The plate was mounted parallel to the ground plane. Plug motion was captured on high-speed film. However, combustion products obstructed viewing of the initial plug motion, hence initial velocity was deduced from the analysis of late time motion. The resulting impulses were fitted to a non-dimensional model, Equation [1], which expresses the spatial distribution of total specific impulse as a function of explosive energy (W), soil density (ρ) and geometry. The latter is defined by the lateral distance from the centre (x), the stand-off between the bottom of the target plate and the centre of the explosive (s) and the depth of burial (d), again defined to the centre of the explosive. These geometric variables are depicted in Figure 1.

$$Y = \frac{0.1352 \tanh^{3.25}(0.9589Z)}{Z^{3.25}} \qquad \text{Equation [1]}$$

where

$$Y = \frac{I_V \sqrt{s}}{\sqrt{\rho W}\left(1+\frac{7d}{9s}\right)} \qquad \text{(Scaled Impulse)}$$

and

$$Z = \frac{xd}{s^{5/4} A^{3/8} \tanh\left(2.2\frac{d}{s}\right)^{3/2}} \qquad \text{(Scaled position)}$$

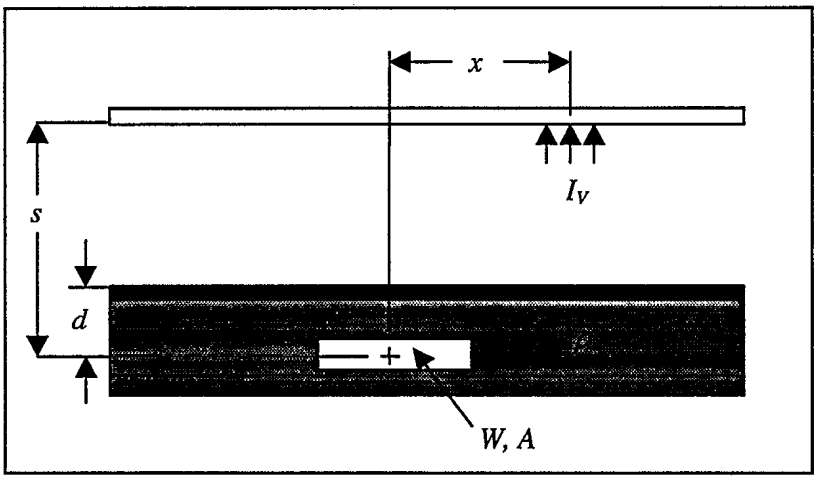

Figure 1: Mine-target geometry

The model was later expanded by Morris[12] to account for plates at an angle from the horizontal. Equation [2] links Equation [1] for total impulse in the vertical direction to total impulse normal to the tilted plate. The relevant geometry is depicted in Figure 2.

$$I_N = I_V \frac{\cos\theta}{\cos\beta}$$ Equation [2]

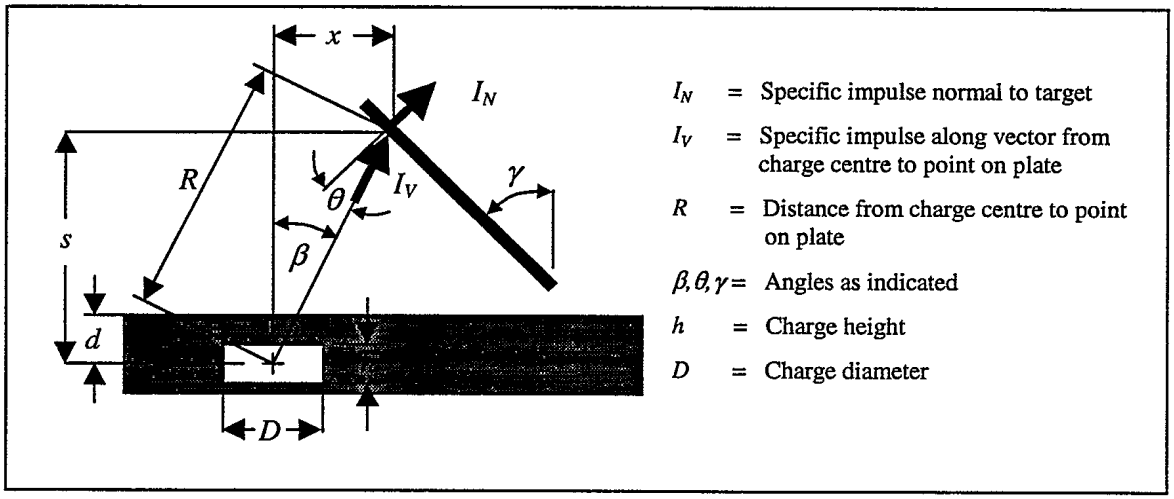

Figure 2: Revised mine-target geometry

It is important to notice here that the definition of depth of burial used by Westine and several other authors is different than the one used by the present authors. Here, the Depth of Burial (DoB) is defined as the distance between the soil surface down to the top of the explosive charge, i.e., the thickness of soil overburden above the charge. It is this definition which is used hereafter in this document.

This work is very useful for design purposes and fits in with accepted design methods based on *P-I* diagrams.[13] However, the total impulse approach does not provide the time-resolved information required to calibrate and validate numerical models used in Computational Fluid Dynamics (CFD) and Computational Structural Dynamics (CSD).

In parallel with the determination of total impulse, substantial effort was devoted to quantifying the effect of these loads on military vehicles. There was -and still is- interest in predicting the response of track and wheel systems[14] for armoured vehicles. Some of the better work involved the development of predictive curves for floor plate response to mine blast. The work of Haskell[15] is worthy of mention. He developed a practical analytical method to determine the response of armoured vehicle bottom hull plates to mine blast. His method is based on a review of 107 experimental tests, conducted at Aberdeen Proving Grounds over a 30-year period, and 244 mine accident reports from Vietnam. The method reportedly predicts final deflection of the plates within 10% accuracy. This information can be very useful for code validation, even if it does not provide the time history of the displacement nor information on the modes of deflection.

1.3 Technical Approach for this Work

One goal of this project is to measure the output of full-scale mines. However, full-scale mines are not required to study the physics of the event. This point is well illustrated by the work of Reichenbach *et al.*[16] who studied shock structure as a function of Depth Of Burial (DOB) using small ½ gram charges. Their Schlieren pictures show how, as DOB increases, shock strength weakens and eventually decays to compression waves. They also relate shock front formation to the piston effect of the overburden material as it is pushed out of the crater, and to the expansion of the

detonation products. Their results also show how soil confinement causes ejecta momentum to be directed more in the vertical direction as DOB increases.

The current work used sub-scale charges with approximately 100 grams of C4 explosive. This made it easier to build the experimental apparatus and decreased set-up time between successive experiments. While small charges present obvious advantages in terms of handling, cost and time, they also require more care to preserve time and spatial accuracy. Much effort went into the design of special jigs and fixtures to ensure that the charge and in-ground sensors were located accurately from one experiment to the next. Bagged, sieved sand was also used to ensure repeatability. Shock propagation was recorded both in air and in soil using pressure gauges and shorting pins. Flash X-ray and high-speed photography were used to measure early soil deformation, detonation products expansion and ejecta release.

The test program consisted of a total of 20 firings divided more or less equally between two separate test series. The principal difference between the first and second test series was a modification to the explosive charges. The charges used during the first series were uncased and easy to deform. Furthermore, the RP-83 detonator used was too powerful and affected the early deformation of the sand overburden. In the second series, thin casings controlled the charge shape and detonation was initiated at the bottom of the charge using a smaller RP-2 detonator. Analysis of the results indicates that the quality of the current data set is relatively high, making it ideal for code validation exercises.

1.4 Organisation of the Report

This report is organised around four sections. The introduction explained the motivation behind this work and presented a synthesis of the physics of a mine detonation based on a search of the literature as well as our own observations and experience. We also justified our decision of using small-scale charges. Given that our interest lies with the interaction between a mine and nearby personnel or equipment, our primary focus is to predict the energy available to impart work on targets. However, what happens above the ground surface depends on what happens in the soil. There is therefore a need to understand the in-soil physics as a prerequisite.

A lot of care and energy went into the design of the experimental apparatus and test procedures. Section 2 provides a detailed description of the set-up and the data acquisition process. Soil characterisation results are also presented along with the motivation behind the test procedures. The level of detail for this section is intentionally high so that readers can evaluate the validity of the procedures and the data, and reproduce the experiments if they wish so.

Section 3 contains the meat of the report. Sample traces of the raw data are presented along with a description of the analysis procedures used to extract information. Plots and curves summarise the time progression of important variables such as shock front position in soil and air. Analysis of the high-speed films yielded the expansion rate of the detonation products and crater diameter. The flash X-ray pictures clearly show the early time evolution of the bubble and give initial particle velocity.

Finally, Section 4 presents key conclusions from this work. It also makes recommendations for possible future experiments to fill in gaps in the characterisation of mine blast output.

Since the intent of this report is to distribute a data package as complete as possible, all x-ray radiographs, selected frames from the high-speed films, and all data traces from the in-ground and air pressure transducers are presented in Annexes A through C.

2. Experimental Setup and Procedures

The purpose of this Section is to describe the physical setup, instrumentation and procedures used for our validation experiments with sufficient detail for anyone else to reproduce them. Two test series were conducted. The first series was in June 1996, but we were not satisfied with the results. We had difficulty controlling the location of the in-ground sensors and the configuration of the explosive charge. This is why the experiments were repeated in August 1996, after the deficiencies observed during the first test series had been corrected.

In the pages that follow, we describe the test setup and the associated instrumentation. The last part is concerned with the accuracy in space and time, measures which are intrinsically linked to the experimental procedures. This is particularly important given the intent of the data presented herein. Note that the present report provides test results from both test series, however, the reader will readily surmise that more emphasis is given to the second series, which is deemed to be more accurate.

2.1 Physical Setup

The experiments were carried out in a "large bucket of sand" as shown in Figure 3. It was constructed from a piece of 12.7-mm thick steel pipe with an 88.9-cm inner diameter and a height of 69.8 cm. A 12.7-mm thick steel plate was welded to the bottom of the pipe to close that extremity. Four pieces of angle iron were welded vertically to the outside of the pipe, two on each side, each pair being diametrically opposed to the other. The spacing between either two pieces of angle iron provided the means for bolting 50.8 × 50.8 × 6.3 mm square tubing uprights. Another piece of square tubing was welded at the top of the uprights to provide an attachment point for the 50.8 x 76.2 x 6.3 mm rectangular tubing used to mount pressure gauges. This last piece of tubing hung suspended vertically above the centre of the tank.

A fixture was welded in place at the bottom of this assembly to bolt in a replaceable blast deflector wedge. The front face of the wedge was parallel and flush to one face of the tubing. The back face sloped away at 60 degrees to meet the 60-degree angle of the fixture, which extended to the 76.2-mm depth of the tubing. The replaceable apex of the wedge (knife-edge) was machined from 6061-T6 aluminium. It was expected that the knife-edge would be damaged regardless of what material was used, therefore a free machining material such as aluminium was used and replaced after each firing.

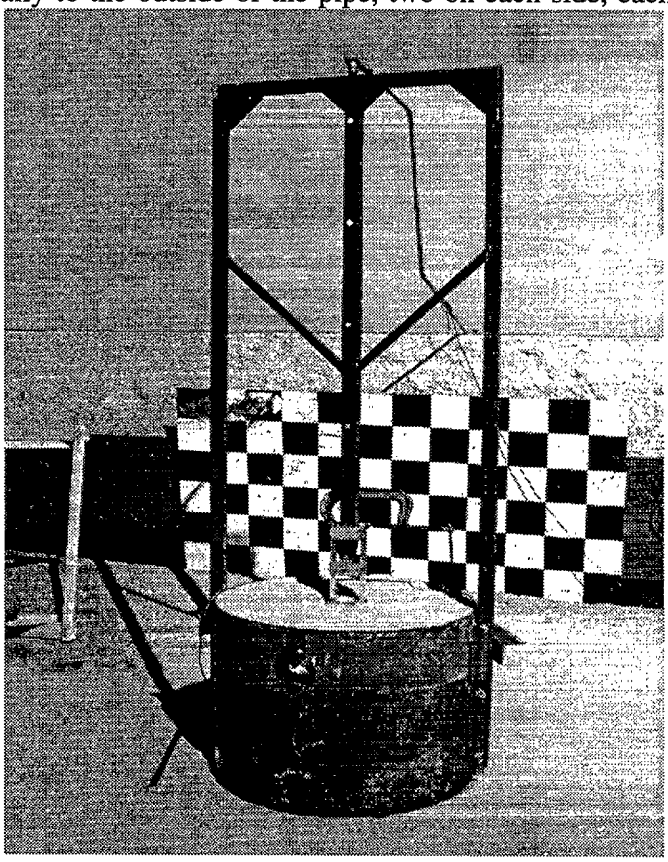

Figure 3. Sand-filled tank (with vertical uprights) used to conduct the two test series. Shown with jig to locate explosive and in-soil transducers.

2.1.1 Soil Selection

The choice of soil for these experiments was guided by the requirement of easy reproducibility. After consideration of a number of options, our selection was 3050-mesh silica sand supplied in 40-kg plastic-lined paper bags. The bags were stacked on pallets that were capped and wrapped in plastic to further protect against moisture absorption during shipment and storage. Target Products of Morinville, Alberta supplied the soil used in all the tests. The result from a sieve analysis of this sand, shown in Figure 4, confirmed that the diameter of the majority (96.2% by mass) of the particles ranged between 160 and 630 microns, with the majority of the particles between 315 and 630 microns.

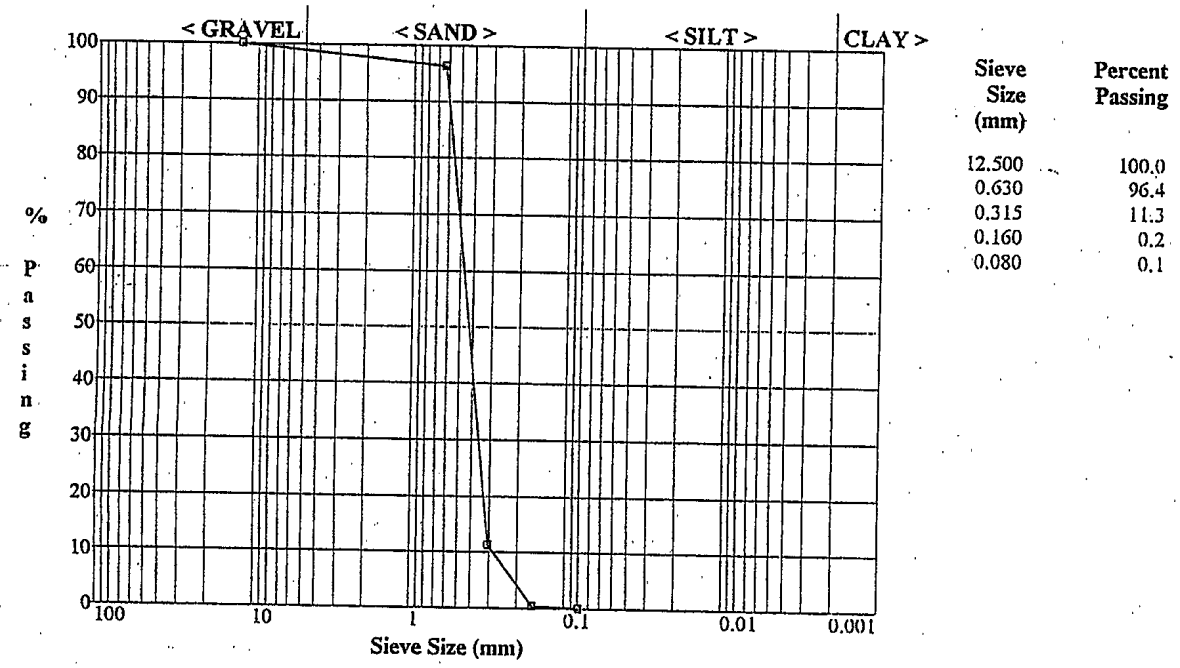

Figure 4. Sieve analysis result for 3050-mesh sand.

The initial filling of the tank required approximately 15 bags of sand, which were simply opened and poured in the tank. When filled, the sand was levelled to the top of the tank using a straight edge. Before the first detonation took place, soil density was measured with a nuclear densitometer (see Table I). The test results indicated a density of approximately 96% Proctor. After the first test firing, a few shovels of sand at the centre of the tank, that contained combustion products and pulverised sand, were removed and the sand density was again measured. These tests indicated that compaction at the centre of the tank had dropped to approximately 87% Proctor. It is suspected that this was produced by a combination of decreased moisture, the driving of combustion products into the sand, and a complex set of compression and tensile stress waves bouncing between the surface of the soil and the bottom of the tank. Further examination of the sand revealed that there were no clumps of solidified sand and that the texture was approximately the same as that of new sand. Preparing the tank for another trial required replenishing the ejected sand and the sand that was shovelled out while getting rid of any debris. This required approximately five 40-kg bags. Once the tank was refilled, density was measured again. Repeating this procedure for most shots during the first test series indicated that the compaction would always return between 94 and 95% Proctor. Because of this high level of repeatability, compaction was not measured for the second test series.

Table I. Summary of Geo-technical Soil Measurements.

Test ID & Date	Description	Depth	Dry Density	Moisture Content	Proctor Density	Optimum Moisture	Percent Proctor
		(mm)	(kg/m^3)	(%)	(kg/m^3)	(%)	(%)
1-17Jun96	Pre-shot 1	300	1577	0.4	1636	2.3	96.4
2- 17Jun96	Pre-shot 1	250	1571	0.4	1636	2.3	96.0
3-17Jun96	Pre-shot 1	200	1571	0.1	1636	2.3	96.0
4-17Jun96	Pre-shot 1	150	1575	0.3	1636	2.3	96.3
5-17Jun96	Pre-shot 1	100	1575	0.3	1636	2.3	96.3
6-17Jun96	Pre-shot 1	50	1575	0.3	1636	2.3	96.3
7-17Jun96	Pre-shot 1	0	1567	0.3	1636	2.3	95.8
1-18Jun96	After detonation	0	1552	-0.1	1636	2.3	94.9
2-18Jun96	After detonation	0	1538	-0.3	1636	2.3	94.0
3-18Jun96	After detonation	0	1533	-0.2	1636	2.3	93.7
4-18Jun96	After detonation	0	1527	-0.4	1636	2.3	93.3
5-18Jun96	After detonation	0	1499	0.0	1636	2.3	91.6
6-18Jun96	After detonation	0	1445	-0.2	1636	2.3	88.3
7-18Jun96	After detonation	0	1408	-0.4	1636	2.3	86.1
8-18Jun96	Tank refilled	0	1563	-0.4	1636	2.3	95.5
9-18Jun96	Tank refilled	0	1548	-0.4	1636	2.3	94.6
10-18Jun96	Tank refilled	0	1555	-0.3	1636	2.3	95.0
11-18Jun96	Tank refilled	0	1553	-0.2	1636	2.3	94.9
12-18Jun96	Tank refilled	0	1568	-0.5	1636	2.3	95.8
13-18Jun96	Tank refilled	0	1575	-0.2	1636	2.3	96.3
14-18Jun96	Tank refilled	0	1571	-0.3	1636	2.3	96.0

2.1.2 Explosive Charges

The explosive used in all trials was C4, which is produced for the Canadian Armed Forces and is supplied in standard block form. For the first series, the charges were made by breaking off pieces of C4, placing them in a metal mould, and manually compressing them into shape using a wooden dowel. The mould produced a charge with a 64-mm diameter, a 20-mm height, and a weight of 100 gram. Detonation of these charges was done with an RP83 detonator forced into the top surface of the C4 charge to a depth of approximately 10 mm.

Two problems where noted with this charge design. First, due to hot weather, the C4 became very pliable and it was difficult to support the detonator in a vertical position. In some cases, the detonator would tilt which made it necessary to pack additional C4 from the top of the charge around it for support. This, of course, changed the mass and configuration of the charge. It was also evident that the diameter was changing when some charge would no longer fit in the sleeve. After only a few trials it was decided that any future trials would require the use of a container to ensure consistency in mass and shape. The second problem was only discovered during examination of the x-ray radiographs. The large size of the detonator relative to the charge height left a substantial portion of the detonator exposed. Detonation of the RP83 above the charge's centre of mass was creating a venting channel that affected the shape of the early ejecta pattern. Furthermore, uncertainties about the charge mass and geometry resulted in greater than desired variability of the pressure records at the first air blast transducer location.

For the second test series, the charge was moulded in a similar manner but the metal mould was replaced with a thin-walled DELRIN plastic container, shown in Figure 5. The C4 was left in the container to ensure that the charge would retain its shape. To account for the 0.76-mm thickness of the container wall, it was decided to modify the dimensions of the C4 explosive from 64 mm to 62 mm in diameter, and from 20 mm to 22 mm in height. The lid for the container was manufactured with a boss and a through hole sized to fit an RP2 detonator. Also machined into the lid, was a 2-mm deep recess into which two discs of DETASHEET, 19-mm in diameter, were installed. This was required, as the RP2 detonator produced insufficient energy to reliably initiate detonation of the C4 explosive. The resulting weight of explosive was consistently 106 gram within a ±1% accuracy.

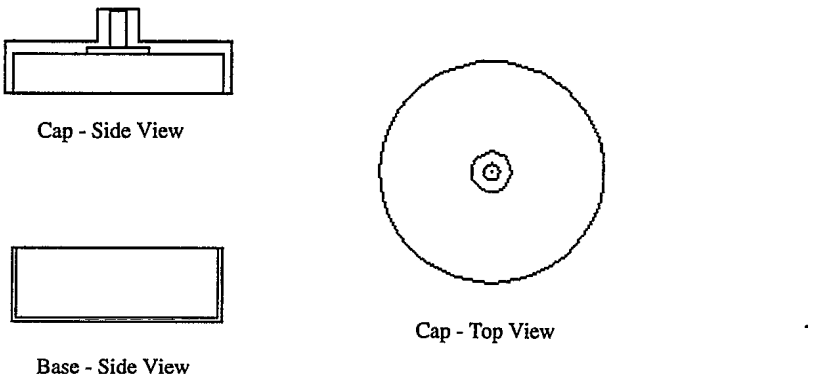

Figure 5. Charge containers used for test series 2.

2.2 Diagnostics

An overview of the instrumentation used during these tests is shown in Figure 6. Five transducers were used to measure air blast propagation while three gauges measured in-ground shock pressure and time of arrival (ToA). Three ToA shorting pins were also used in parallel with the in-soil pressure gauges. Finally, flash x-ray radiography and high-speed photography were used along with simple eyeball examination of the "craters" resulting from the explosion.

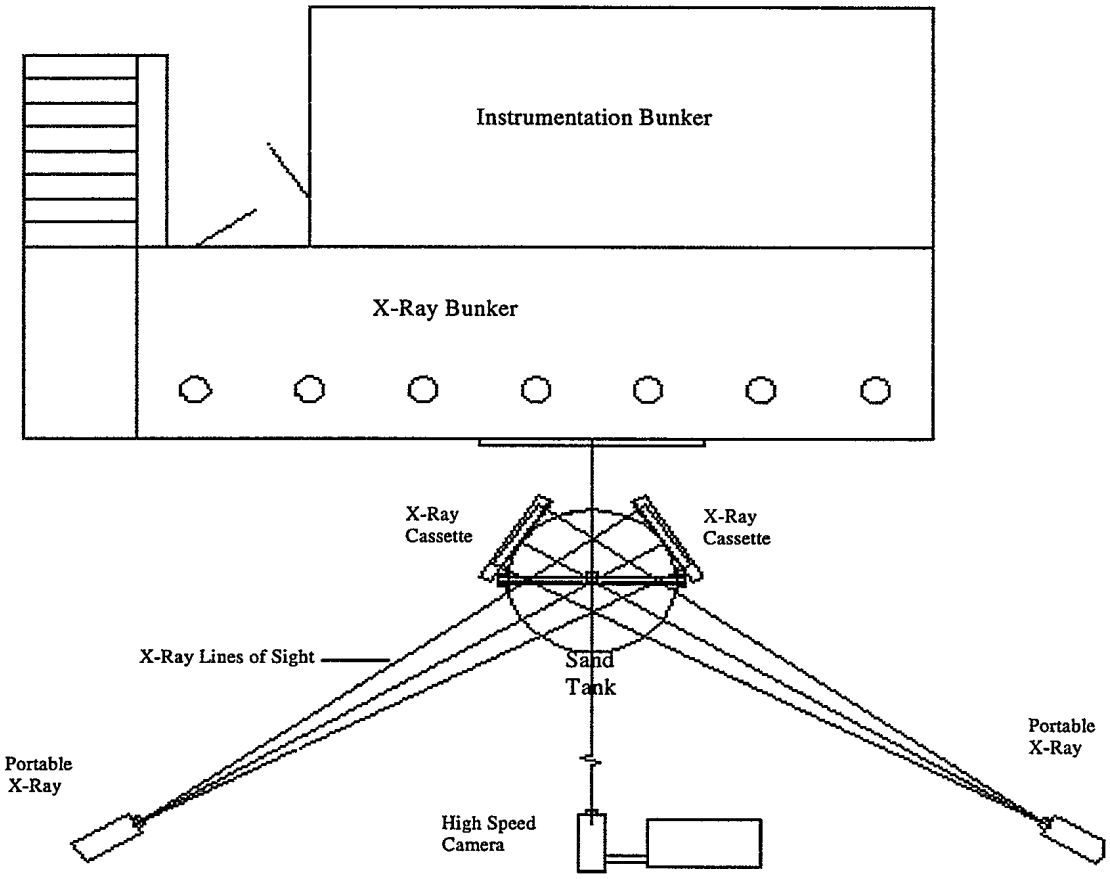

Figure 6. Plan view of the experimental setup with diagnostics.

2.2.1 Air Blast Pressure

Five Endevco pressure transducers were mounted on the front face of the vertical 50.8 × 76.2-mm tubing. Figure 7 shows their location at 30, 70, 110, 150 and 190 cm above the soil surface. The transducers were first threaded into DELRIN inserts that also had an external thread. The insert and transducer, now functioning as a single unit, were then threaded into the rectangular tubing so that the insert and transducer face were flush to the front face of the tubing. The mismatch in material impedance, introduced by the density discontinuity between steel and DELRIN, attenuates shock transmission to the transducer. This, in turn, improves the signal-to-noise ratio for the pressure measurements. The type and range of the transducers used is listed in Table II.

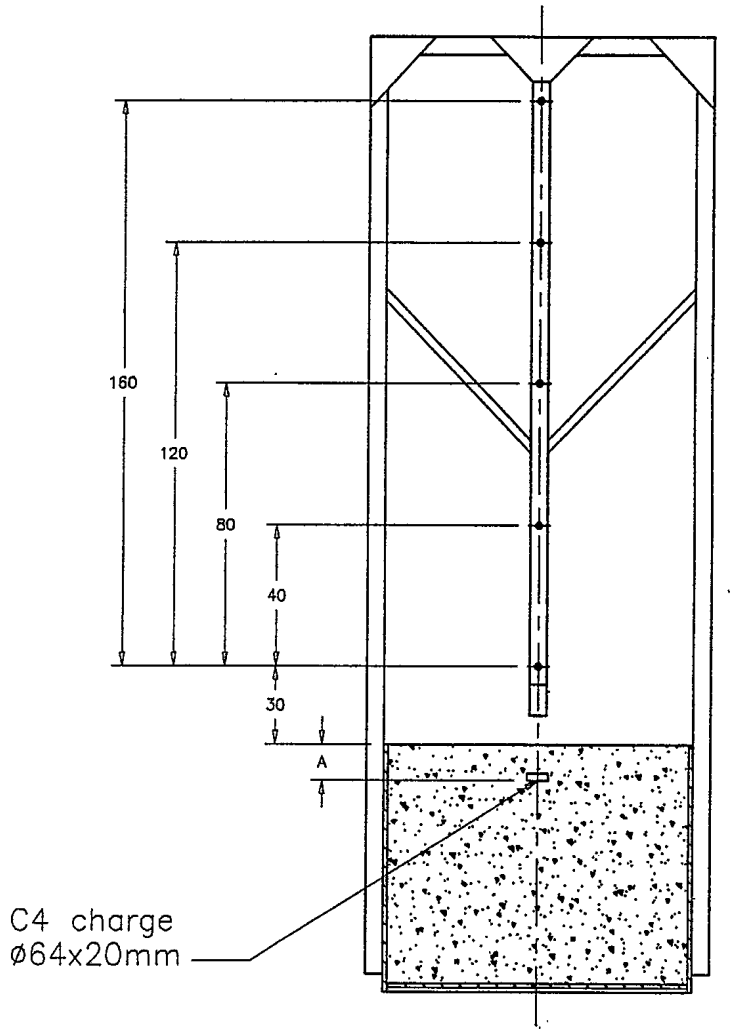

Figure 7. Location of the air blast transducers relative to the soil surface.

Table II. List of Air Blast Transducers.

Location (cm)	Gauge Type	Model No.	Range (psi)	Transducer ID
30	Endevco	8530A/B	200-1000	TP1
70	Endevco	8530A/B	200-500	TP2
110	Endevco	8530C	100	TP3
150	Endevco	8530C	50	TP4
190	Endevco	8530C	15-50	TP5

2.2.2 In-Soil Pressure

The test plan called for in-soil pressure measurements to be taken close to the explosive, which meant that any instrument used would very likely be damaged. It was therefore decided to construct low-cost, expendable pressure gauges using commercial carbon composition resistors. The resistor type selected for this application is a 1/8 W carbon composition resistor made by the Allen-Bradley Company with a nominal resistance of 470 ohms (±5%). Each resistor was embedded in the centre of a Plexiglas™ cylinder 12.7 mm in diameter and 12.7 mm in length using epoxy. The cylinders were cut to length from a commercial 12.7-mm rod to a tolerance of 0.025 mm. To insure that the location of the resistor relative to the top or bottom of the cylinder was the same for each gauge, the hole was drilled using a drilling fixture. Two additional holes were drilled in the cylinder, on either side of the resistor hole, for mounting purposes as will now be explained.

It was important to maintain the spacing between the in-soil Carbon Resistor Gauges (CRGs), a task particularly difficult while the transducers were being buried under the explosive charge. During the first test series, the CRGs were mounted on wooden support members using electrical tape, as shown in Figure 8, but the accuracy of this arrangement, particularly with respect to the distance beneath the explosive, was less than desired (a few mm). But more importantly, the vertical stacking of the CRGs was believed to mask the second and third gauges, thus preventing the measurement of full shock strength.

A special test fixture (Figure 9) was therefore constructed for the second test series. It was formed from a piece of 3.18-mm aluminium cut in the shape of a "U". The outside height and width of the frame were 20.8 and 25.4 cm, respectively. The corresponding inside height and width were 15.7 and 15.2 cm. The CRGs were attached to the U-frame with guitar tuning pegs and 18 pound test monofilament fishing line. One end of each line was anchored to the side of the U-frame housing of the tuning peg. The other end was fed through one hole in the Plexiglas™, then through a hole in the opposite leg of the U-frame, back through the second hole in the Plexiglas™, and finally attached to the tuning peg. The line was drawn taut by turning the tuning peg. The reader should note that the thickness of the U-frame was adjusted to match the spacing of the holes in the Plexiglas™ and that a

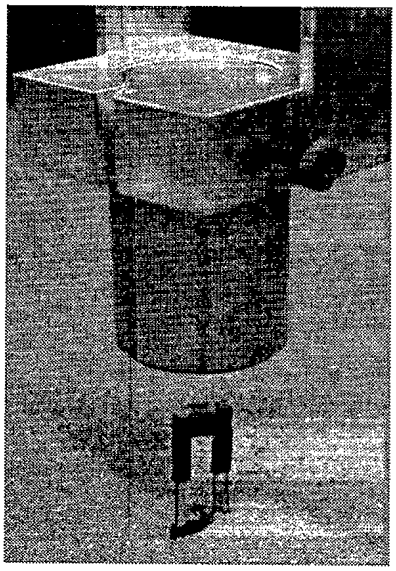

Figure 8. Vertical stacking of CRGs using wooden posts and electrical tape for test series 1.

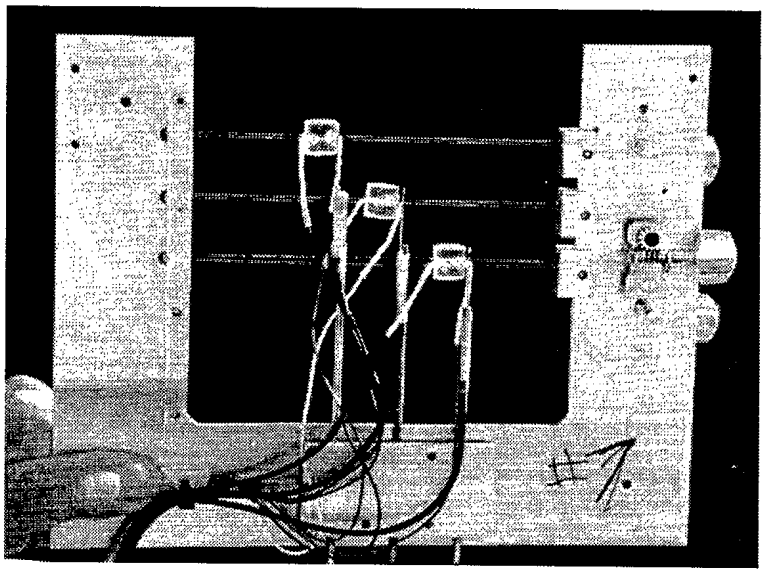

Figure 9. U-frame used to mount the CRGs with lateral offset during the second test series. The Dynasen shorting probes were mounted next to each CRG.

lot of attention went into mounting the CRGs with their upper face parallel to the bottom of the explosive. The CRGs were also offset from one another to prevent masking of the shock as it impinged upon successively deeper gauges. Vertical spacing between gauges was 2.5 cm and the distance from the bottom of the explosive to the sensing element of the first CRG was 8.73 cm. One exception to this spacing is for test number 14, when the U-frame was moved 2.5 cm closer to the charge.

The cabling for the in-soil gauges ran below the U-frame, across to the side of the tank, up along the side of the tank, over the edge and down along the 50.8 × 50.8-mm upright. It was connected to a junction box on the ground near the bottom of the upright. Signals from the box were fed to a bank of Digistar II recorders located inside the bunker. The cables from the junction box to the gauges, as well as the gauges themselves, were replaced after each test. All cables were shielded against EMP spikes.

2.2.3 In-Soil Time of Arrival

Three ToA shorting pins were mounted parallel to the CRGs to detect the arrival of the shock at the upper face of each Plexiglas™ cylinder (see Figure 9). The instruments used were model No. CA-1043-C, purchased from Dynasen Inc. of Goleta, California. They were mounted on steel rods, 3 mm in diameter, which were attached to the bottom of the U-frame. The height of each pin was adjusted on a surface table using a Vernier gauge. Comparison of the ToA values obtained from the pins to those obtained with the CRGs provides information about the reaction time of the CRGs.

2.2.4 Flash x-ray Radiography

Two 150 kV flash x-ray heads were used to image the early deformation of the soil surface. The heads were located 2.9 m from the centre of the tank and the angle between the two heads was 115°, as shown on Figure 6. The film cassettes rested on two horizontal pieces of angle iron welded to the tank. Their top edge was lightly attached to the 50.8 × 50.8 uprights using duct tape. This method of attachment was sufficient to hold the cassettes in place until they were hit by the blast, yet "soft" enough to release the cassettes without damage thereafter.

To accurately locate the cassettes for each firing, a V notch was filed into the edge of the tank at each cassette location. The external vertical cross hair mark on the cassette was aligned with this notch. The horizontal cross hair mark was located near the bottom of the cassette, just above the edge of the tank. A laser transit was used to set a horizontal datum for both cassettes. The alignment procedure was repeated for all tests so that all radiographs have a common datum.

2.2.5 High-Speed Photography

A 10,000 frame per second PHOTEC camera was used during these tests. The camera was located mid-way between the x-ray heads at a radial distance of approximately 9 m from the centre of the tank. The lens chosen provided a field of view of 2 m above the tank surface. During the first test series, a checker board backdrop was provided for the camera. It was hoped that motion of the shock front could be observed against this background, but no visual disturbance was observed for any of the first test series shots. The backdrop was therefore changed to alternate black and white strips at 45° for the second test series, but again, motion of the shock front could not be observed.

Despite the failure to observe motion of the shock front, the high-speed photography produced a lot of other data. This included the early deformation of the soil surface (for buried charges), the expansion rate of the detonation products, and the angle at which ejecta was being expelled.

2.2.6 Crater Measurements

Crater measurements were taken after selected shots. However, it became apparent early in the test program that the cohesion of the sand used bears little resemblance to actual soil. In fact, it was observed that 3050-mesh sand behaves more like a liquid. Hence the craters produced are not representative of what would be found in a more realistic scenario.

2.3 Experimental Resolution and Accuracy

A detailed analysis of the absolute accuracy of the results presented herein is a complex process. It is also beyond the scope of this report. The reader should simply be aware that uncertainties are associated with each step of an experiment. The choice of transducers, the signal conditioning and the resolution of the digitalisation process itself, are all factors that affect the final accuracy of the measurement. However, the experimentalist has little control over these factors and must simply make sure that the instrumentation used is operating as close as possible to accepted standards. By the same account, there are several factors over which direct control can be exerted. These include the physical geometry of the experiment, the mass and dimensions of the explosive charge, the selection of soil medium, the gains used to bracket the expected signal range, and the sampling rate for digital recorders.

During these experiments, a lot of attention went towards maintaining a reasonably high degree of accuracy with respect to mass, time and space. Factors relating to mass include soil density and compaction, as well as the amount of explosive used. The sieve analysis confirmed that the sand used was uniform in size, with more than 95% of the particles having a diameter between 160 and 630 micron. Likewise, in-situ measurements of soil compaction proved that the latter was repeatedly 95 ± 1%. The mass of the explosive was weighted to be 106 gram within a ±1% accuracy.

2.3.1 Accuracy in Time

Time resolution is a direct function of the speed of the instruments used or of the sampling rate selected. For flash x-ray, the firing time for each x-ray head was pre-programmed on the firing console and the actual firing time was confirmed with time counters to within a 0.1 μsec accuracy. It is therefore reasonable to assume that the timing for the x-rays is accordingly accurate.

The PHOTEC high-speed cameras used was operated near its maximum framing rate of 10,000 frames per second. The actual framing rate is determined from the spacing of 1 msec timing marks on the film. The framing rate determines the time resolution of the instrument. Hence, the maximum resolution for the high-speed film is 100 μsec. Reconciliation of the film results with the radiographs requires careful interpolation of the data.

The Digistar II recorders were run at a 1 MHz sampling rate. Their time accuracy is controlled by the clock cycles, which should ensure good accuracy. However, other factors affect accuracy, such as the frequency response of the sensors and bandwidth of the signal conditioning hardware. The signal conditioning suite of the Digistar II recorder was designed to meet or exceed the 1 MHz specification, hence, the frequency response of the sensor is the limiting factor in the present case.

Three sensor types were connected to the recorders, the Endevco pressure transducers, the Dynasen shorting pins and the CRGs. The manufacturer specifications for the Endevco transducers quote a 2 to 3 μsec rise time, which is 3 to 5 times faster than the typical rise time of the shock wave, and 300 to 500 smaller than the duration of the pressure pulse. Regular calibration of the transducers in the laboratory also confirm that their linearity is within ±0.5% and their absolute accuracy is within ± 2 to 3%. The shorting pins operate on the principle that two very thin wires are crushed together by

the passage of the shock, thereby creating a short. The limiting factor in this case is the time required to physically crush the structure. This time is estimated to be better than 1 μsec.

The frequency response and accuracy of the CRGs is the one with the greatest uncertainty. Recall that these cheap gauges were designed for single use only. They are constructed with resistor components that already have a ±5% uncertainty. The formula used to transform their resistance change was extracted de facto from the literature[17,18] and applied directly. Consequently, the CRG signals should be considered to provide only a rough order of magnitude estimate of in-ground pressure. Their frequency response can be ascertained from comparison with the shorting pins, which will be addressed in the results' section. Nevertheless, considering the extreme environment where these gauges operated, the results obtained provide insight into the nature of the in-soil pressure wave.

2.3.2 Accuracy in Space

Spatial accuracy is where the authors had the greatest influence. The spacing of the five air blast transducers relative to each other remained constant. Since it was machined in steel, the accuracy was of the order of 0.1 mm. The vertical position of the first gauge above the sand surface was measured at 30 cm using a ruler and straight edge across the top of the tank. The uncertainty associated with reading a mm-graduated ruler is ±0.5 mm, but other factors, such as flexing of the ruler and vertical alignment, can affect the accuracy of the measurement. Hence, a conservative estimate of the overall accuracy is ±1 mm.

One of the primary concerns was to locate the centre of the explosive charge vertically below the air blast column, accurately and repeatedly within ±1 mm. To solve this challenge, the charge-locating fixture depicted in Figure 10 was used. It consists of a split sleeve held together as a cylinder by a block. The diameter of the annulus at the top of the block was machined to the same diameter as the split sleeve. The block and sleeve were then referenced laterally to the knife-edge by cross members on the support arms, which were clamped to the 50.8 x 76.2 mm rectangular tubing supporting the air blast gauges. Two dowel pins spaced at 38.1 mm were press-fitted into the cross member. By sliding the fixture upward, the two dowel pins contacted the knife-edge ensuring constant vertical spacing between the knife-edge and the soil surface. Once in position, the fixture assured that the explosive charge was directly centred to the column supporting the gauges. Also, the top of the block supporting the split sleeve was on the same plane as the sand surface.

This configuration was used throughout the first test series. For the second test series, the switch to cased charges required a minor modification to the fixture. Since the detonator was now at the bottom of the charge, the wiring needed to be drawn taut over the side of the container and taped to the top. A recessed groove needed to be machined in one half of the split sleeve to account for this localised increase in the diameter of the charge.

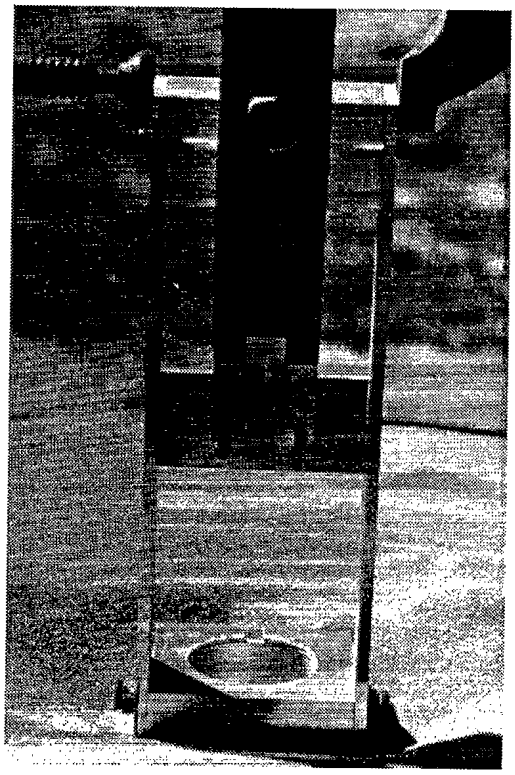

Figure 10. Charge locating fixture clamped to main vertical post housing the pressure

When the apparatus was in place and securely clamped to the vertical column, a depression would exist in the sand in the centre area of the tank. The fixture was first used to locate the array of CRGs; the spatial accuracy of this operation is discussed later in this section. Once the CRGs had been properly located, sand was poured from the 40-kg bags to fill the cavity and bring the sand level to the top of the tank and the block holding the split sleeve. A DELRIN plug (Figure 11) was used to tamp the sand at the bottom of the sleeve at the pre-selected depth of burial. Tamping ensured that the surface at the bottom of the sleeve would be flat, ready to receive the explosive charge. The latter was armed before insertion. The apparatus was then removed by loosening the screws holding the split sleeve to the block and lifting upward. The split sleeve was left in the sand with the charge and detonator. The wiring to the detonator was undisturbed during the removal procedure due to the opening in the block. Sand was then poured into the sleeve to cover the charge and each half was carefully removed, leaving only a slight depression that was filled and levelled using a straight edge across the top of the tank.

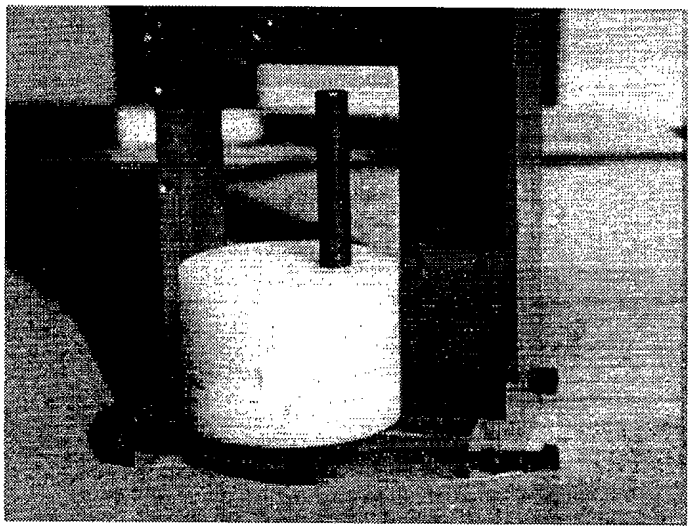

Figure 11. DELRIN plug used to tamp the bottom of hole and set the depth of burial for the explosive.

Accurate placement of the CRGs below the explosive charge presented its own challenges. During the first test series, the CRGs were assembled on a wooden frame with electrical tape. This operation was performed in the laboratory and the spacing between successive CRGs was measured by hand with a ruler, therefore the positional uncertainty was as mentioned previously. The tips of the ToA gauges were then positioned flush to the top of the Plexiglas and also taped to the wooden supports. In the field, when positioning these assemblies, they were held by hand below the charge fixture while sand was poured in around the unit. The distance to the top gauge was then measured with a ruler, as shown in Figure 12. This method of placement does not ensure that the CRGs are centred under the explosive, hence the positional accuracy is considered to be of the order of a few mm. Furthermore, it was difficult to ensure consistency from shot to shot and the authors were concerned about this deficiency. On the other hand, it can be argued that the footprint of the CRGs is much less than the diameter of the explosive, thereby nullifying any error introduced with lateral placement.

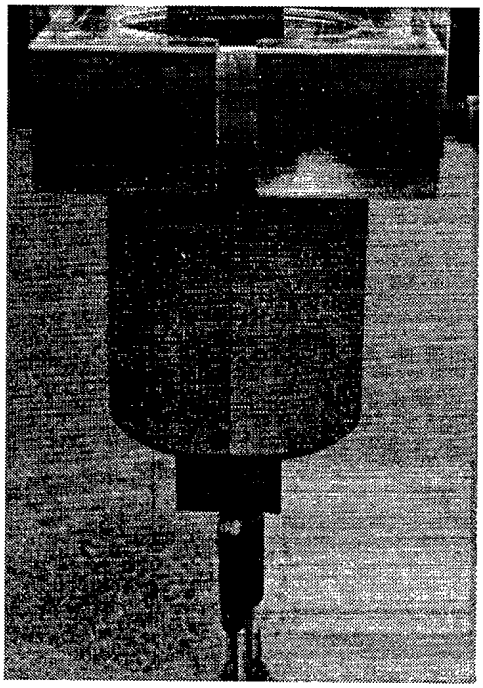

Figure 12. Emplacement of the CRGs during the first test series.

Given the above arguments, the whole concept of mounting the CRGs and locating them below the explosive was modified. The gauges were mounted in the U-frame with lateral offset from one another, and their relative position within the frame was again verified in the laboratory with a ruler. Although the accuracy of this mounting method is

judged to be an improvement over that used during the first test series, the use of strings to mount the gauges introduced its own positional uncertainties. Tension in the strings had to be controlled, but the gauges are now free to rotate. However, the angle of rotation was small, less than 1° or 2°. It was largely dependent on the tension of the electrical leads to the CRG resistors.

In the field, the U-frame was attached to the charge fixture as shown in Figure 13. This arrangement provided a repeatable method to position the in-soil gauges accurately relative to the base of the charge. Once in position, sand was poured in while making sure that the assembly remained vertical. This procedure required a larger cavity in the sand but as it turned out, this was approximately the required volume of five 40-kg bags. Once the gauges and the connecting electrical cabling were buried, the thumbscrews at the top of the U-frame were loosened which released the frame from the bracket connected to the charge fixture. This bracket could then be released from the charge fixture leaving the in-ground gauges precisely positioned relative to the fixture. Sand was again poured in to fill the rest of the cavity with the exception of the volume within the sleeve. During this time, the in-soil gauges were connected electrically to the junction box on the ground outside the tank. Once completed, the charge was placed in the split sleeve by munitions personnel and the final leveling off of the sand was completed once the sleeve had been removed.

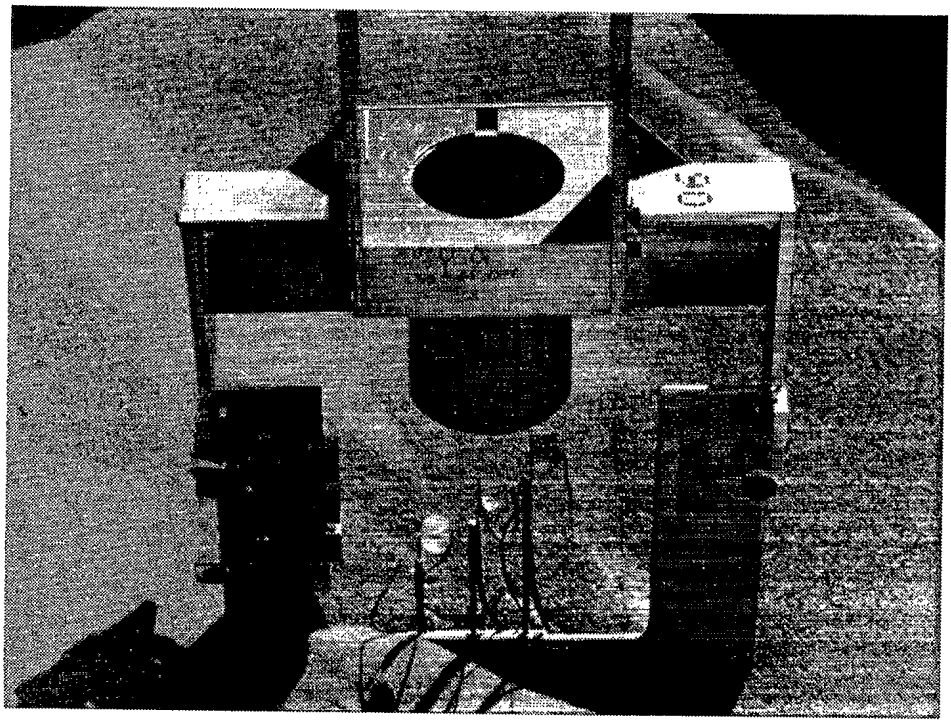

Figure 13. Extra fixture used to accurately position the CRGs and shorting pins during the second test series.

3. Results and Discussion

This section presents the results from test series 1 and 2 as a combination of tables and figures or graphs. Wherever appropriate, an interpretation or other comments are also given. The reader is reminded that the aim of the present publication is to disseminate a data set for code validation. Hence, the information herein must be used in concert with the description of the experimental apparatus and test conditions given in the previous sections.

3.1 Early Soil Deformation

Flash x-ray photography was used to capture the early motion at the soil surface. The photographic records from series 1 and 2 tests are shown at Annex A. The same test conditions were repeated three times for each depth of burial. For any given test, up to two x-rays were obtained at pre-set delay times after initiation of the detonation. In some instances, x-rays for a given delay time were obtained for more than one experiment in order to check repeatability. Otherwise, the delay was varied to capture the shape of the soil surface for six different times. This is a valid approach under the assumption that soil motion is repeatable, hence more x-ray times yield a more complete "picture" of the early surface motion.

Figures 14a and 14b show the surface deformation about 350 μsec after detonation of the charge for an 8-cm overburden. Comparison of these two figures clearly demonstrates the influence of the detonator size and method of initiation on the bubble. For the series 1 x-rays, metal fragments from the detonator casing and a venting channel on the upper portion of the bubble are visible. However, it is also seen that venting takes place only on the upper portion of the bubble and that the shape of its lower portion remains well defined. Hence, the data may still be used.

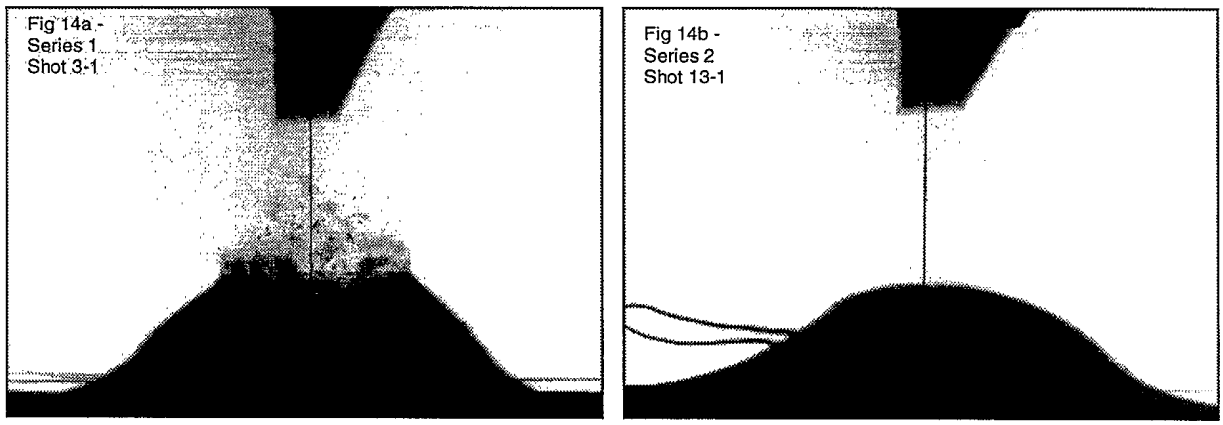

Figure 14. Comparison of soil surface deformation for an 8-cm overburden, 351 μsec after detonation. a) Series 1, b) Series 2.

The information extracted from the original x-rays includes the maximum height of the bubble, which is tabulated in Tables III and IV. Note that for series 1, height was estimated given that venting destroyed the top portion of the bubbles. Tables III and IV also include measurements of the width of the bubbles taken at the base, 1/3rd and 2/3rd heights. These points may be used to fit a quadratic or cubic function to describe the shape of the bubble cap.

Table III. Early soil deformation data extracted from the x-ray films, Series 1

Shot ID	Time (μs)	Charge depth (cm)	Base width (cm)	1/3 width (cm)	2/3 width (cm)	Bubble height (cm)
2-2	55.9	8	-[1]	-	-	-
8-1	150.9	8	9.7	7.8	6.5	0.6[2] (v) [3]
8-2	(250) [4]	8	12.8	10.1	8.1	1.6 (v)
3-1	350.8	8	15.6	11.2	8.2	1.7 (v)
2-1	450.8	8	21.8	13.3	10.7	5.1 (v)
3-2	731.0	8	23.1	17.4	17.4	12.8 (v)
5-1	50.9	3	7.9	5.9	3.2	1.8 (v)
4-1	100.9	3	13.4	8.6	7.7	3.1 (v)
6-1	150.9	3	16.4	9.9	7.8	4.8 (v)
5-2	201.2	3	17.7	11.9	10.8	8.0 (v)
6-2	246.0	3	18.4	14.3	13.7	9.1 (v)
4-2	301.9	3	20.8	15.3	16.6	14.2 (v)
9-1	24.0	0	7.2	-[5]	-	-
9-2	51.0	0	9.7	-	-	-
10-1	100.9	0	13.7	-	-	-
10-2	201.0	0	19.0	-	-	-
11-1	250.8	0	17.5	-	-	-
11-2	301.1	0	17.7	-	-	-

[1] Nothing visible on x-rays from Shots 1-1, 1-2, and 2-2.

[2] Bubble heights for vented shots are extrapolated from bubble curvature.

[3] (v) denotes detonation products have vented through ejecta bubble.

[4] X-ray apparatus did not record exact time for Shot 8-2. 250 μs was preset time.

[5] No ejecta bubbles formed for 0 cm DoB. Lateral expansion of ejecta only.

Figure 15 presents bubble height as a function of time for the 3 and 8-cm DoB cases. No data is included for the flush buried charges since no overburden exists for that case. Data is presented for both test series. It is seen that for any given time and DoB, the displacement during series 2 is greater than for series 1. This difference is likely attributable to the method of initiation. Recall that top initiation was used for series 1, while that bottom initiation was used for series 2.

From inspection of the shot 2-2 x-ray (Annex A) for an 8-cm overburden, it is seen that surface motion has not yet occurred 55.9 μsec after detonation due to the finite amount of time required for the compression wave to reach the surface. The time at which initial surface motion takes place is estimated from a linear fit through the early portion of the data. These times are approximately 30 and 80 μsec for the 3-cm and 8-cm cases, respectively. This yields an average wave velocity of 1000 m/sec through the soil cap. The material accelerates until the detonation products burst through the upper portion of the bubble. Estimates of the final velocity of the soil cap, obtained from quadratic curve fits through the data and taking the first derivative, yield final velocities of the order of 870 and 1690 m/sec for the 3-cm cases, and 210 and 425 m/sec for the 8-cm cases. Although these numbers vary significantly, they show there is a definite dependence of ejecta velocity on DoB. The decrease of ejecta propagation speed with overburden is due to the greater energy absorbed by compaction of the granular sand, behaviour consistent with the existence of *camouflets*.

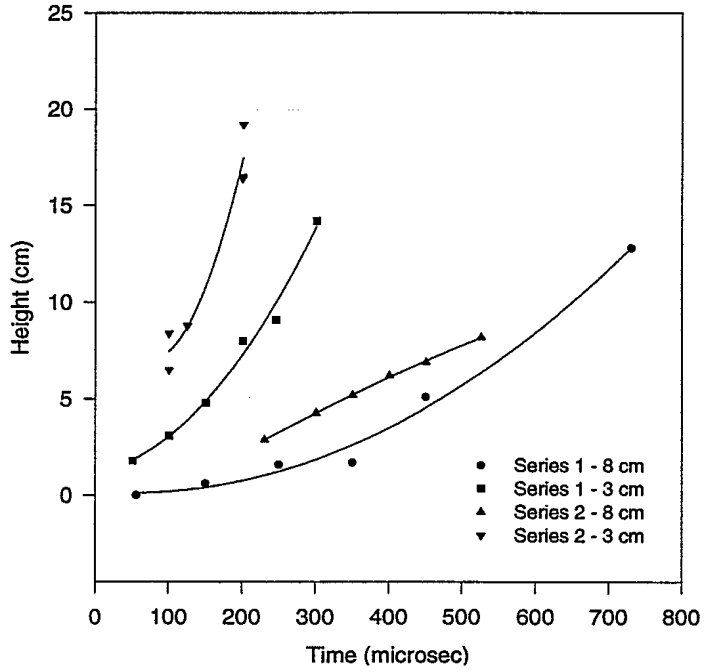

Figure 15. Early displacements of ejecta front for test series 1 and 2, 3-cm and 8-cm overburden.

Table IV. Early soil deformation data extracted from the x-ray films, Series 2

Shot ID	Time (μs)	Charge depth (cm)	Base width (cm)	1/3 width (cm)	2/3 width (cm)	Bubble height (cm)
12-1	230.9	8	19.9	13.0	9.4	2.9
12-2	301.1	8	22.9	14.5	9.8	4.3
13-1	351.0	8	27.9	16.1	11.1	5.2
13-2	401.1	8	29.1	16.7	11.9	6.2
14-1	451.0	8	32.8	17.7	11.8	6.9
14-2	526.1	8	31.1	17.6	12.4	8.2
16-1	100.8	3	17.3	11.5	7.8	6.5
15-1	100.9	3	17.7	12.3	9.8	8.4
17-1	125.9	3	19.9	13.1	10.1	8.8
16-2	201.1	3	22.0	17.3	13.8	16.4
17-2	201.1	3	24.6	17.3	14.3	16.5
15-2	201.9	3	24.2	20.7	18.5	19.2
20-1	25.9	0	10.4	[1]	-	-
20-2	51.0	0	13.6	-	-	-
18-1	50.8	0	14.1	-	-	-
19-1	50.9	0	14.7	-	-	-
18-2	101.1	0	16.9	-	-	-
19-2	101.9	0	17.0	-	-	-

[1]. No ejecta bubbles formed for 0 cm DoB. Lateral expansion of ejecta only.

3.2 Expansion of the Detonation Products

The high-speed films show that soil overburden has a strong effect on the expansion rate of the detonation products and the associated phenomenology. Annex B illustrates the dynamics of this process using frames extracted from the films. Trace overlays of the detonation products cloud are also presented for six of the nine series 2 shots. The time evolution of the height and width of the clouds are listed in Table V and plotted in Figures 16a and 16b. Recall that the time resolution of the high-speed film is about 100 μsec, which is coarse relative to the time scale of the chemical reactions, but appropriate to describe the expansion of the detonation products.

In general, the vertical velocity of the cloud is maximum at its early stages, and slows down with time. The initial cloud vertical velocity is estimated for each DoB by fitting a quadratic through the data and taking the initial slope. For a flush buried charge, the initial vertical and lateral expansion rates are about 2660 m/sec and 1300 m/sec, respectively. They remain very strong right across the field of view of the camera for the time period considered. The event is also very bright, indicating intense burning of the hot combustion products long after the initial detonation wave has travelled through the explosive. The strong rate of expansion makes it possible for the hot, unburned products to mix with fresh oxygen to sustain the combustion process. Jetting is also apparent, thereby indicating that a lot of turbulent mixing takes place at the interface between the products and the air. The cloud turns dark, starting near the surface and moving upwards, as the combustion gets quenched. This observation may be used in code validation to correlate with temperature.

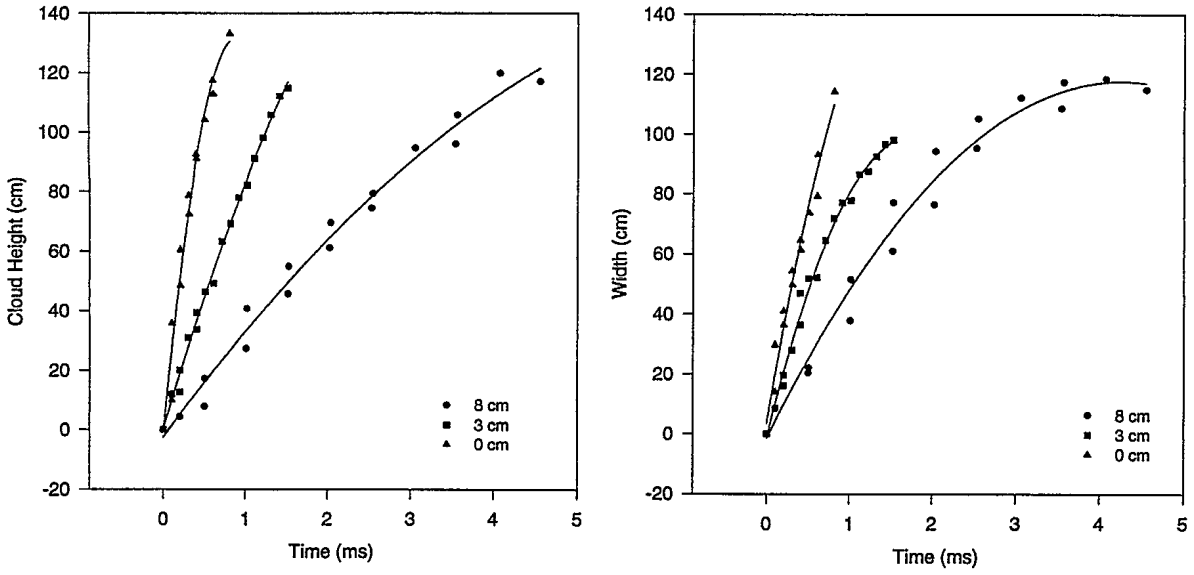

Figure 16. Time growth of maximum height and width of the cloud of detonation products.

The sand overburden slows down the expansion rate and chemistry of the detonation products. The first observation from the high-speed films is the appearance of a "milky" region at the surface above the explosive. This is likely caused by a dilute suspension of sand particles when the initial compression wave arrives at the surface, phenomenon also observed in underwater explosions. The products then continue to push on the sand material as described in the previous section. The push appears to be quite uniform at first, which generates a uniform semi-hemispherical bubble of sand. However, density of the soil cap thins out rapidly and the detonation products are seen to "burst" through the top of the bubble, which marks the beginning of the cloud expansion process.

Table V. Time growth of maximum height and width of the detonation products cloud.

Shot #	DoB (cm)	Time (ms)	Width (cm)	Height (cm)
12	8	0.2035	16.12	4.2
		0.5087	22.08	17.17
		1.0173	51.51	40.65
		1.5260	77.09	54.66
		2.0347	94.26	69.38
		2.5434	105.12	79.19
		3.0520	112.13	94.61
		3.5607	117.38	105.82
		4.0694	118.44	119.84
14	8	0.5052	20.32	7.71
		1.0104	37.84	27.33
		1.5156	60.97	45.55
		2.0209	76.39	60.97
		2.5261	95.31	74.28
		3.5365	108.62	96.01
		4.5469	114.93	117.03
16	3	0.1014	8.41	11.91
		0.2028	19.62	19.97
		0.3042	28.03	30.84
		0.4056	46.95	39.24
		0.5070	51.86	46.25
		0.7097	64.47	63.07
		0.9125	77.09	77.79
		1.1153	86.55	91.10
		1.3181	92.51	105.82
		1.5209	98.11	114.93
17	3	0.2030	16.12	12.61
		0.4060	36.44	33.64
		0.6090	52.21	49.06
		0.8120	71.83	69.03
		1.0150	77.79	81.99
		1.2180	87.60	98.11
		1.4210	96.71	112.13
19	0	0.1015	29.78	35.74
		0.2031	41.00	60.27
		0.3046	54.31	78.49
		0.4061	64.47	92.51
		0.6092	79.19	117.38
		0.8123	114.23	133.15
20	0	0.1024	14.02	9.81
		0.2048	36.44	48.36
		0.3072	49.76	72.18
		0.4096	61.32	91.10
		0.5120	73.58	104.07
		0.6144	93.21	112.83

It is clear from the photographic records that the overburden quenches the combustion, thereby resulting in dark clouds. However, it is also apparent that the extent of quenching depends on the thickness of the overburden. For the 3-cm overburden case, an orange glow can be seen through the upper portion of the cloud. It is speculated that combustion is sustained within the core of the cloud where the detonation products are still hot enough to react with fresh air. The external portion has probably cooled off too much to react chemically. Overhead cinematography is required to confirm or infirm this fact. For the 8-cm overburden case, the cloud is very dark, which may be linked to the fact that the hot products are trapped in the soil much longer than in the other cases. This allows more cooling of the products before they have an opportunity to mix with fresh air.

Soil overburden combined with quenching of the combustion influence the cloud expansion rate. The general trend is that a greater overburden results in slower expansion rates. For the 3-cm case, the initial vertical and lateral expansion rates are about 940 m/s and 1200 m/sec, respectively. The corresponding expansion rates for the 8-cm overburden case are 400 m/s and 590 m/sec.

3.3 Late Ejecta Flow

The early motion of the soil surface and "blow off" of the soil cap above the explosive were described above. Long after these events, significant soil motion continues. The net effect can be seen on flash x-rays (see Annex A, flush buried and 3-cm cases) and on the high-speed films. A time sequence overlay depicts the motion in Annex B. As the in-soil compression wave propagates in the radial direction, it causes the soil surface to swell. Further back towards the centre, soil particles are entrained due to the venting of the detonation product gases. These particles move along curved paths due to the combination of upward thrust and rapid radial acceleration of the hot gases.

Two measures of ejecta flow are used here to describe this phenomenon: the time variation of the minimum visible outer diameter, or neck of the crater, and the nominal flow angle of the sand particles after their acceleration phase is [nearly] over. The results are listed in Table VI and depicted in Figure 17. The crater diameter data may be used to estimate the amount of material expelled with time if a crater shape is assumed.

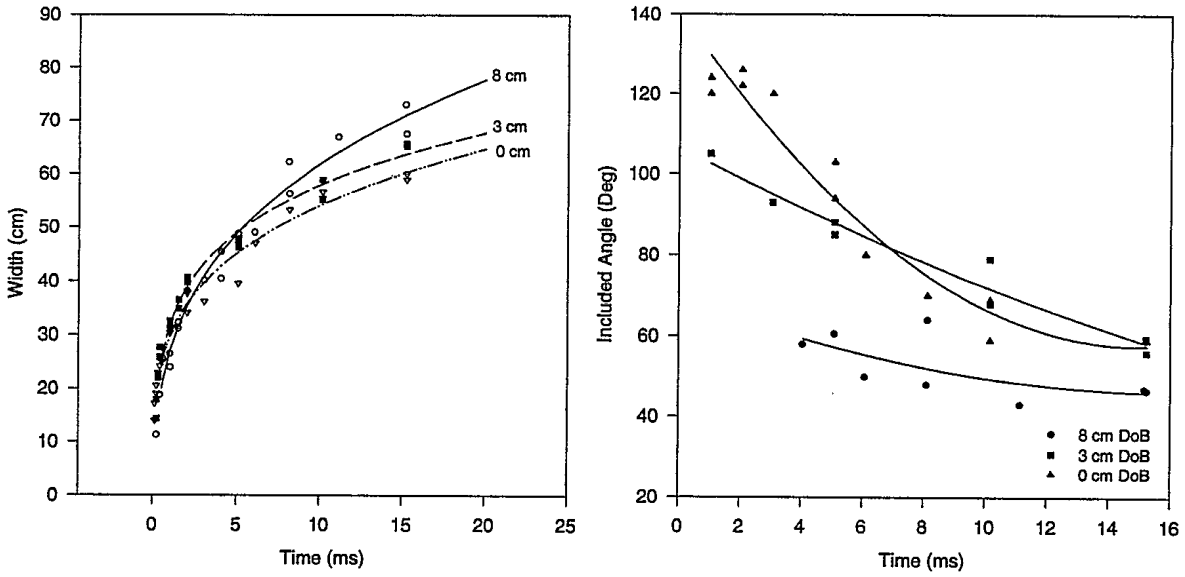

Figure 17. Minimum outer width and nominal included angle of the ejecta zone.

The nominal angle at which ejecta flows after it has undergone radial acceleration may be related to momentum, a vector quantity. It is apparent from Figure 17b that DoB plays an important role. The total included flow angle for the ejecta reaches a maximum of 126° for the flush buried case, 105° for the 3-cm overburden case and 64° for the 8-cm overburden case. Note that these values are strictly valid for loose dry silica sand and they are expected to change considerably as a function of soil type and compaction (or cohesion). In all cases, the included flow angle reduced with time, to values between 47° for the 8-cm overburden case, and 59° for the flush buried case. It is unclear how much influence the container dimensions had on the final flow angles.

Table VI. Summary of craters' minimum outer width and included angle of ejecta zone.

Shot no. 12 - 8 cm DoB			Shot no. 14 - 8 cm DoB		
Time (ms)	Width (cm)	Angle (deg)	Time (ms)	Width (cm)	Angle (deg)
0.203	11.3		1.010	26.4	
0.406	18.8		1.516	32.3	
0.609	24.0		2.021	38.1	
1.015	25.5		4.042	40.4	58
1.523	31.1		6.063	48.9	50
2.030	37.9		8.083	62.2	48
3.045	40.1		11.115	66.9	43
4.060	45.4		15.157	73.1	47
5.075	48.8	60.5			
8.120	56.3	64			
15.225	67.5	46.5			
Shot no. 16 - 3 cm DoB			Shot no. 17 - 3 cm DoB		
Time (ms)	Width (cm)	Angle (deg)	Time (ms)	Width (cm)	Angle (deg)
0.203	14.3		0.203	17.9	
0.304	22.0		0.305	22.4	
0.406	25.8		0.406	27.7	
1.014	31.4		1.015	32.6	105
1.521	34.9		1.523	36.4	
2.028	39.8		2.030	40.6	
3.042	-	93	5.075	46.2	88
5.069	47.5	85	10.150	58.8	68
10.139	55.1	79	15.225	65.1	56
15.209	65.6	59.5			
Shot no. 18 - 0 cm DoB			Shot no. 19 - 0 cm DoB		
Time (ms)	Width (cm)	Angle (deg)	Time (ms)	Width (cm)	Angle (deg)
0.102	13.9		0.101	17.1	
0.203	19.1		0.203	20.6	
0.406	24.2		0.305	22.9	
0.609	27.3		0.508	25.0	
1.015	30.4	120	1.015	31.2	124
2.031	34.1	122	2.031	37.7	126
3.046	36.1	120	5.077	47.9	94
5.077	39.5	103	10.154	55.5	69
6.092	47.1	80	15.231	58.9	59
8.123	53.2	70			
10.154	56.6	59			
15.231	60.0	59			

3.4 Wave Propagation Speed in Soil

Soil data was obtained only for Series 2. The corresponding time traces from the CRGs are shown in Annex C. The important data, i.e., time of arrival, peak pressure and positive phase impulse is summarised in Table VII. The time of arrival data is also presented graphically in Figure 18 along with the Dynasen ToA shorting pin data. The CRGs have a finite response time associated with their larger physical size and the offset between their top surface and the carbon resistor at their centre. The time delay increases from about 6 μsec to 11 μsec as the distance from the explosive increases. This also bears a direct relationship to the decrease of shock propagation speed with distance.

The distance from the bottom of the explosive charge to the centre of the gauges varied from 6.23 to 13.73 cm. The time of arrival data ranges from roughly 50 μsec to 185 μsec. The ground shock velocity is estimated from the slope of a curve fit through the data. It is seen that the shock is initially overdriven and slows down rapidly, as shown the velocity drops from 760 m/s down to 230 m/s over the range measured. The limited range over which measurements were taken does not yield where and when the shock reached its final sonic velocity.

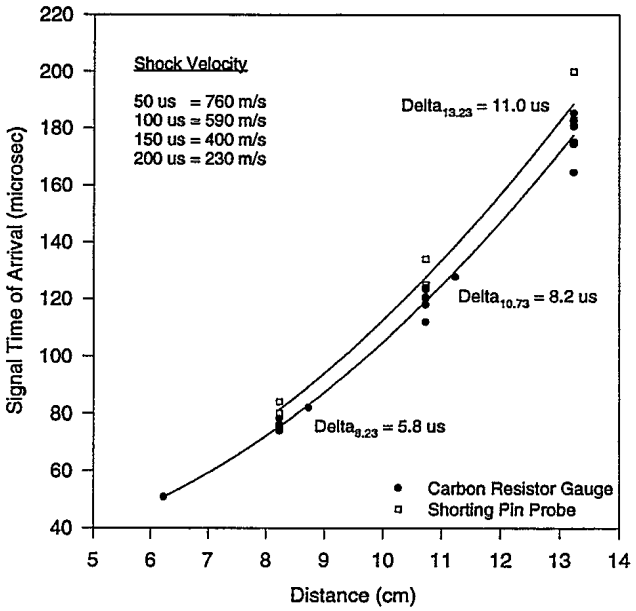

Figure 18. Wave propagation speed in soil.

3.5 Shock Pressure and Impulse in Soil

The CRG data for the in-soil pressure is presented in Annex C along with its time integral, i.e., impulse. The most important information is tabulated in Table VII while pressure and impulse are plotted in Figure 19.

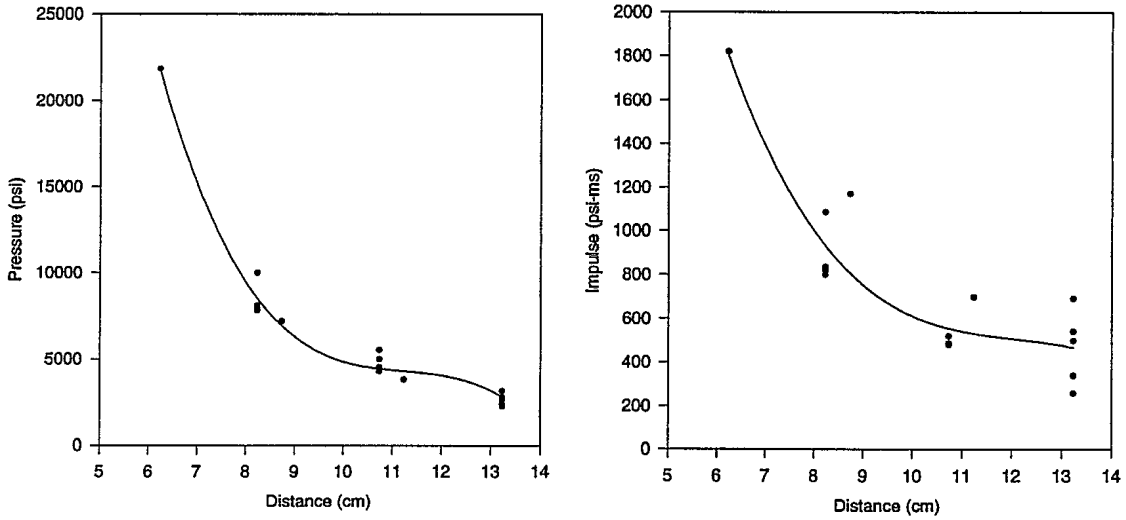

Figure 19. In-soil pressure and impulse data from CRG gauges.

Table VII. Summary of in-soil pressure measurements for Series 2.

Shot ID	DoB (cm)	Standoff to charge (cm)			Time of Arrival (μs)			Peak pressure (psi)			Impulse (psi-ms)		
		P6	P7	P8	P6	P7	P8	P6	P7	P8	P6	P7	P8
12	8	8.73	10.23	13.73	76.3	117.9	174.4	7814	5543	3182	829	676	539
13	8	8.73	10.23	13.73	73.8	120.8	181.2	8124	5003	2809	835	710	691
14[1]	8	6.23	8.73	11.23	50.8	82.1	127.9	21818	7182	3850	1819	1169	697
15	3	8.73	10.23	13.73	78.3	119.9	185.3	8031	4457	2429	1084	477	258
16[2]	3	8.73	10.23	13.73	-	123.3	-	3067	1651	1272	237	154	-
17	3	8.73	10.23	13.73	76.2	120.1	164.5	7895	4558	2669	797	517	497
18[2]	0	8.73	10.23	13.73	74.2	124.0	182.6	3024	1900	1771	568	-	273
19	0	8.73	10.23	13.73	74.9	111.9	175.3	9985	4284	2315	816	478	337
20[3]	0	8.73	10.23	13.73	75.3	118.2	180.7	5853	3373	2058	-	485	418

[1] Reduced distances between charge and gauges

[2] Serious EM interference to gauges – data suspect

[3] Gauge destroyed before full signal captured

The scatter of the data for pressure is relatively small, particularly when compared to the impulse data. However, it can be surmised from the trend lines that peak pressure at least, if not also impulse, drop by roughly an order of magnitude over the short range of our measurements. This may be related to the physical observations made after each experiment. Typically, the top gauge sustained substantial mechanical and thermal damage, thereby indicating that it was at least within the plastic zone, and more likely in the hydrodynamic zone. The location of this transducer was normally exposed after the experiment and a layer of carbon was left over from the detonation products. Hence, this transducer saw a combination of soil motion and high thermal load. The transducer furthest away (7.5 cm lower) would typically "look" intact, hence it was either in the elastic or plastic zone. Damage to the central transducer was anywhere from light to heavy. This data and the corresponding observations may be used to correlate with computer code outputs.

3.6 Wave Propagation Speed in Air

The gas phase pressure traces are reproduced in Annex C. The important data, i.e., time of arrival, peak pressure and positive phase impulse, is summarised in Tables VIII and IX for Series 1 and 2, respectively. Figure 20 compares the time of arrival data for Series 1 and 2. The method of initiation had little effect on the wave propagation speed through air. However, DoB has a strong influence as indicated by the distinct spacing and different average slope of the three curves. Curvature is also important. It shows that deceleration of the shock front is most important for the flush buried charges while it is almost negligible for the 8-cm DoB case. The propagation speed of the shock, estimated from the slope of each curve fit, yields initial speeds of 440, 1200 and 3730 m/s for the 8-cm, 3-cm and flush buried cases, respectively. These speeds reduce to 380, 390 and 440 m/s over the 160-cm distance between the bottom and top transducers. The time delay associated with the shock travel through the overburden is also apparent from the intercept of the three curves with the y-axis.

The air shock propagation speed is coupled to the expansion of the detonation products. The latter act as a piston and the air shock runs ahead of it. However, the recording methods used in the present experiments, namely high-speed film with a time resolution of 100 μsec and electronic pressure transducers with a time resolution of 2-3 μsec, do not permit the accurate resolution of the spacing between the air shock and the front of the detonation products.

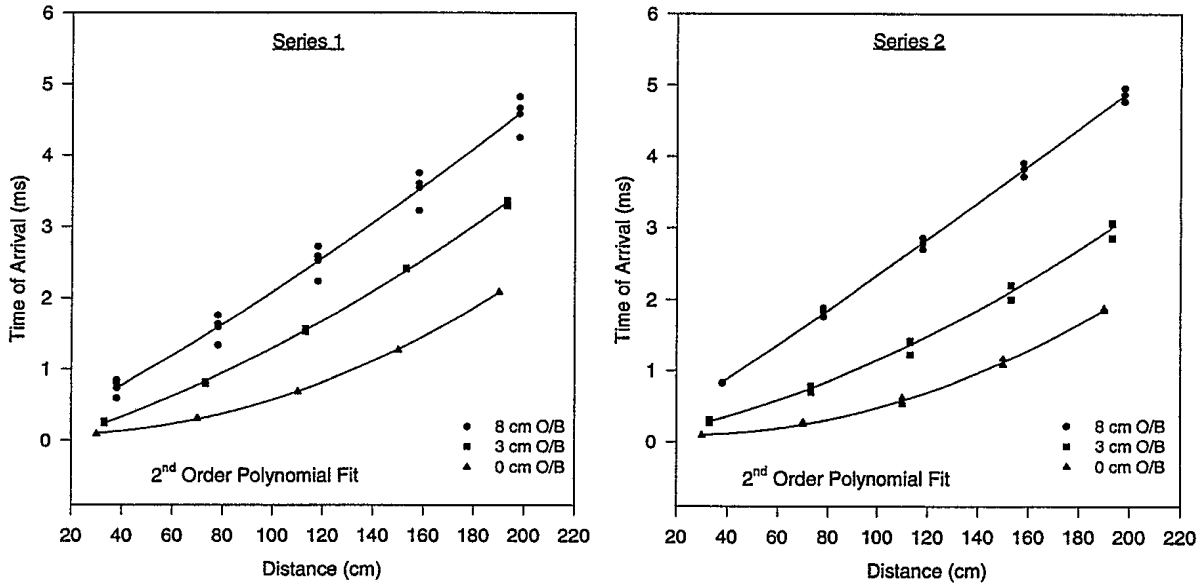

Figure 20. Time of Arrival of air shock for Series 1 and 2.

Table VIII. Summary of air shock results for test Series 1.

Shot	DoB	Standoff - charge top/gauge (cm)					Time of Arrival (ms)					Peak Pressure (psi)					Positive Phase Impulse (psi-ms)				
ID	(cm)	P1	P2	P3	P4	P5	P1	P2	P3	P4	P5	P1	P2	P3	P4	P5	P1	P2	P3	P4	P5
1	8	38	78	118	158	198	0.84	1.76	2.72	3.75	4.82	20.5	11.5	5.39	4.45	2.73	7.93	5.64	3.80	2.57	2.02
2	8	38	78	118	158	198	0.74	1.59	2.52	3.54	4.58	43.0	11.8	7.75	5.52	3.33	11.0	6.39	4.40	2.92	2.33
3	8	38	78	118	158	198	0.59	1.34	2.23	3.22	4.25	39.3	15.4	9.95	6.53	3.52	9.07	5.78	4.96	3.06	2.35
4	3	33	73	113	153	193	0.27	0.82	1.57	2.42	3.29	101	30.5	18.9	18.7	11.3	9.83	6.71	6.90	5.66	4.90
5	3	33	73	113	153	193	0.24	0.81	1.53	2.41	3.32	60.1	30.1	18.5	13.3	10.5	8.91	8.94	6.61	5.41	4.92
6	3	33	73	113	153	193	0.24	0.80	1.53	2.41	3.36	76.1	33.9	20.9	12.9	9.93	9.48	6.90	6.68	5.61	4.99
8	8	38	78	118	158	198	0.80	1.64	2.58	3.60	4.66	27.8	11.9	8.62	5.47	3.07	10.82	6.11	4.24	2.86	2.28
10	0	30	70	110	150	190	0.094	0.317	0.682	1.27	2.09	316	106	63.0	25.5	11.2	13.37	14.1	9.59	7.24	5.98
11	0	30	70	110	150	190	-	0.307	0.696	1.28	2.09	-	98.7	59.8	24.7	13.4	-	18.04	8.77	7.67	6.15

No data available for shots no. 7 and no. 9 due to a misfire and a recorder malfunction, respectively. No trigger on P1 for Shot # 11.

Table IX. Summary of air shock results for test Series 2.

Shot	DoB	Standoff - charge to gauge (cm)					Time of Arrival (ms)					Peak Pressure (psi)					Positive Phase Impulse (psi-ms)				
ID	(cm)	P1	P2	P3	P4	P5	P1	P2	P3	P4	P5	P1	P2	P3	P4	P5	P1	P2	P3	P4	P5
12	8	38	78	118	158	198	0.83	1.76	2.70	3.72	4.77	19.5	13.9	7.31	5.40	3.28	-	-	4.75	3.53	2.57
13	8	38	78	118	158	198	0.83	1.83	2.79	3.82	4.87	23.5	10.3	6.58	5.00	3.13	-	6.56	4.59	3.34	2.43
14	8	38	78	118	158	198	0.83	1.88	2.86	3.90	4.96	20.9	9.30	5.89	4.40	2.59	-	7.96	4.36	3.02	2.11
15	3	33	73	113	153	193	0.27	0.70	1.23	2.01	2.86	201	68.0	28.2	22.7	14.5	25.5	-	7.88	6.31	4.71
16	3	33	73	113	153	193	0.31	0.79	1.42	2.20	3.07	313	53.4	29.2	18.4	13.1	23.7	9.51	7.61	6.01	4.76
17	3	33	73	113	153	193	-	0.78	1.41	2.20	3.06	-	48.2	28.2	18.4	11.7	-	9.30	7.34	5.97	4.70
18	0	30	70	110	150	190	0.090	0.273	0.626	1.17	1.87	627	246	90.0	48.2	22.5	14.15	18.29	13.98	9.20	7.00
19	0	30	70	110	150	190	0.102	0.254	0.533	1.09	1.88	398	210	95.4	33.8	20.0	12.05	18.24	13.35	8.65	6.80
20	0	30	70	110	150	190	0.093	0.277	0.566	1.08	1.85	286	202	163	41.2	17.9	10.25	16.05	13.45	8.47	6.70

For Shot nos. 12 to 17, several signal spikes/drops on P1 and P2 make questionable the integration of pressure trace to get impulse.

3.7 Shock Pressure and Impulse in Air

The complete air pressure records for Series 1 and 2 are presented in Annex C. A close examination of this data led the authors to believe that three mechanisms affect the pressure-time histories. They are DoB, the method of initiation of the detonation and the presence of early venting. During series 1, a fourth mechanism was also at work because a second RP-83 detonator was used as a time zero visual cue for the high-speed films. This RP-83, located on the side of the tank 10 to 15 cm below the rim, contains 1 gram of RDX-type explosive that generates an air blast of its own, which contaminates the primary signal generated by the charge buried in the sand. Had there been a direct line-of-sight between the second RP-83 and the pressure transducers, it would have generated an overpressure of approximately 4 psi at the first transducer. This level of contamination is significant for the 8-cm cases, less so for the 3-cm cases and insignificant for the flush-buried charges. The second RP-83 was replaced by a regular flash bulb for series 2.

Examination of the pressure traces in Annex C reveals that the pressure data is of generally good quality. The only exception, aside possible contamination by the secondary RP-83 detonators during series 1, is for the P1 position on the 8-cm shots for series 2, an example of which is shown in Figure 21 below. There are strong pressure spikes on the P1 traces. It could not be determined whether these are caused by a real physical phenomenon, by a transducer malfunction, or by a poor electrical connection. However, these spikes were not present during series 1 and the general magnitude of the signals was in the 20-40 psi range despite early venting of the detonation products. The portion of "clean" signal prior to the spikes is sufficiently long to allow us to extract peak pressure, but the spikes corrupt the integration of the signal and the impulse data for the three series 2 8-cm shots could not be used. The reader should also note that signal drop occurred on P2 for shot # 12.

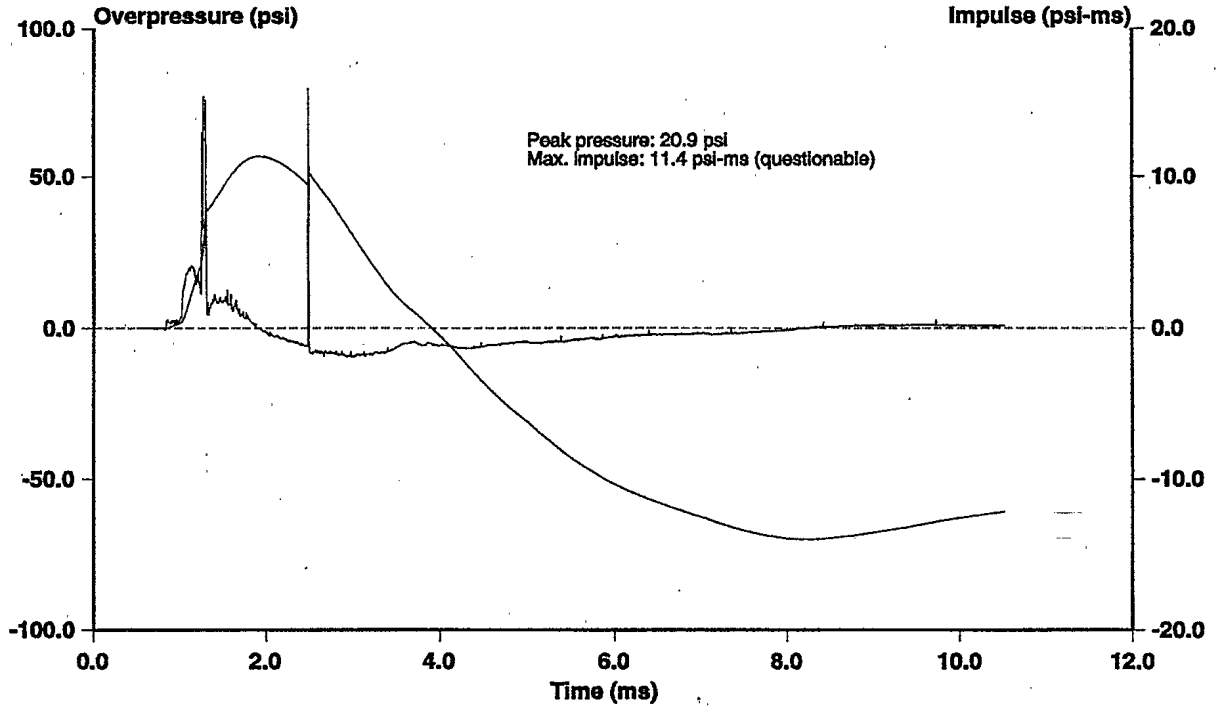

Figure 21. Sample pressure trace for an 8-cm DoB shot.

Side-on peak pressure for the series 1 and 2 tests is plotted in Figure 22 and the corresponding values of impulse are presented in Figure 23. It is apparent that substantial scatter of the data exists, particularly at P1. Note that integration of the data has a mild smoothing effect, but the scatter remains significant. In general, there is more scatter for the flush-buried case and it decreases as DoB increases. This may be due to jetting and the high level of turbulence associated with the detonation of flush-buried explosives. Scatter also reduces strongly as a function of distance from the charge. For the flush-buried case of series 2, this is demonstrated from the percent variation of peak pressure computed as the difference between the largest and smallest peak pressure values at a given location, divided by the average at that same location. Using this measure of scatter, the variation 78% at P1 and reduces to 23% at P5. The same trend is observed for other DoB values. The reader should be aware, though, that the use of statistics using very small samples (3 shots in this case) could be dangerous. Such statistics are subject to large uncertainties, but they are nevertheless useful to point out data trends.

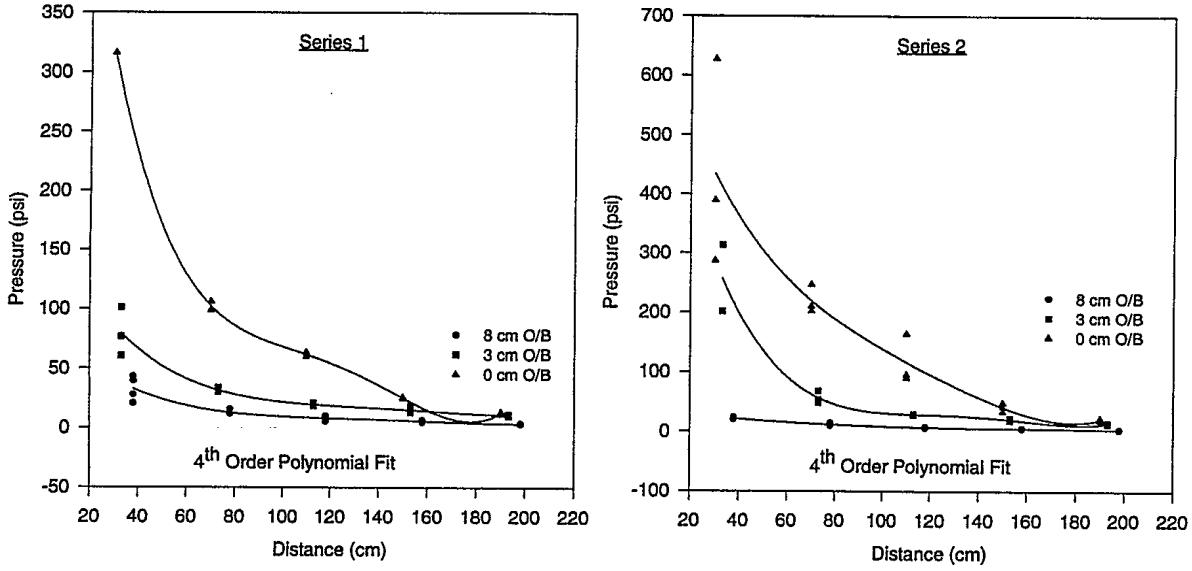

Figure 22. Side-on peak pressure of air shock for Series 1 and 2.

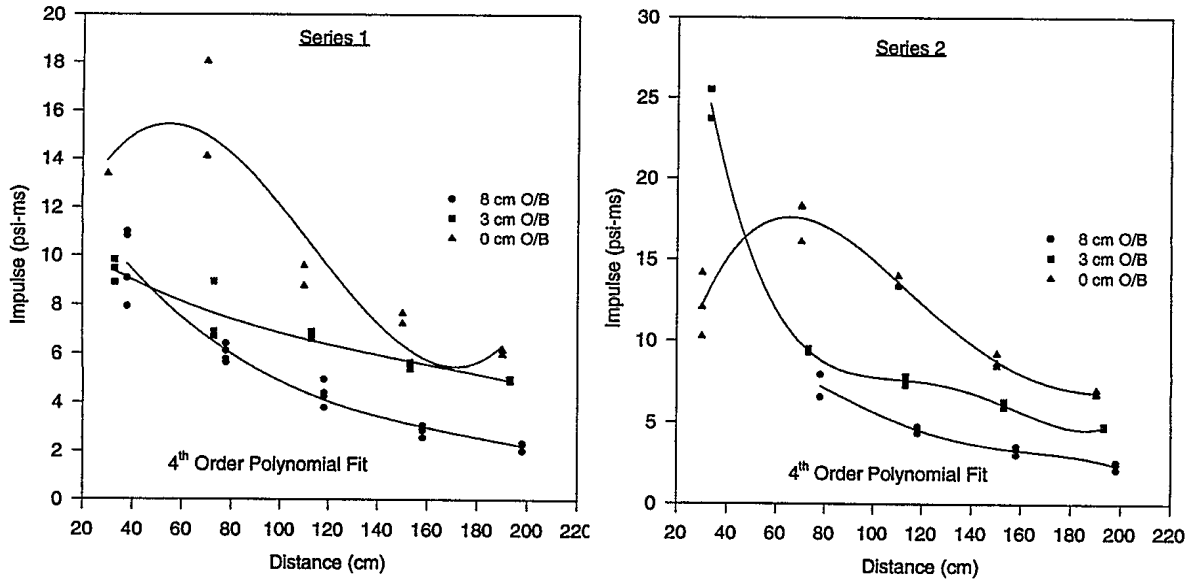

Figure 23. Side-on impulse of air shock for Series 1 and 2.

The average values for peak pressures and impulses are listed in Tables X and XI, respectively. One obvious trend for peak pressure is that it decreases with distance. The dependency on distance is well documented in the literature[19] as reflected by the various scaling laws. In general, peak pressure is plotted at a function of the distance scaled by the cube root of the explosive energy. Curve fits with 2nd or 3rd order polynomials are then often used to give a relationship between peak pressure and distance, irrespective of the geometry and chemistry of the explosive source. These empirical relationships are also valid only for the "far-field" where distance plays a smoothing role. Similar relationships are published for time-of-arrival, impulse and positive phase duration. It should also be pointed out that for the flush-buried case, impulse increases from P1 to P2, and decreases afterwards. The integration process brings out this phenomenon, also well documented in the literature. Peak pressure decreases with distance but duration increases. The net effect is that the area under the pressure curve increases over a short distance near the explosion source. This is linked to the coalescence of multiple shocks near the explosive source as waves bounce back and forth between the centre of the explosion and the outer limit of the fire ball.

Table X. Average side-on peak pressure for series 1 and 2.

DoB	Series	P1	P2	P3	P4	P5
8	1	32.6	12.6	7.92	5.49	3.16
	2	21.3	11.2	6.59	4.93	3.00
3	1	79.1	31.5	19.4	14.9	10.6
	2	257	56.5	28.5	19.8	13.1
0	1	316	102	61.4	25.1	12.3
	2	437	219	116	41.1	20.1

Table XI. Average side-on impulse for series 1 and 2.

DoB	Series	P1	P2	P3	P4	P5
8	1	9.71	5.98	4.35	2.85	2.25
	2	-	7.26	4.57	3.30	2.37
3	1	9.41	7.52	6.73	5.56	4.94
	2	24.6(?)	9.40	7.61	6.10	4.72
0	1	13.37	16.07	9.18	7.45	6.06
	2	12.15	17.53	13.59	8.77	6.83

In the present case, it is also evident that soil plays a very important role. The trend observed is that side-on peak pressure and impulse decrease with DoB. As the charge is buried deeper, more of the explosive energy goes into compaction of the particle bed and creation of ejecta. As a result, there is less energy for the air blast, as reflected by the current results. The reader should note however, that side-on pressure accounts only for part of the overall energy. From anecdotal mine strike stories, it is known that some combinations of soil and DoB increase the lethality of a mine. The present authors believe that a substantial amount of the explosive energy is transferred in dynamic pressure, and that the soil focuses this flow of energy in the upward direction. Additionally, a portion of the explosive

energy goes into ejecta momentum. These forms of energy are of great importance to the mine output problem and should be measured in future experiments of this type, keeping in mind that what matters is the amount and forms of energy deposited on the target. On the same note, the reader is reminded that the goal of present experiments is to produce a data package for code validation, not to fully characterise mine output.

When comparing the average values of peak pressure and impulse for series 1 and 2, Tables X and XI point to another interesting phenomenon. Neglecting the peak pressure values for the 8-cm case, which we will address later, peak pressure and impulse is almost always larger for series 2. This is caused by the directionality of the detonation wave due to how the explosion was initiated. During series 1, the initial detonation wave propagated downward and radially outward within the explosive. During series 2, bottom initiation resulted in the initial detonation wave propagating principally upward. Hence, the second method of initiation results in a stronger air shock passing by the transducers. The only exception is peak pressure for the 8-cm DoB. For this case, the series 1 values are consistently higher than those for series 2. This is attributed to the early venting of the overburden caused by the method of initiation of the detonation. Early venting meant that less soil was in the way of the expanding gases thereby resulting in a less pressure attenuation. Closer examination of the pressure traces for position P1 also reveals that the shock fronts were sharp for series 1 while pressure increased more gradually for series 2. Hence, well-formed shock existed during series 1 while the overburden caused the latter to decay to multiple compression waves during series 2. This is consistent with a model that shows multiple mini-shock fronts venting through the solid particles of the soil cap.

3.8 Crater Dimensions

The average crater dimensions, if one can refer to the displaced volume of sand in our experiments as such, were measured after each experiment. The nominal volume of ejecta increased with DoB as depicted in Figure 24 for each depth of burial (measured to the bottom of the charge). Recall that the silica sand used for the current experiments was dry and "flowed" like a liquid. Hence soil cohesion was almost nil. The crater shapes obtained would have been very different if the experiments had been carried out in another soil medium. Nevertheless, with the geometry provided, the amount of material ejected may be computed and used in computer code validation.

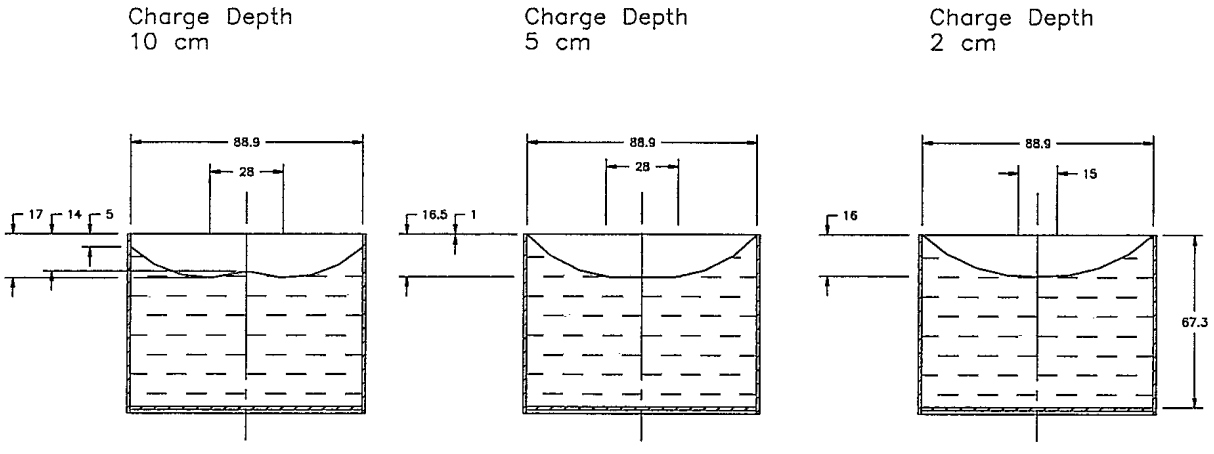

Figure 24. Nominal shape of craters for each DoB.

4. Conclusions and Recommendations

This work was undertaken to (i) further the understanding of the physics governing the detonation of a land mine, and (ii) to generate a high-quality data set suitable for use in the validation of computer codes. This report goes a long way towards achieving these goals. The following conclusions are drawn from our results:

- Tight control of the experimental geometry and procedures must be maintained to insure data quality for this type of experiment. Even with this control, the physical processes taking place in the near field of an explosion are highly stochastic and lead to a large variance of the results. These variances varied between 20% and 80% in the present case due to the small number of repetitions done for each setup.
- The use of x-ray and high-speed film methods for this type of experiment yield the majority of the information necessary to understand the physics occurring in the near-field of a mine explosion. The pressure measurements help to quantify the process.
- These experiments provide sufficient information to allow for the basic calibration of a multi-phase CFD model for loose dry silica sand. This is a first step in the development of CFD predictive tools.
- Controls of the explosive charge geometry, the location of the initiation point and the size of detonator are all important. Use of a plastic explosive such as C4 makes economic sense, however, it is required to use a container to maintain the geometry constant. A low initiation point is preferred as it results in greater velocity of the early soil motion, as well as in higher side-on overpressure and impulse values. Finally, a poor choice of detonator, such as the RP-83 versus the RP-2, affects the repeatability and consistency of the results.
- The detonation of a buried mine generates a bubble of hot gas that causes the soil cap to deform, break down and be ejected. The initial ejection velocity depends on the soil overburden. In general, the ejection speed decreases with increasing depth of burial. Eventually, the hot gas breaks through and overtakes the soil cap.
- Soil overburden has a strong influence on the expansion rate of the detonation products. The expansion rate slows down substantially as the thickness of the overburden increases. Additionally, continued combustion occurs when the charge is buried flush with the ground or lightly buried. It is quenched when the charge is buried deeper.
- The early flow of soil ejecta is more vertical as the charge is buried deeper. It is speculated that this is due to greater confinement of the hot gas.
- The in-soil wave propagation is overdriven near the explosive source, but decelerates rapidly within 2 charge diameters for the soil conditions used in these experiments.
- In-soil pressure and impulse drop rapidly, within 2 charge diameters, as the shock propagates away from the centre of the explosion.
- Propagation of the air shock is strongly influenced by the thickness of the soil overburden. The greatest propagation speeds, in the order of km/sec, are obtained when the charge is buried flush to the soil surface.
- Side-on peak pressure and shock rise time decrease sharply as depth of burial is increased. For the flush buried charges, the impulse curves display the characteristic dip near the explosive charge, as observed in air explosions.

As with any research project, one learns as events unfold and the data comes in. During this project, it became clear that some important information is missing from the data set. Hence, for future experiments, it is recommended that:

- New experiments be carried out to investigate the effect of other soil types for variables such as particle size, bulk density, compaction, water content and cohesion. This large number of variables makes it impractical to investigate all possible combinations, however, two or three combinations should be selected to bracket a wide range of conditions encountered in real life situations. Possibilities include gravel, silty sand and clay. Fully dry and water saturated conditions should be investigated.
- New experiments be planned to investigate the effect of the explosive mass and chemical composition. For example, it is known that the fuel-to-oxidiser ratio varies from one explosive to another. It is possible that this factor plays a significant role on target loads in the near field.
- A vertical camera position, directly above the charge, should be used to determine the processes in the cloud of expanding detonation products.
- More in-soil pressure transducers need to be used to establish the final wave propagation velocity in the soil medium. It is suggested to locate these new transducers near the bottom of the soil container in future experiments.

References

1. Anonymous, "Mine Clearance Operations Evaluation Study", J3 Engineers, Directorate of Military Engineers, National Defence Headquarters, Ottawa, Canada, 1996.
2. Bangash, M.Y.H., *Impact and Explosion - Analysis and Design*, CRC Press, Boca Raton, Florida, USA, 1993.
3. Drake, J.L., and Little, C.D., "Ground Shock from Penetrating Conventional Weapons", Presented to the Symposium on the Interaction of Non-Nuclear Munitions with Structures, Colorado Springs, Colorado, USA, 1983.
4. Prakash, S., *Soil Dynamics*, McGraw-Hill Book Company, New York, USA, 1981.
5. Shukla, A., and Prakash, V., "Wave Propagation in a Porous Media as a Function of Fluid Saturation", Proceedings of the Society for Experimental Mechanics, Vol. XLVII, Portland, Oregon, USA, pp. 80-87, 1988.
6. Veyara, G.E., "Uniaxial Stress-Strain Behaviour of Unsaturated Soils at High Strain Rates," US Air Force Report WL-TR-93-3523, Wright Laboratory, Tyndall AFB, Florida, USA, 1992.
7. Woods, R.D., "Screening of Surface Waves in Soils", *Journal of Soil Mechanics and Foundation Engineering*, ASCE, Vol. 94, No. SM4, pp. 951-979, 1968.
8. Lamb, H., "On the Propagation of Tremors over the Surface of an Elastic Solid", Philos. Trans. R.S., London, England, Ser. A, Vol. 203, pp. 1-42, 1904.
9. Johnson, S.M., "Explosive Excavation Technology", NCG Technical Report No. 21, U.S. Army Engineer Nuclear Cratering Group, Livermore, California, 1971.
10. Unruh, J.F., Scheidt, D.C. and Pomerening, D.J., "Data Analysis of Scale Model Armored Vehicle Response to Ballistic Impulses", Volume 1, contract report no. 13112 for U.S. Army TACOM Research and Development Center, 1985.
11. Westine, P.S., Morris, B.L., Cox, P.A. and Polch, E.Z., "Development of Computer Program for Floor Plate Response from Land Mine Explosions", contract report no. 13045 for U.S. Army TACOM Research and Development Center, 1985.
12. Morris, B.L., "Analysis of Improved Crew Survivability in Light Vehicles Subjected to Mine Blast", Final report for contract no. DAAK70-92-C-0058 for the U.S. Army Belvoir RDEC, Ft. Belvoir, Virginia, 1993.
13. Anonymous, "Structures to Resist the Effects of Accidental Explosions", TM5-1300, AD-A243 272, Departments of the Army, Navy and Air Force, 1990.
14. Morris, B.L., Westine, P.S. and Wauters, D.K., "Determination of Blast Response of Armored Vehicle Track and Wheel Systems", contract report no. 12913 for U.S. Army TACOM Research and Development Center, 1984.
15. Haskell, D.F., "Deformation and Fracture of Tank Bottom Hull Plates Subjected to Mine Blast", BRL report No. 1587, 1972.
16. Reichenbach, H., Behrens, K. and Kuhl, A.L., "Airblast Environments from buried HE Charges", Ernst-Mach-Institut, E 1/93, 1993.

17. Ginsberg, M.J., and Asay, B.W., "Commercial carbon Composition Resistors as Dynamic Stress Gauges in difficult Environments:, Review of Scientific Instruments, Vol. 62, No. 9, pp. 2218-2227, 1991.

18. Austing, J.L., et. al., "Carbon Resistor Gauges for Measuring Shock and Detonation Pressures, III. Revised Calibration Data and Relationships", Propellants, Explosives and Pyrotechniques, Vol. 20, pp. 159-169, 1995.

19. Baker, W.E., *Explosions in Air*, University of Texas Press, Austin and London, 1973.

ANNEX A

Individual X-Ray Exposures

Table of Contents

Series 1 - 100 g C-4 Top Initiated by RP 83 Detonators

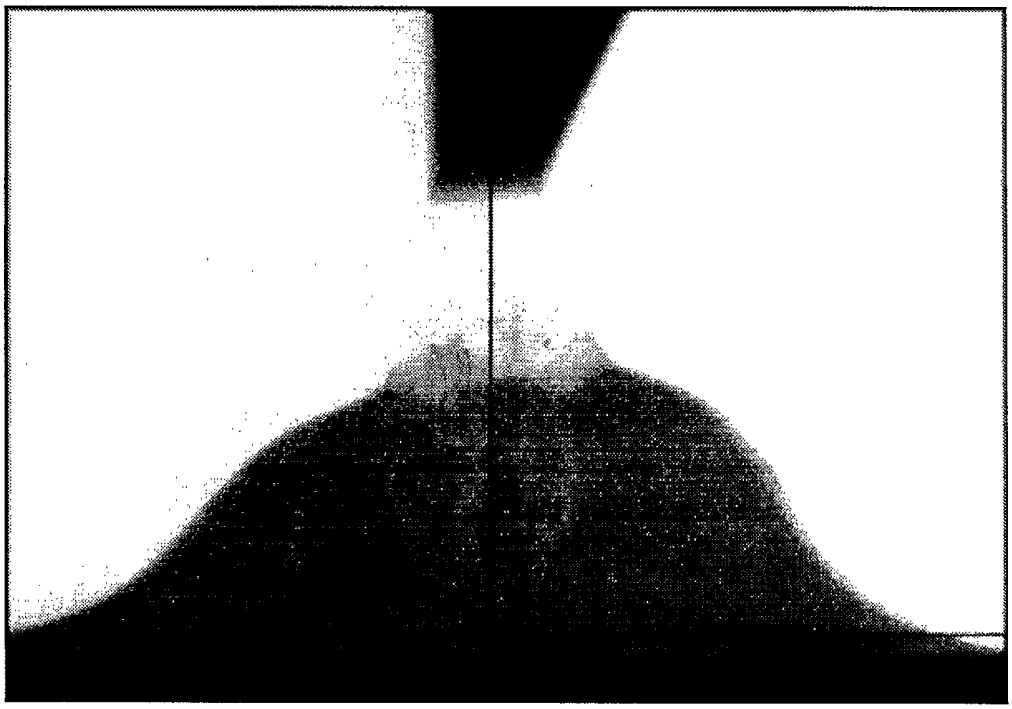

Shot 2-1 450.8 μs 8 cm DOB

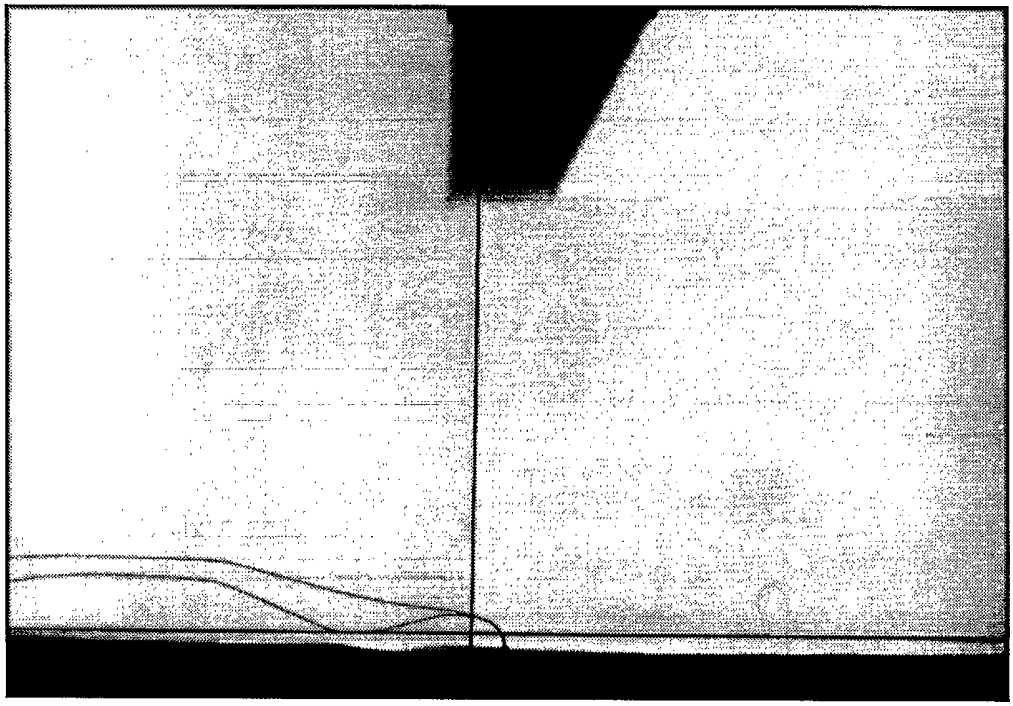

Shot 2-2. 55.9 μs 8 cm DOB

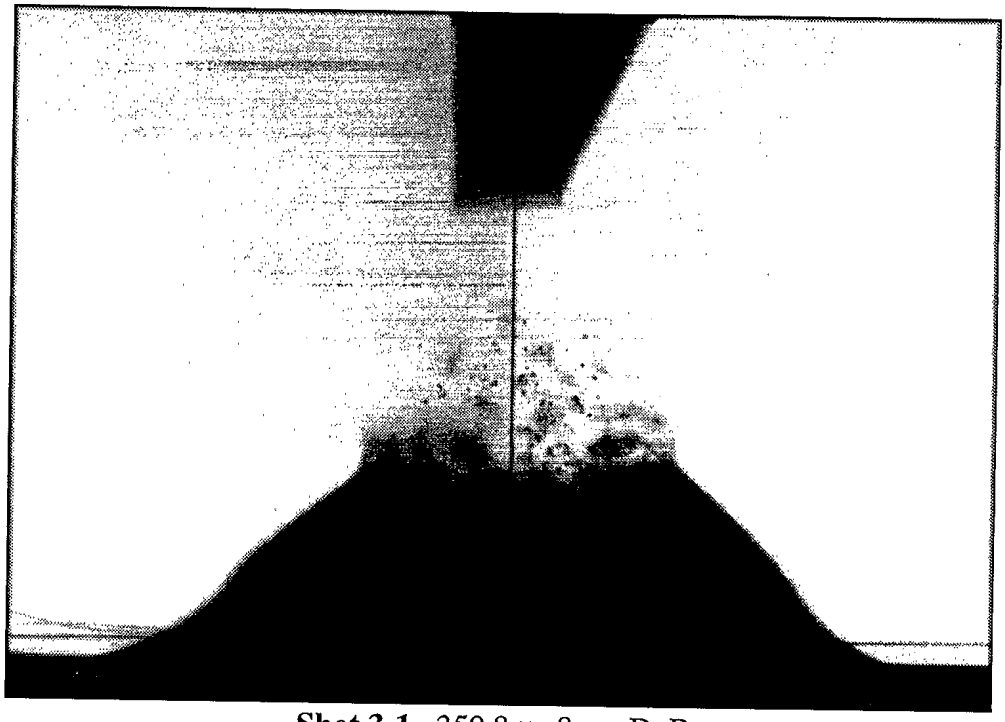

Shot 3-1. 350.8 μs 8 cm DoB

Shot 3-2. 731 μs 8 cm DoB

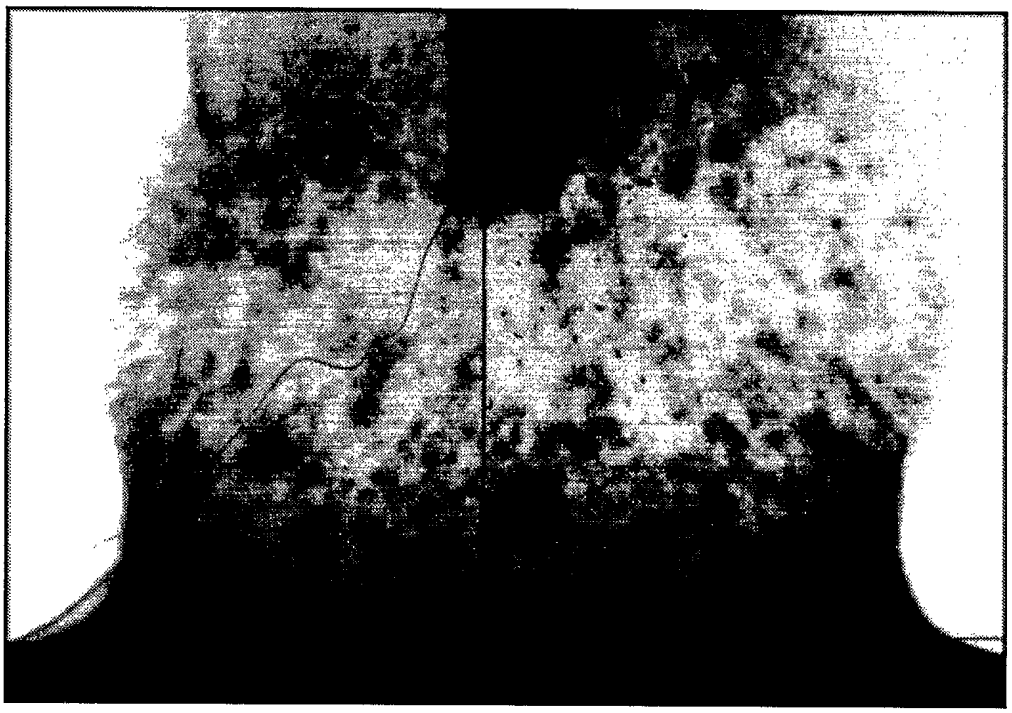

Shot 4-1. 100.9 μs 3 cm DoB

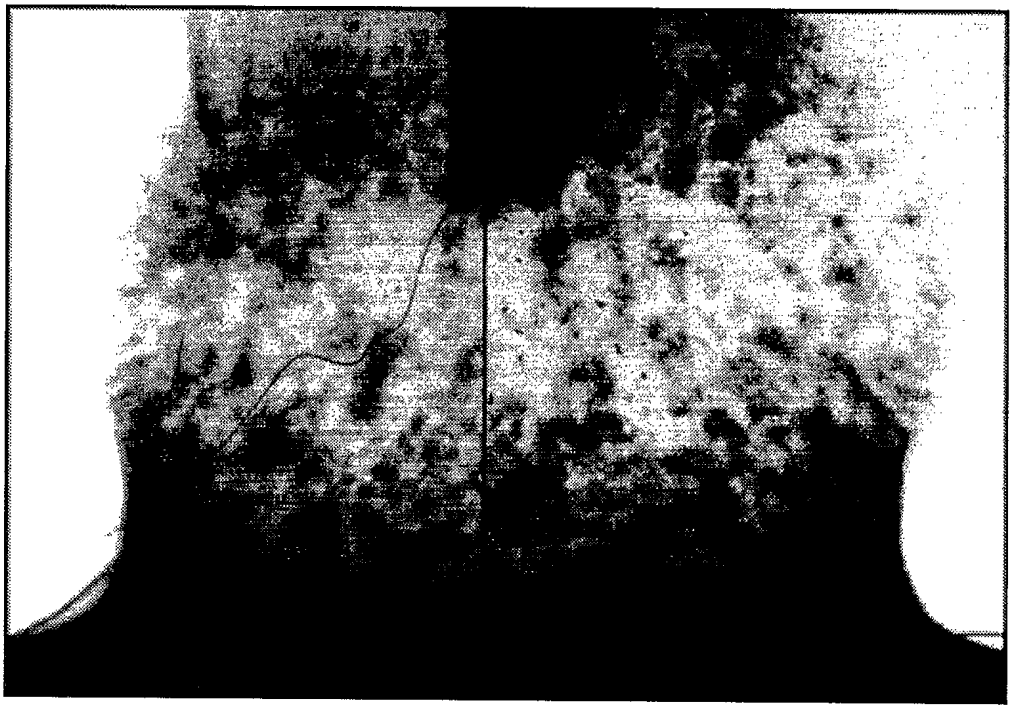

Shot 4-2. 301.9 μs 3 cm DoB

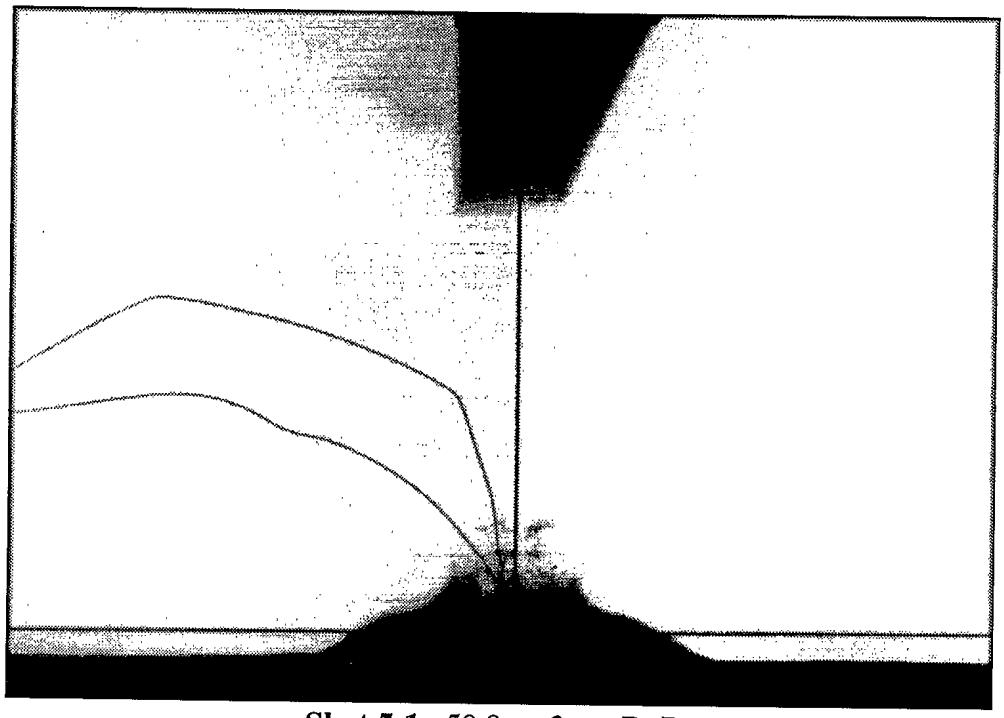

Shot 5-1. 50.9 μs 3 cm DoB

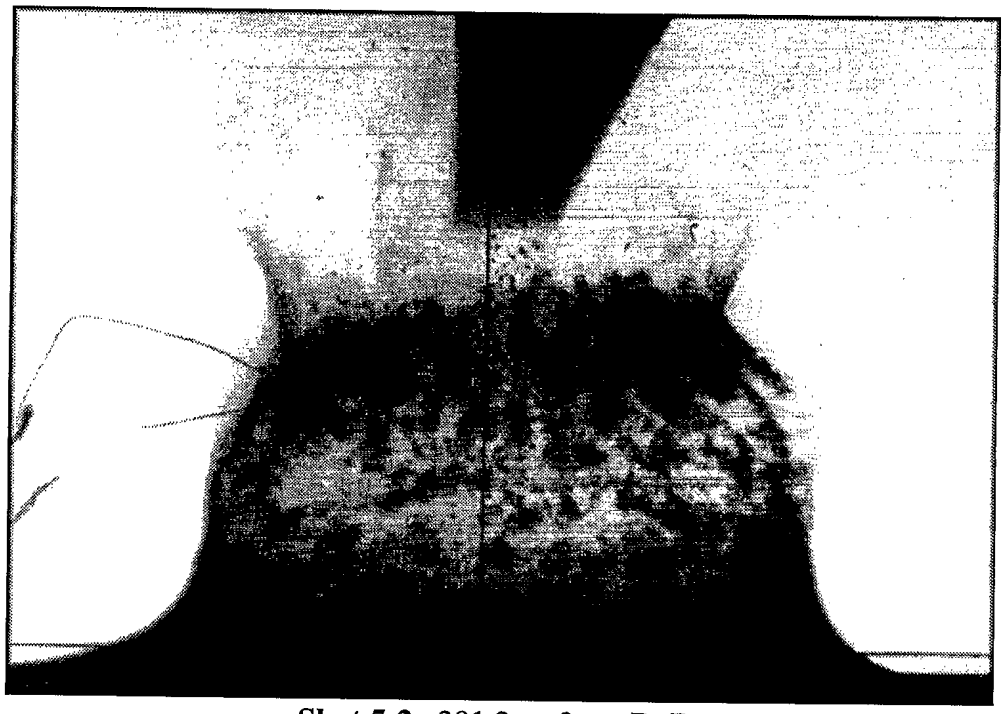

Shot 5-2. 201.2 μs 3 cm DoB

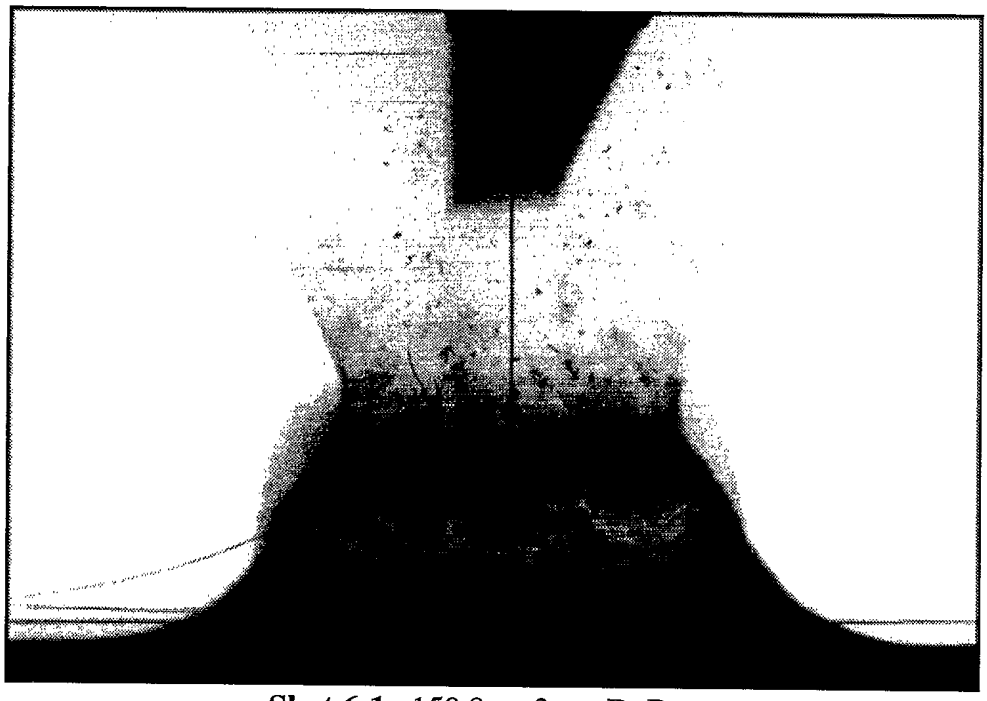

Shot 6-1. 150.9 μs 3 cm DoB

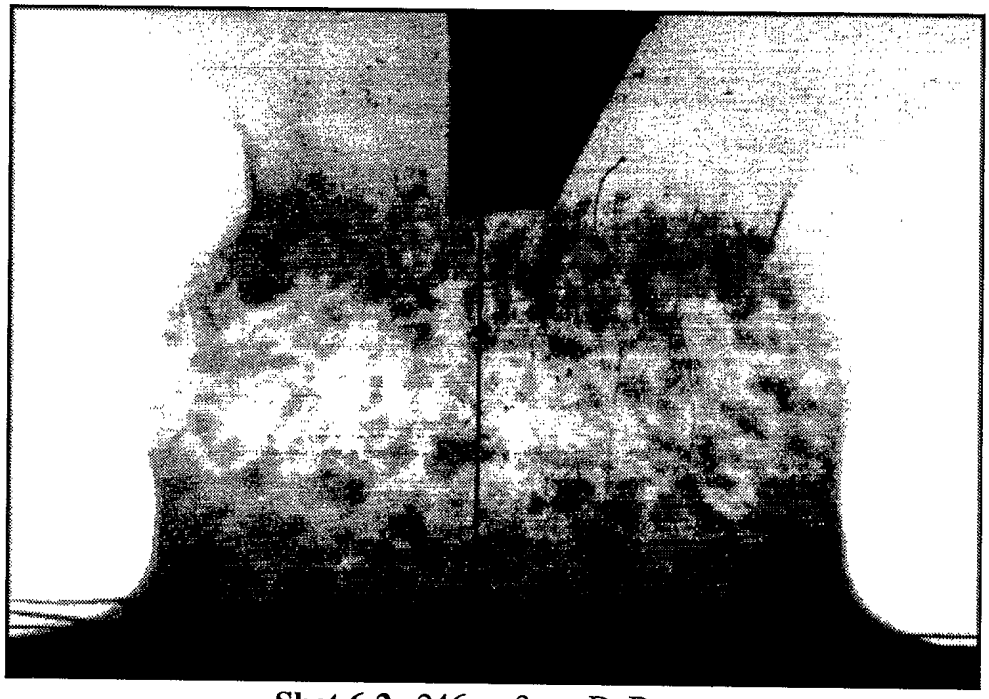

Shot 6-2. 246 μs 3 cm DoB

Note: Shot 7 was a misfire - no X-Ray photographs

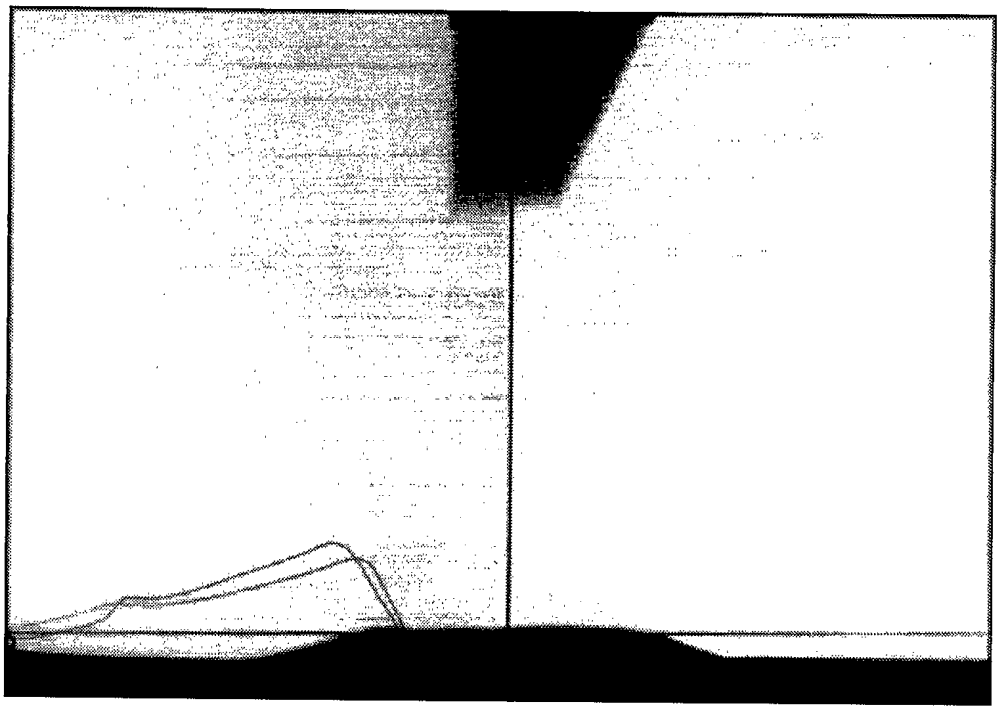

Shot 8-1. 150.9 μs 8 cm DoB

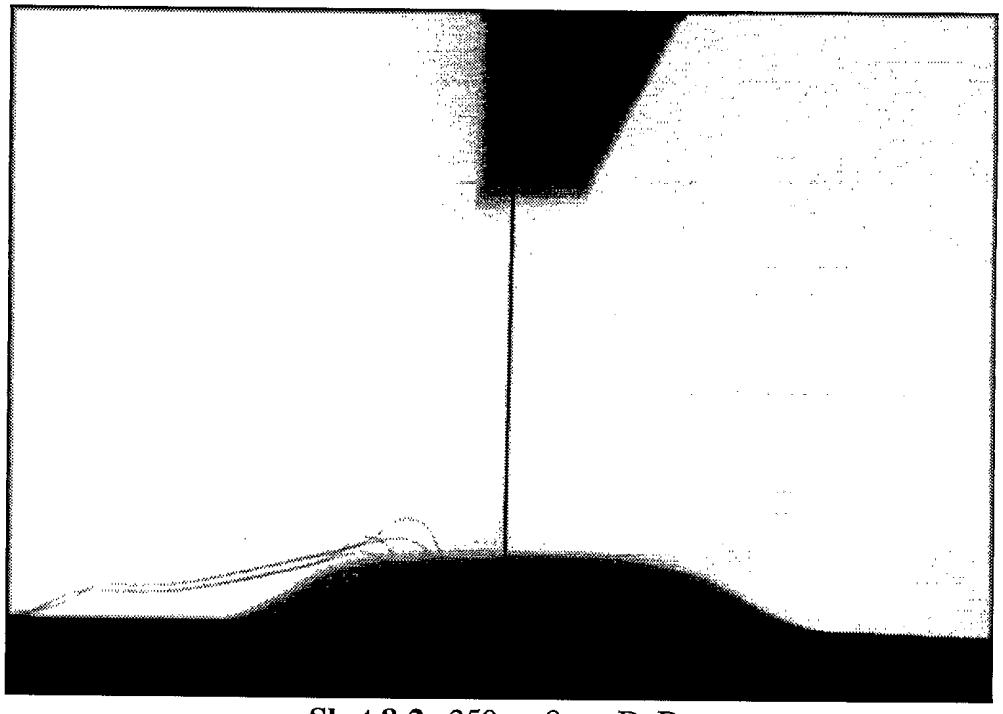

Shot 8-2. 250 μs 8 cm DoB

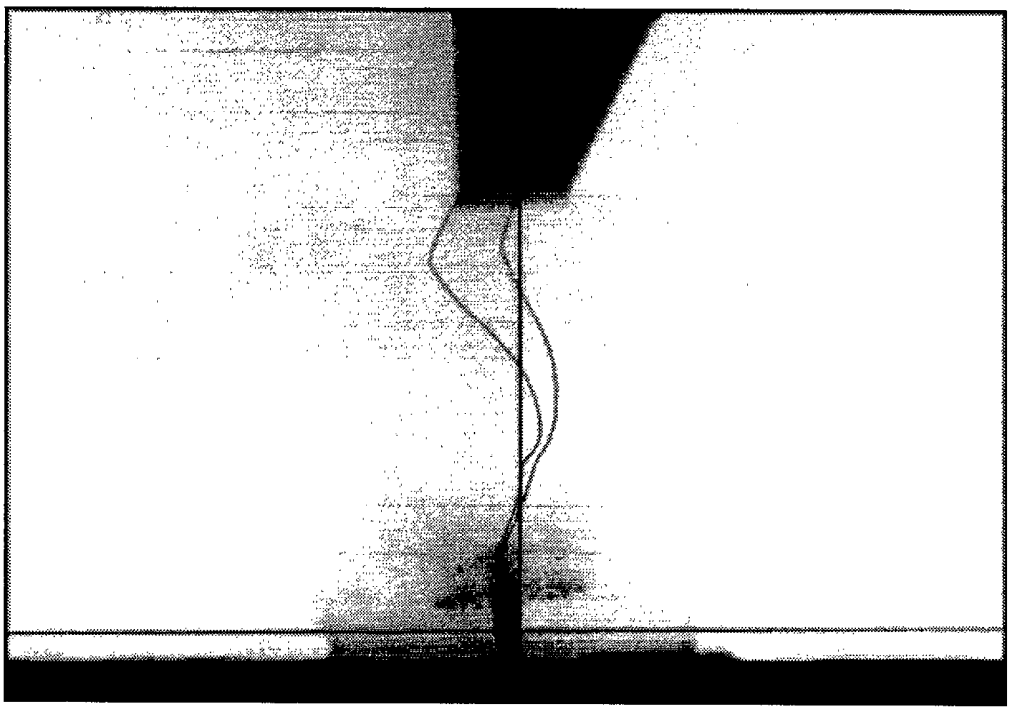

Shot 9-1. 24 μs 0 cm DoB

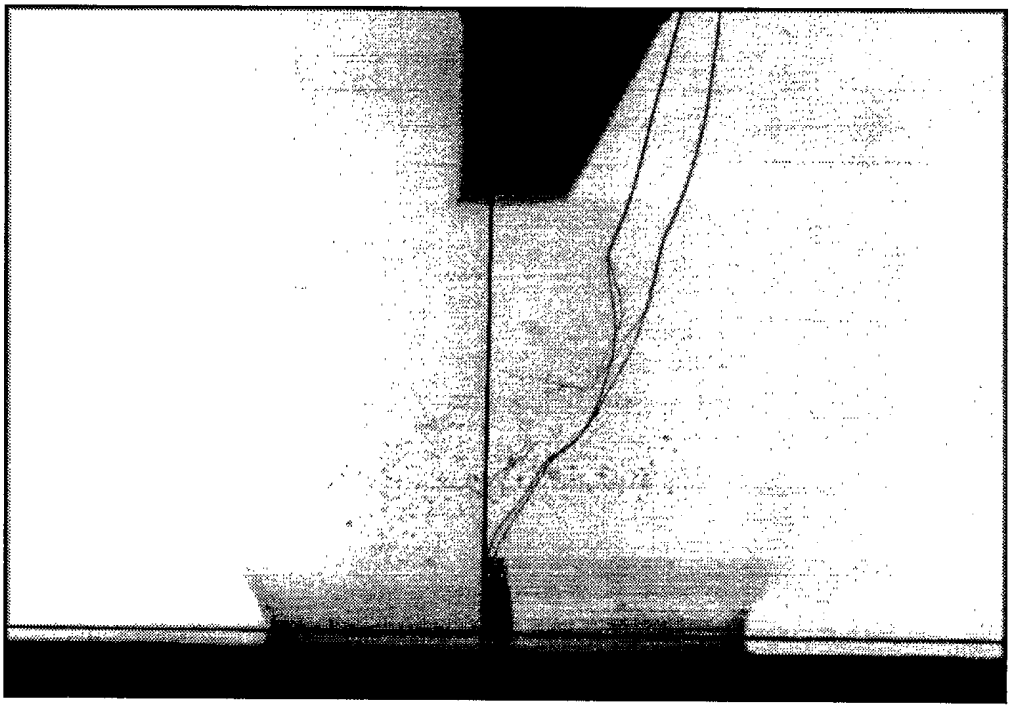

Shot 9-2. 51 μs 0 cm DoB

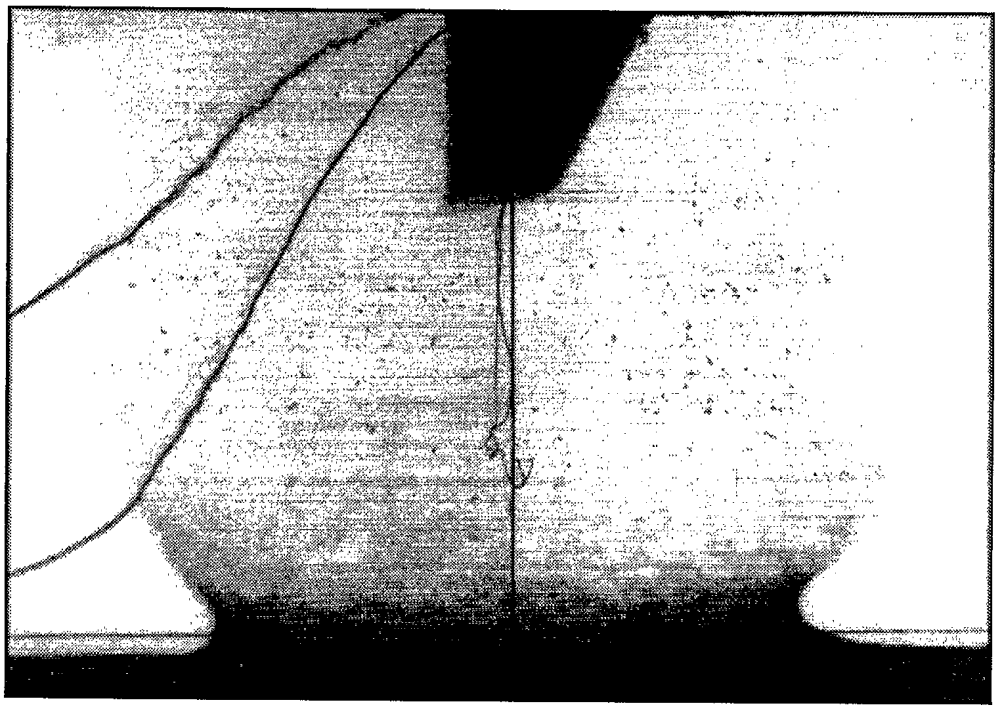

Shot 10-1. 100.9 μs 0 cm DoB

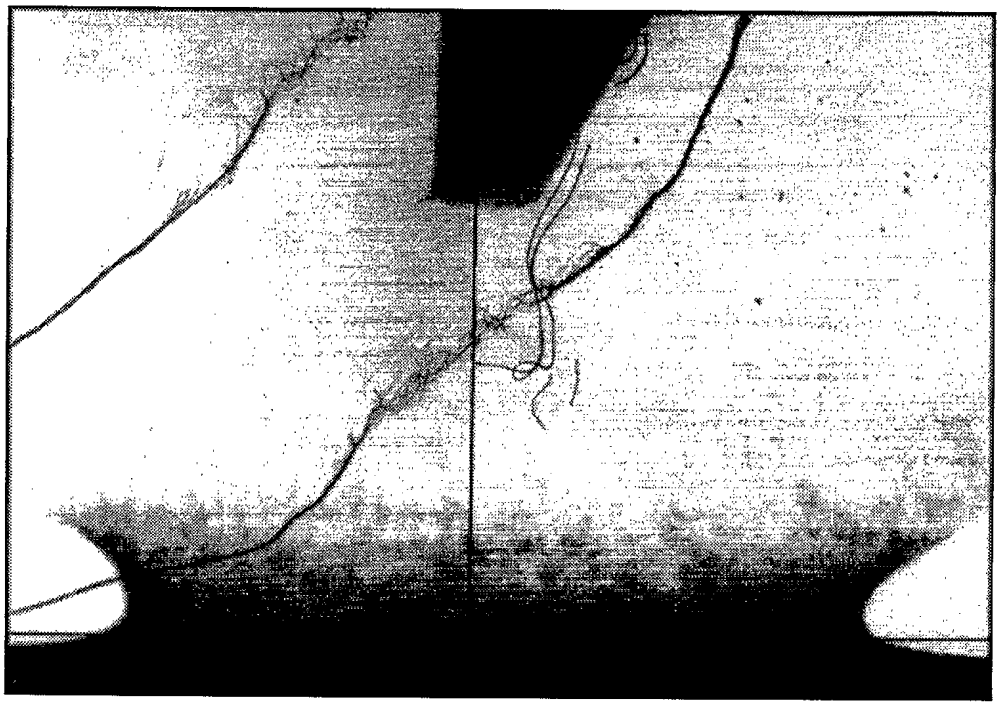

Shot 10-2. 201 μs 0 cm DoB

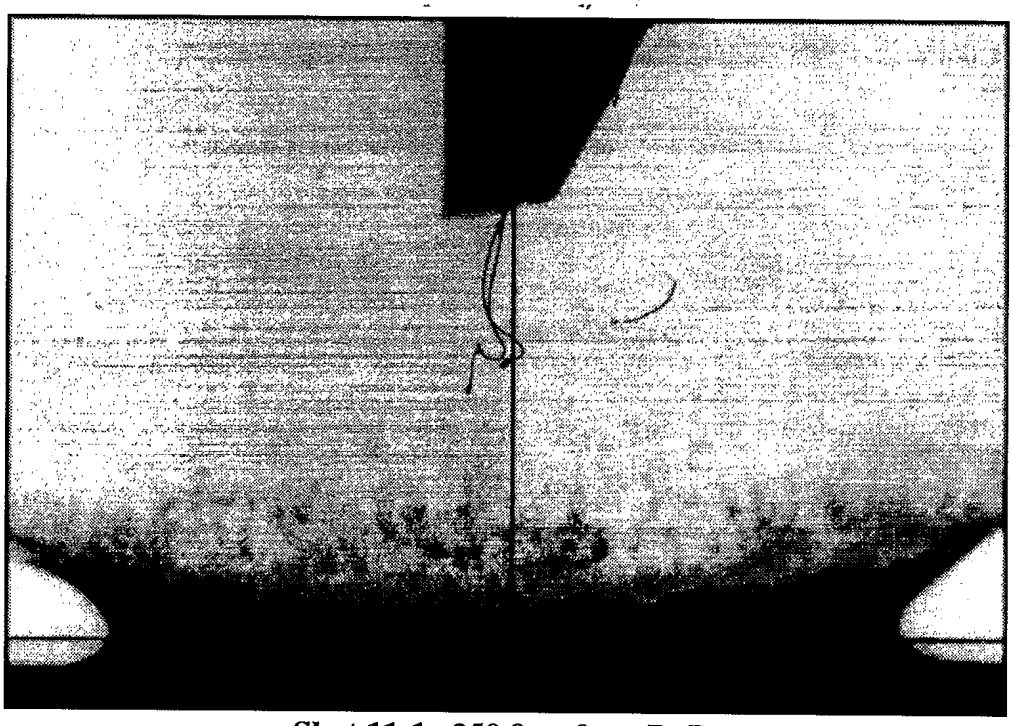

Shot 11-1. 250.8 μs 0 cm DoB

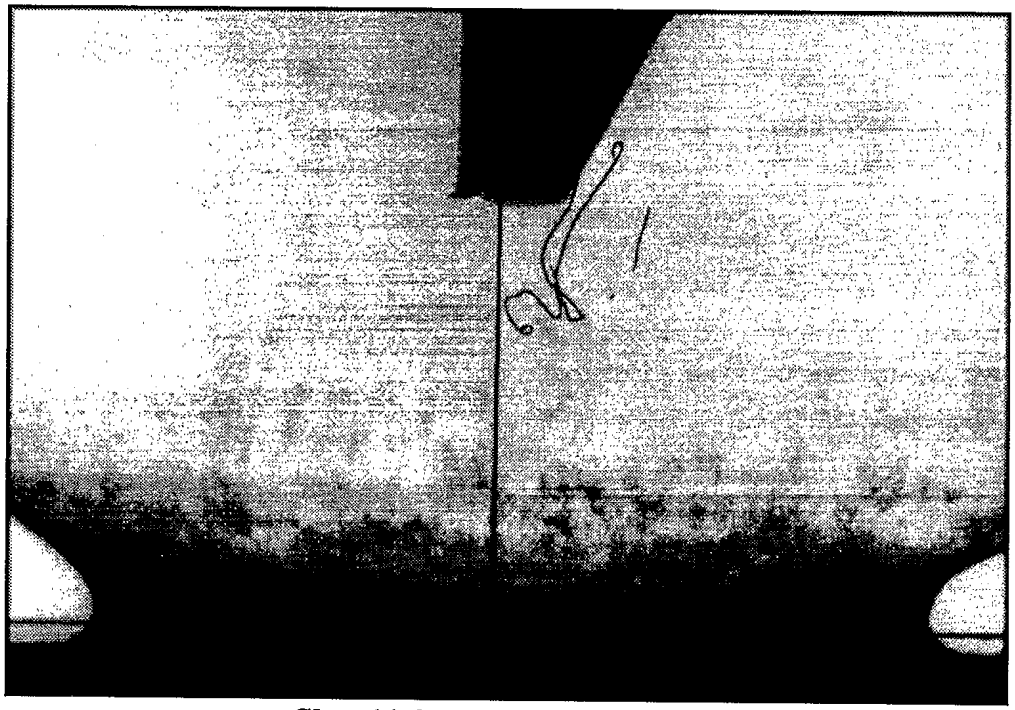

Shot 11-2. 301.1 μs 0 cm DoB

Series 2 - 100 g C-4 Bottom Initiated with RP2 Detonators

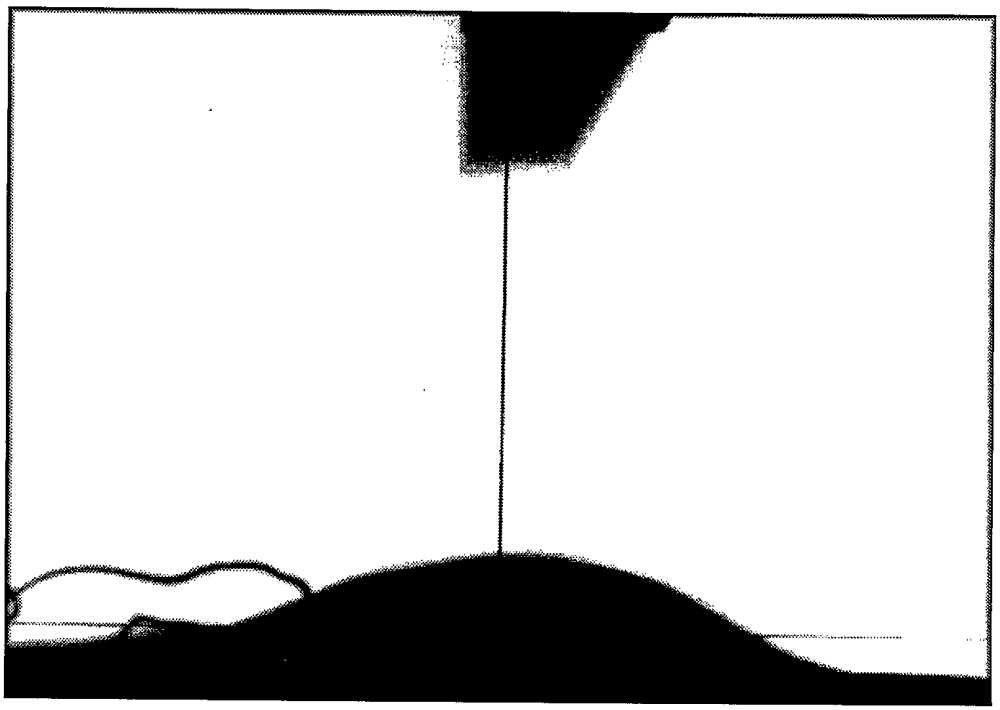

Shot 12-1. 230.9 µs 8 cm DoB

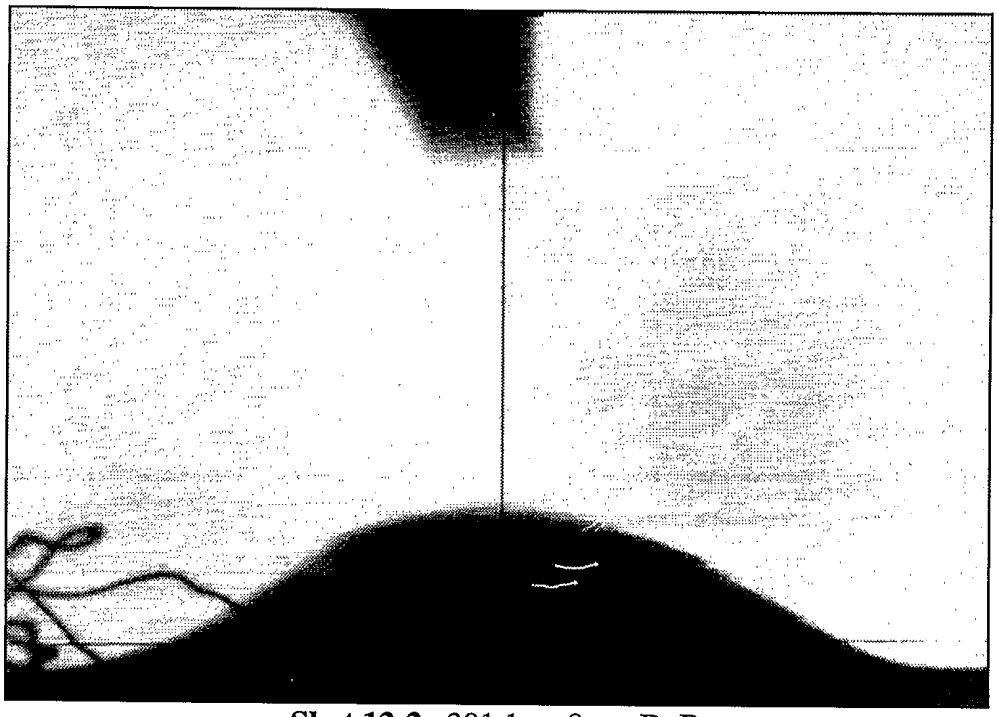

Shot 12-2. 301.1 µs 8 cm DoB

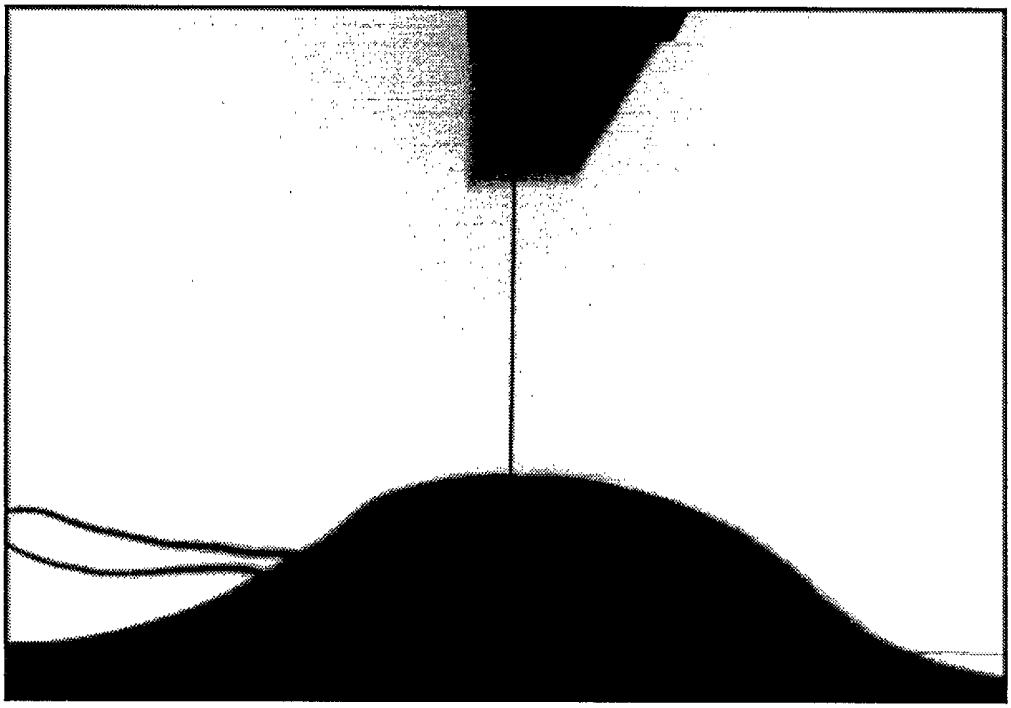

Shot 13-1. 351 μs 8 cm DoB

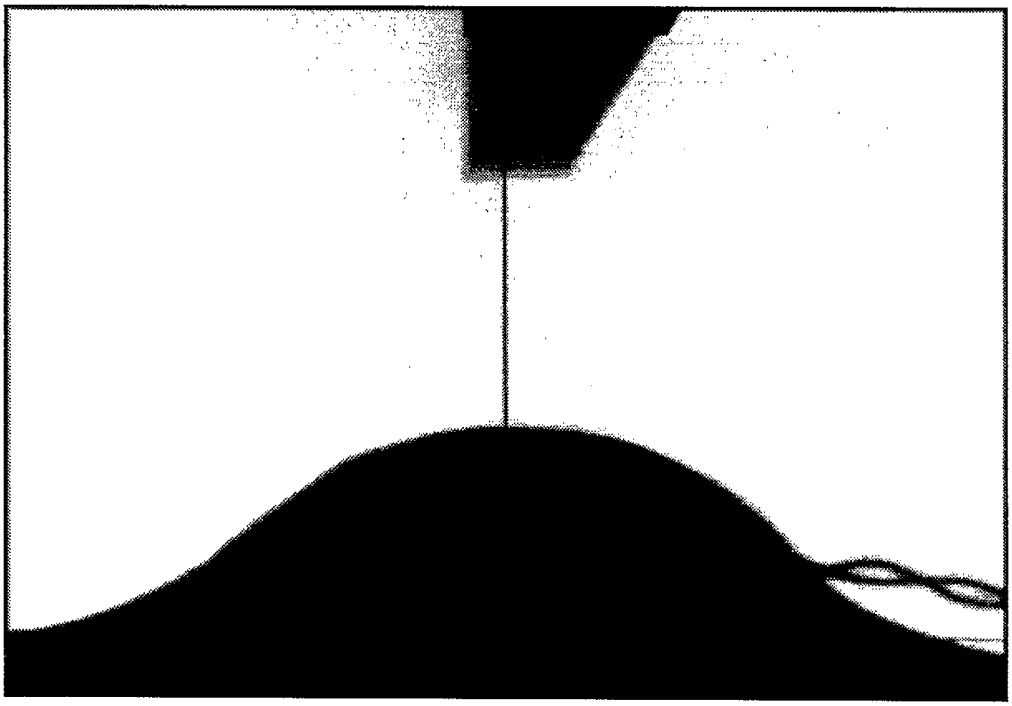

Shot 13-2. 401.1 μs 8 cm DoB

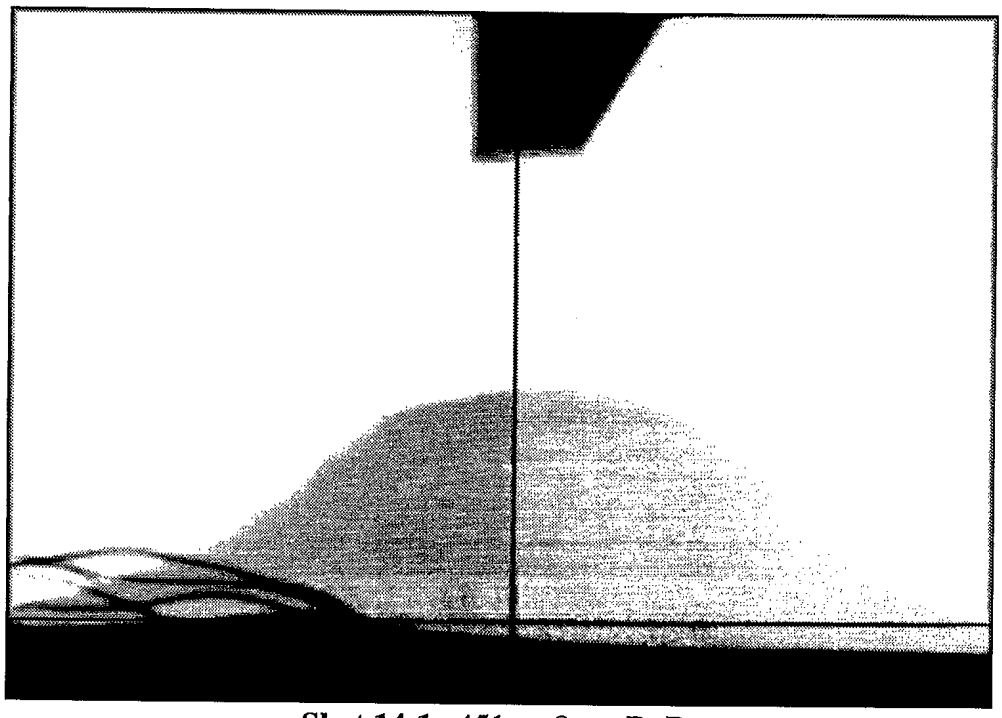

Shot 14-1. 451 μs 8 cm DoB

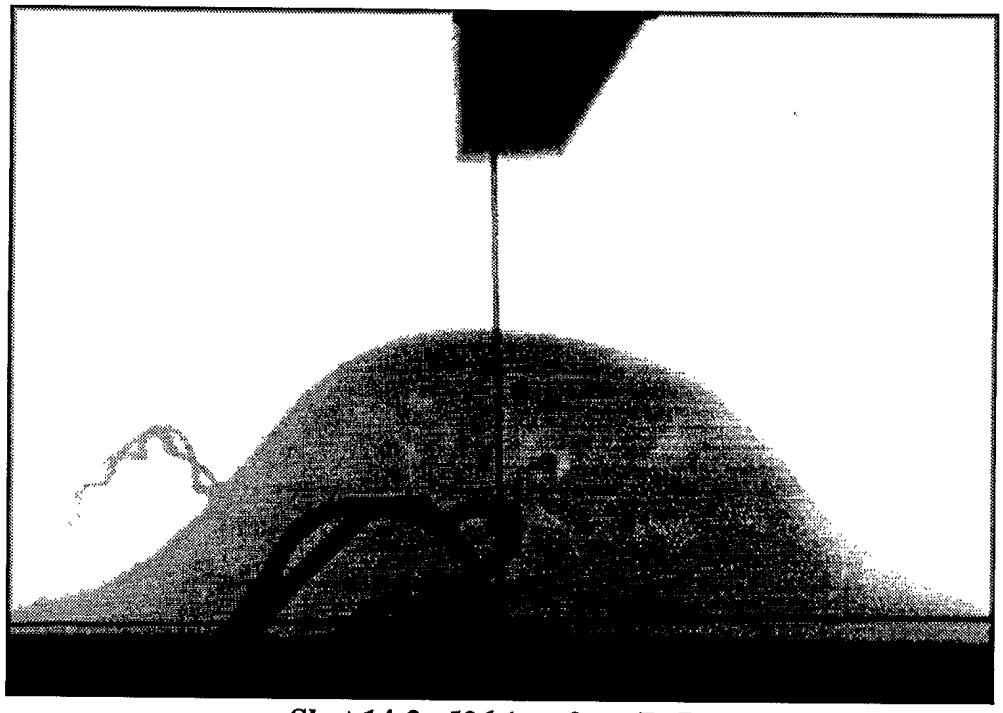

Shot 14-2. 526.1 μs 8 cm DoB

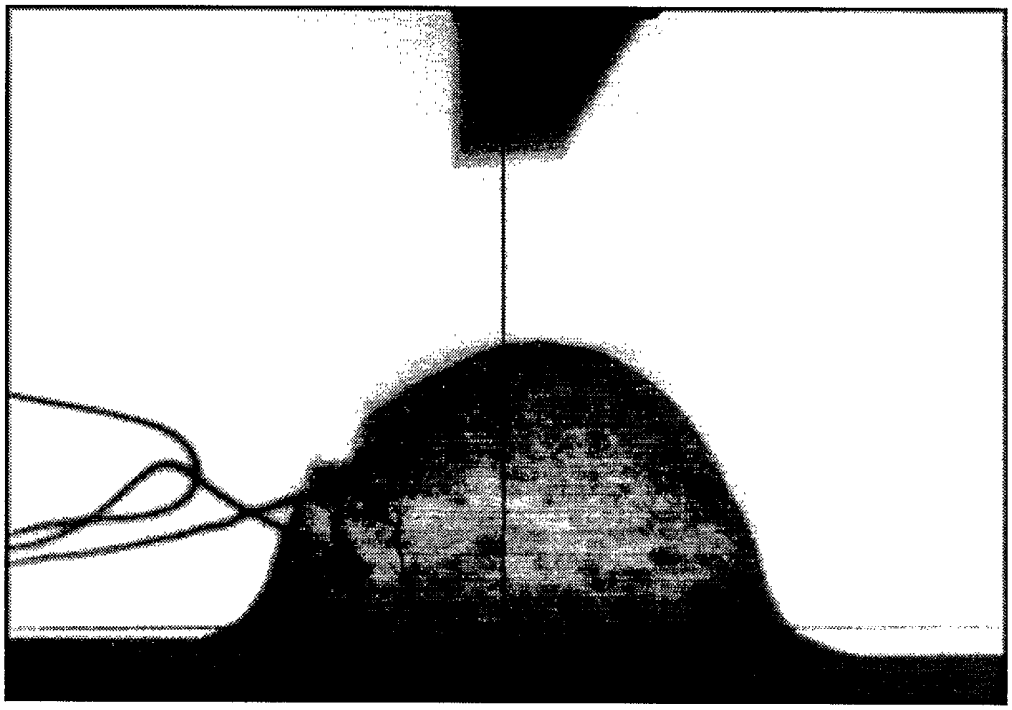

Shot 15-1. 100.9 μs 3 cm DoB

Shot 15-2. 201.9 μs 3 cm DoB

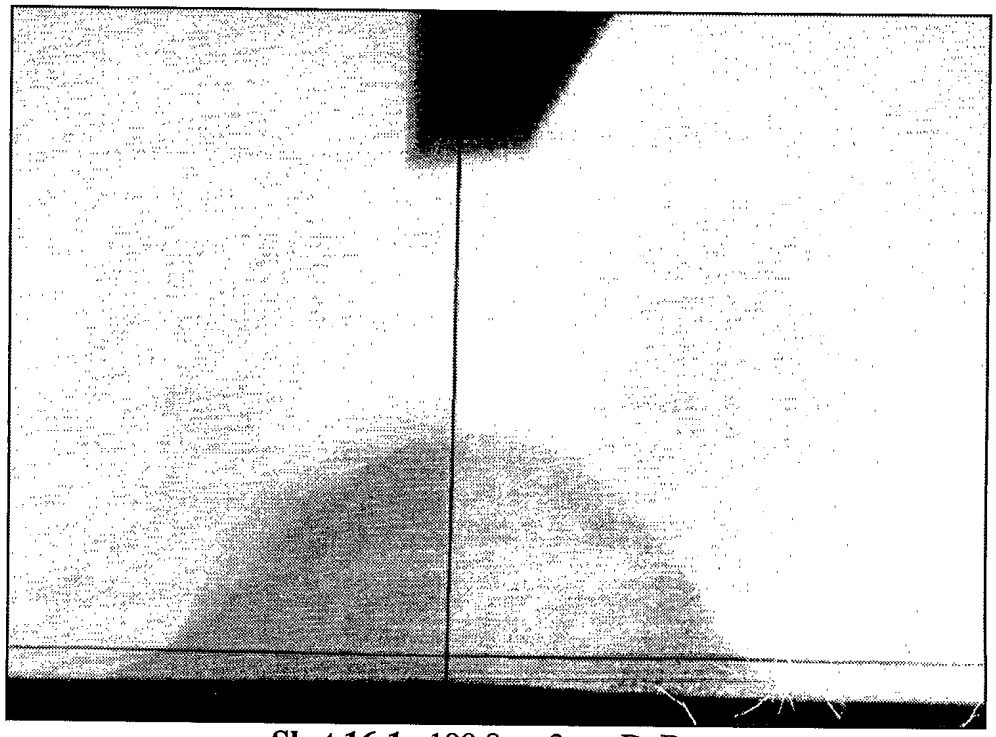

Shot 16-1. 100.8 μs 3 cm DoB

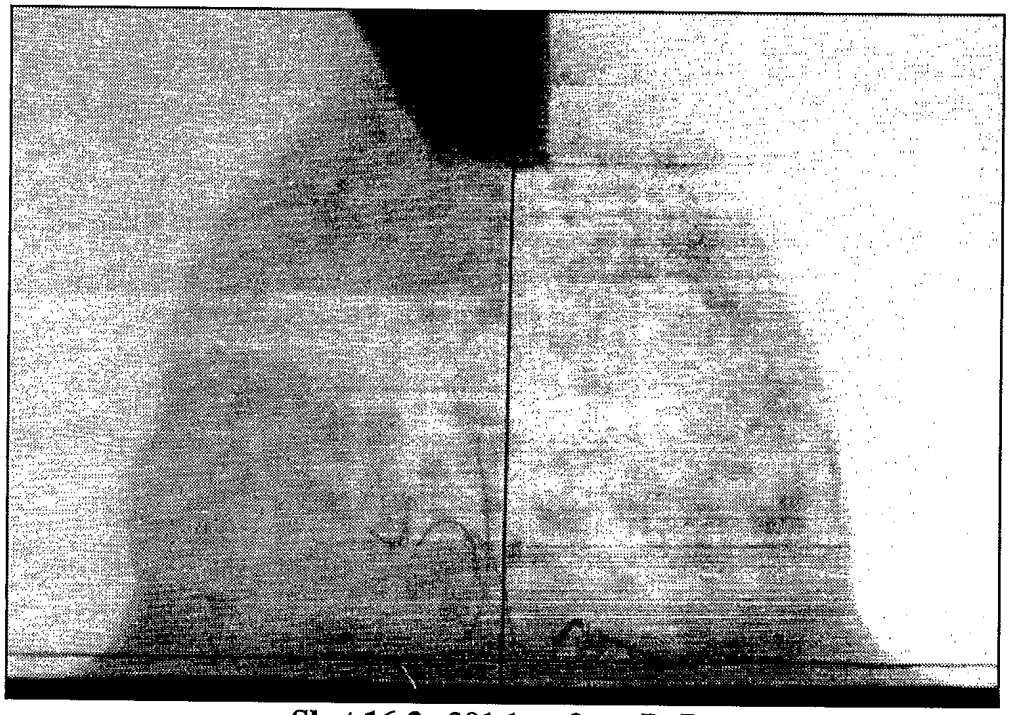

Shot 16-2. 201.1 μs 3 cm DoB

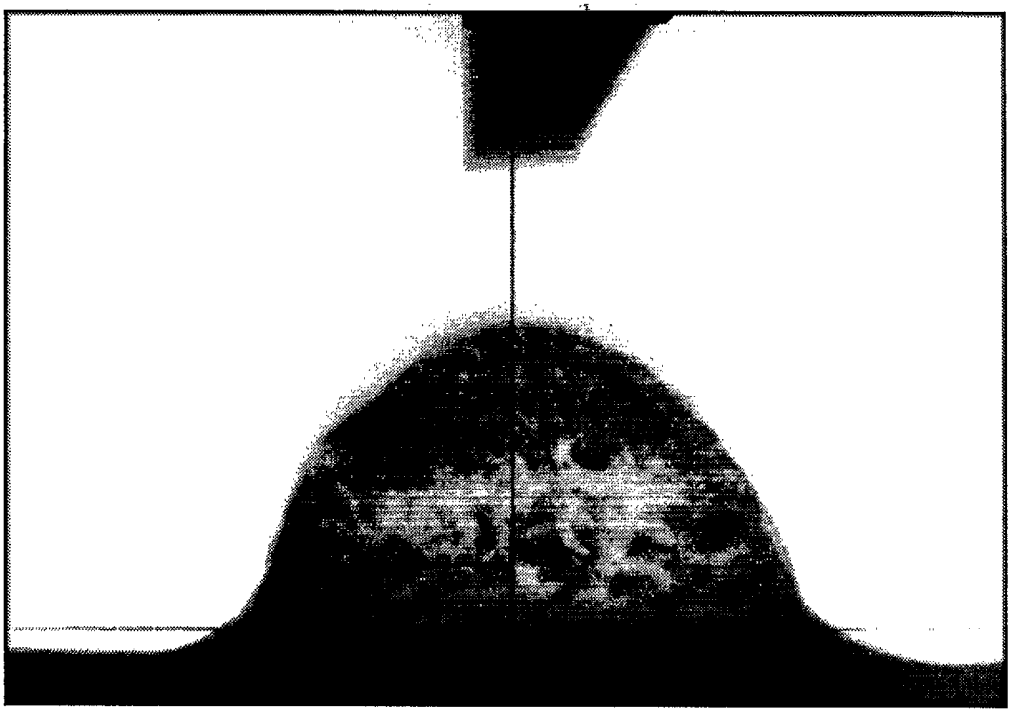

Shot 17-1. 125.9 μs 3 cm DoB

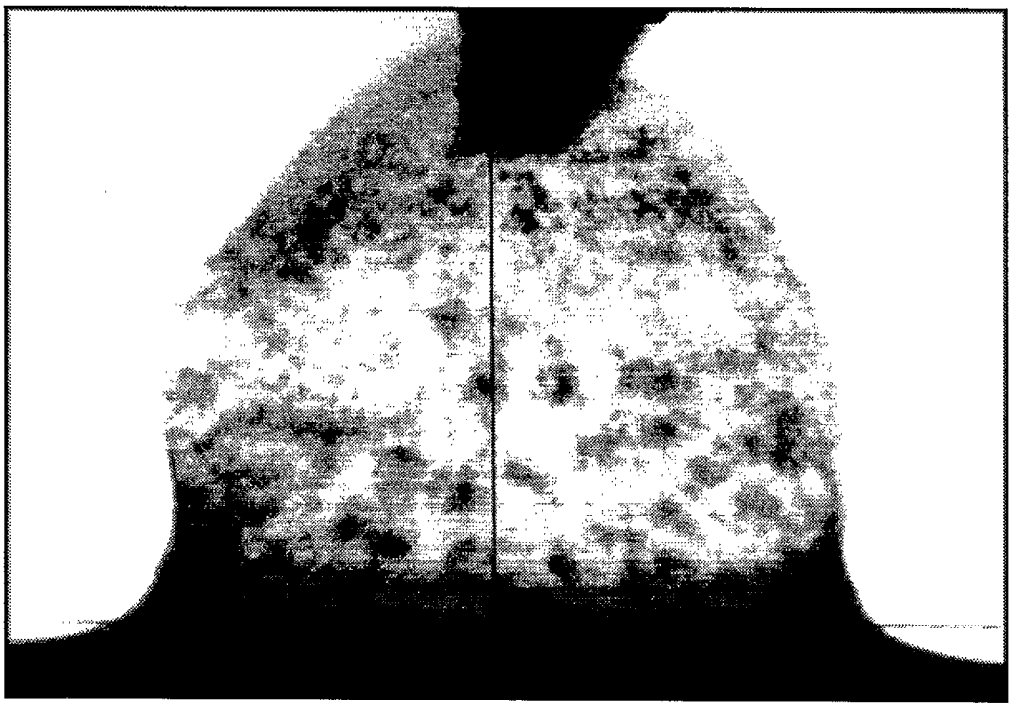

Shot 17-2. 201.1 μs 3 cm DoB

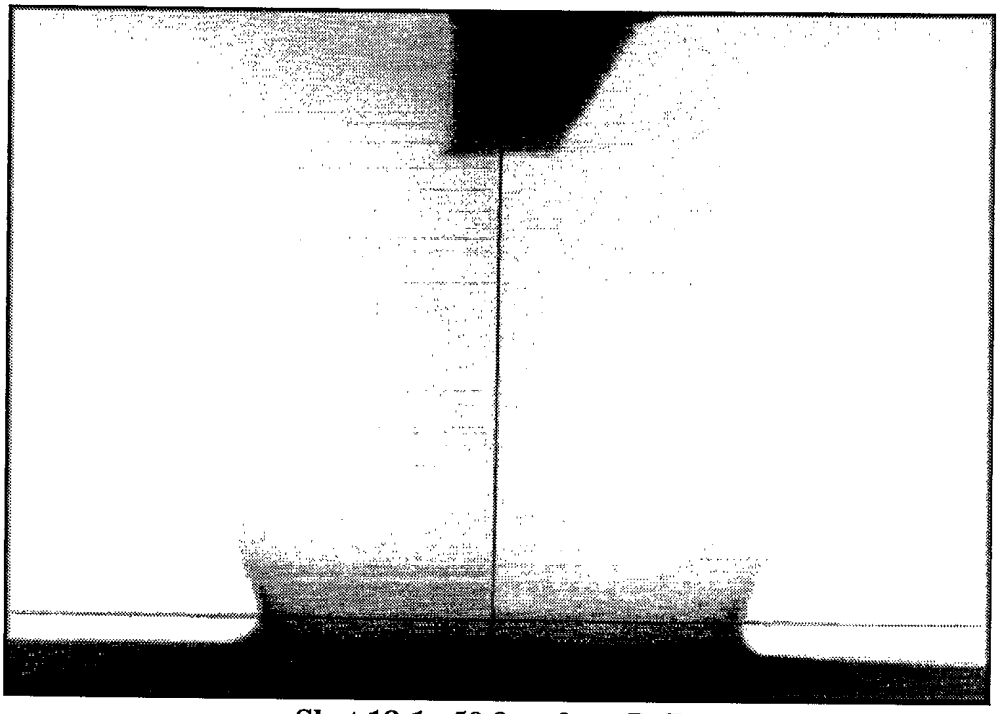

Shot 18-1. 50.8 μs 0 cm DoB

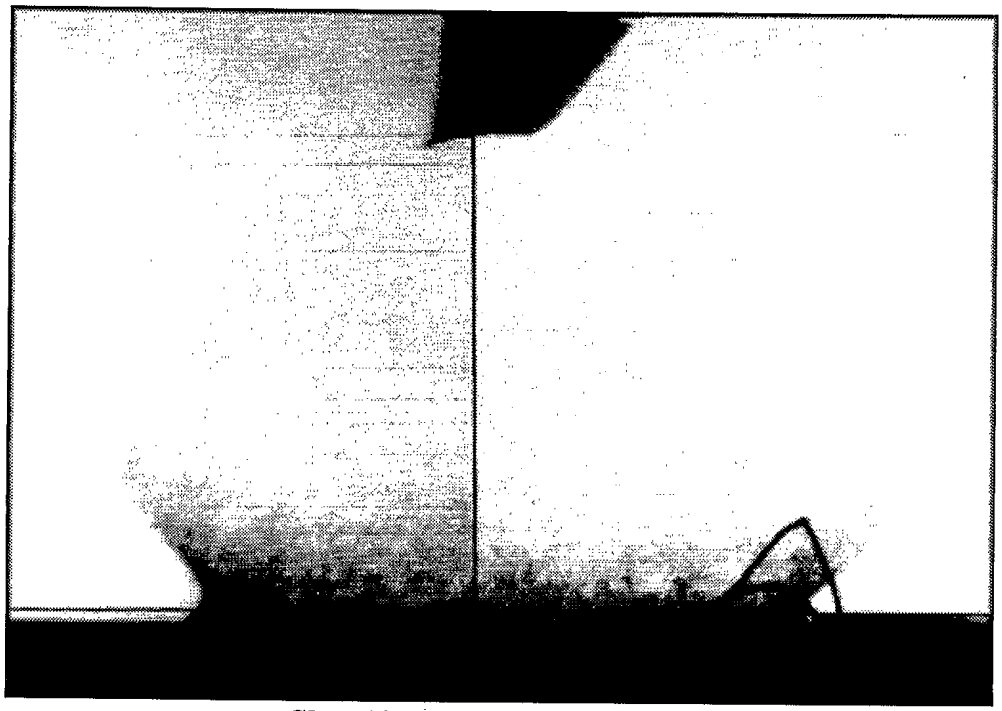

Shot 18-2. 101.1 μs 0 cm DoB

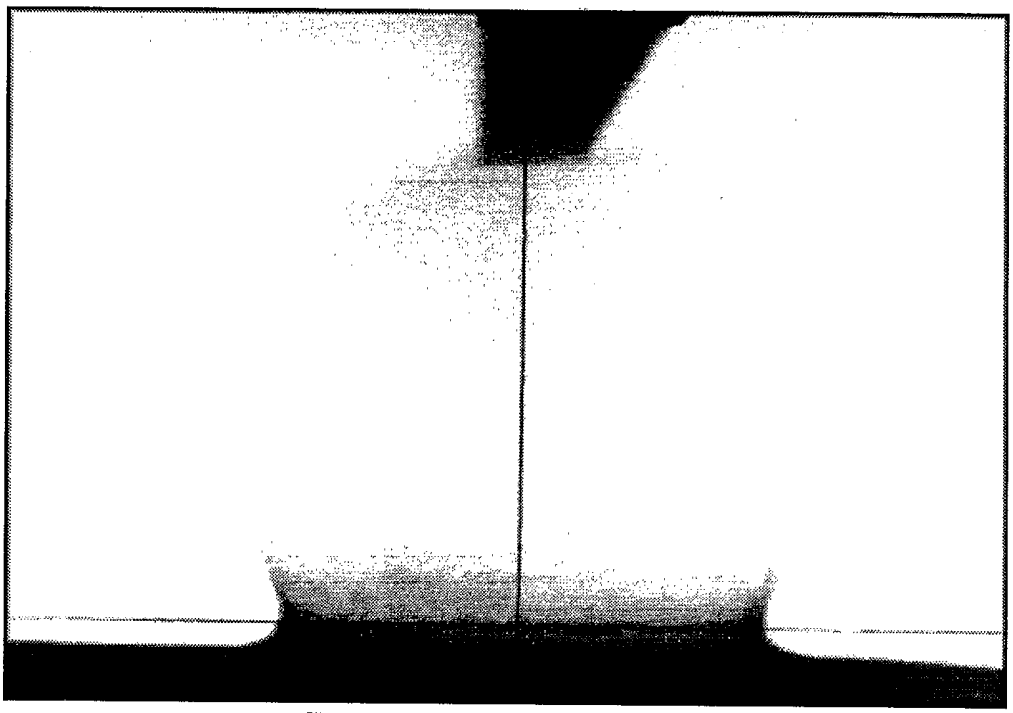

Shot 19-1. 50.9 μs 0 cm DoB

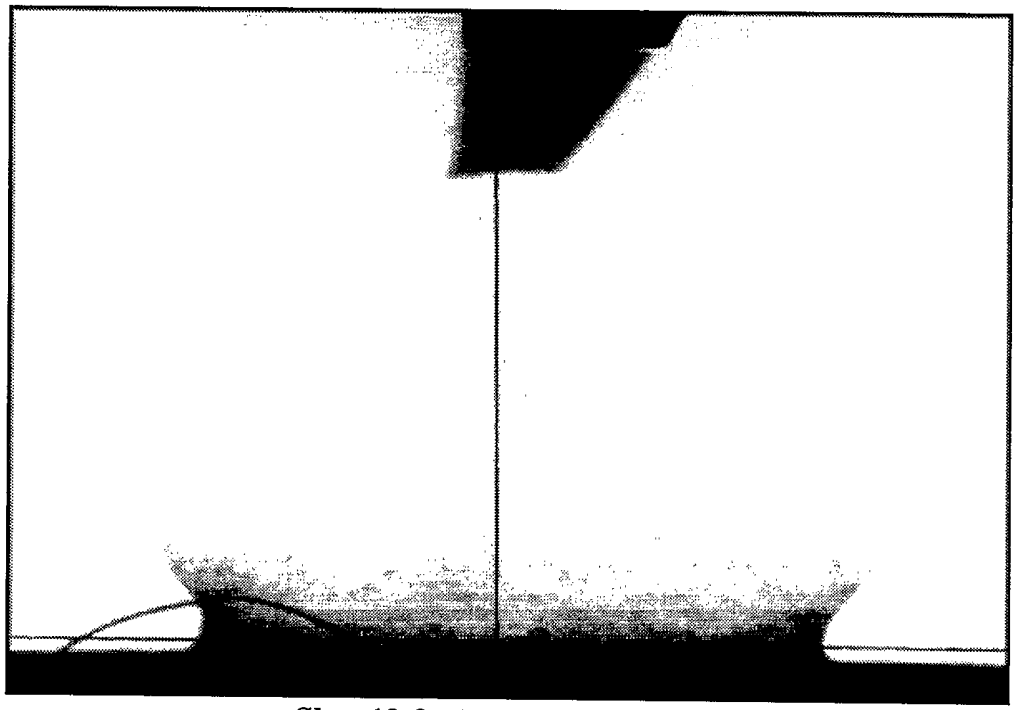

Shot 19-2. 101.9 μs 0 cm DoB

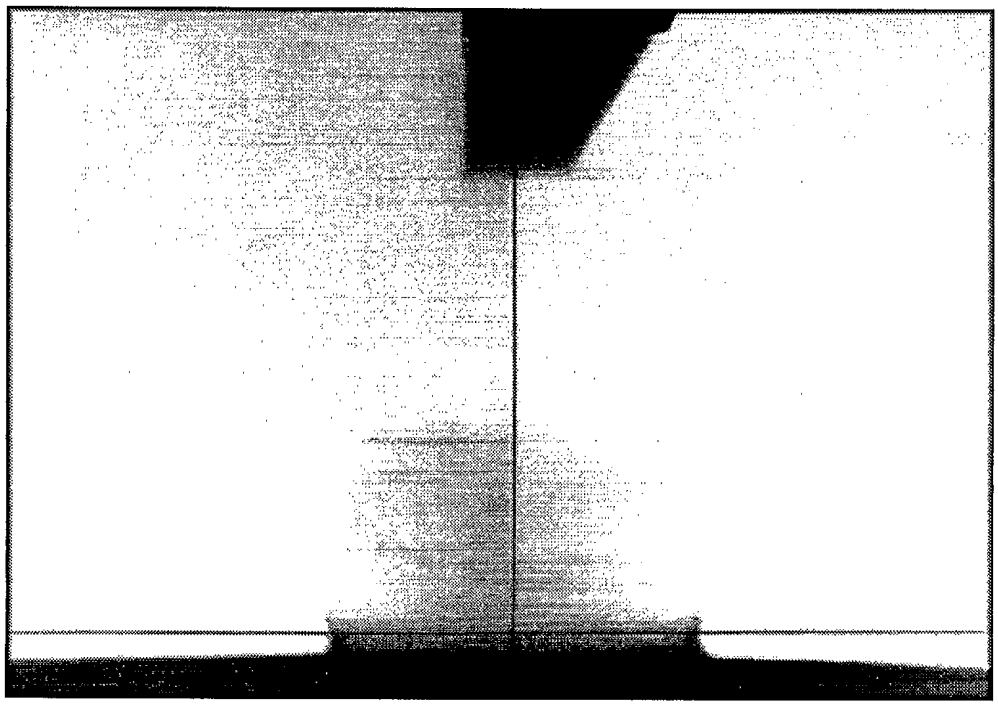

Shot 20-1. 25.8 μs 0 cm DoB

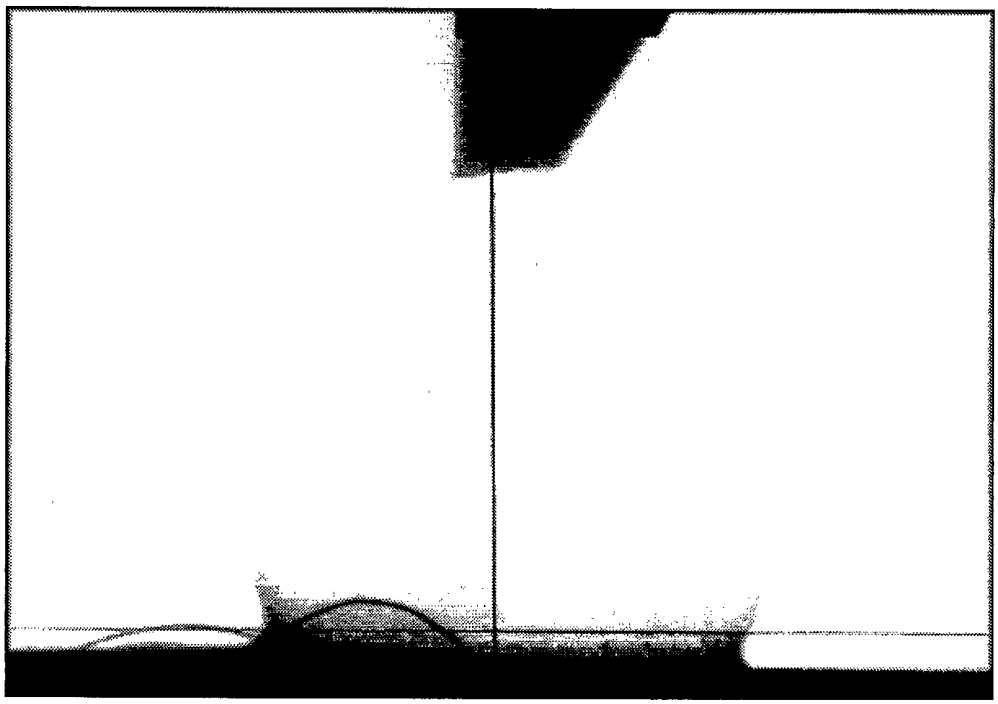

Shot 20-2. 51 μs 0 cm DoB

ANNEX B

Selected High Speed Film Shots From Series 2

Annex B - Table of Contents

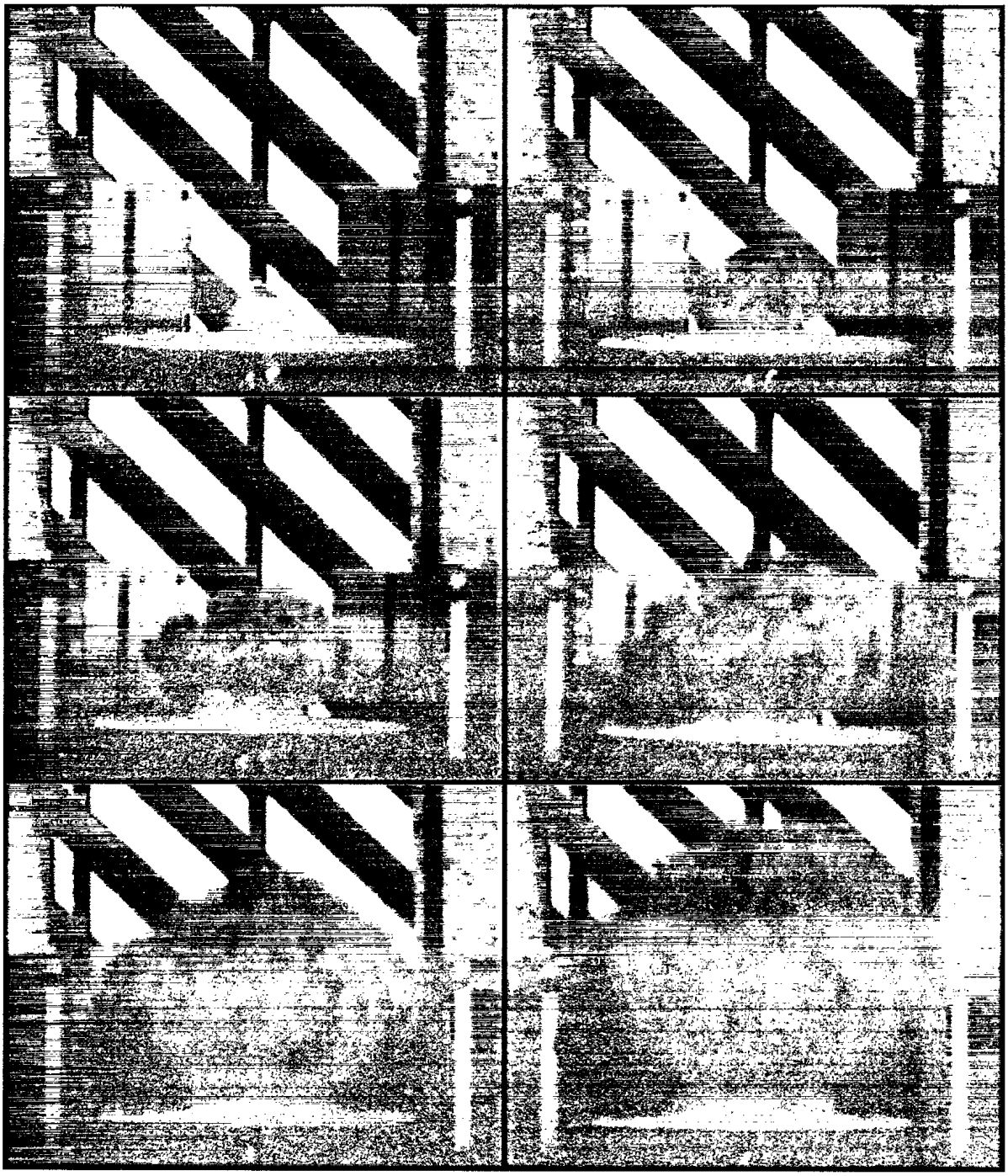

Figure B1. Sequential images from detonation of a 100 g charge of C-4 with 8 cm loose dry silica sand overburden

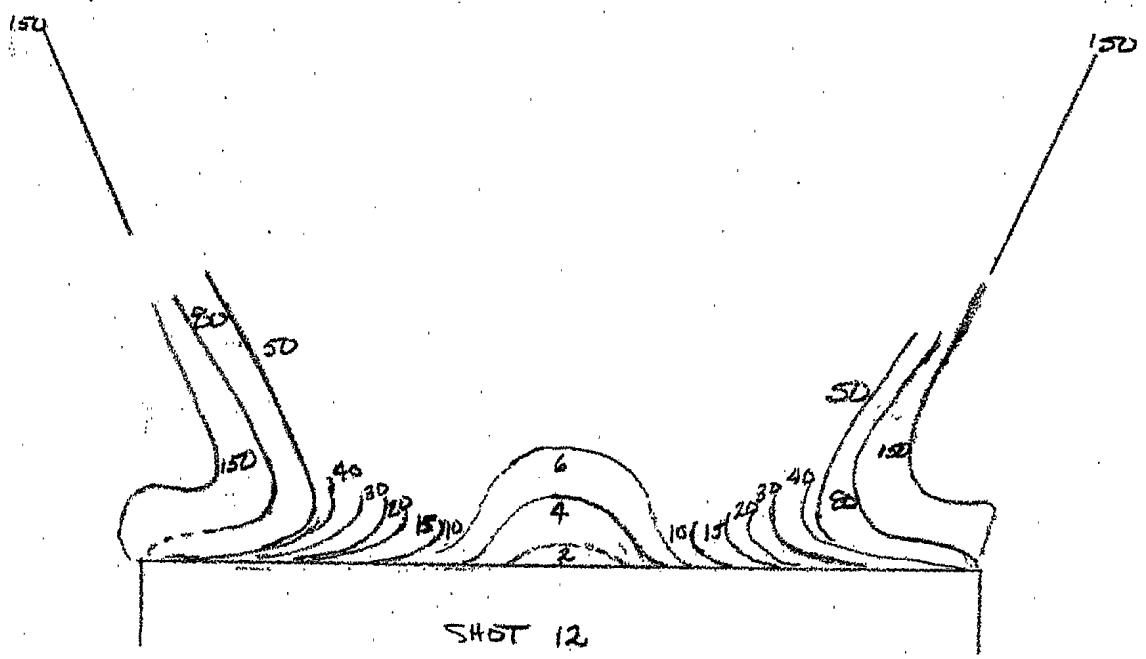

Figure B2. Sequential traces of ejecta expansion for Shot 12 (8 cm O/B).

(To convert frame contour lines to elapsed time multiply frame number by 1.017 x 10^{-4} sec).

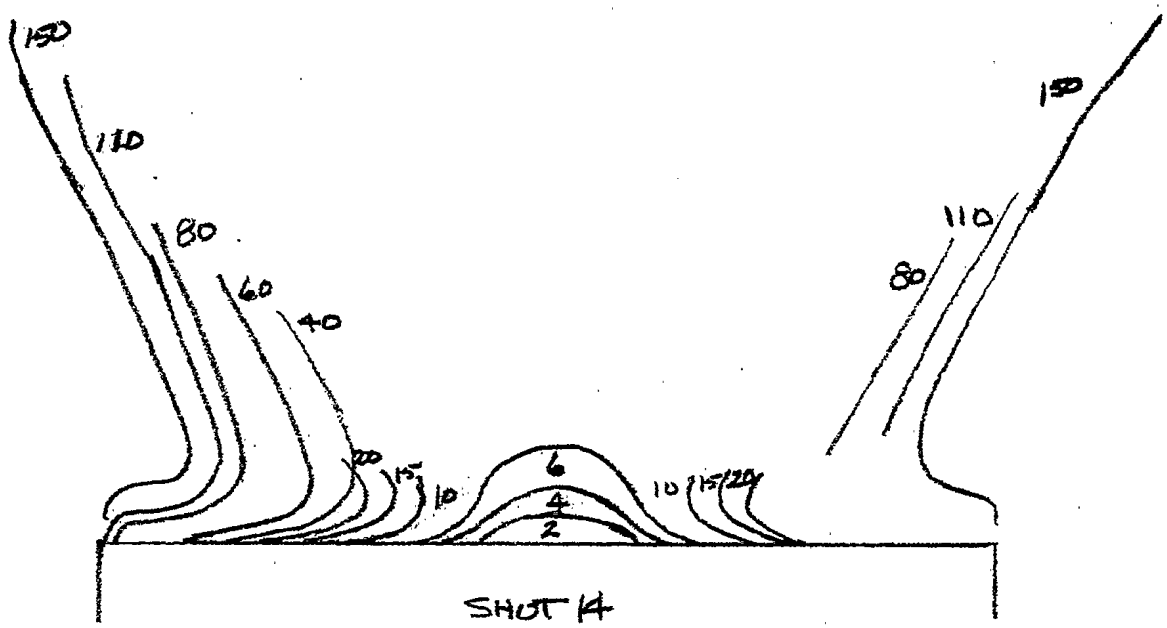

Figure B3. Sequential traces of ejecta expansion for Shot 14 (8 cm O/B)

(To convert frame contour lines to elapsed time multiply frame number by 1.01 x 10^{-4})

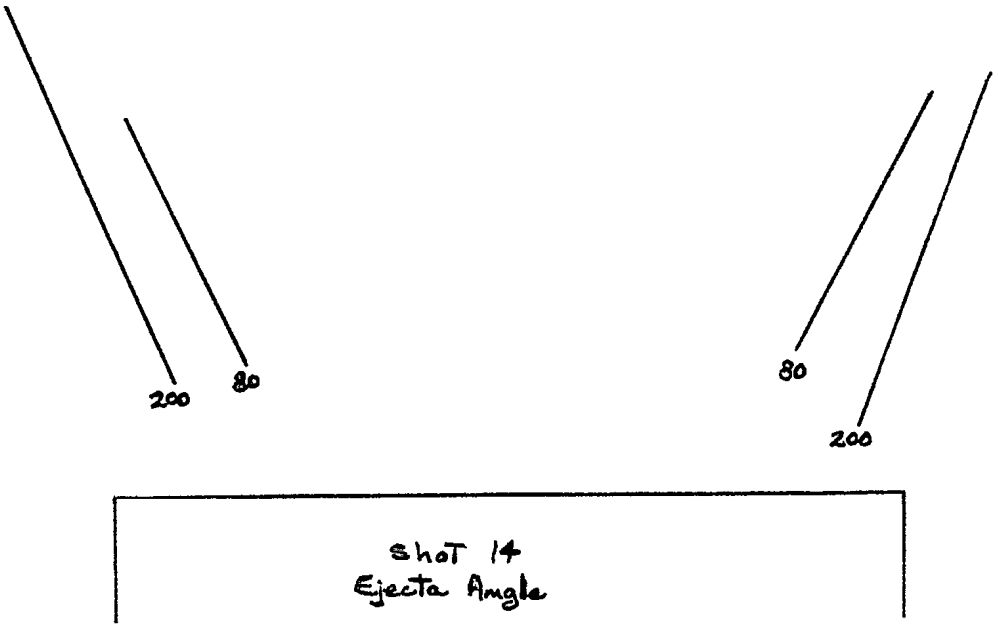

Figure B4. Angles of ejecta at 80 and 200 ms for Shot 14 (8 cm O/B)

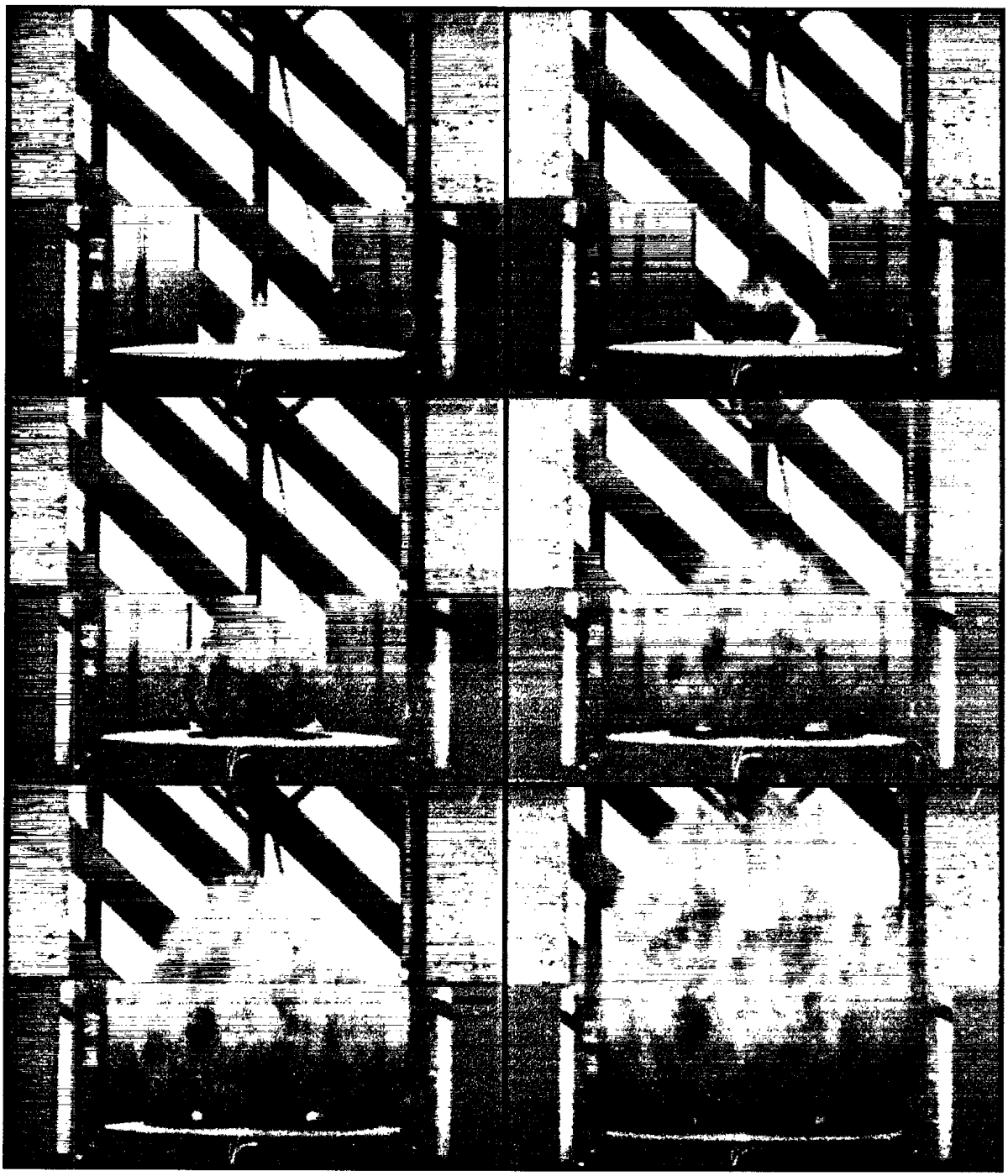

Figure B5. Sequential images of the detonation of 100 g C-4 with 3 cm of loose drv silica sand overburden.

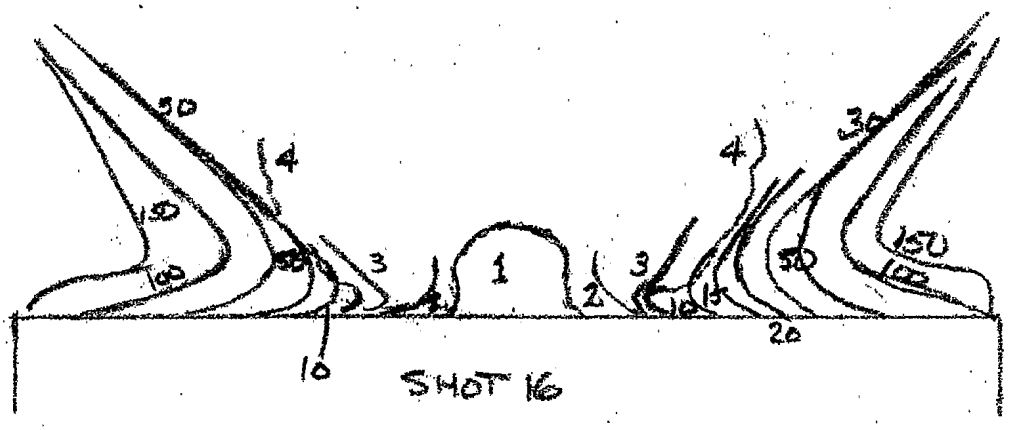

Figure B6. Sequential traces of ejecta expansion from Shot 16 (3 cm O/B). (To convert frame number to elapsed time multiply by 1.013×10^{-4} sec).

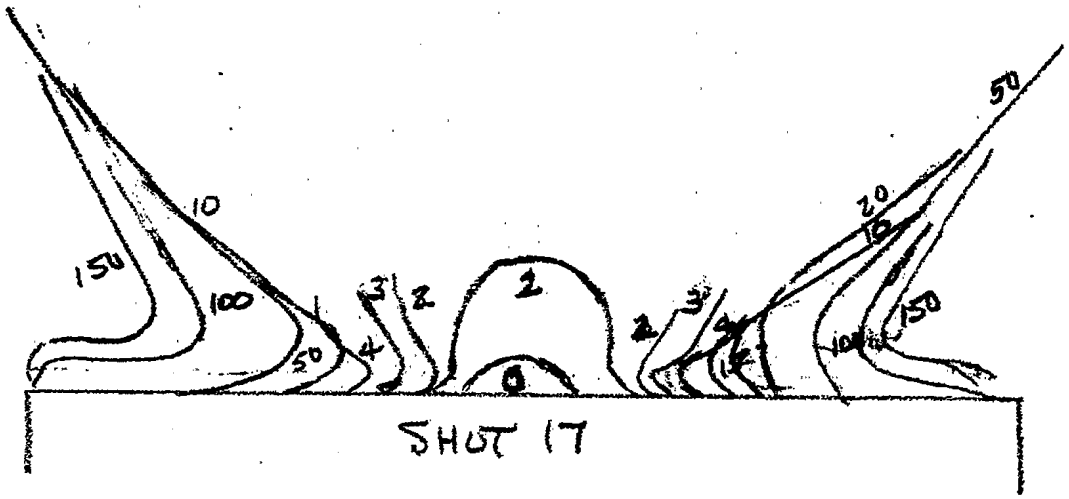

Figure B7. Sequential traces of ejecta expansion from Shot 17 (3 cm O/B). (To convert frame number to elapsed time , multiply by 1.015 x 10^{-4} sec).

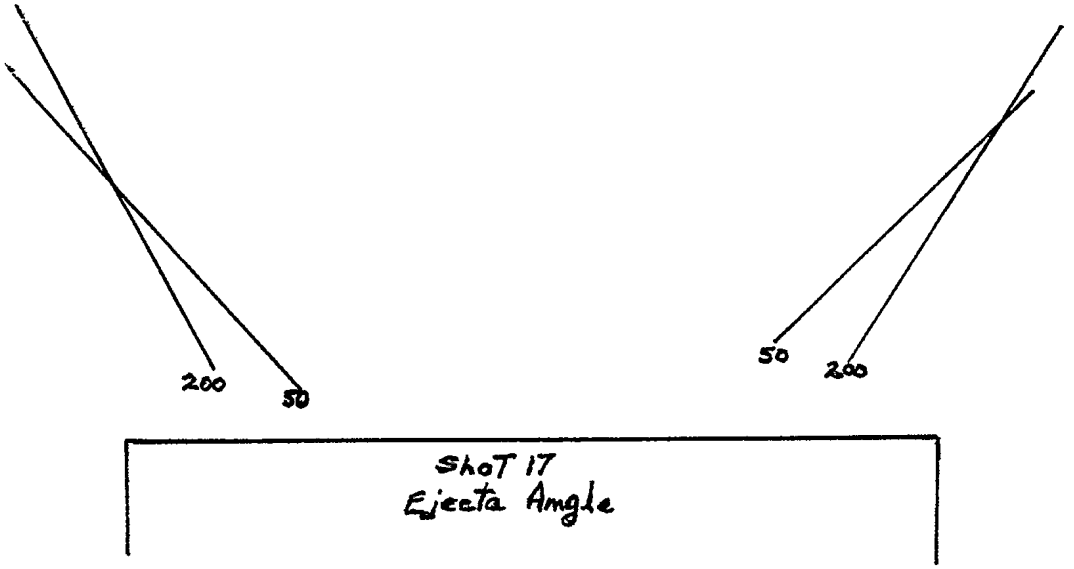

Figure B8. Angles of ejecta at 50 and 200 ms from detonation of 100 g C-4 with 3 cm of loose dry silica sand overburden.

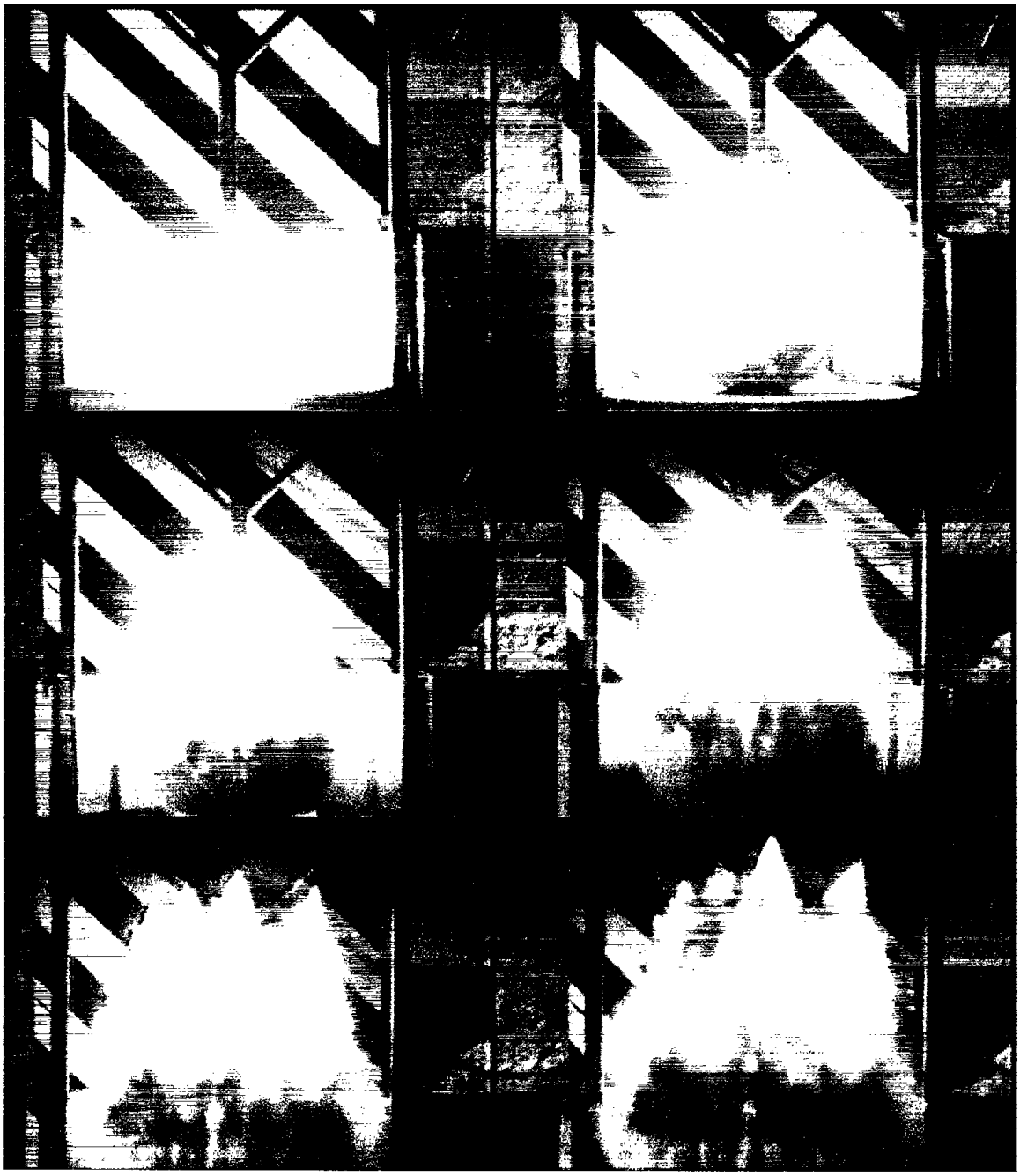

Figure B9. Sequential images from the detonation of 100 g C-4 with 0 cm loose dry silica sand overburden.

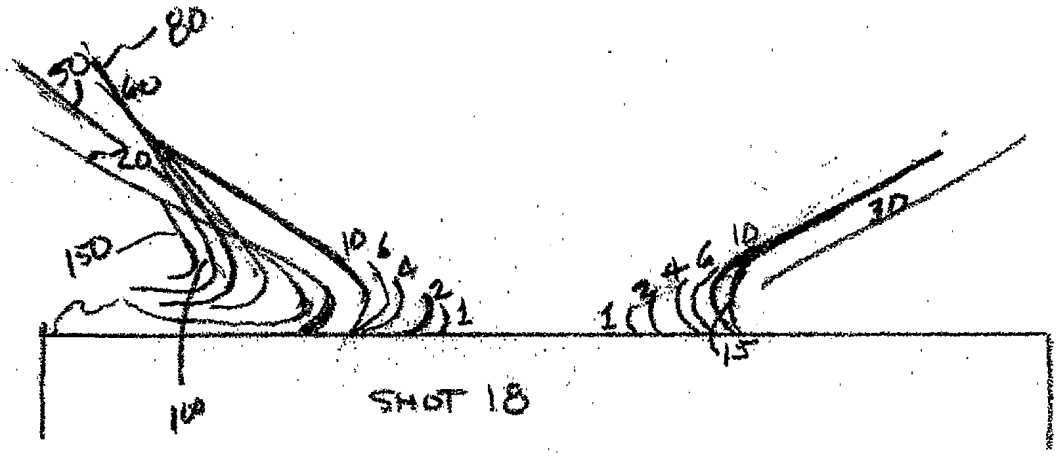

Figure B10. Sequential traces of ejecta expansion from Shot 18 (0 cm DoB). (To convert frame number to elapsed time, multiply by 1.015 x 10^{-4} sec).

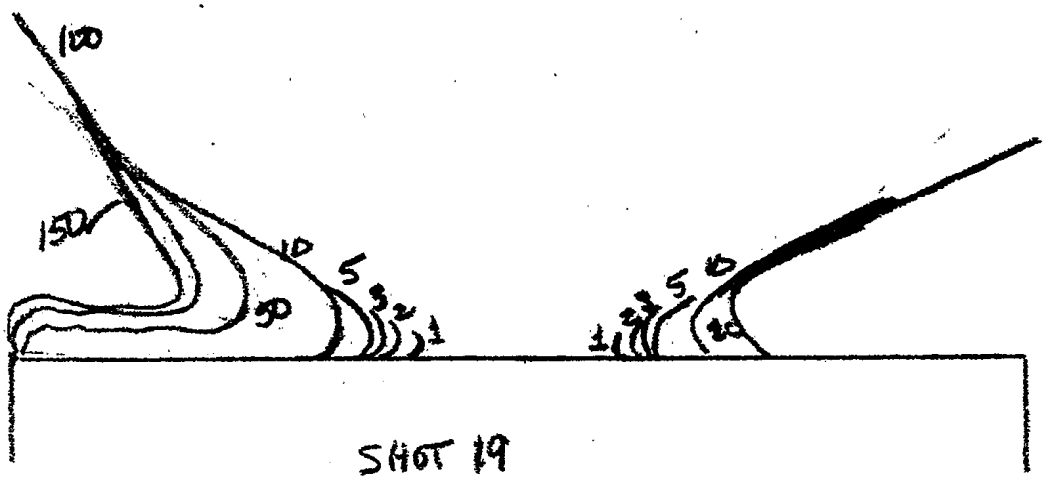

Figure B11. Sequential traces of ejecta expansion from Shot 19 (0 cm DoB). (To convert frame numbers to elapsed time, multiply by 1.015 x 10^{-4} sec).

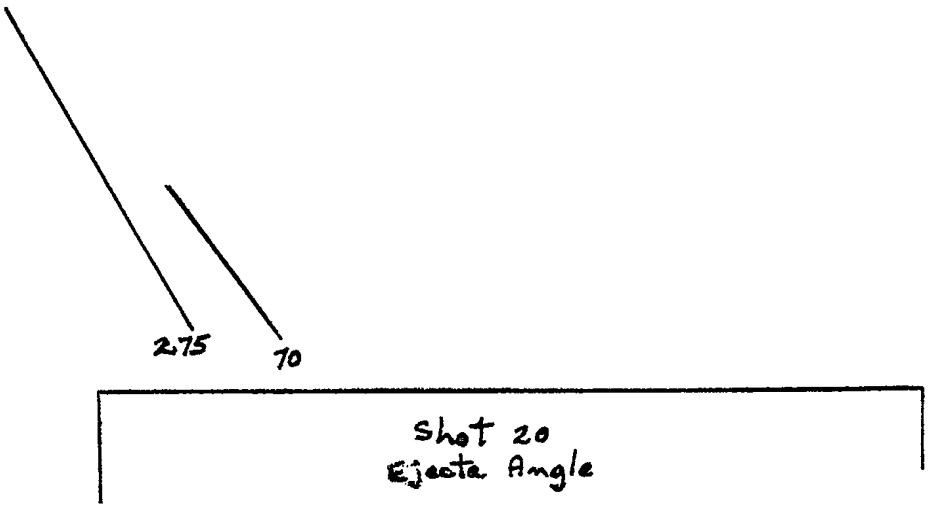

Figure B12. Angle of ejecta at 70 and 275 ms from Shot 20 (0 cm DoB).

ANNEX C

Individual Transducer Records from all Shots

Annex C - Table of Contents

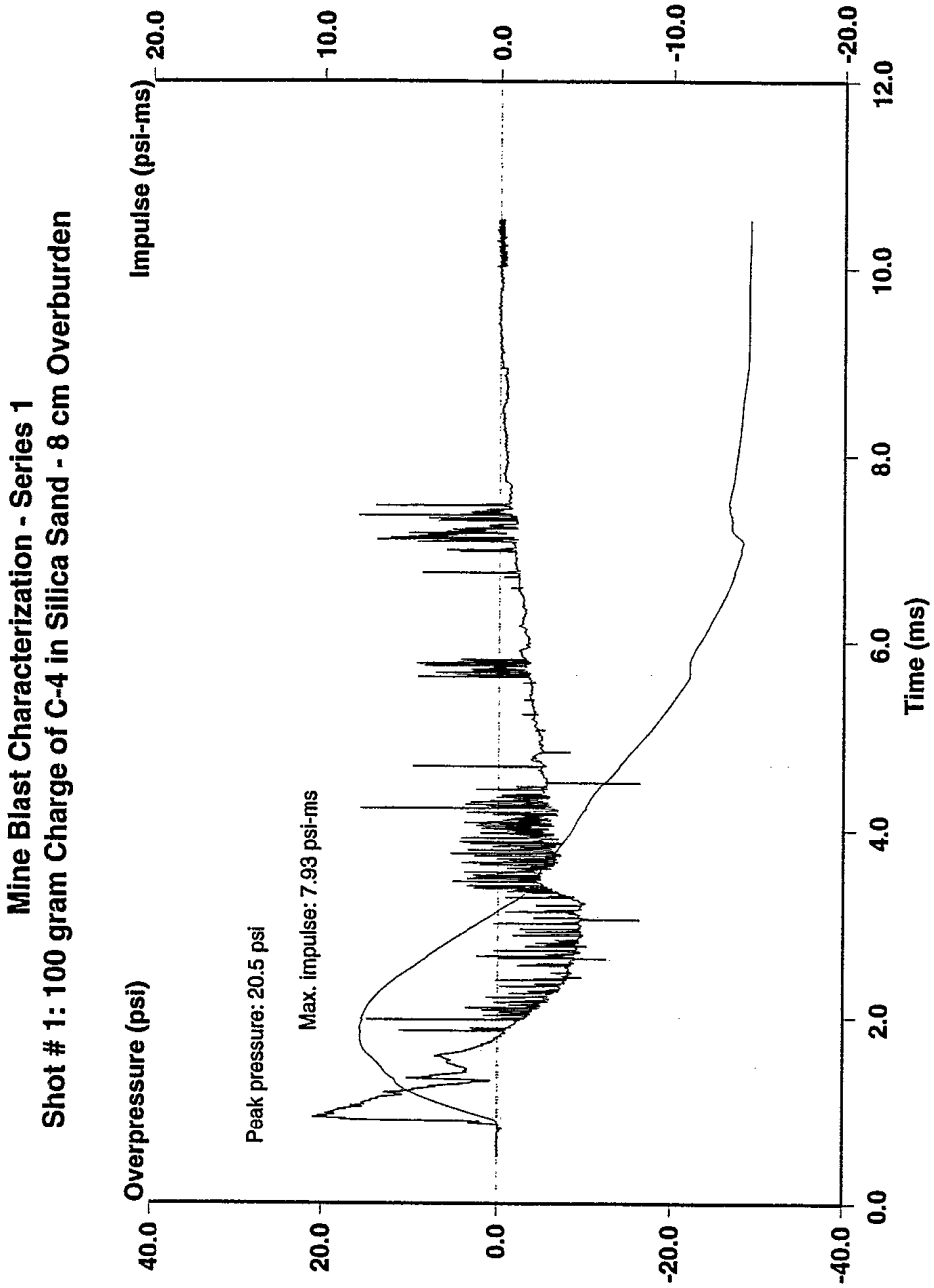

Position 1 (38 cm), Air Shock, 2nd Order 100 kHz Butterworth Filter

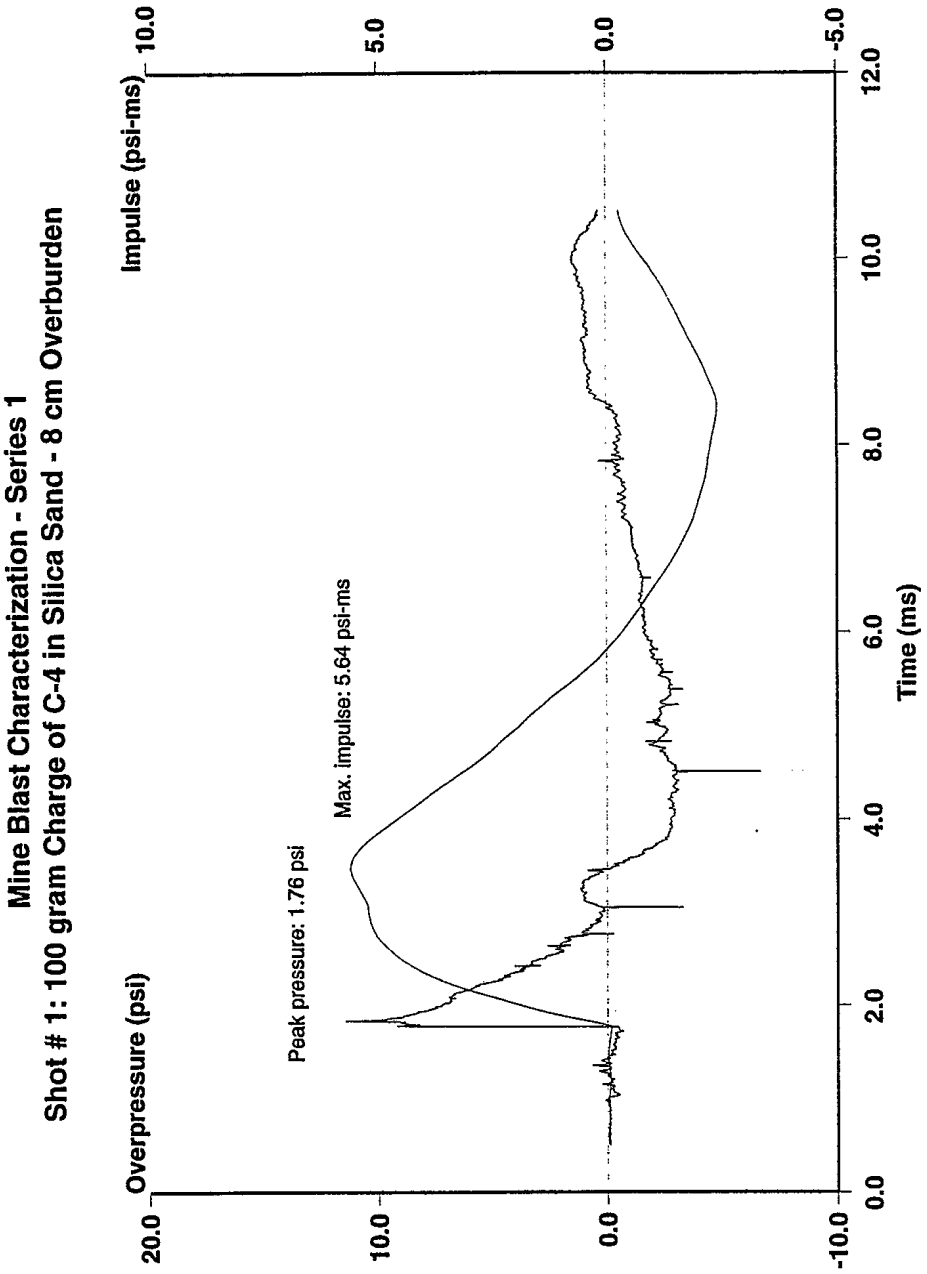

Position 2 (78 cm), Air Shock, 2nd Order 100 kHz Butterworth Filter

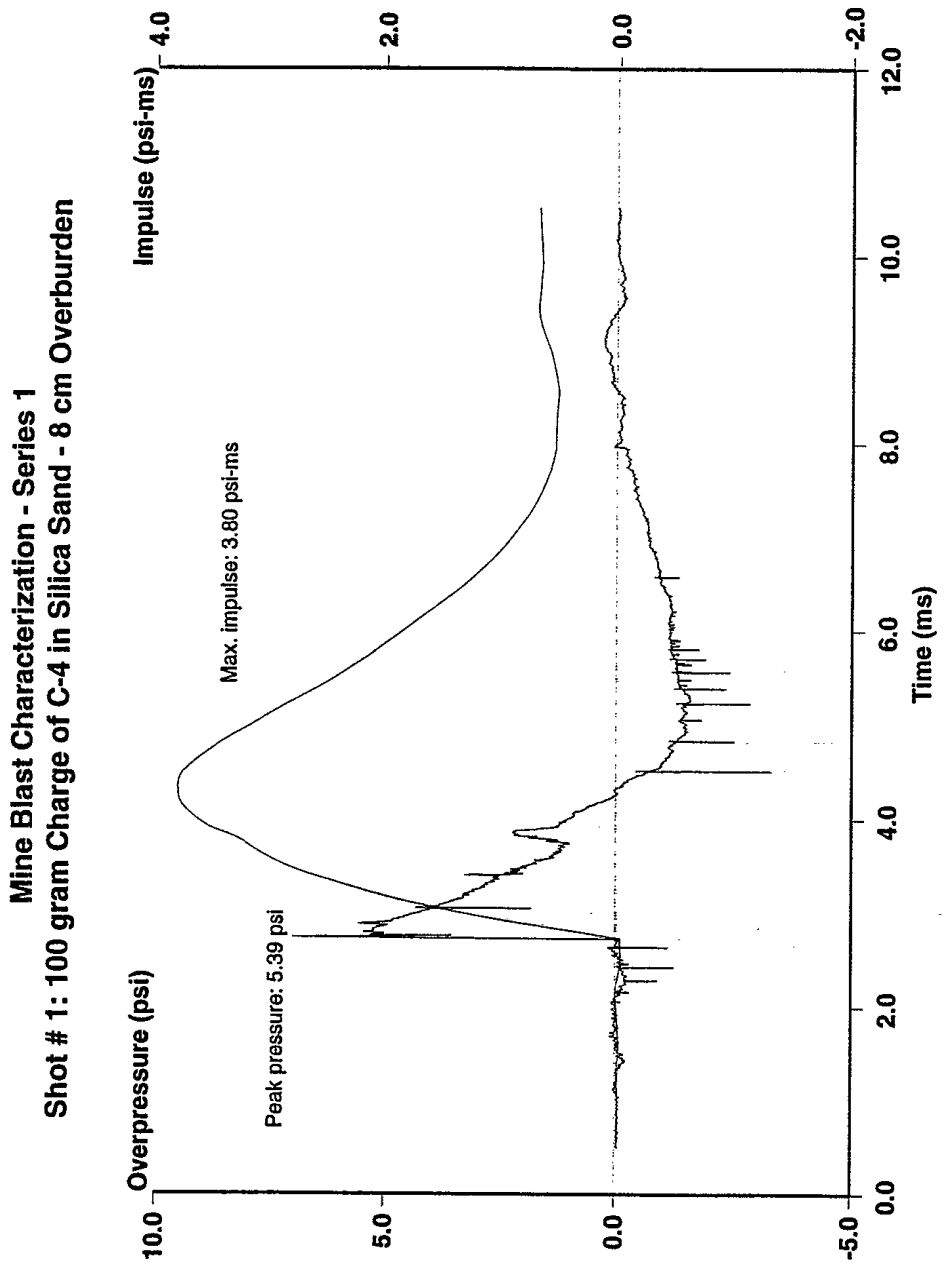

Position 3 (118 cm), Air Shock, 2nd Order 100 kHz Butterworth Filter

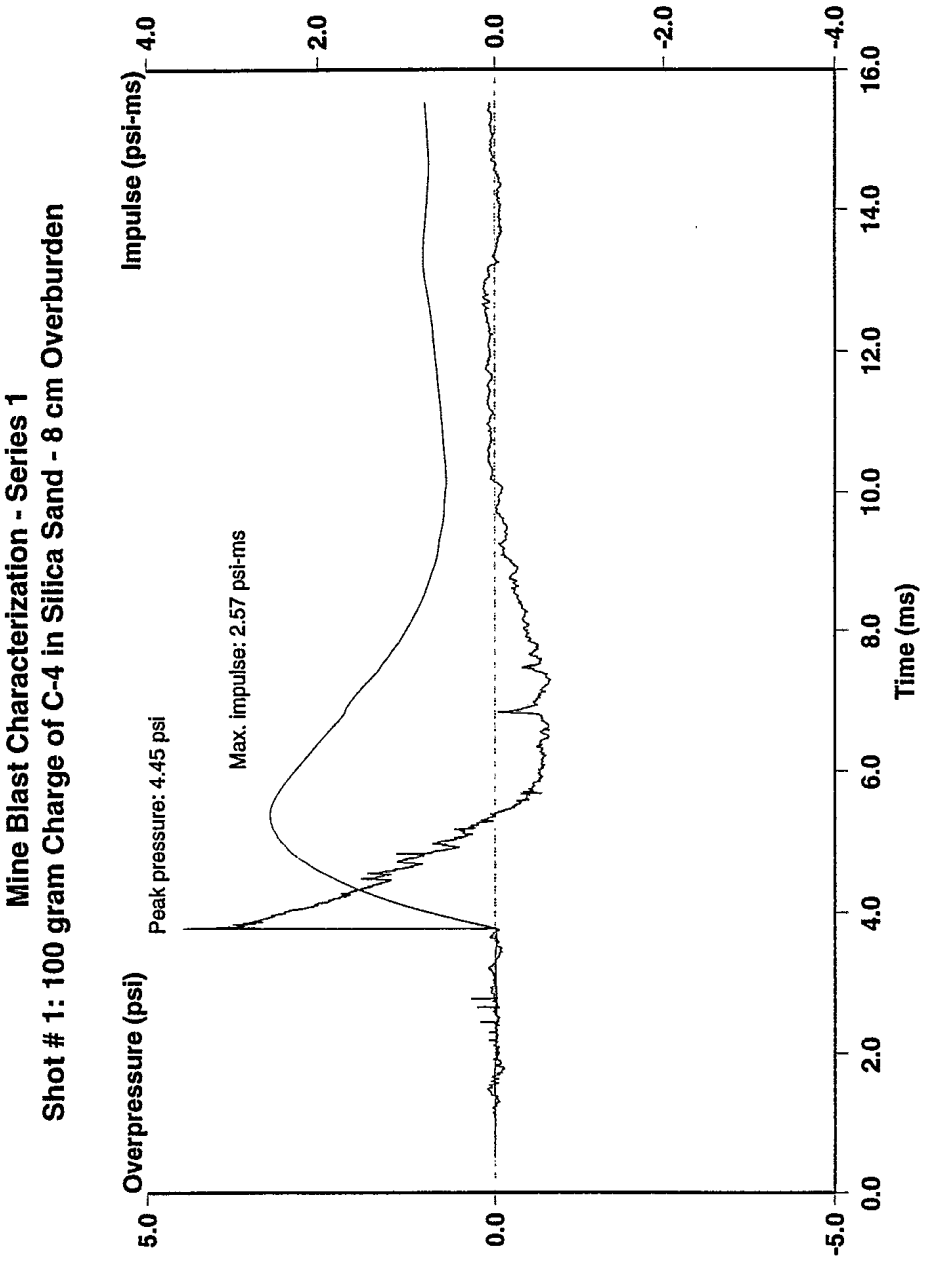

Position 4 (158 cm), Air Shock, 2nd Order 100 kHz Butterworth Filter

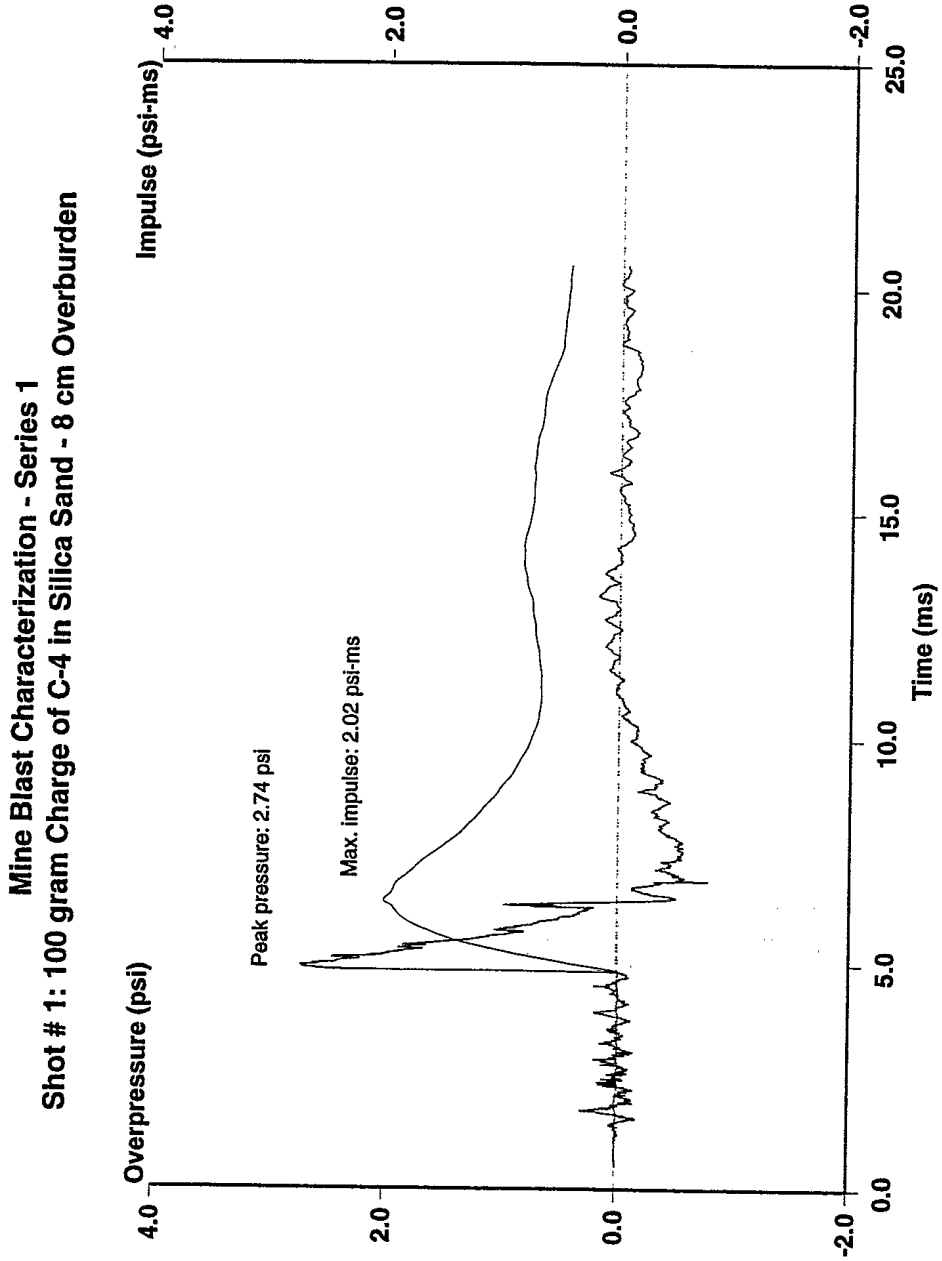

Position 5 (198 cm), Air Shock, 2nd Order 100 kHz Butterworth Filter

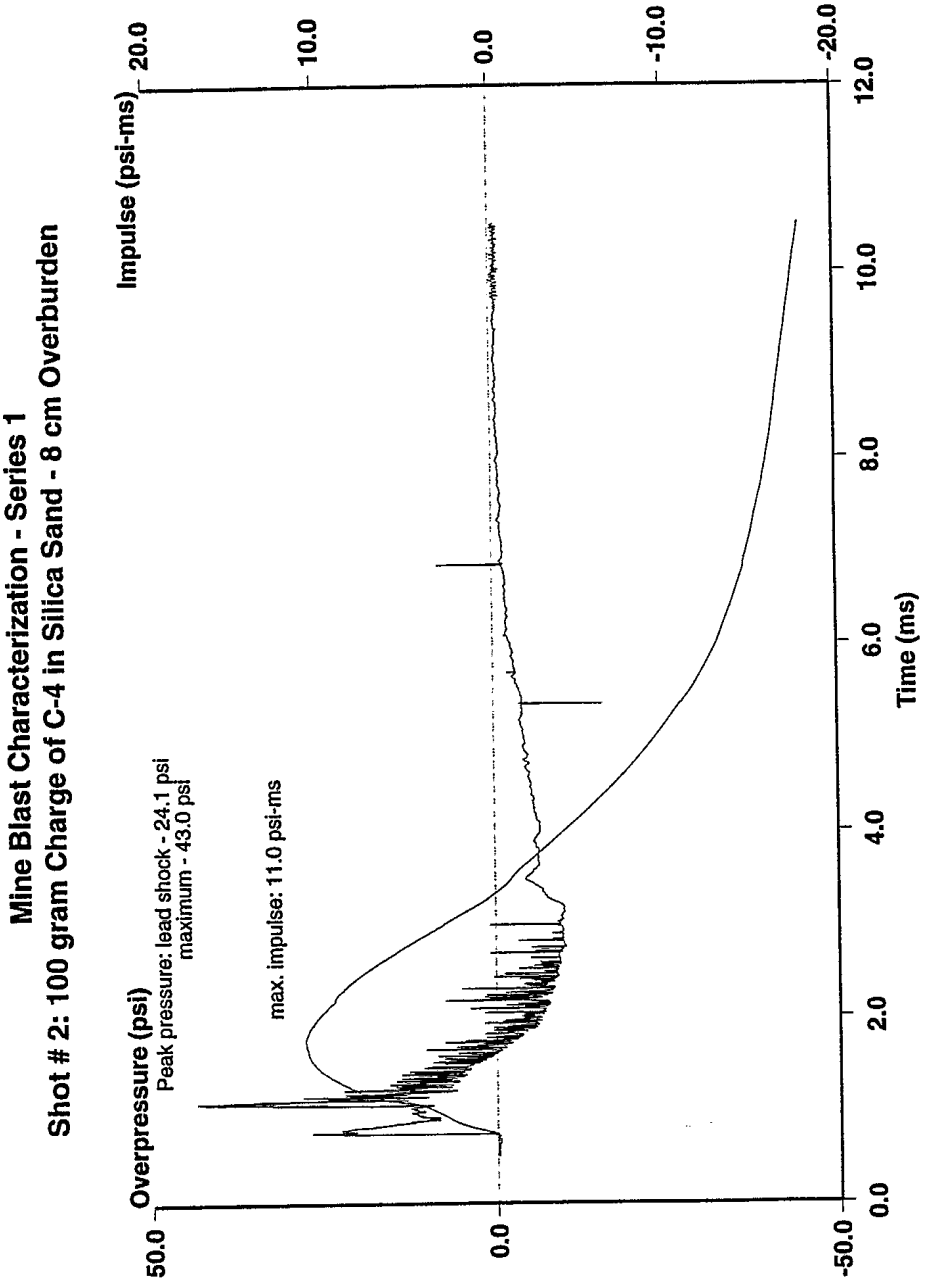

Position 1 (38 cm), Air Shock, 2nd Order 100 kHz Butterworth Filter

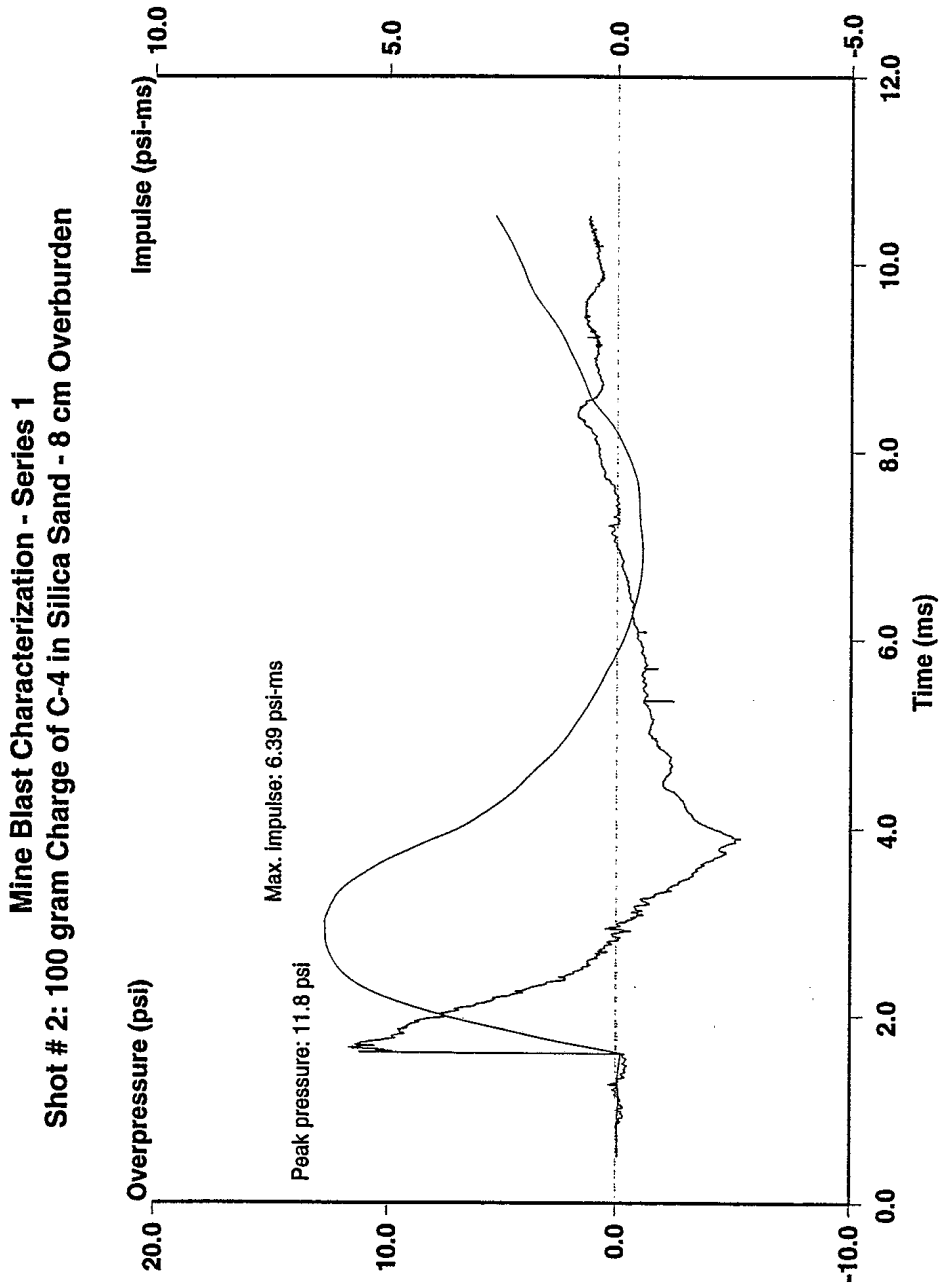

Position 2 (78 cm), Air Shock, 2nd Order 100 kHz Butterworth Filter

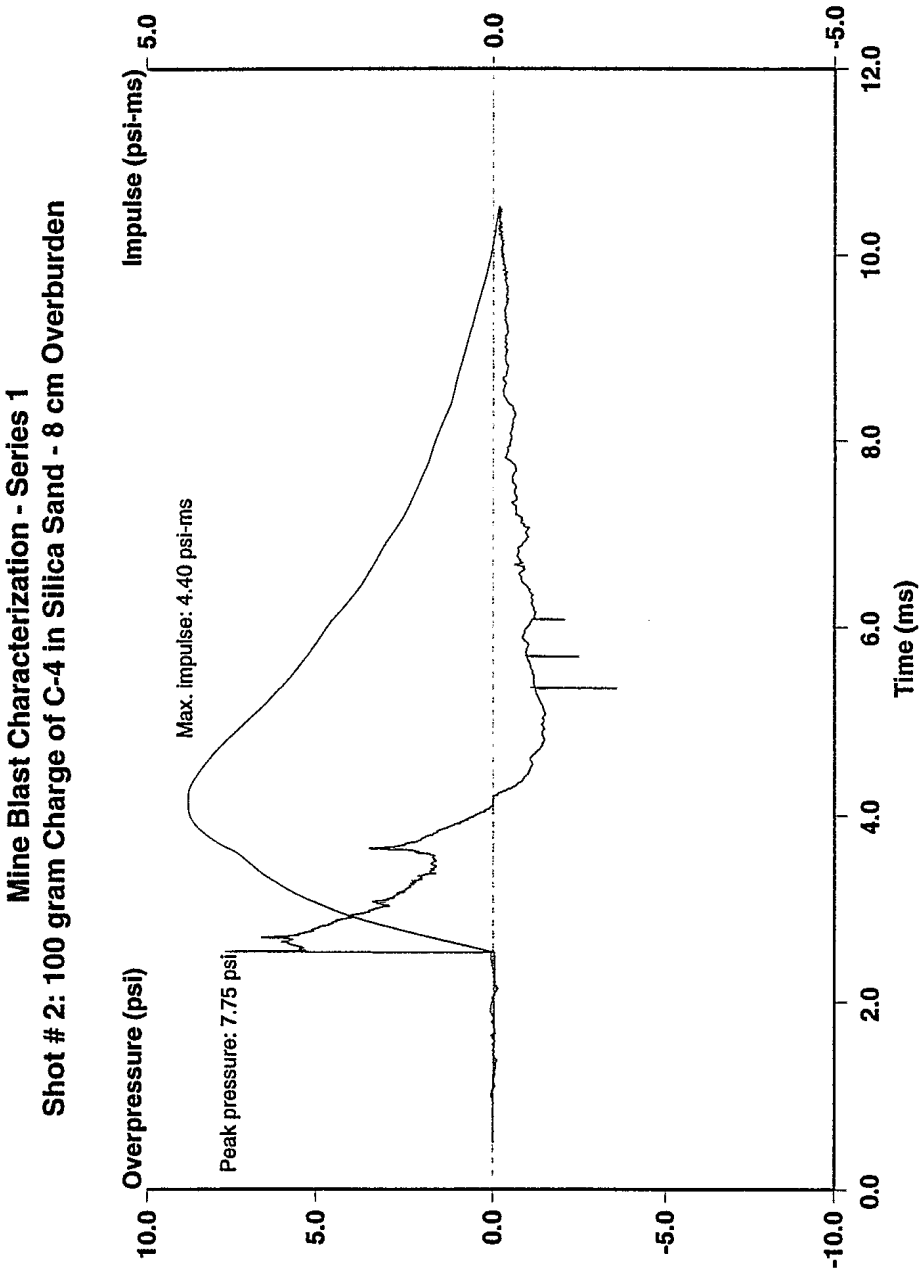

Position 3 (118 cm), Air Shock, 2nd Order 100 kHz Butterworth Filter

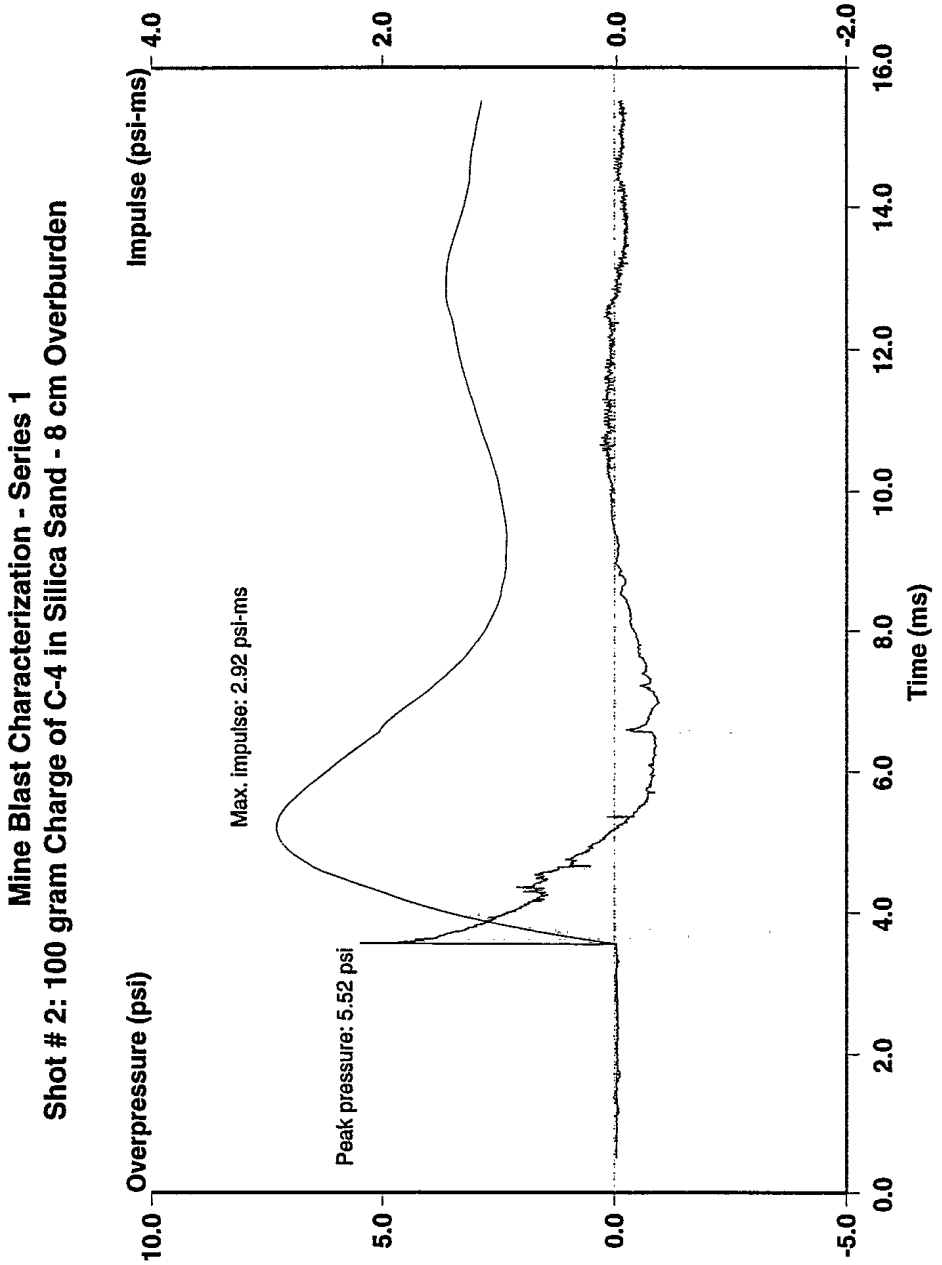

Position 4 (158 cm), Air Shock, 2nd Order 100 kHz Butterworth Filter

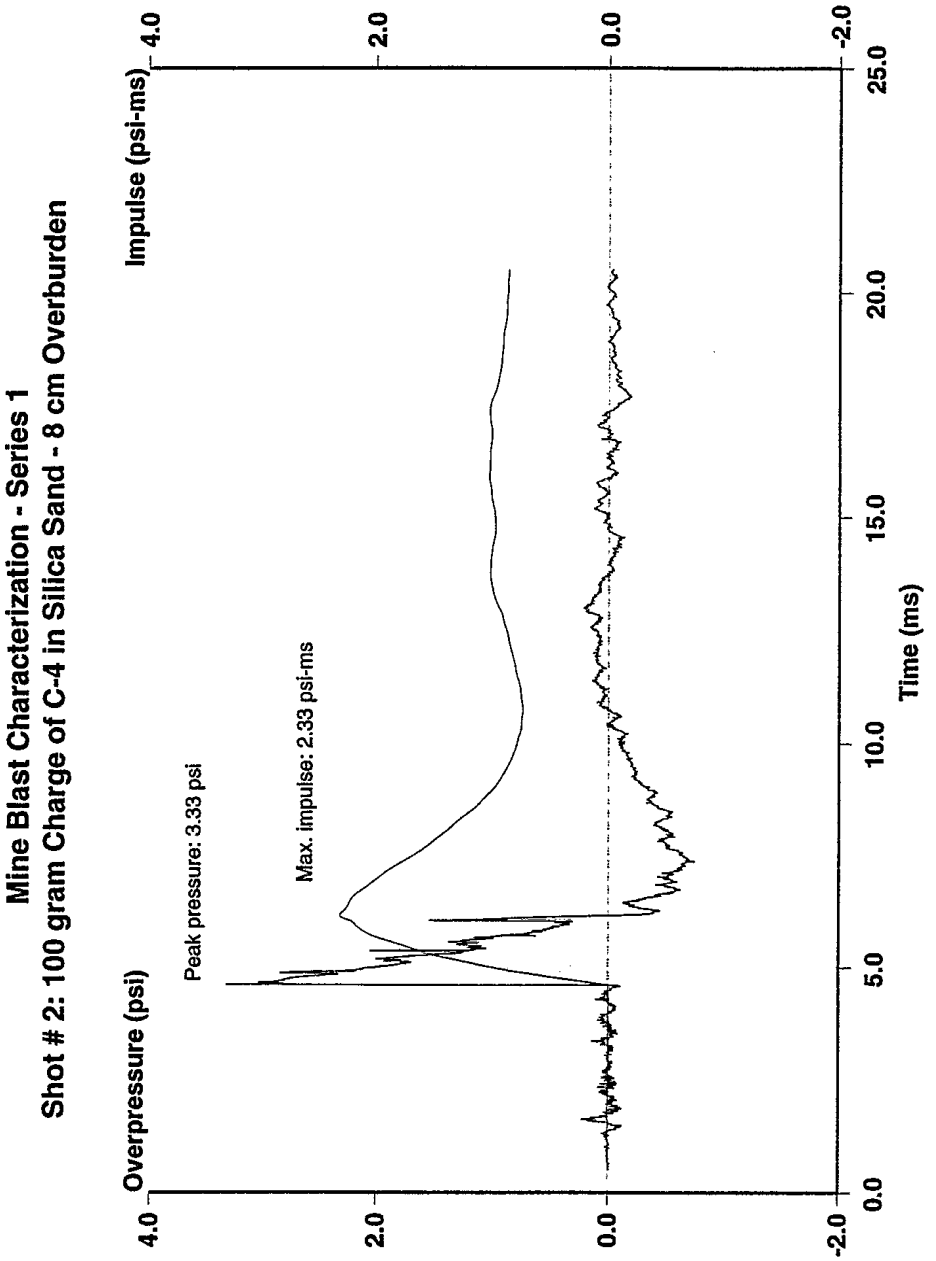

Position 5 (198 cm), Air Shock, 2nd Order 100 kHz Butterworth Filter

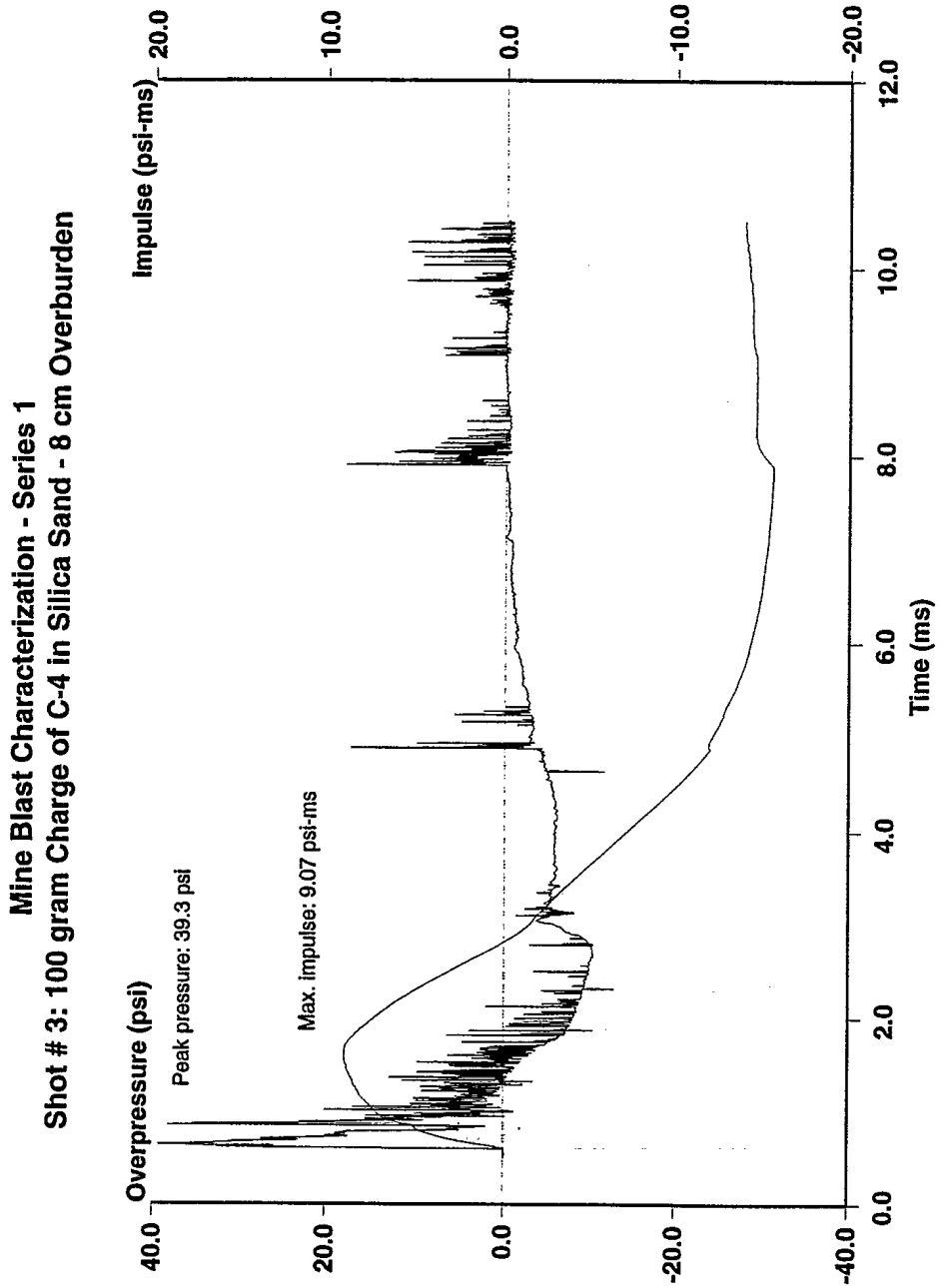

Position 1 (38 cm), Air Shock, 2nd Order 100 kHz Butterworth Filter

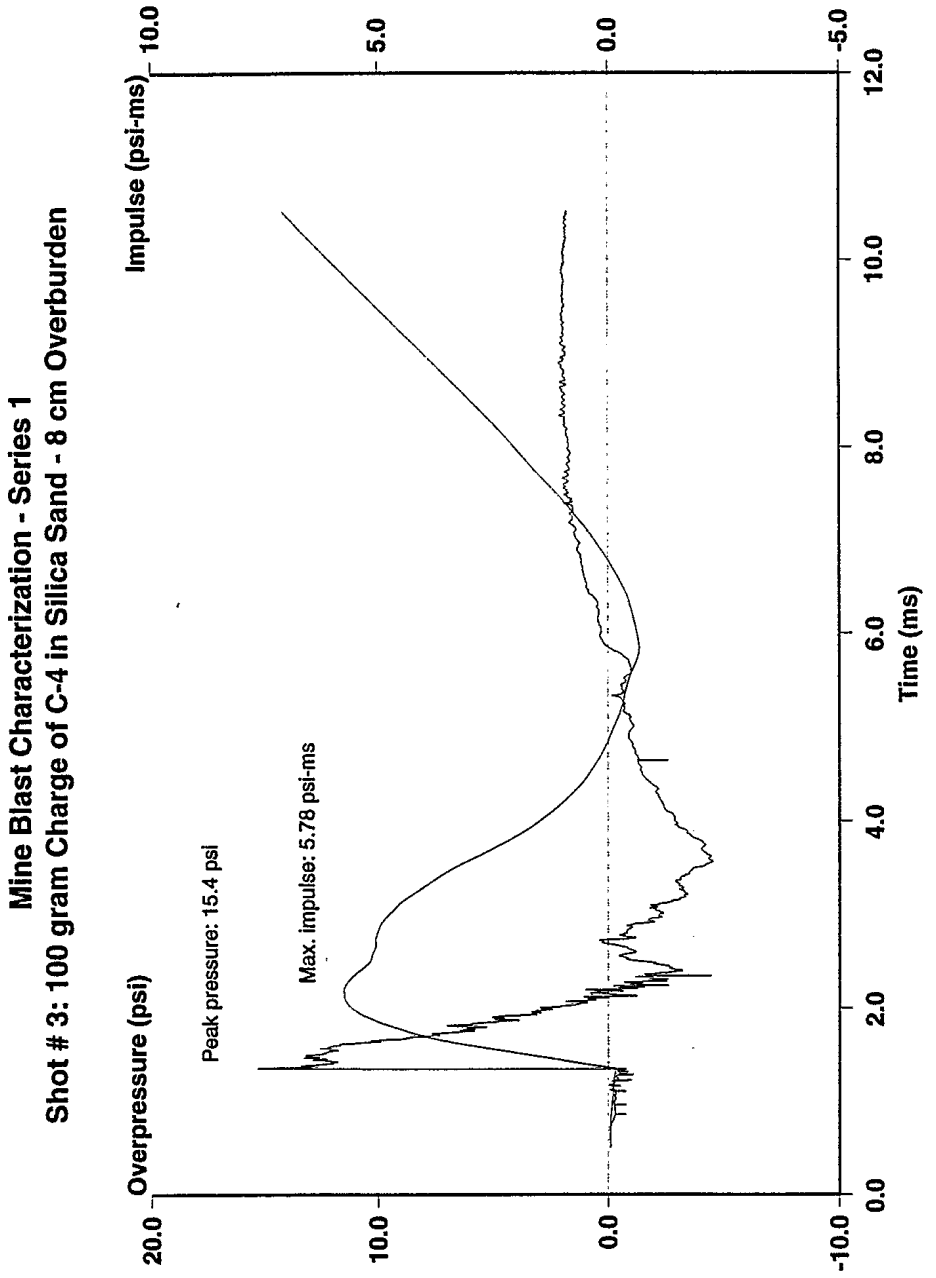

Position 2 (78 cm), Air Shock, 2nd Order 100 kHz Butterworth Filter

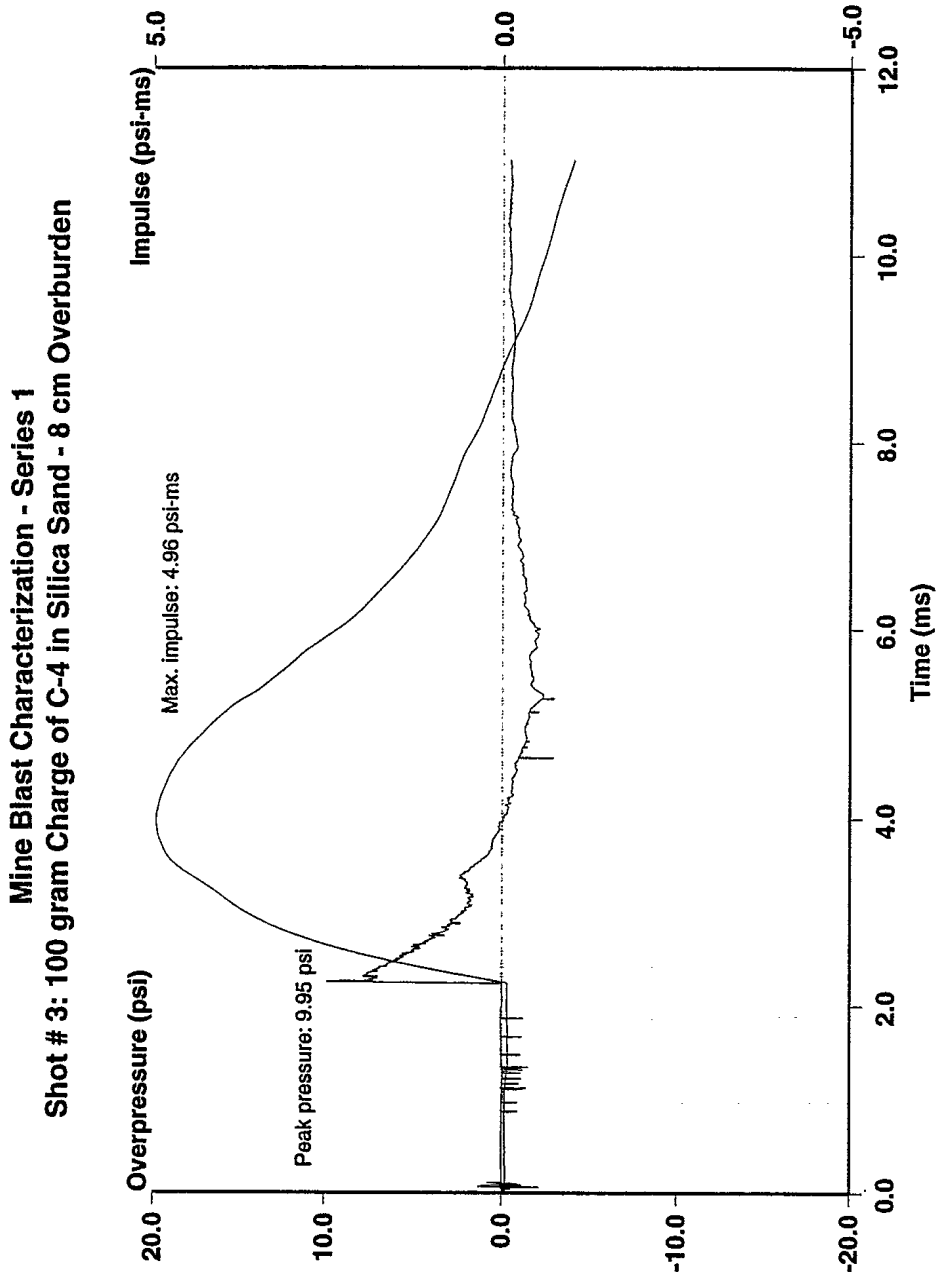

Position 3 (118 cm), Air Shock, 2nd Order 100 kHz Butterworth Filter

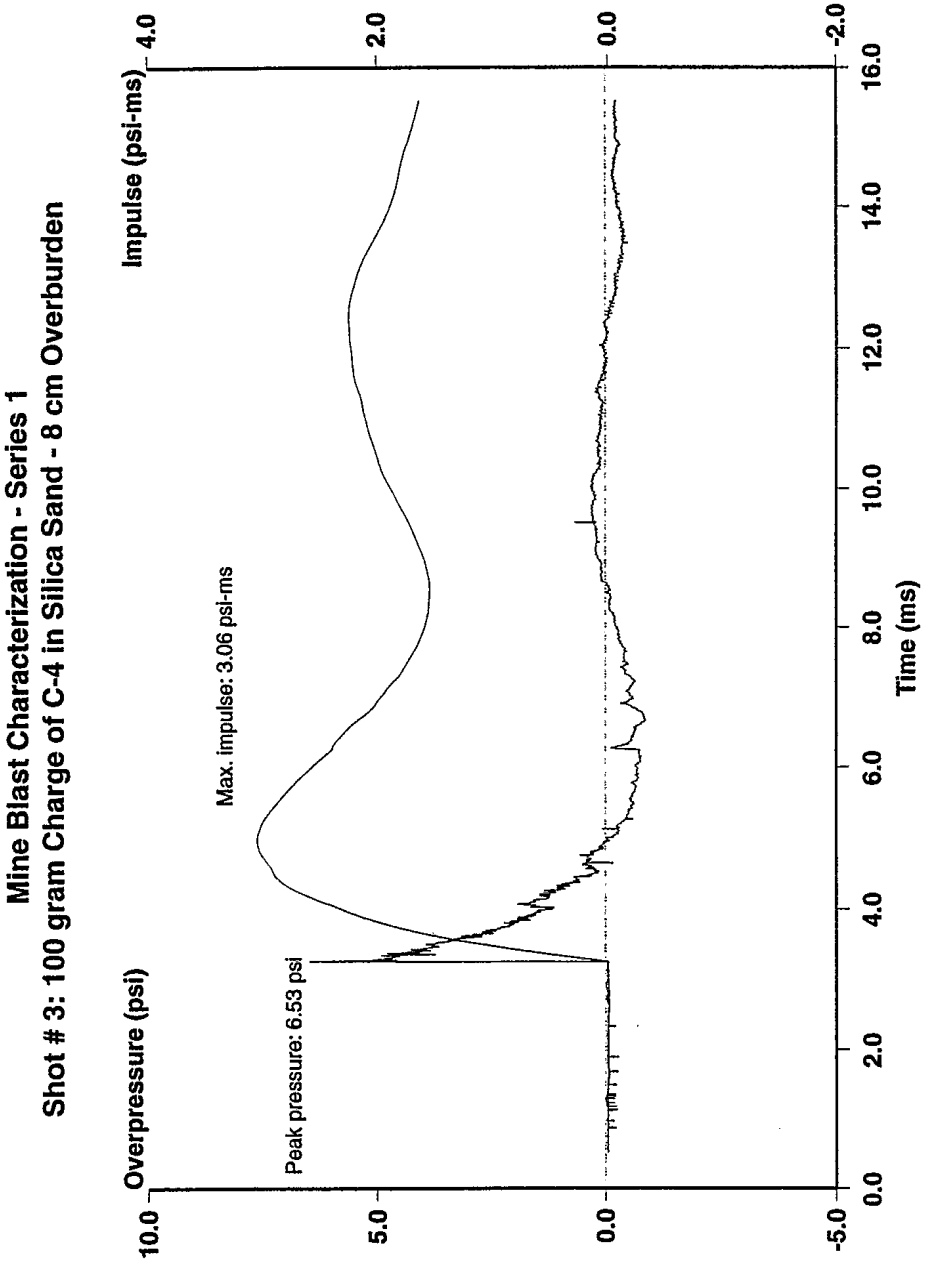

Position 4 (158 cm), Air Shock, 2nd Order 100 kHz Butterworth Filter

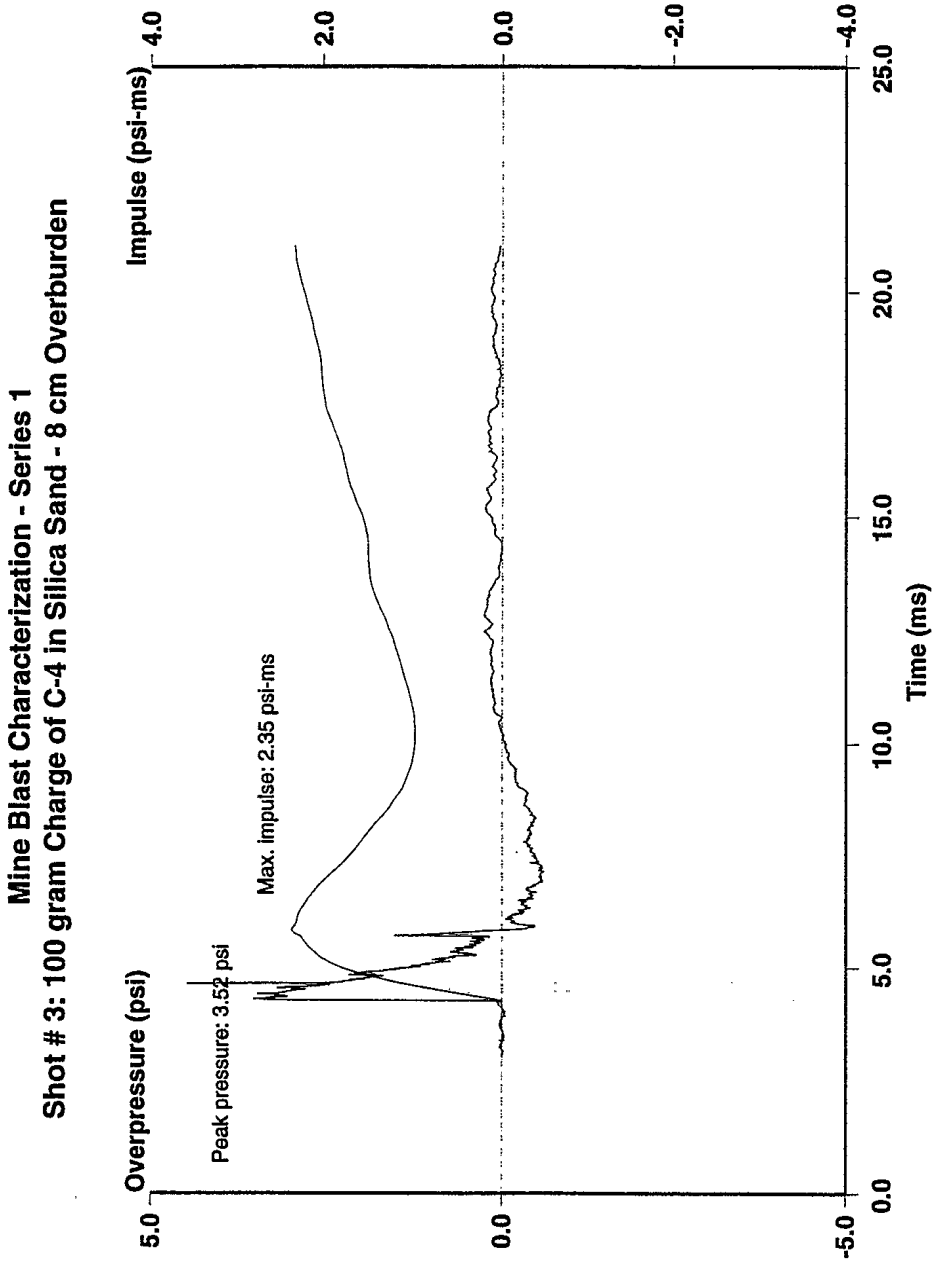

Position 5 (198 cm), Air Shock, 2nd Order 100 kHz Butterworth Filter

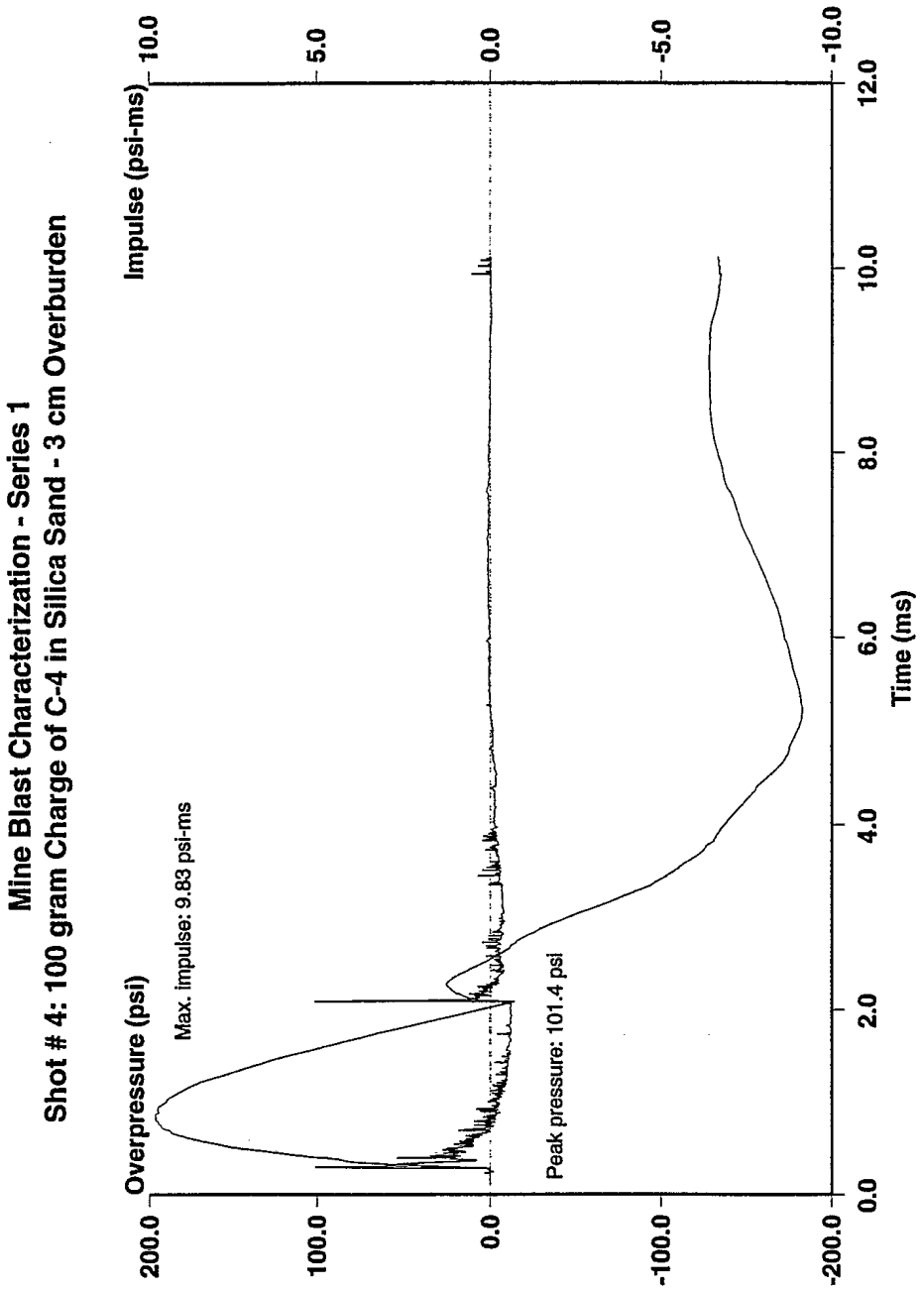

Position 1 (33 cm), Air Shock, 2nd Order 100 kHz Butterworth Filter

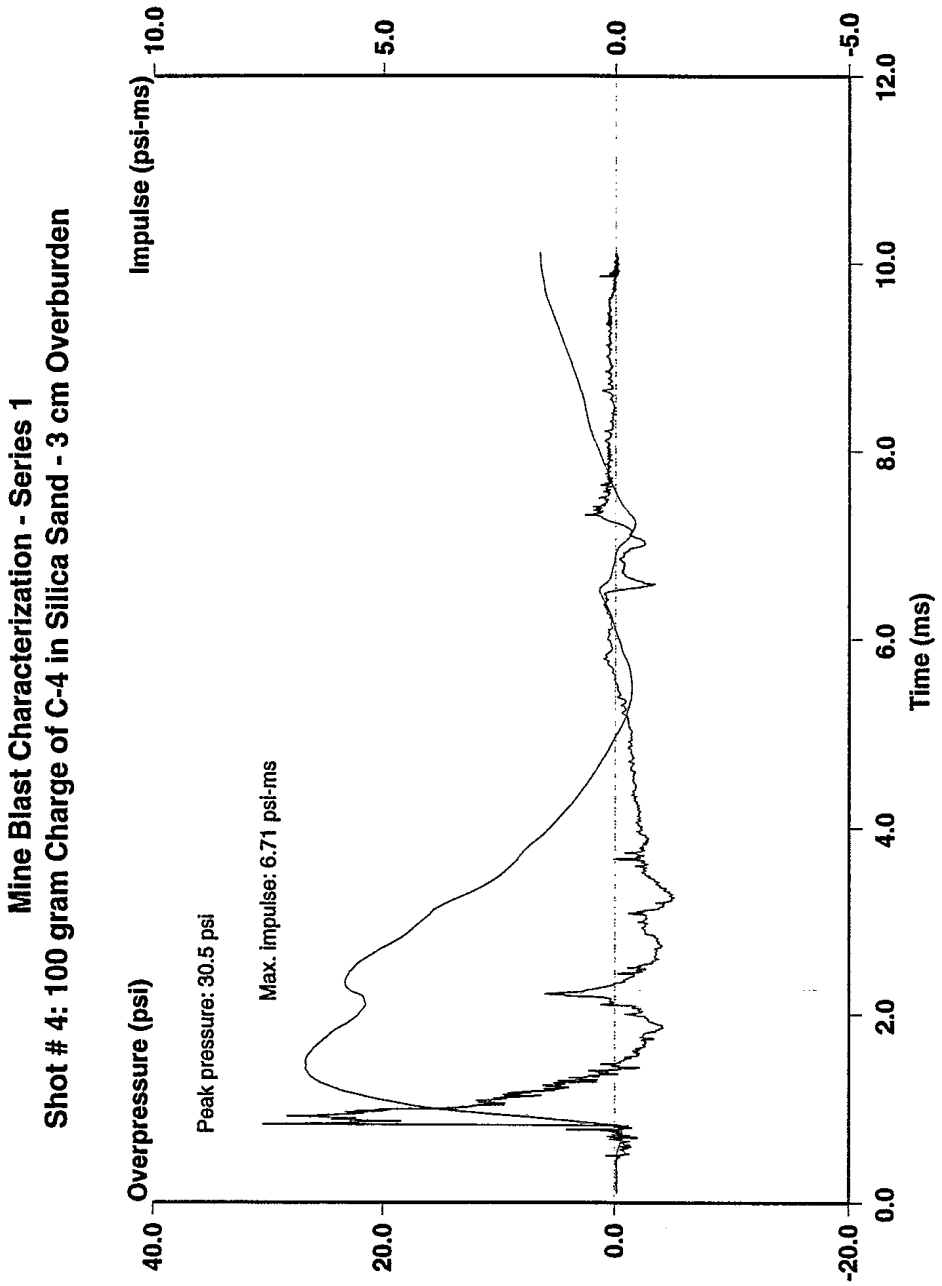

Position 2 (73 cm), Air Shock, 2nd Order 100 kHz Butterworth Filter

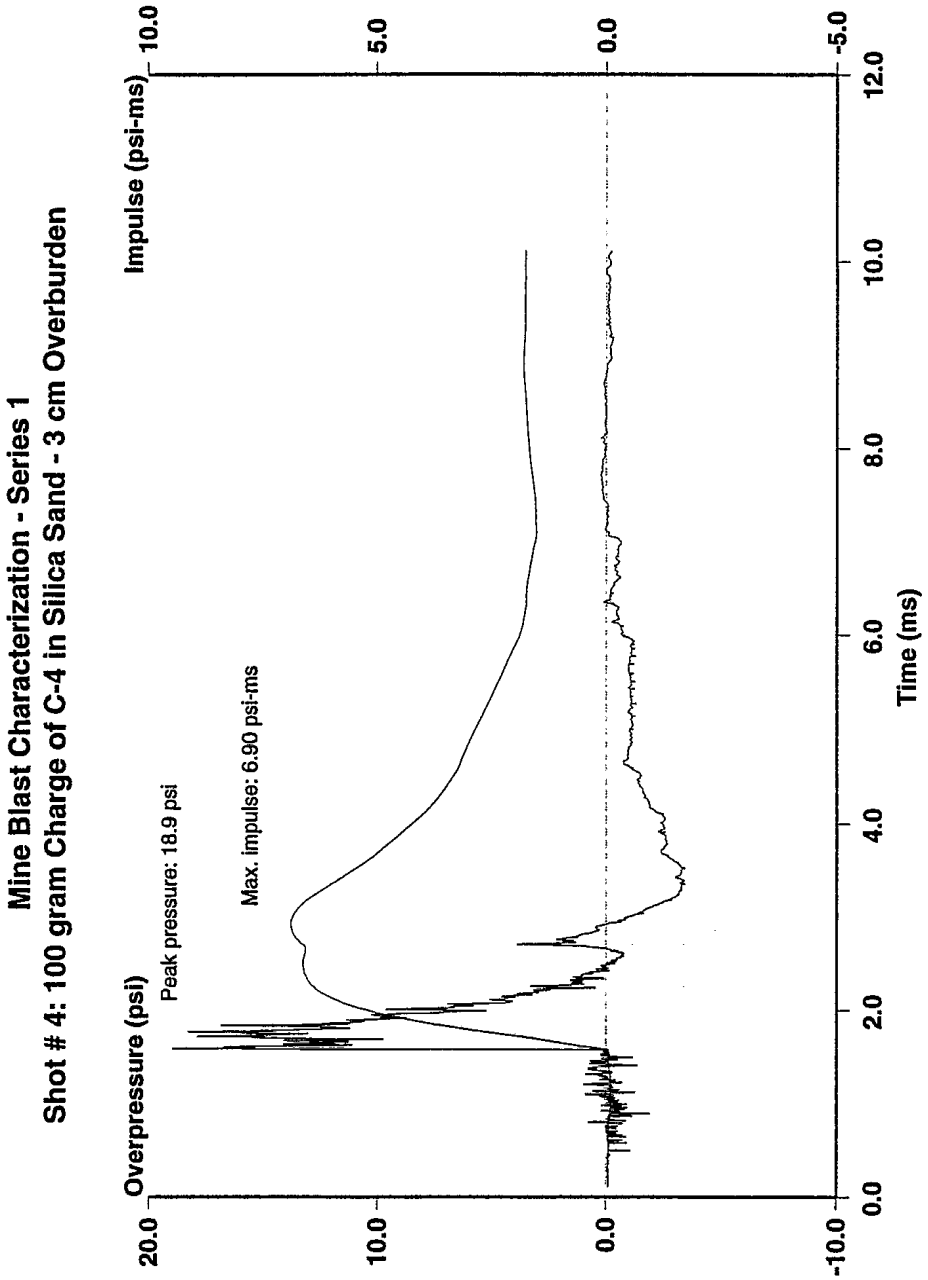

Position 3 (113 cm), Air Shock, 2nd Order 100 kHz Butterworth Filter

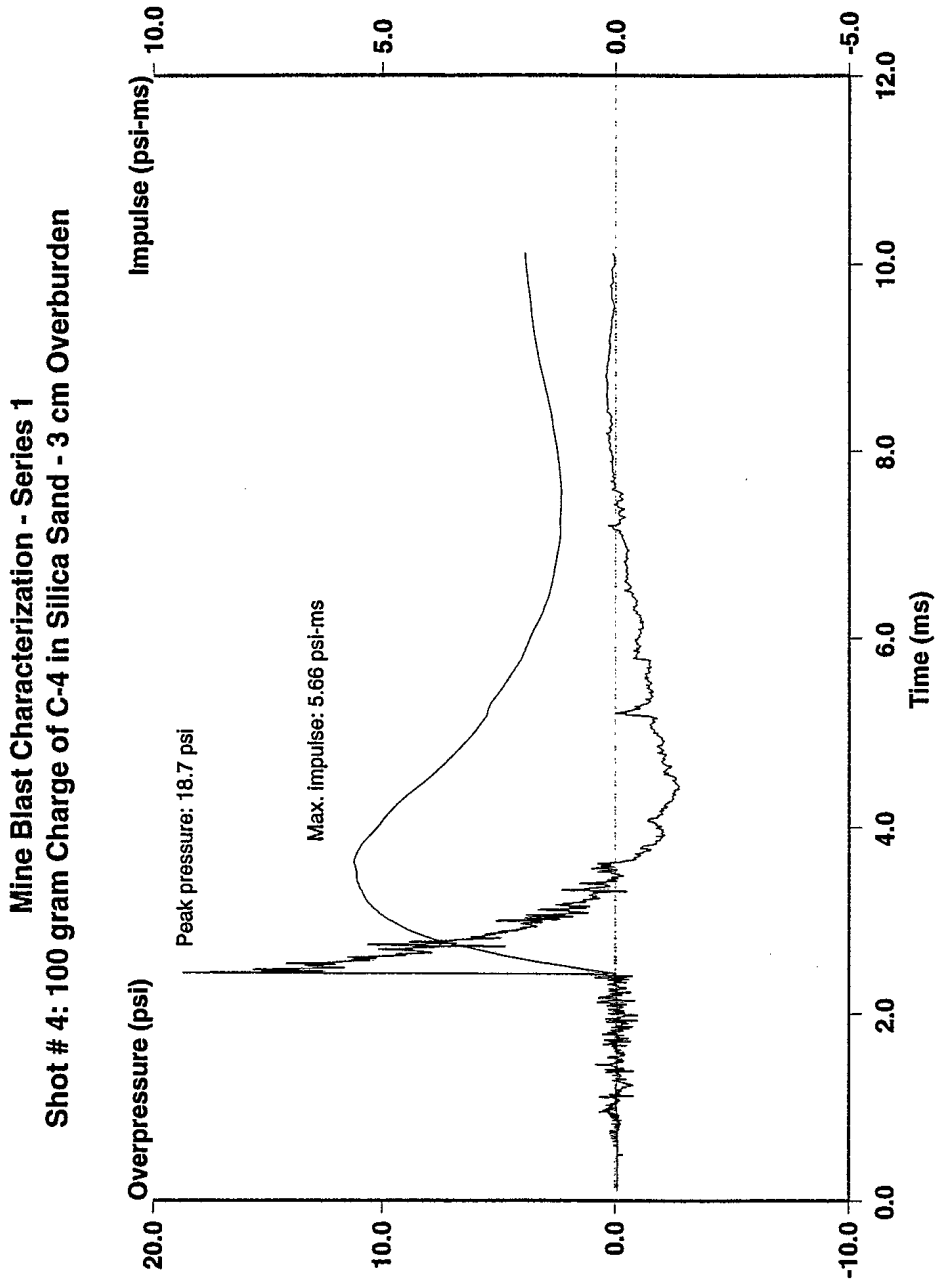

Position 4 (153 cm), Air Shock, 2nd Order 100 kHz Butterworth Filter

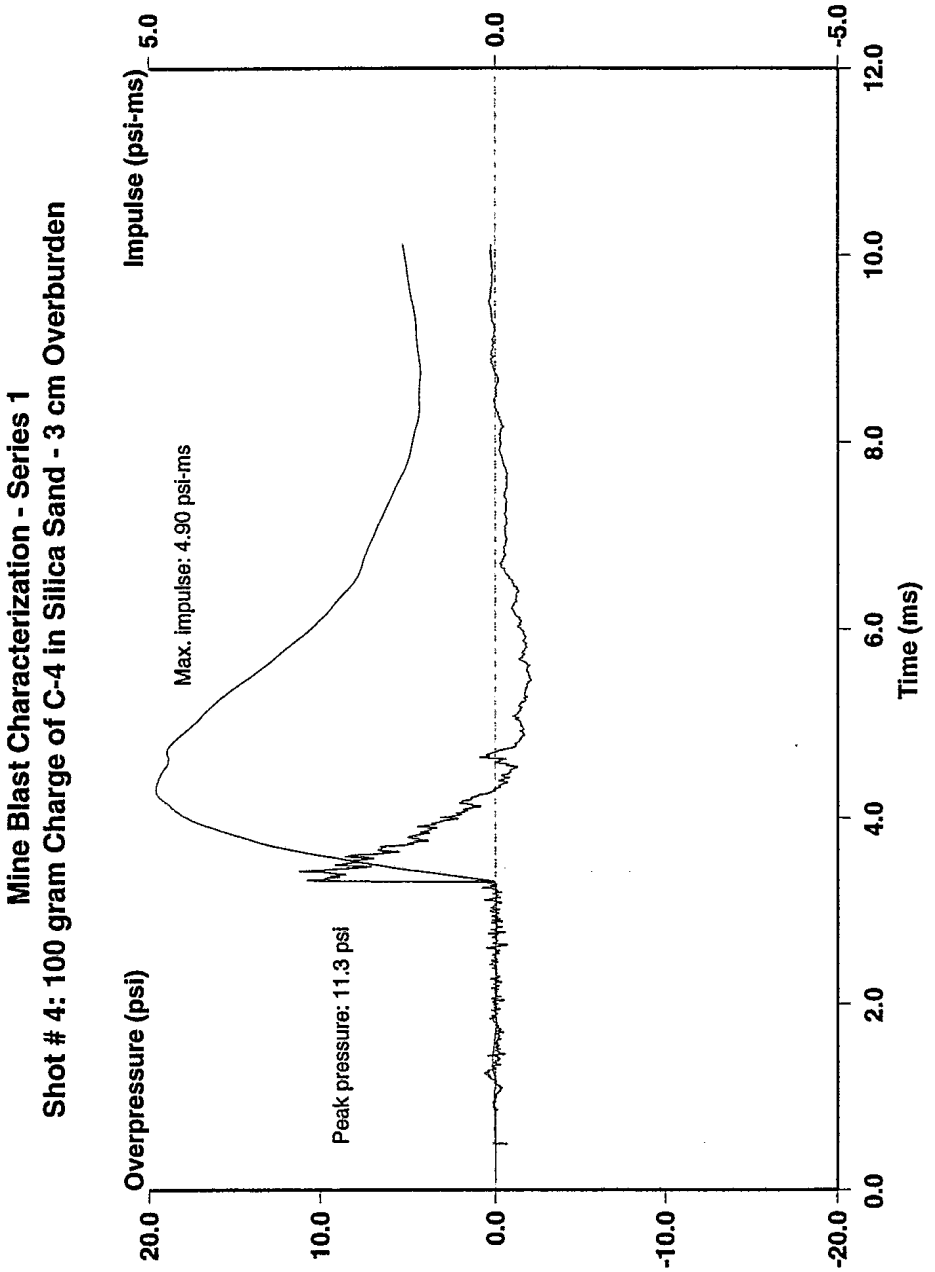

Position 5 (193 cm), Air Shock, 2nd Order 100 kHz Butterworth Filter

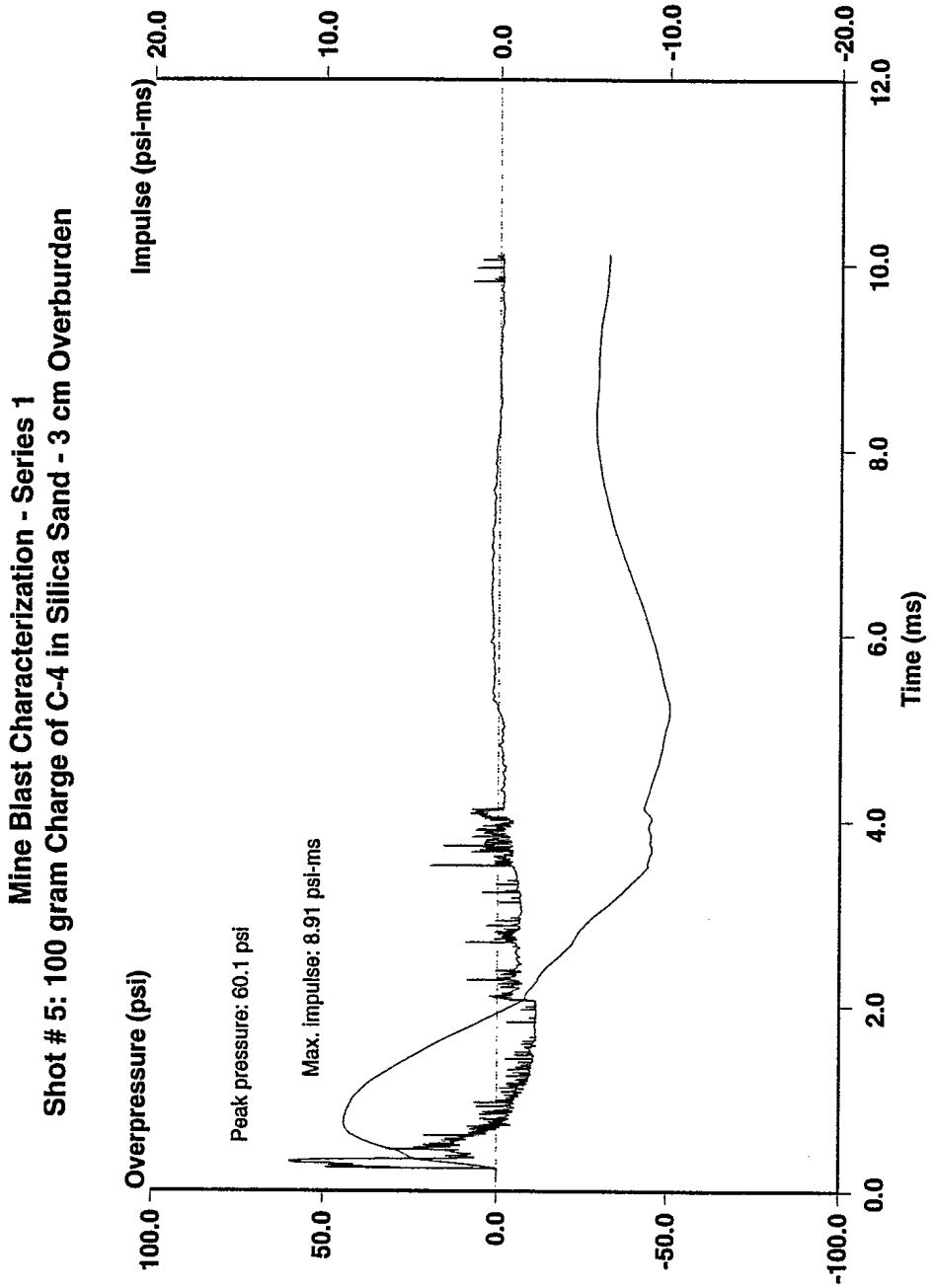

Position 1 (33 cm), Air Shock, 2nd Order 100 kHz Butterworth Filter

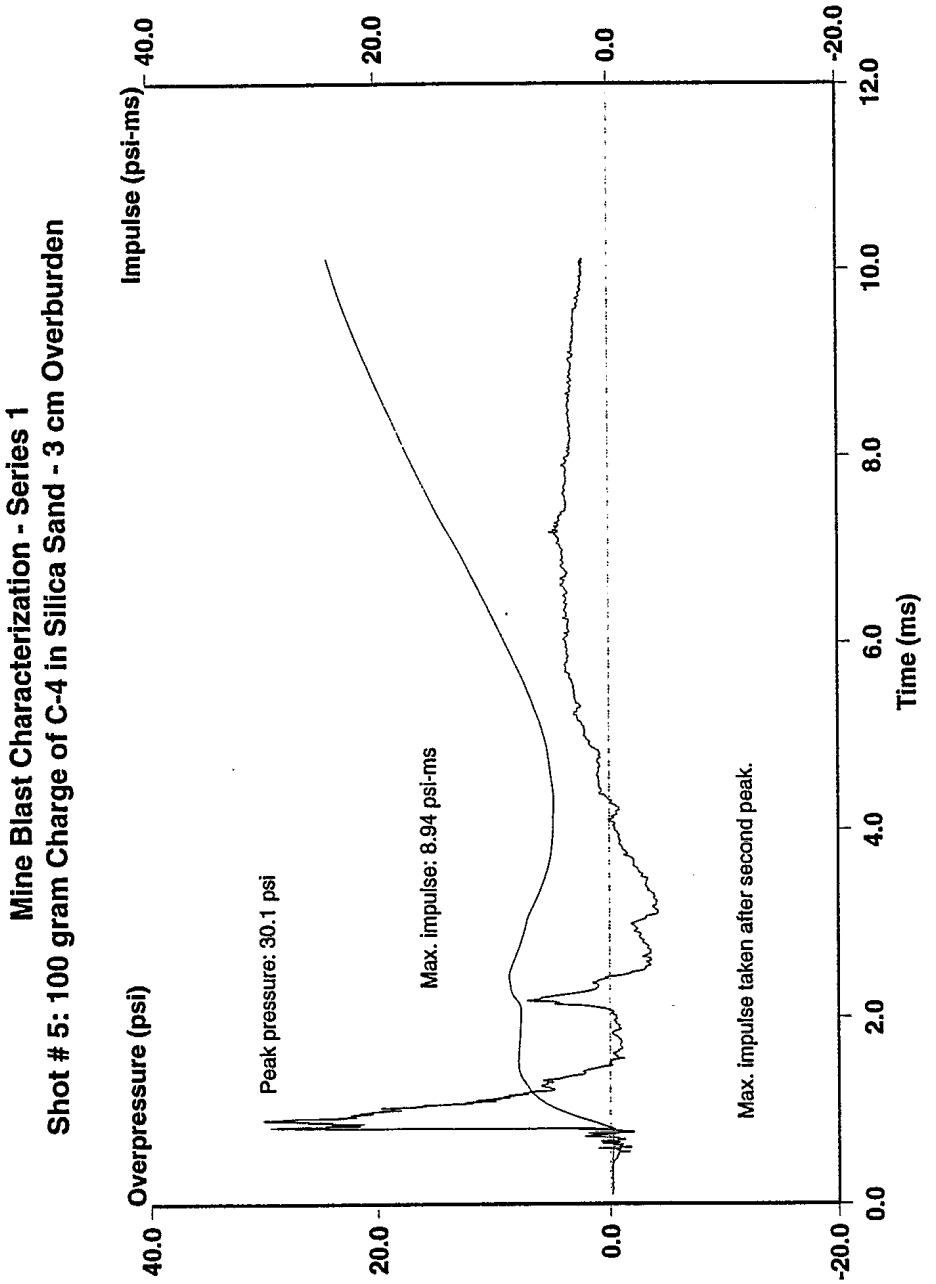

Position 2 (73 cm), Air Shock, 2nd Order 100 kHz Butterworth Filter

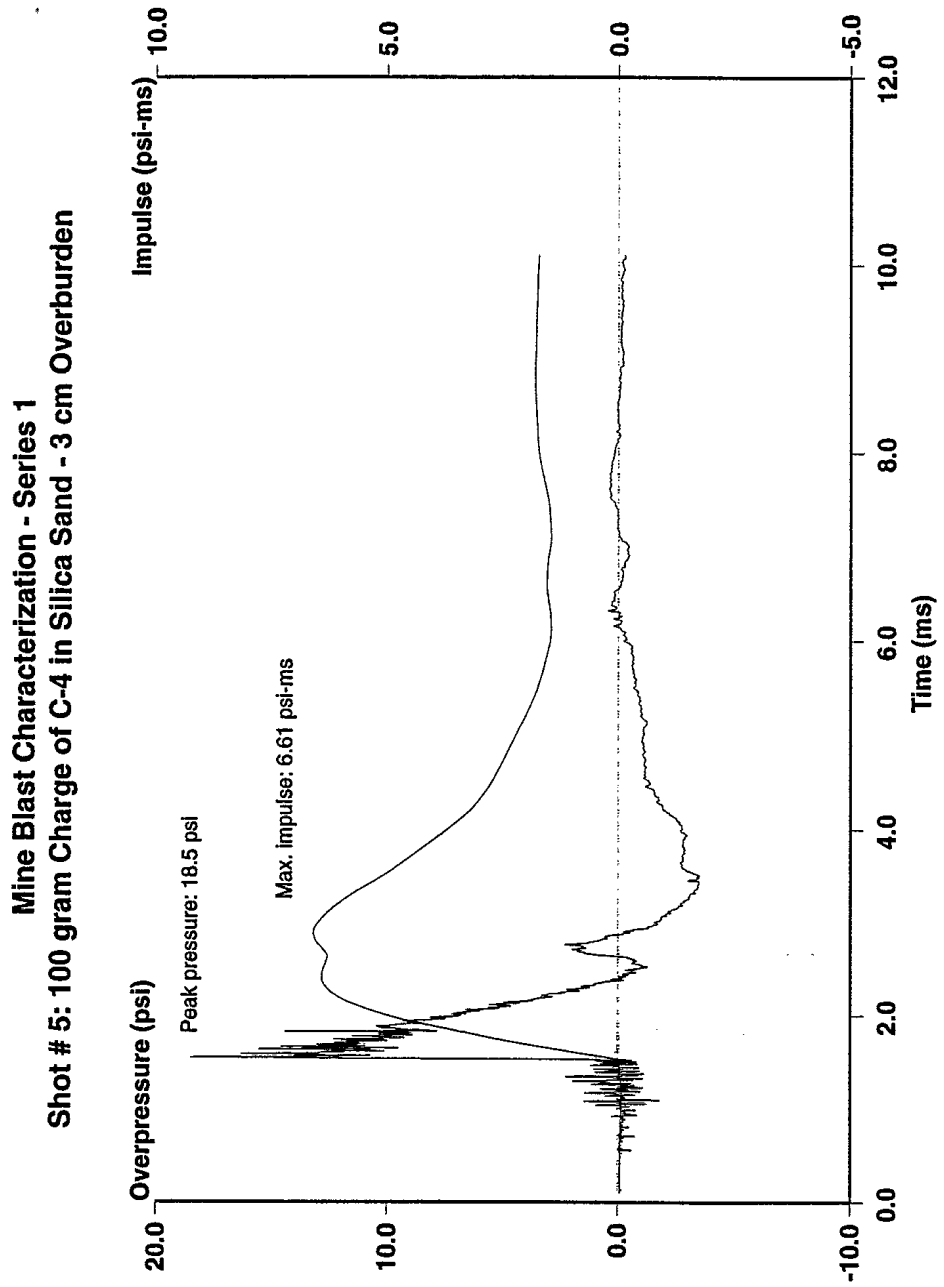

Position 3 (113 cm), Air Shock, 2nd Order 100 kHz Butterworth Filter

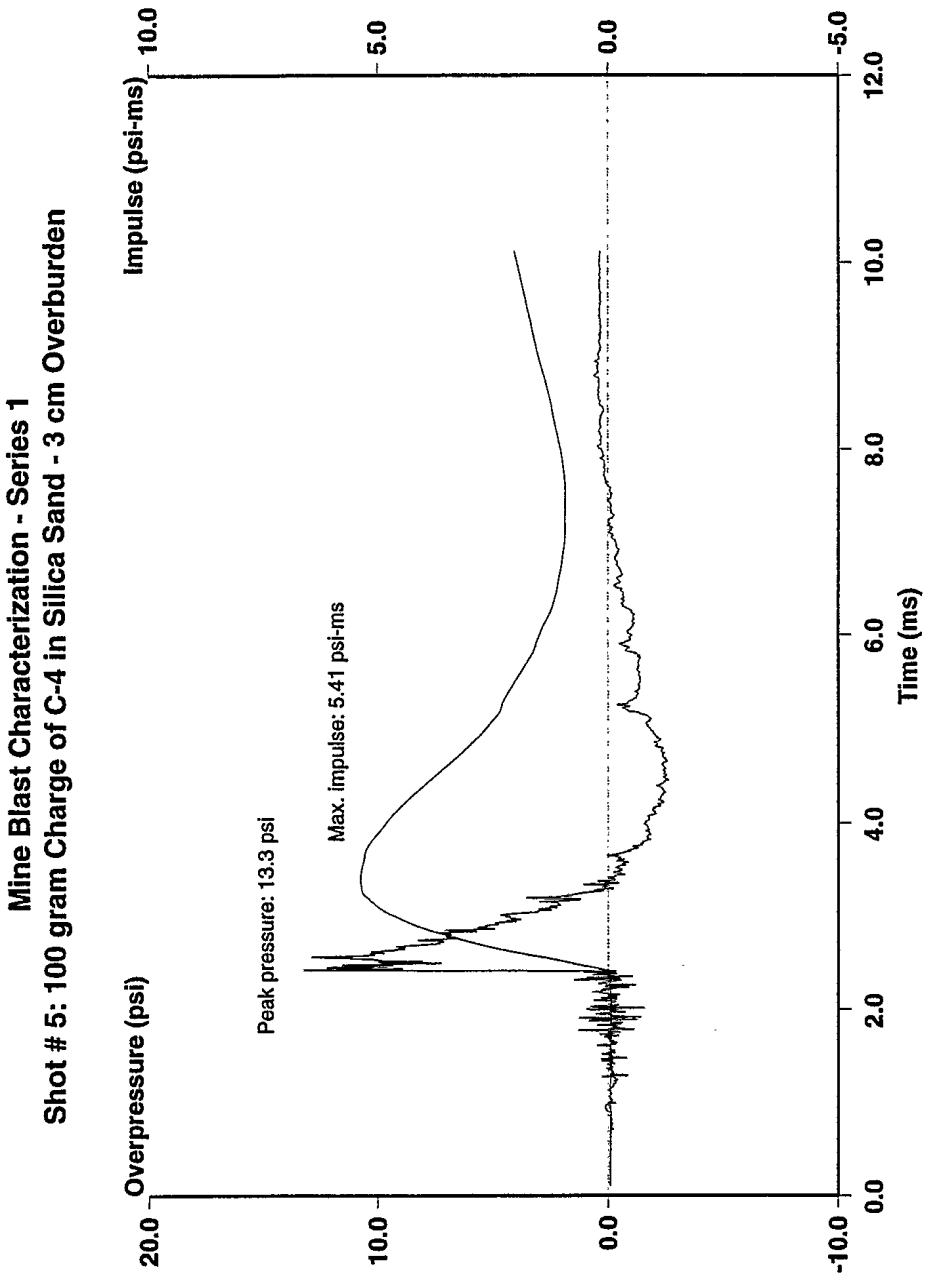

Position 4 (153 cm), Air Shock, 2nd Order 100 kHz Butterworth Filter

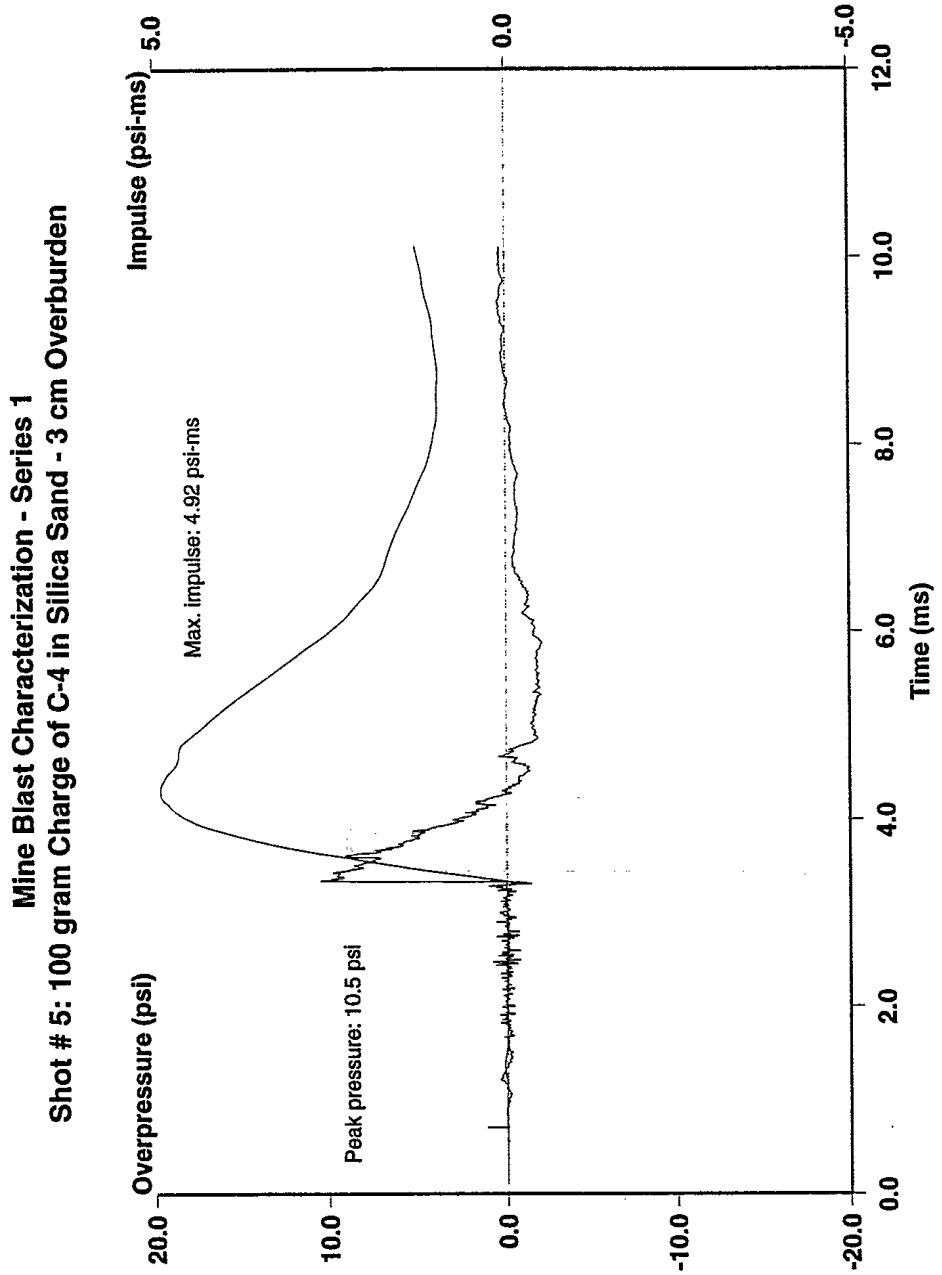

Position 5 (193 cm), Air Shock, 2nd Order 100 kHz Butterworth Filter

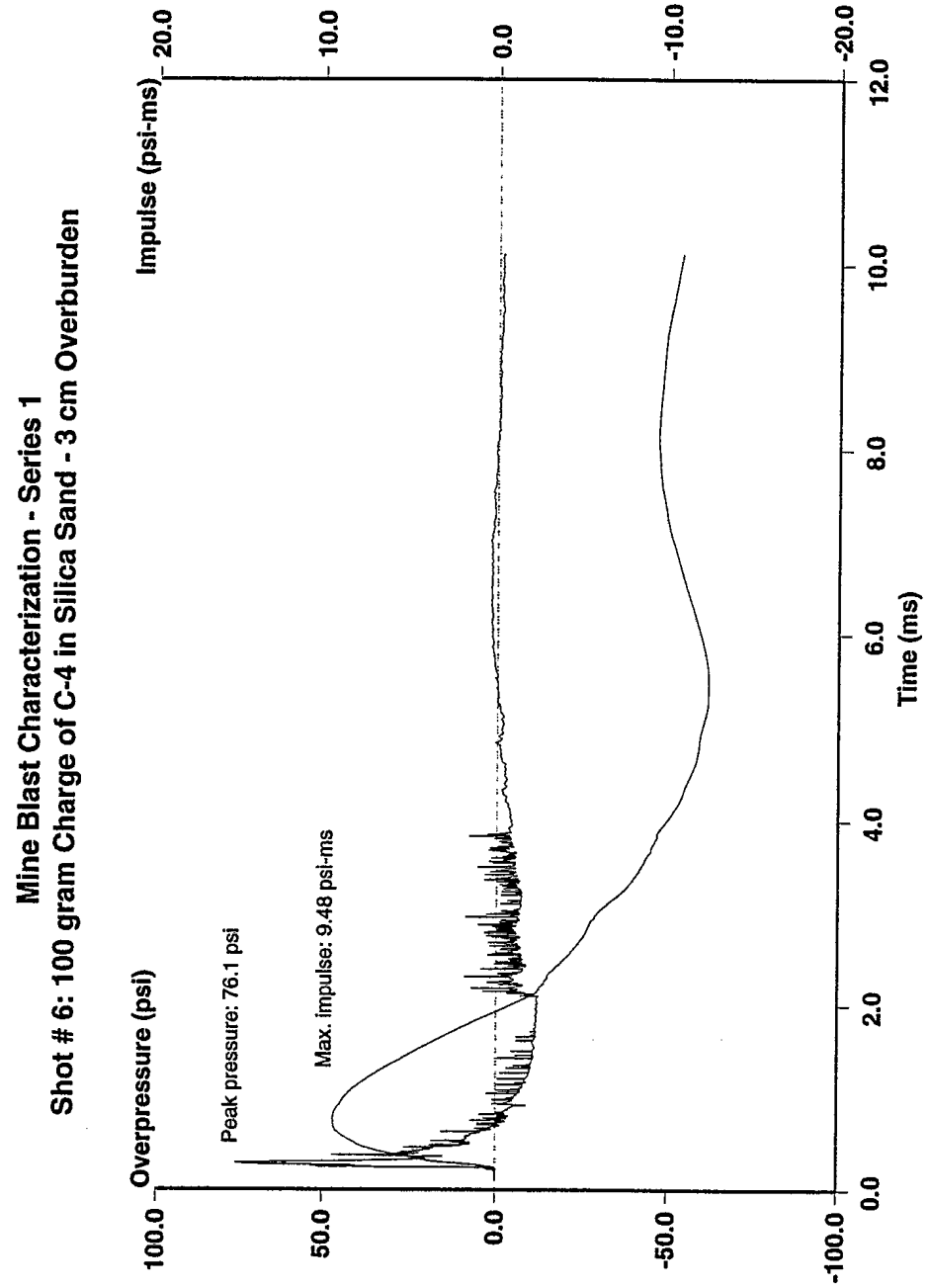

Position 1 (33 cm), Air Shock, 2nd Order 100 kHz Butterworth Filter

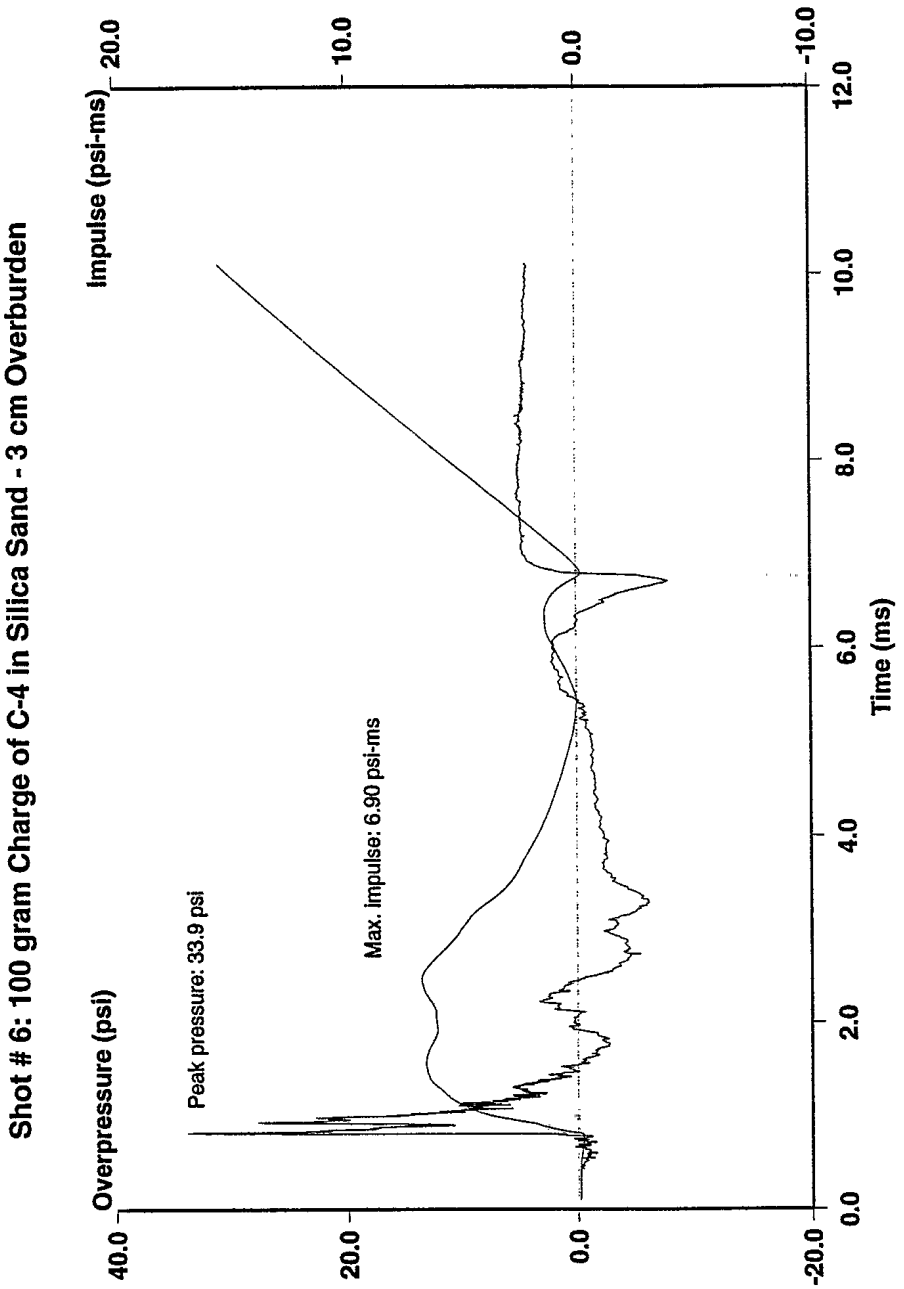

Position 2 (73 cm), Air Shock, 2nd Order 100 kHz Butterworth Filter

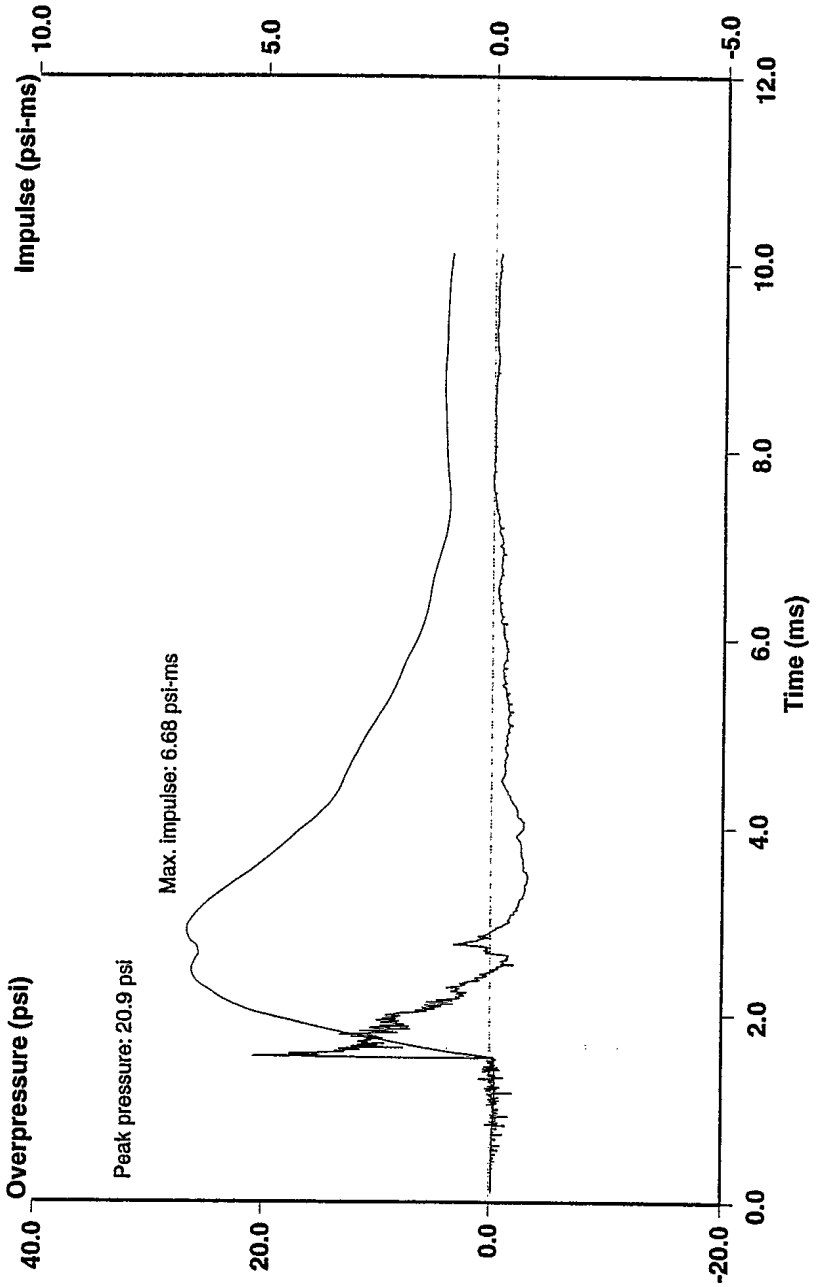

Position 3 (113 cm), Air Shock, 2nd Order 100 kHz Butterworth Filter

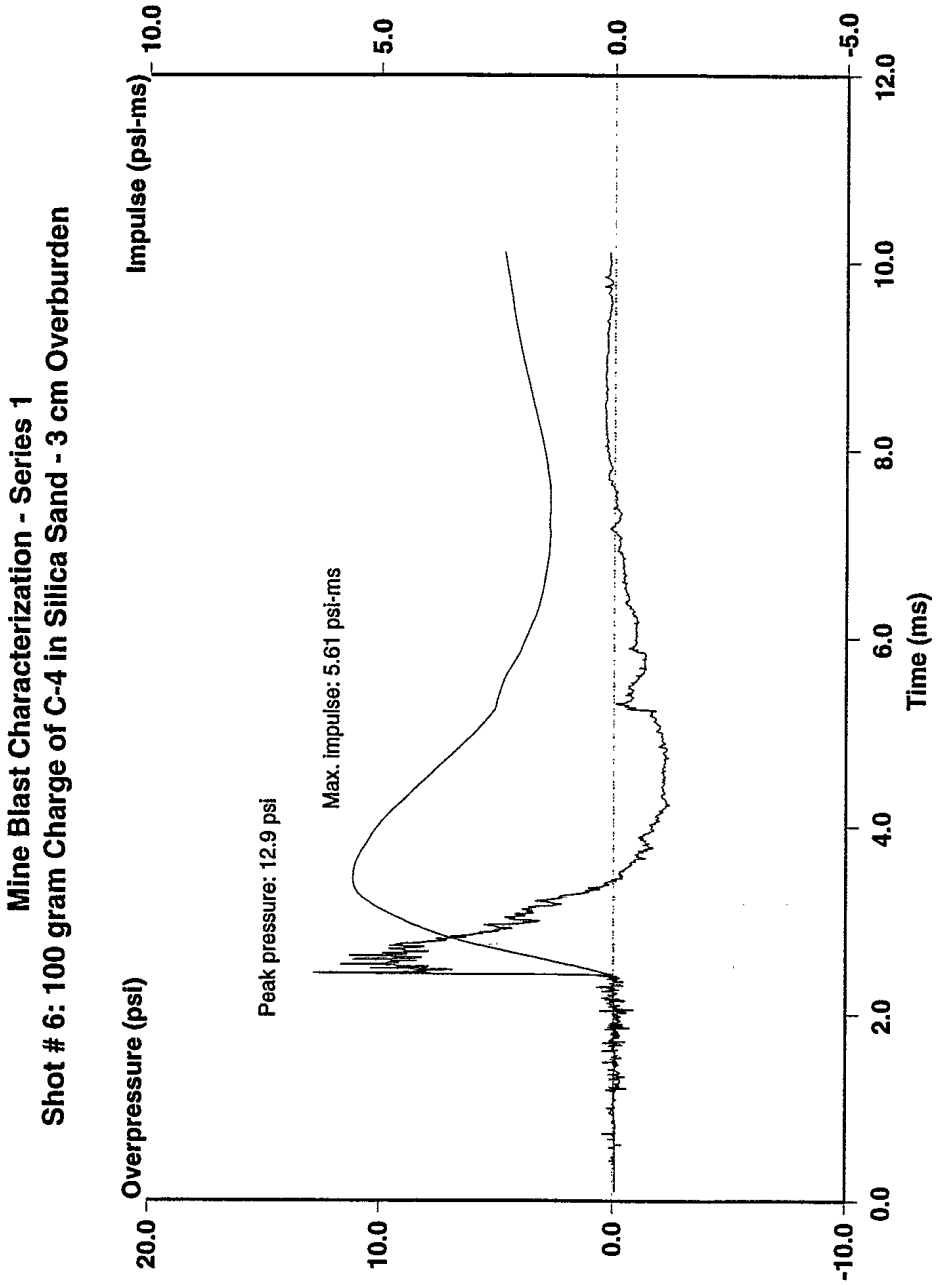

Position 4 (153 cm), Air Shock, 2nd Order 100 kHz Butterworth Filter

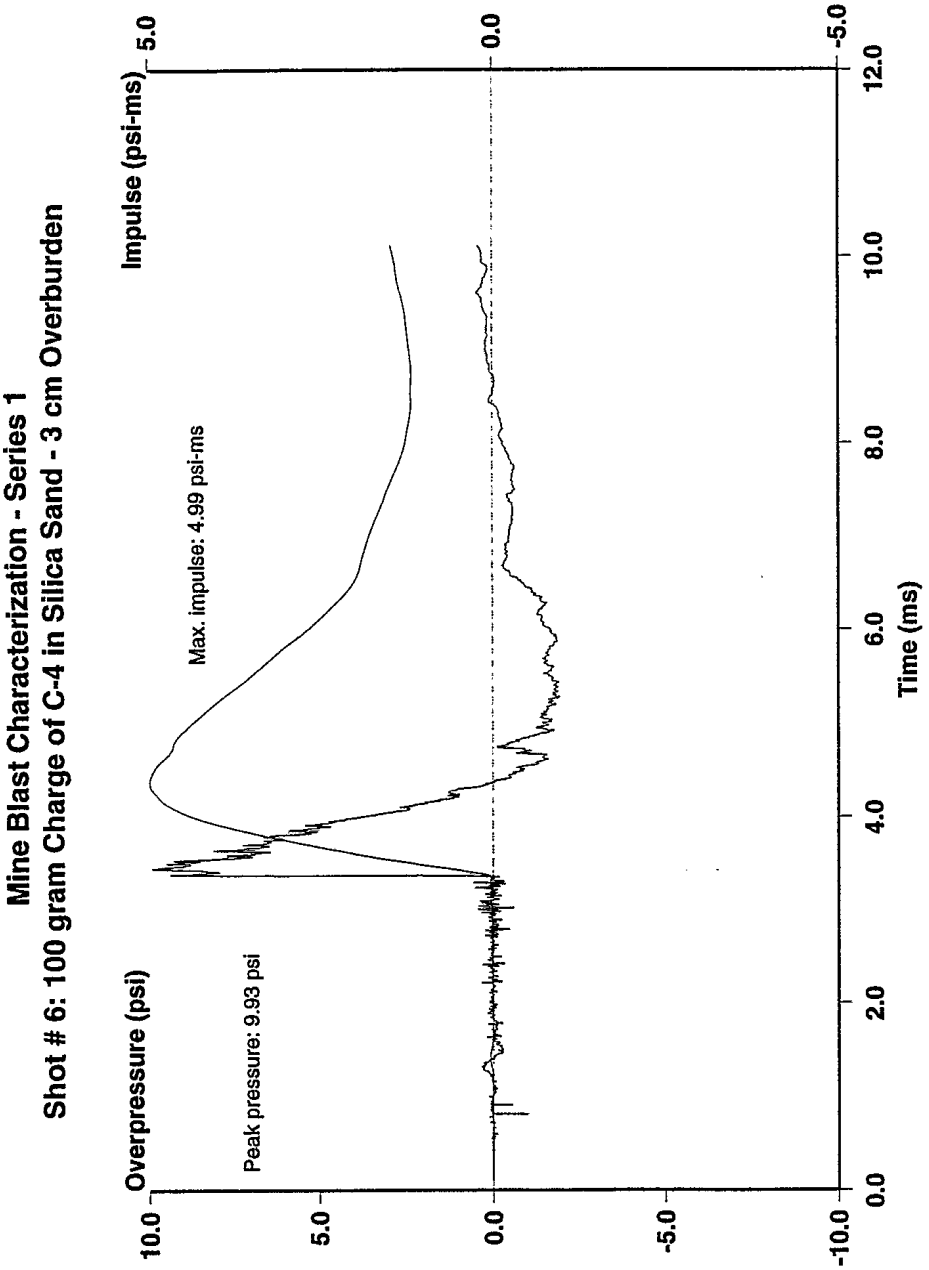

Position 5 (193 cm), Air Shock, 2nd Order 100 kHz Butterworth Filter

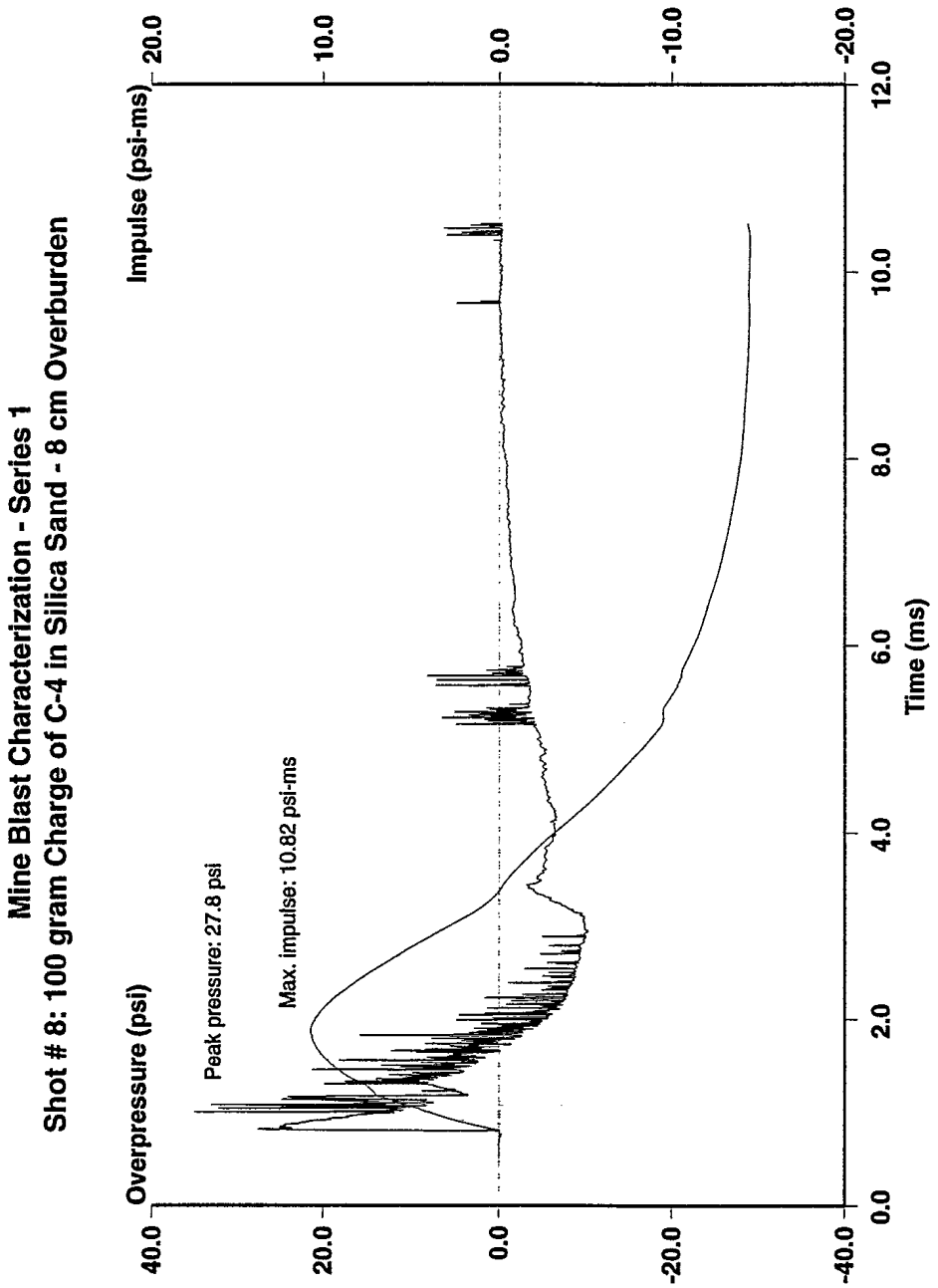

Position 1 (38 cm), Air Shock, 2nd Order 100 kHz Butterworth Filter

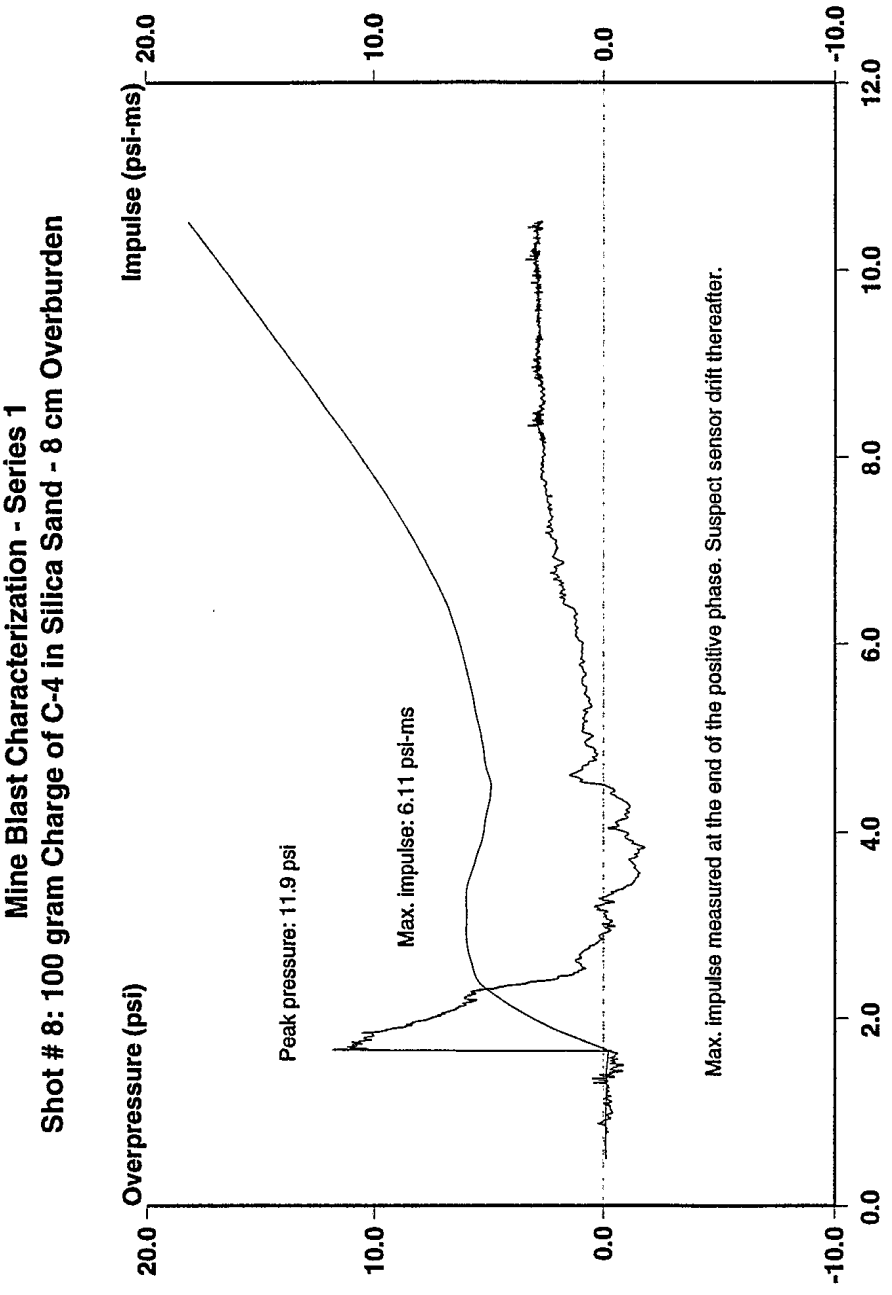

Position 2 (78 cm), Air Shock, 2nd Order 100 kHz Butterworth Filter

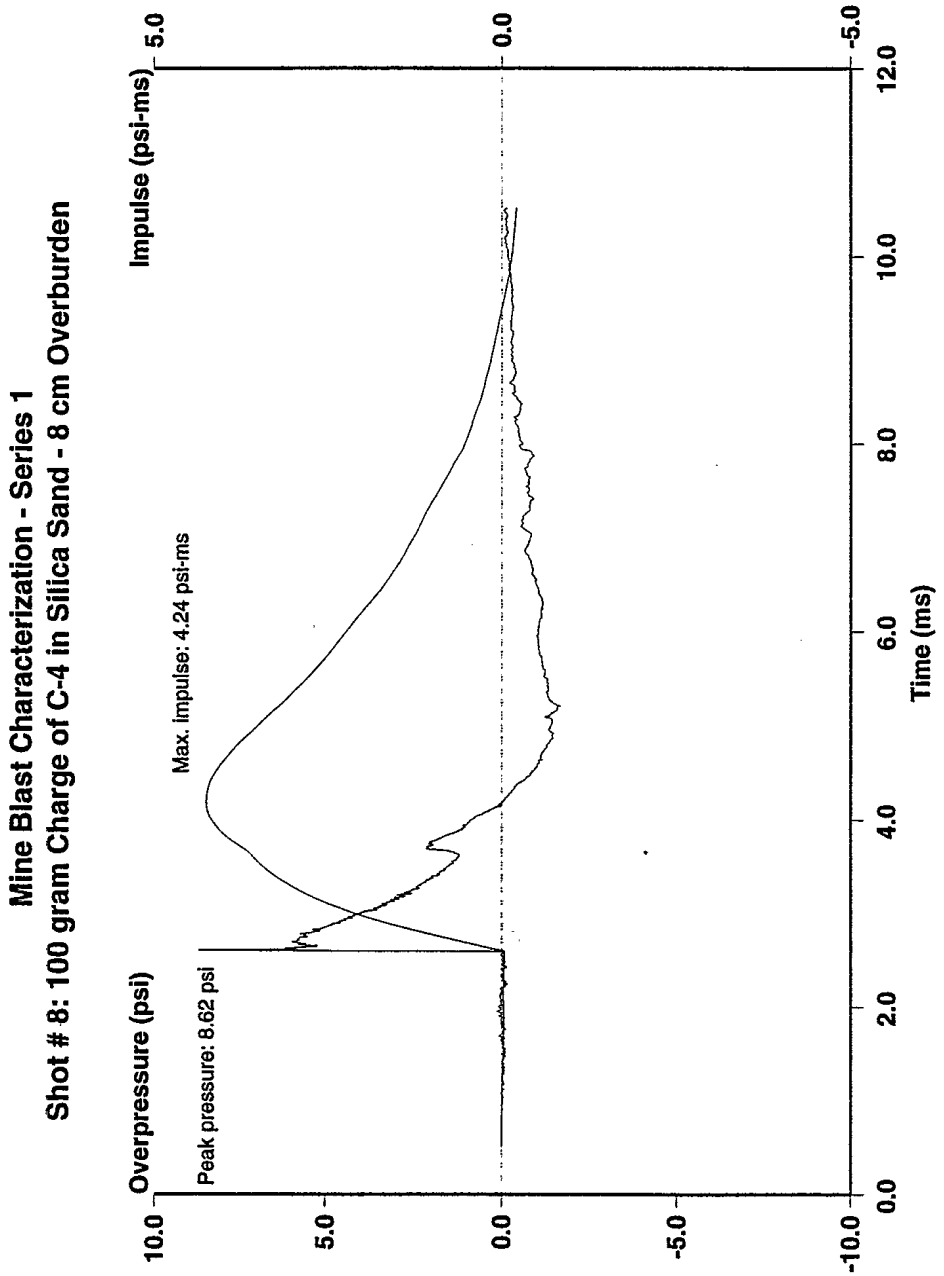

Position 3 (118 cm), Air Shock, 2nd Order 100 kHz Butterworth Filter

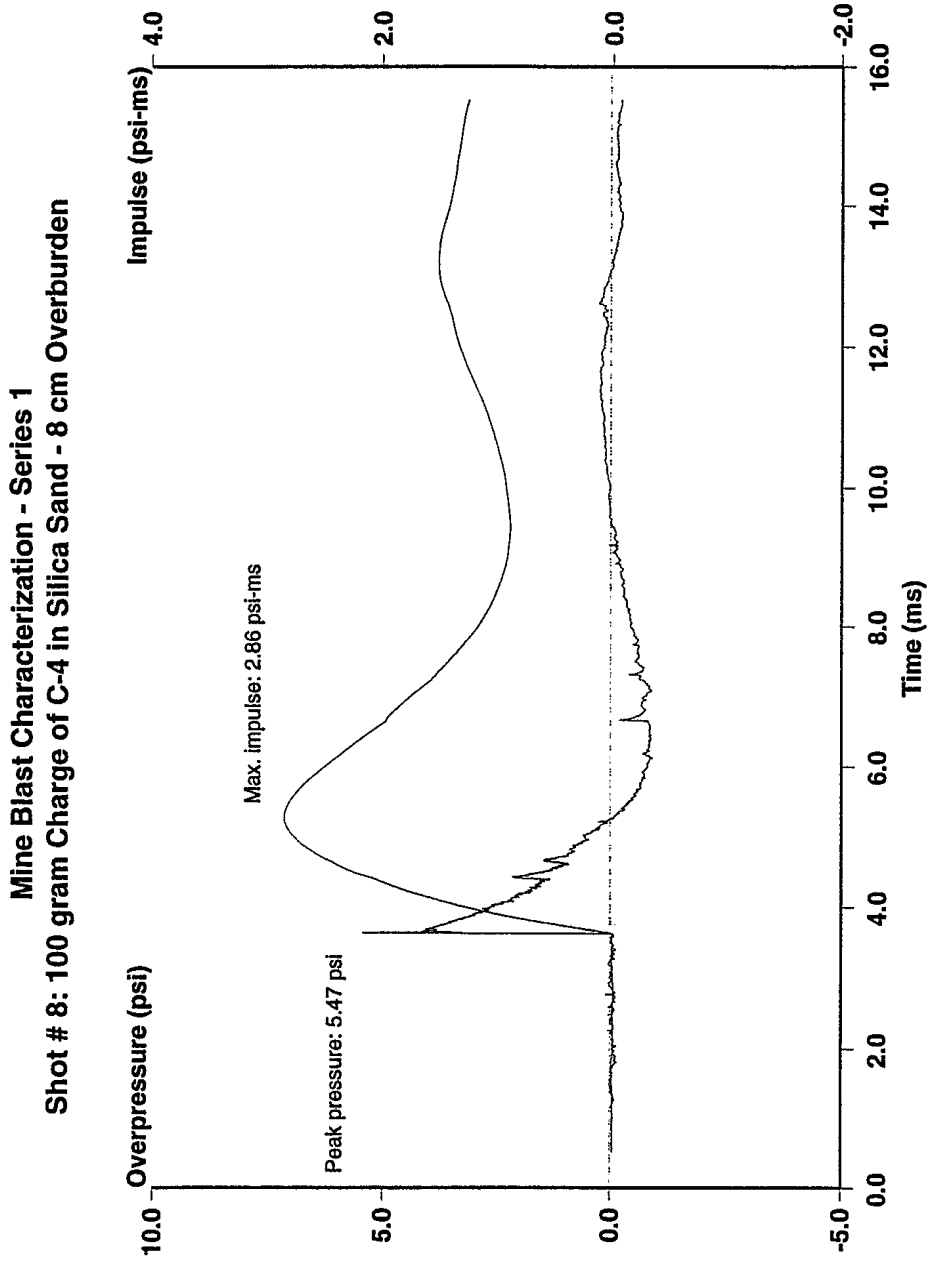

Position 4 (158 cm), Air Shock, 2nd Order 100 kHz Butterworth Filter

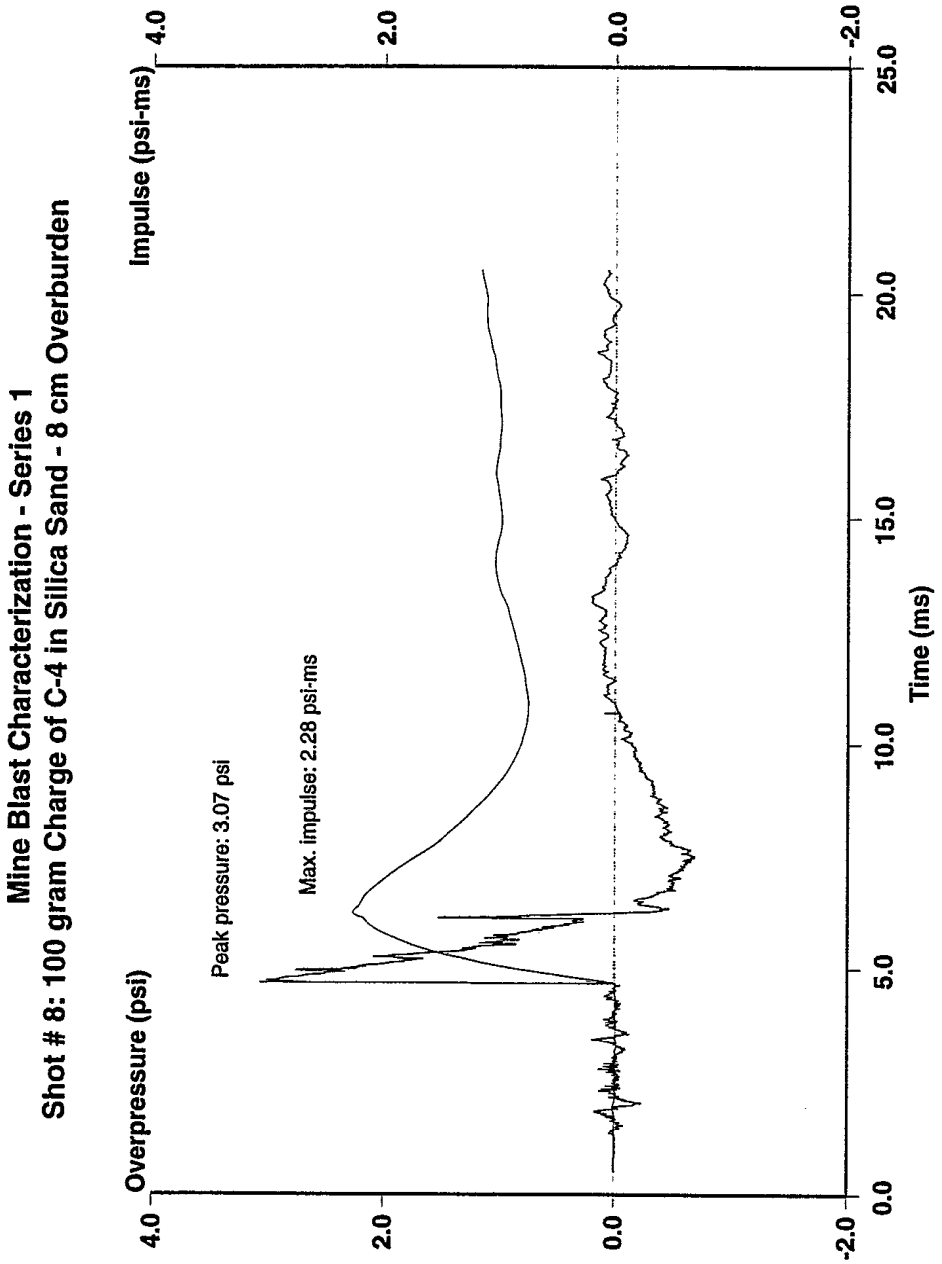

Position 5 (198 cm), Air Shock, 2nd Order 100 kHz Butterworth Filter

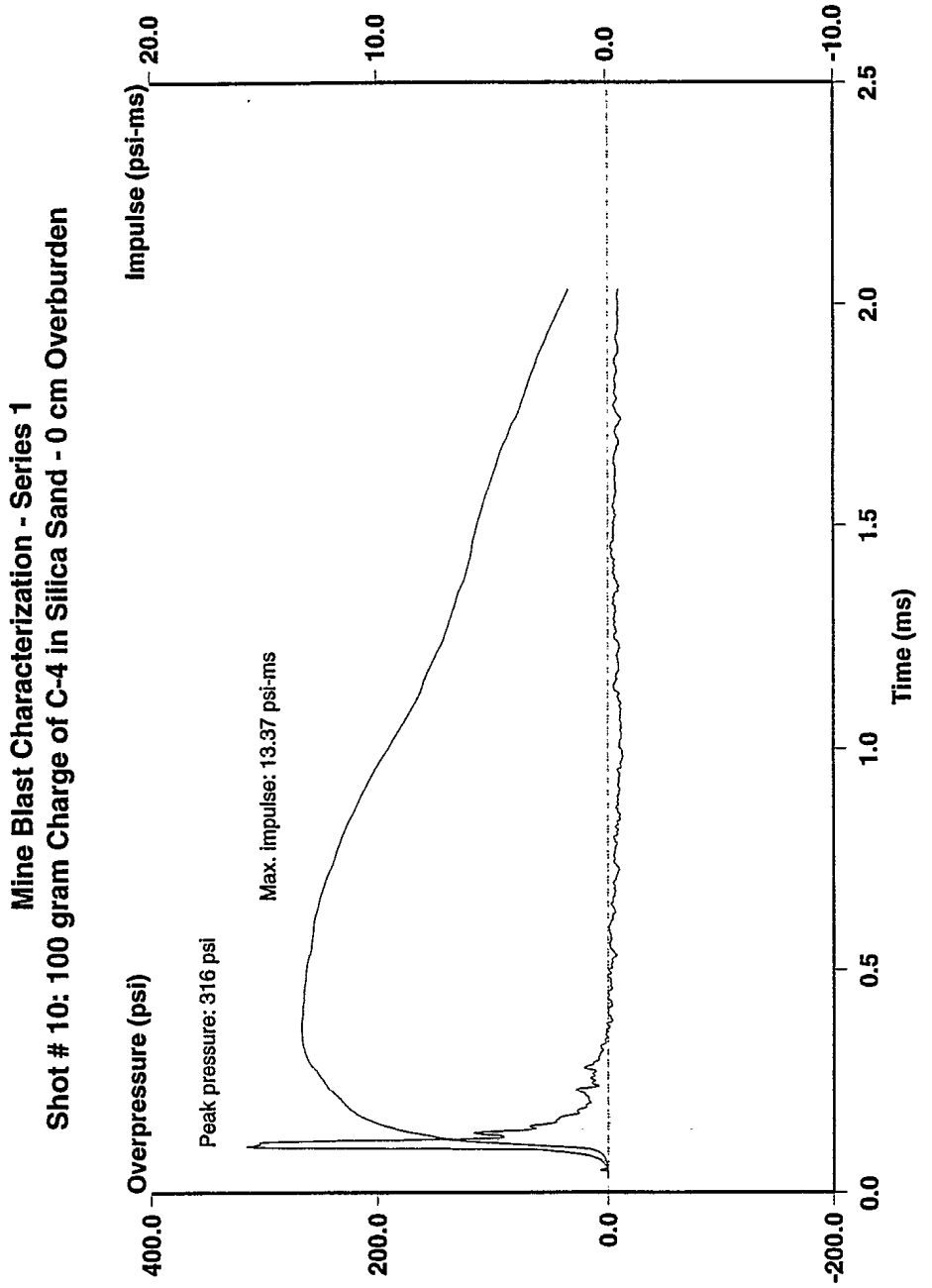

Position 1 (30 cm), Air Shock, 2nd Order 100 kHz Butterworth Filter

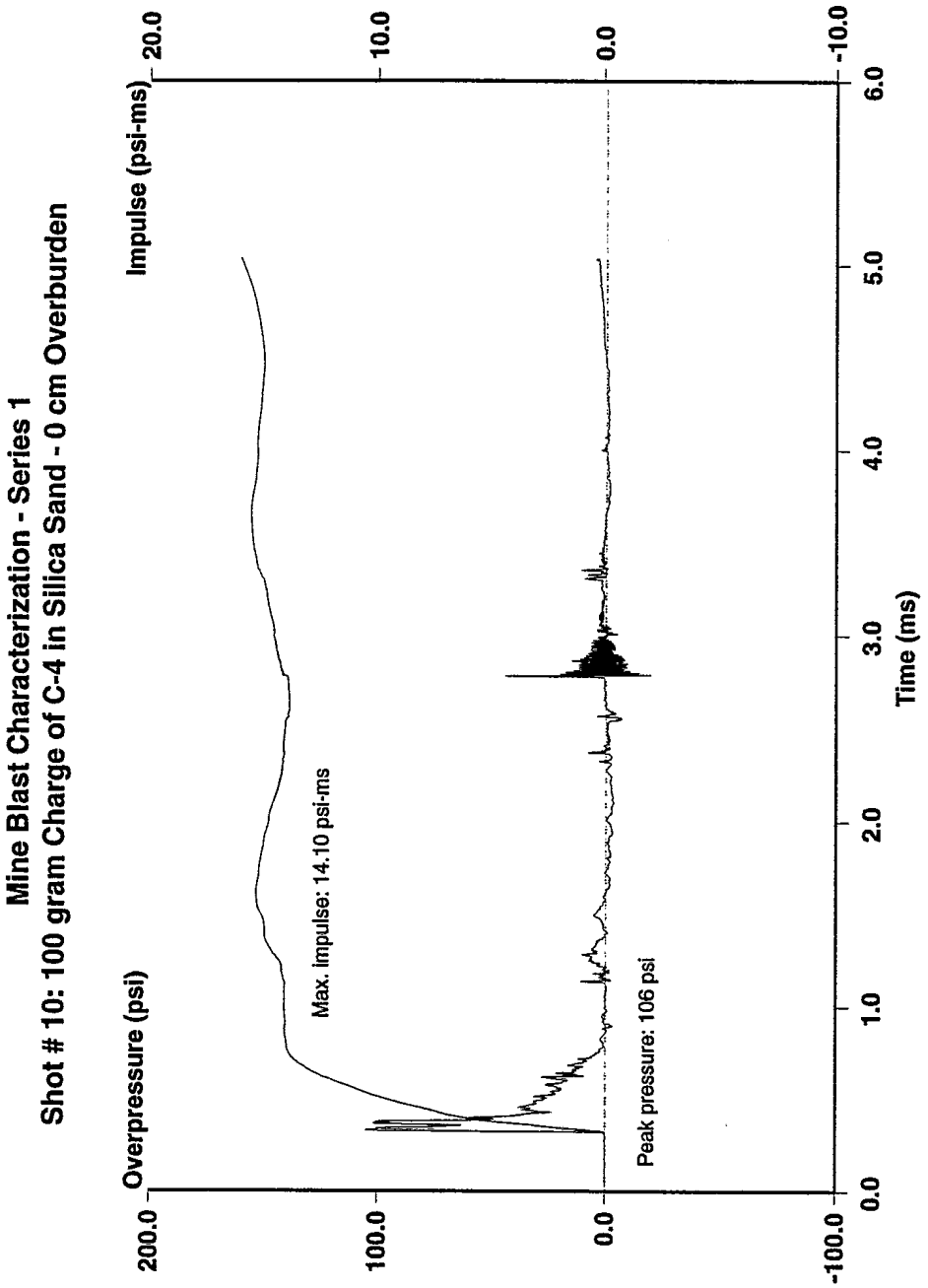

Position 2 (70 cm), Air Shock, 2nd Order 100 kHz Butterworth Filter

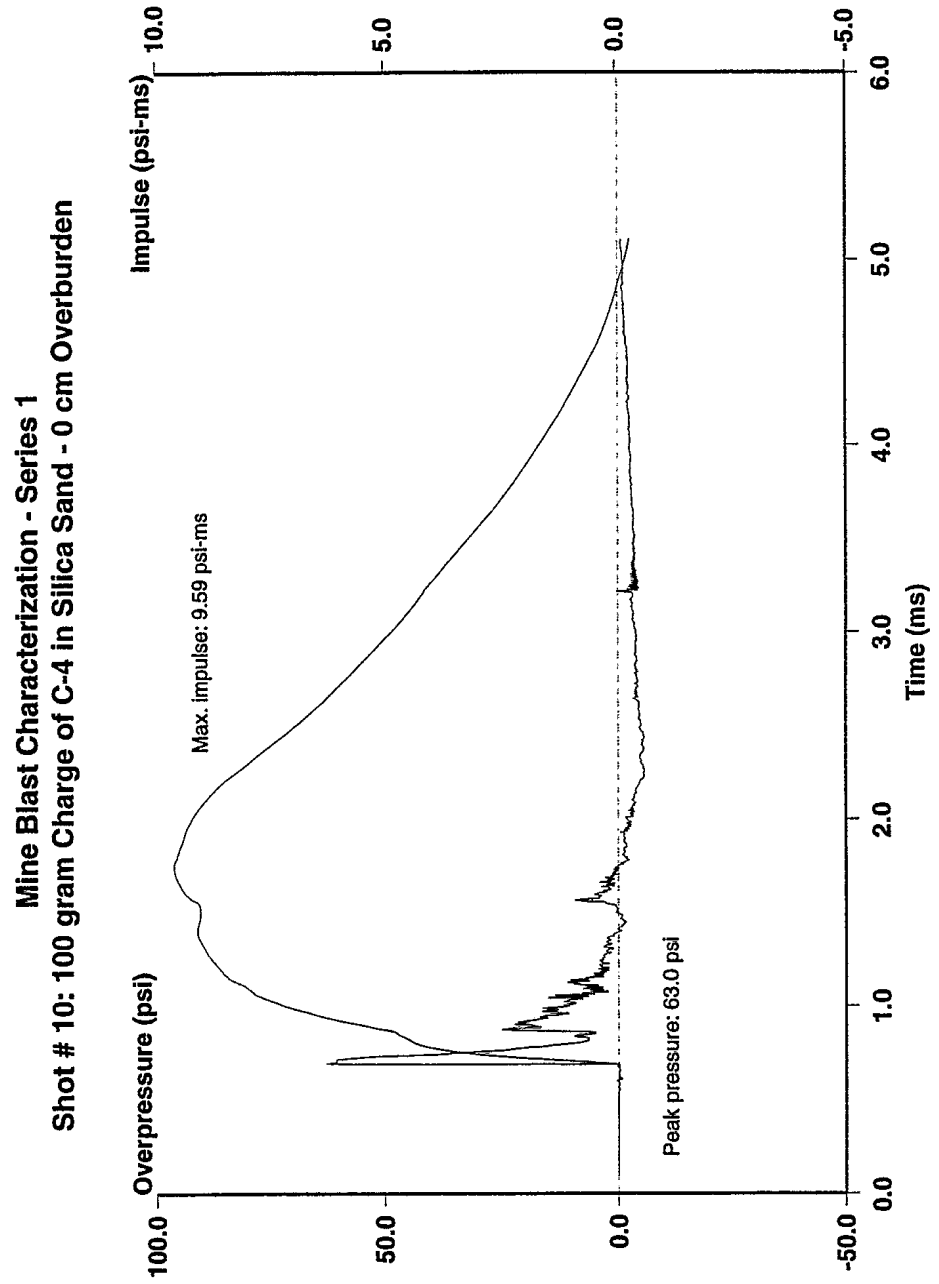
Mine Blast Characterization - Series 1
Shot # 10: 100 gram Charge of C-4 in Silica Sand - 0 cm Overburden
Overpressure (psi)
100.0
50.0
0.0
-50.0
Impulse (psi-ms)
10.0
5.0
0.0
-5.0
Max. impulse: 9.59 psi-ms
Peak pressure: 63.0 psi
0.0
1.0
2.0
3.0
4.0
5.0
6.0
Time (ms)
Position 3 (110 cm), Air Shock, 2nd Order 100 kHz Butterworth Filter

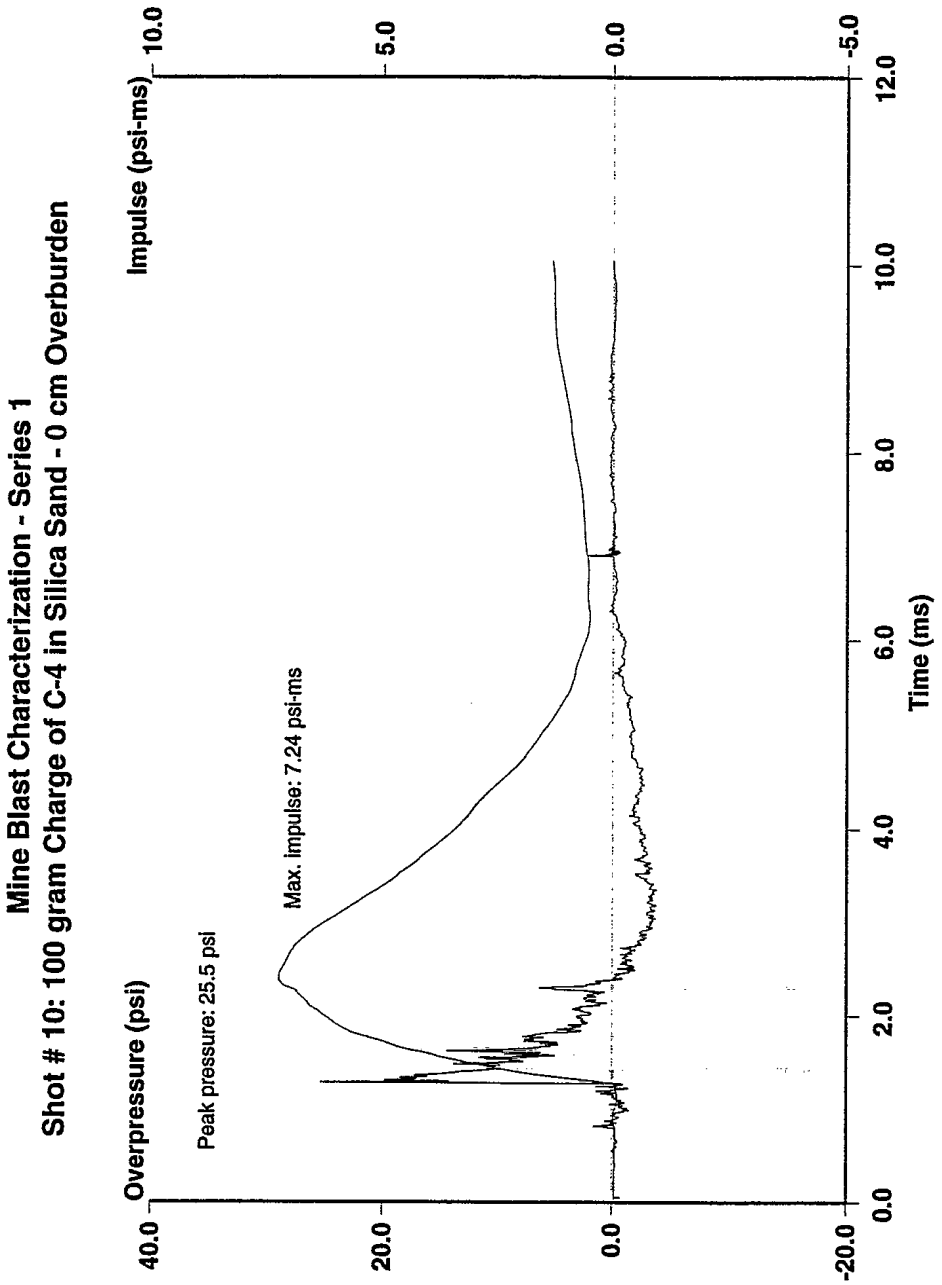

Position 4 (150 cm), Air Shock, 2nd Order 100 kHz Butterworth Filter

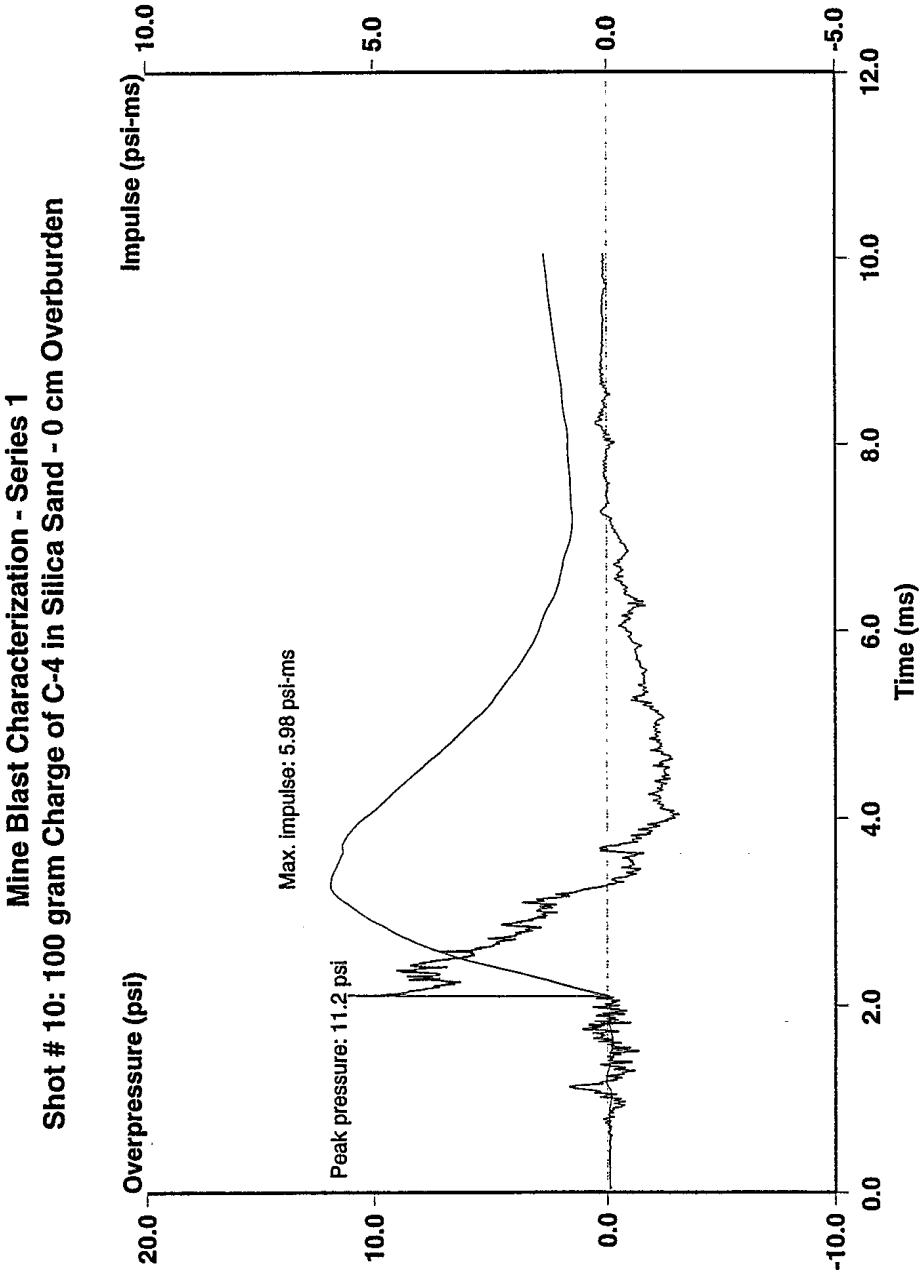

Position 5 (190 cm), Air Shock, 2nd Order 100 kHz Butterworth Filter

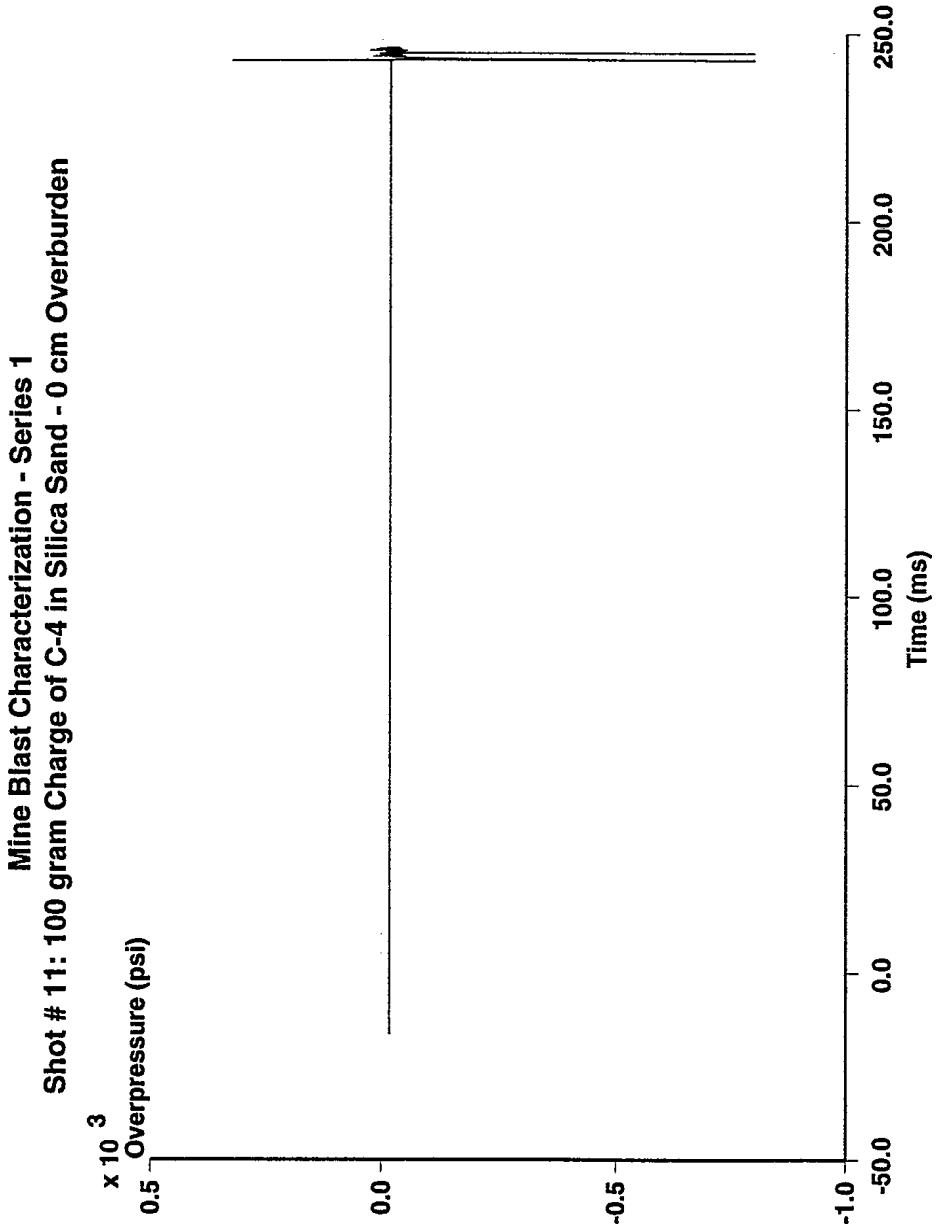

Position 1 (30 cm), Air Shock, 2nd Order 100 kHz Butterworth Filter

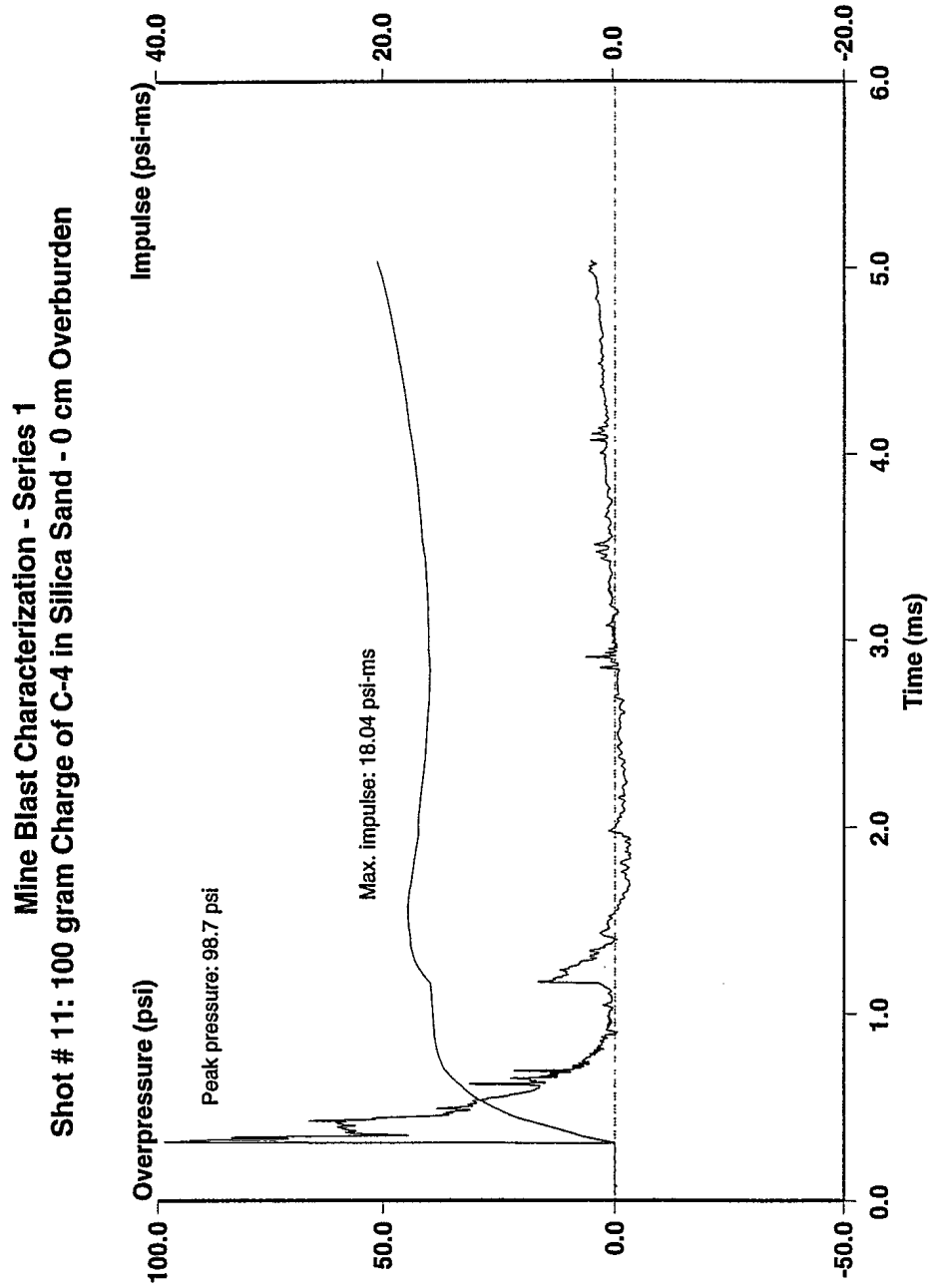

Position 2 (70 cm), Air Shock, 2nd Order 100 kHz Butterworth Filter

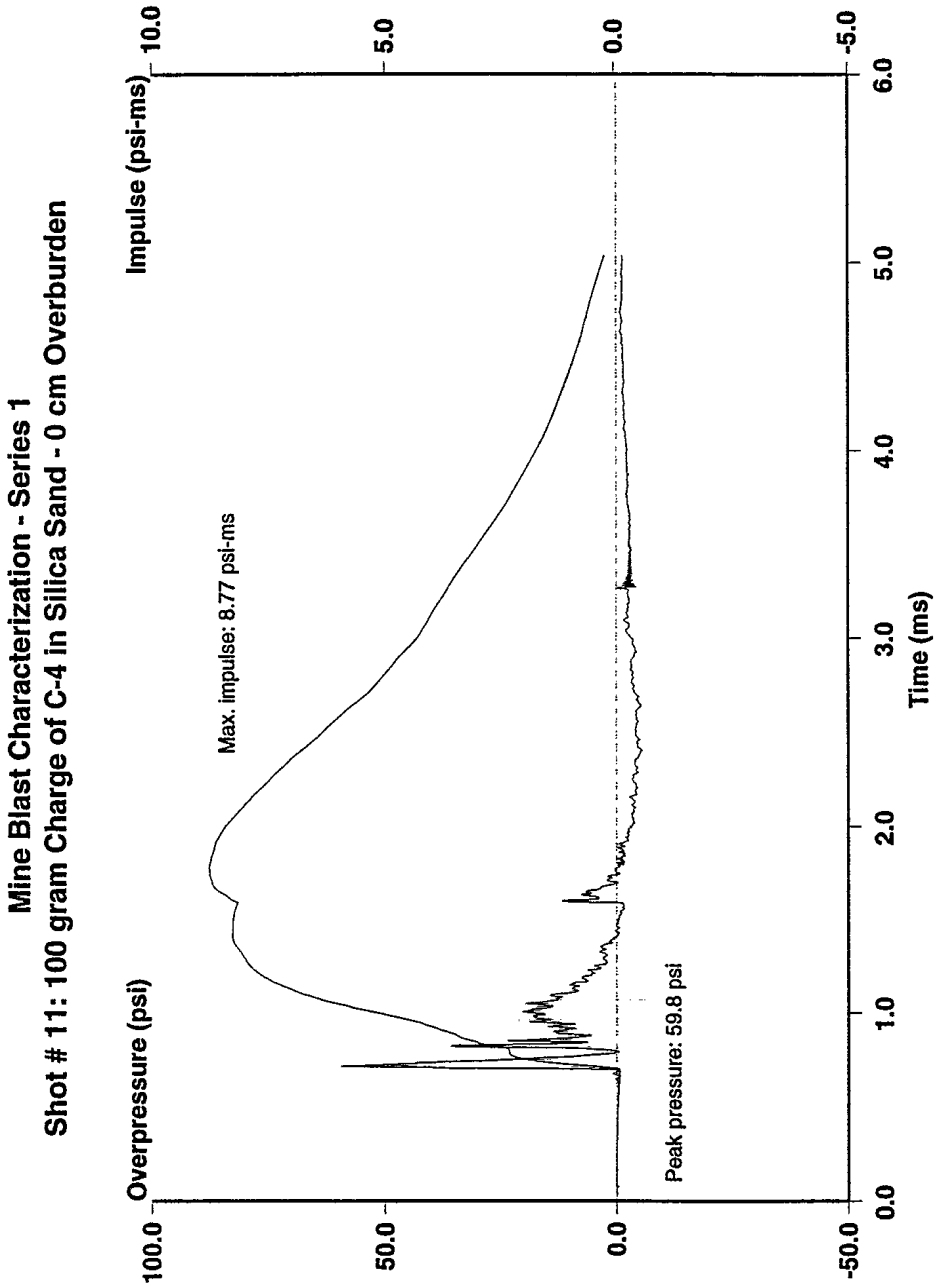

Position 3 (110 cm), Air Shock, 2nd Order 100 kHz Butterworth Filter

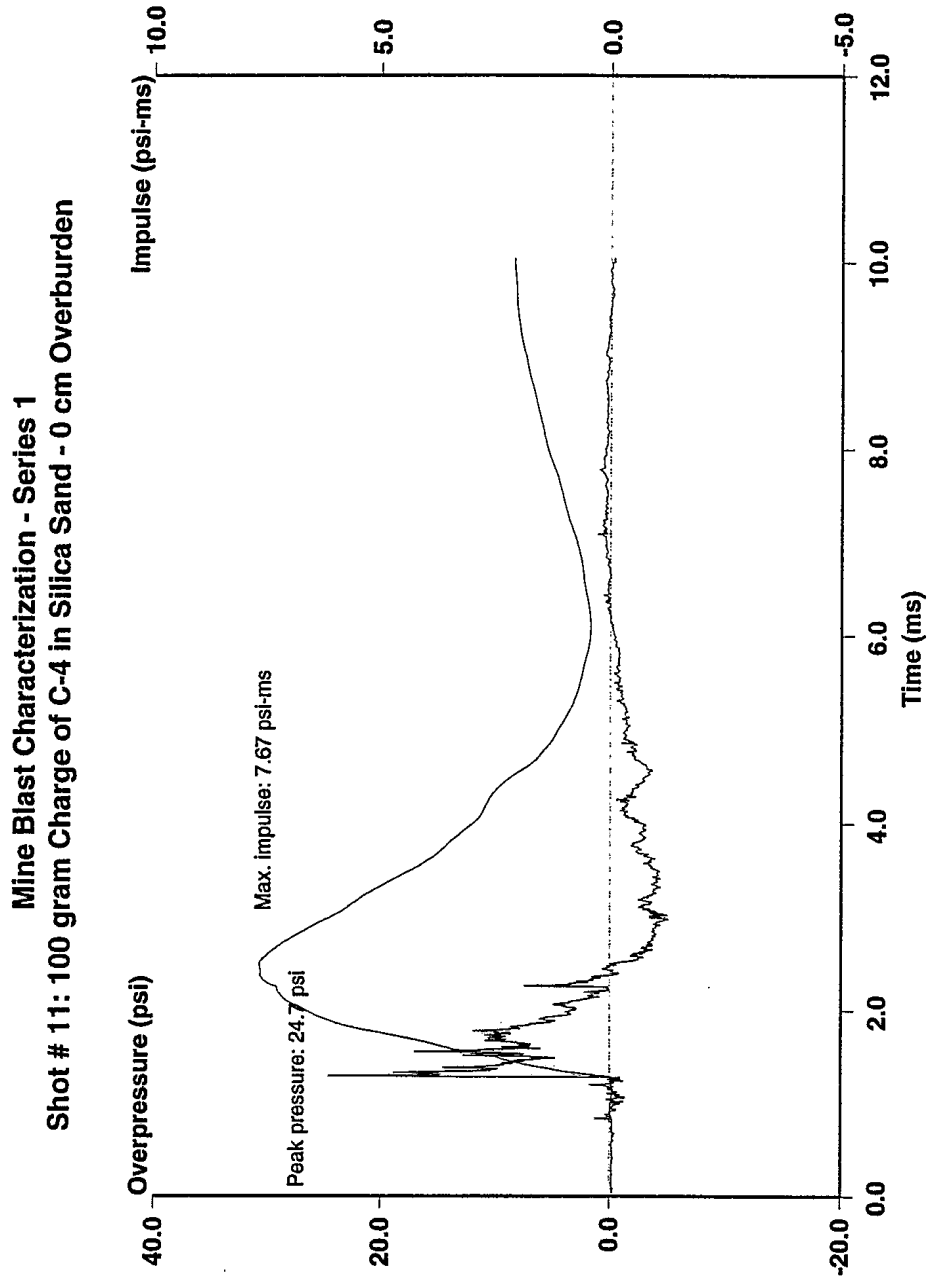

Position 4 (150 cm), Air Shock, 2nd Order 100 kHz Butterworth Filter

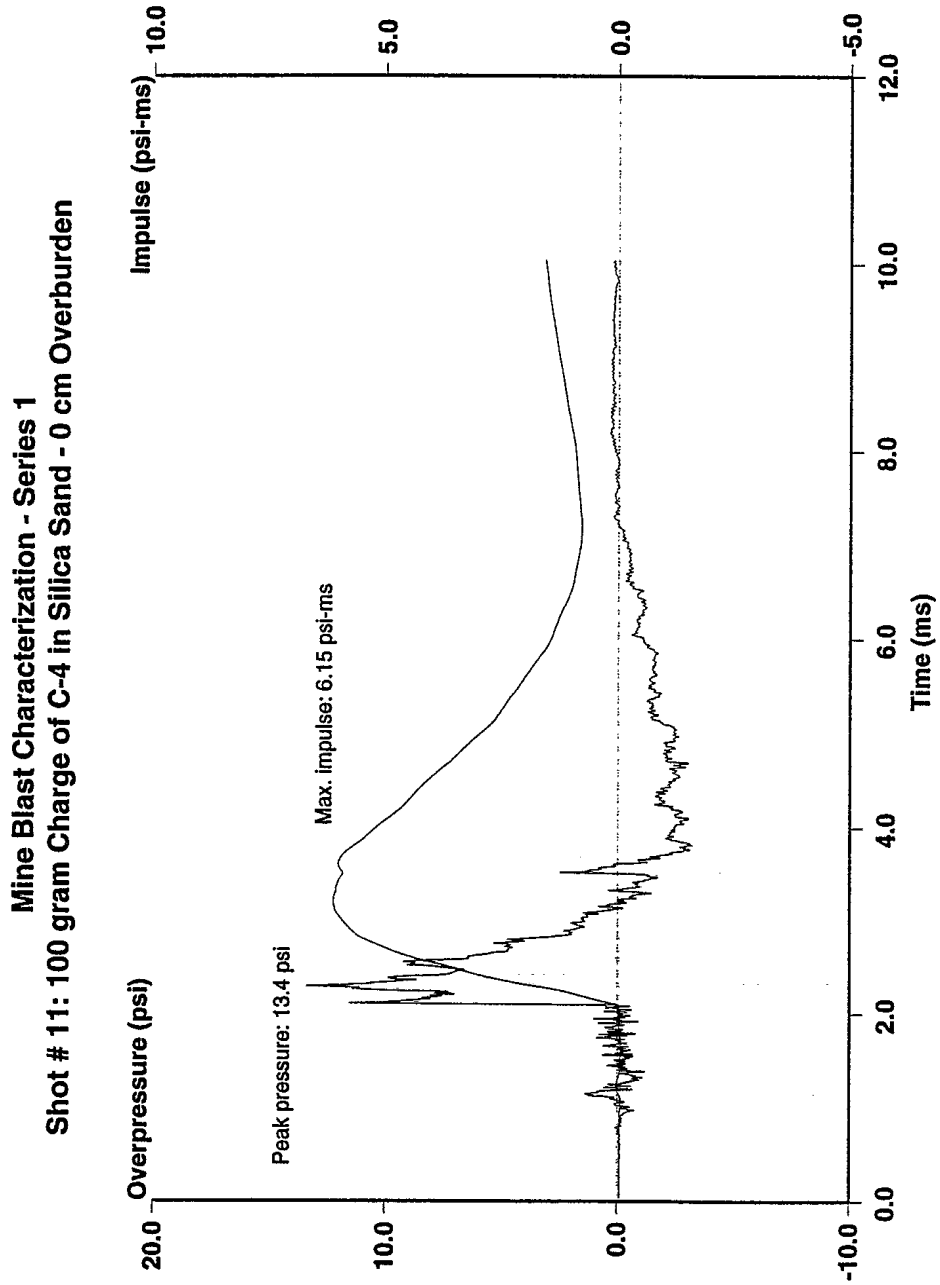

Position 5 (190 cm), Air Shock, 2nd Order 100 kHz Butterworth Filter

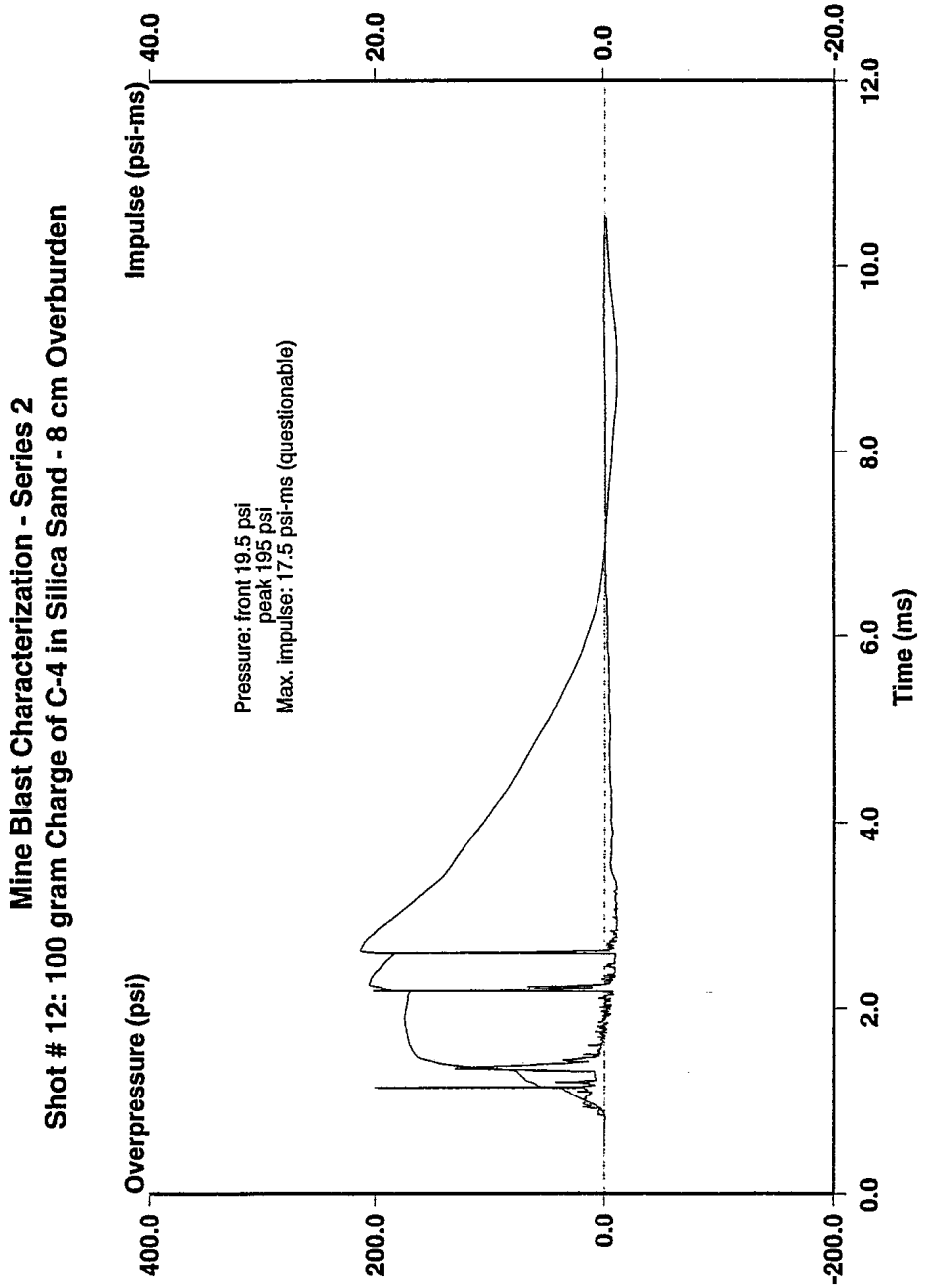
Mine Blast Characterization - Series 2
Shot # 12: 100 gram Charge of C-4 in Silica Sand - 8 cm Overburden
Overpressure (psi)
400.0
200.0
0.0
-200.0
Impulse (psi-ms)
40.0
20.0
0.0
-20.0
Pressure: front 19.5 psi
peak 195 psi
Max. impulse: 17.5 psi-ms (questionable)
0.0
2.0
4.0
6.0
8.0
10.0
12.0
Time (ms)
Position 1 (38 cm), Air Shock, 2nd Order 100 kHz Butterworth Filter

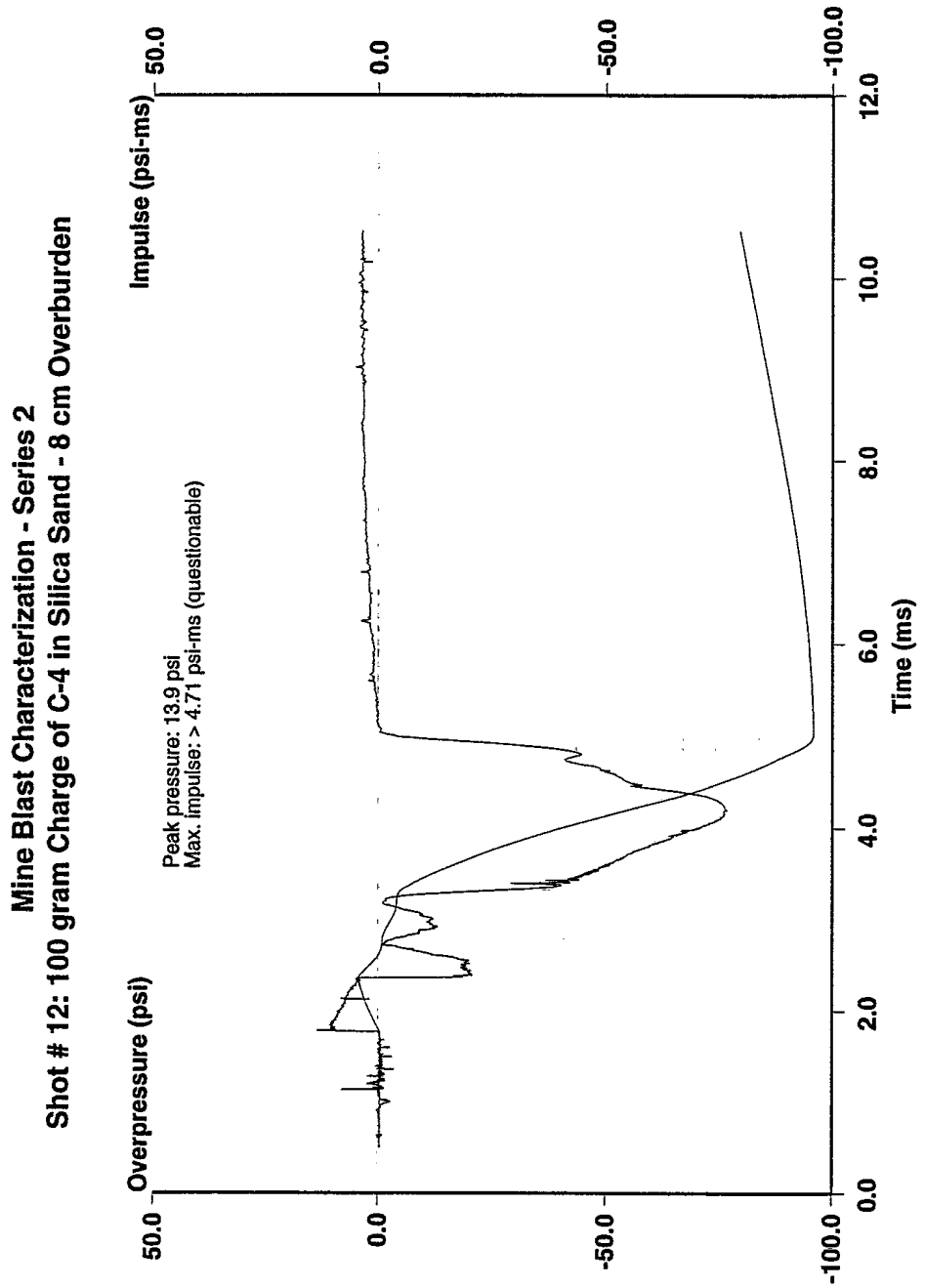

Position 2 (78 cm), Air Shock, 2nd Order 100 kHz Butterworth Filter

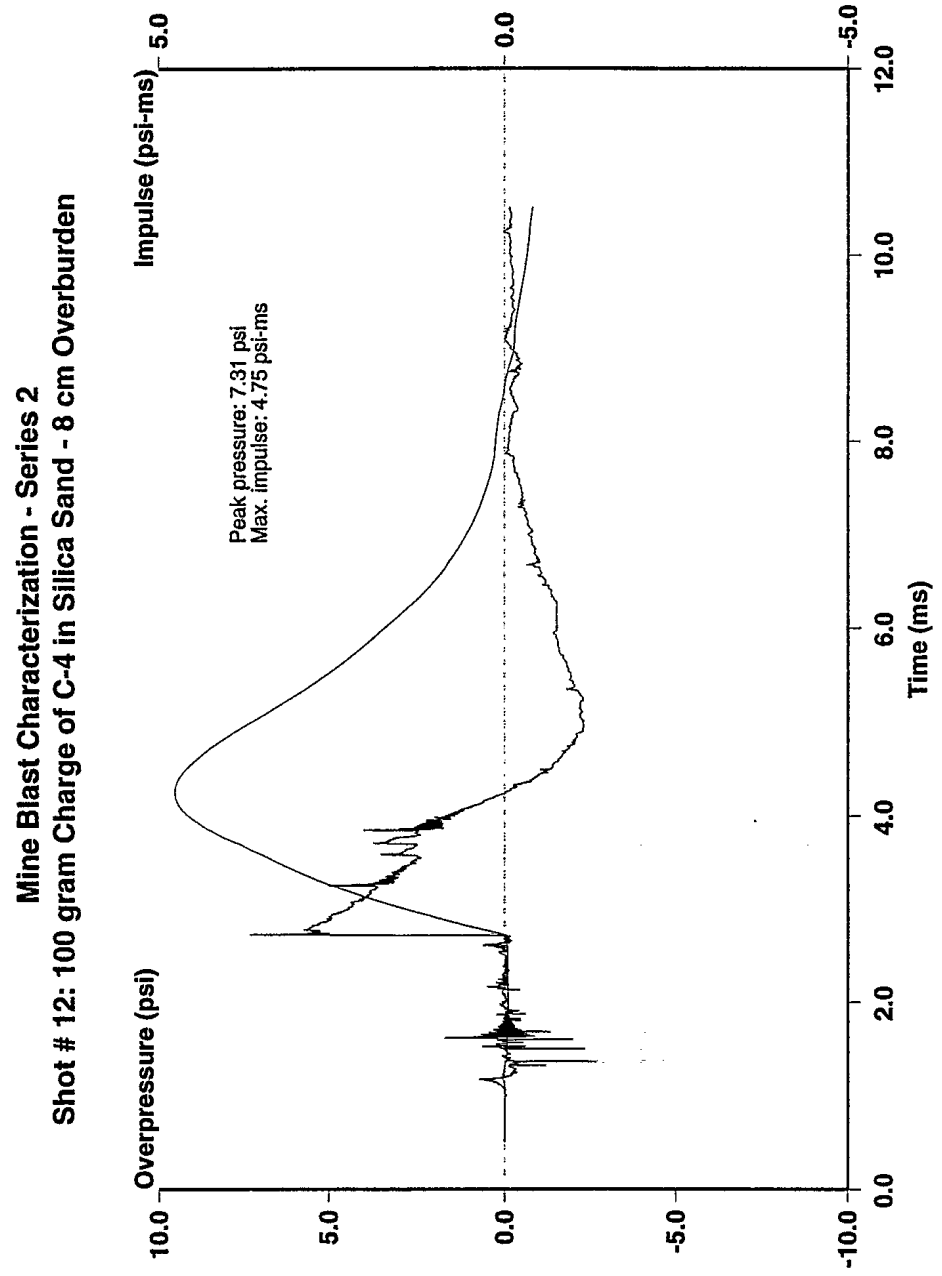
Mine Blast Characterization - Series 2
Shot # 12: 100 gram Charge of C-4 in Silica Sand - 8 cm Overburden
Overpressure (psi)
Impulse (psi-ms)
Time (ms)
Peak pressure: 7.31 psi
Max. impulse: 4.75 psi-ms
10.0
5.0
0.0
-5.0
-10.0
5.0
0.0
-5.0
0.0
2.0
4.0
6.0
8.0
10.0
12.0
Position 3 (118 cm), Air Shock, 2nd Order 100 kHz Butterworth Filter

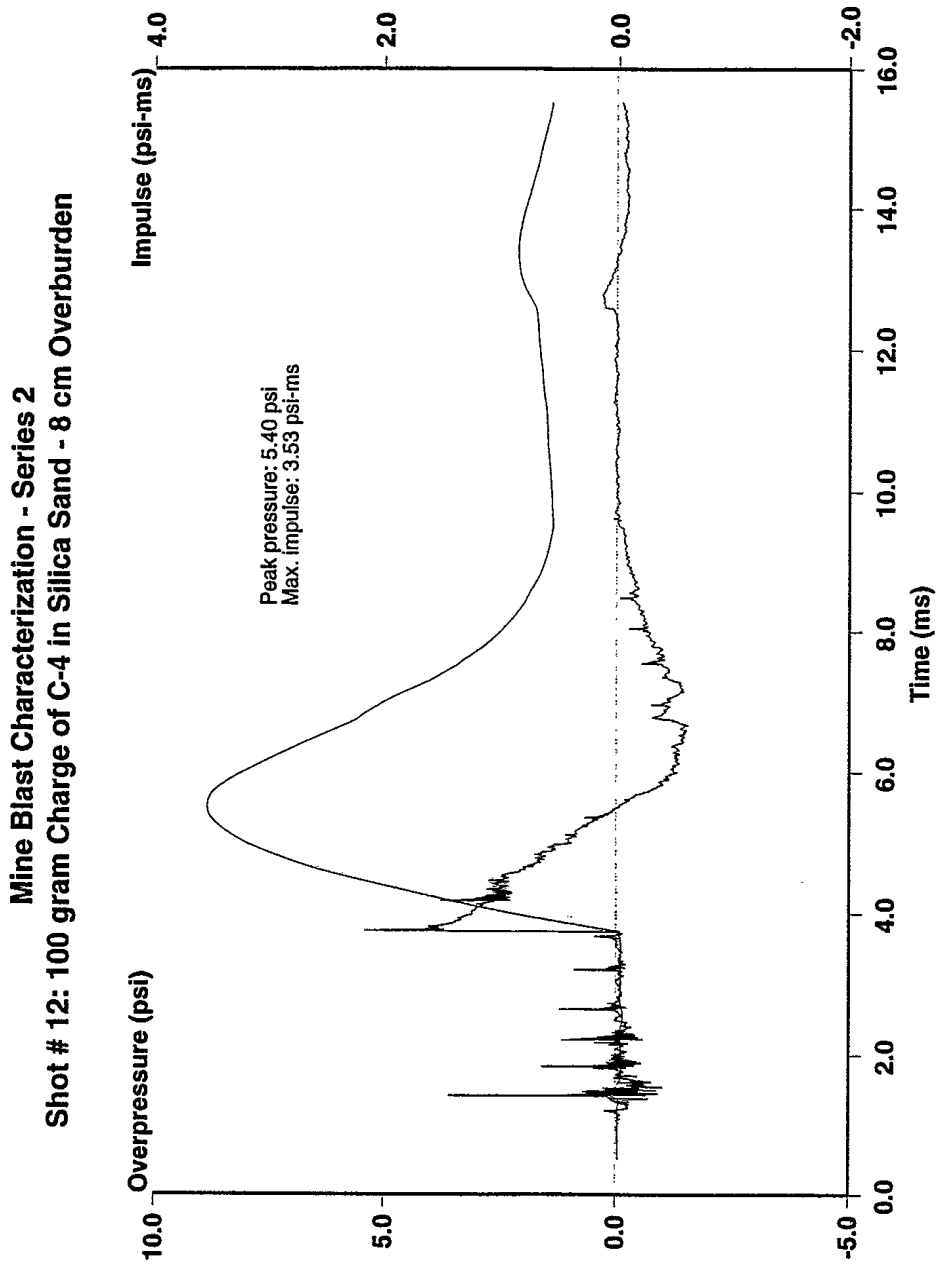

Position 4 (158 cm), Air Shock, 2nd Order 100 kHz Butterworth Filter

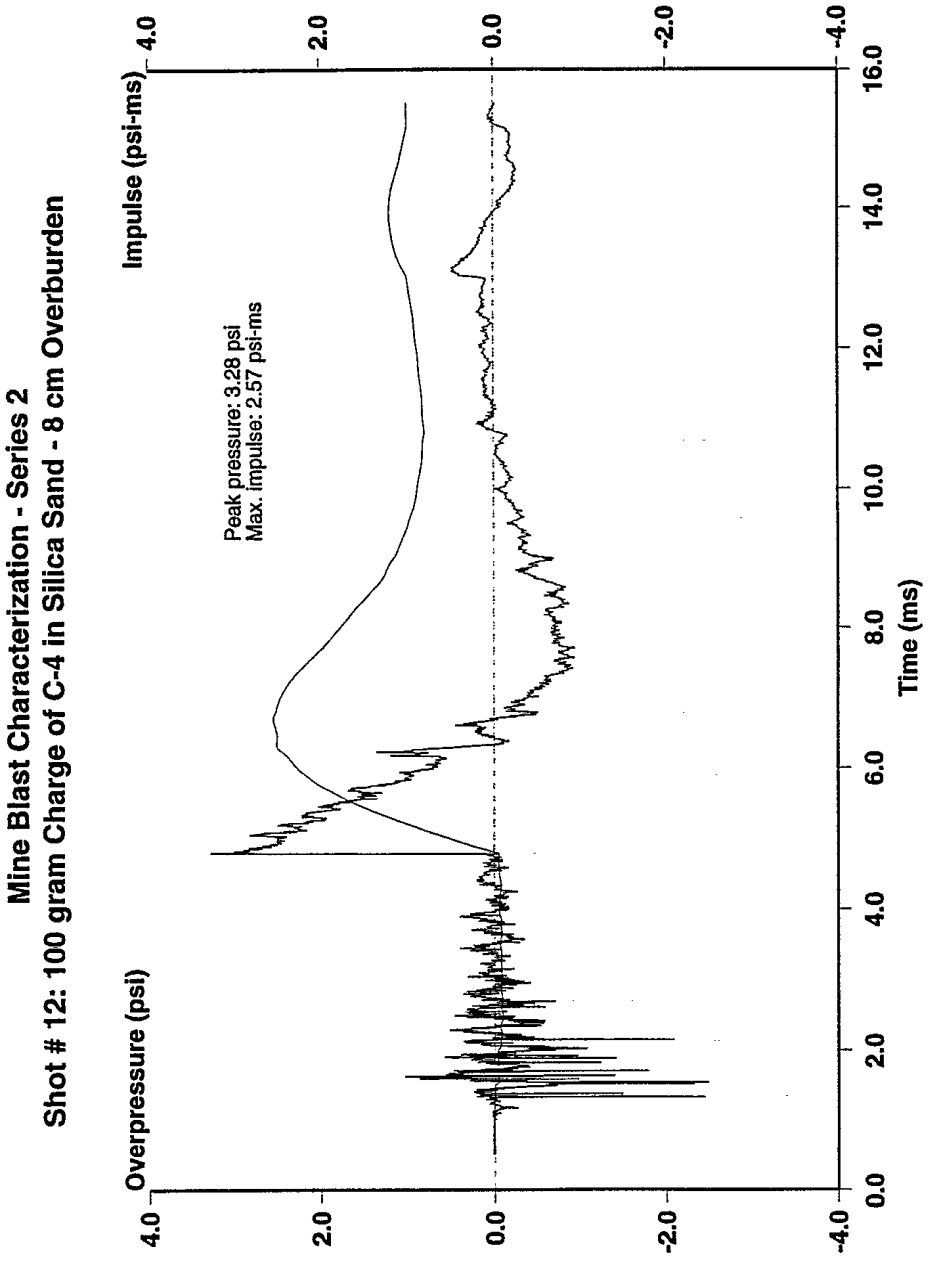

Position 5 (198 cm), Air Shock, 2nd Order 100 kHz Butterworth Filter

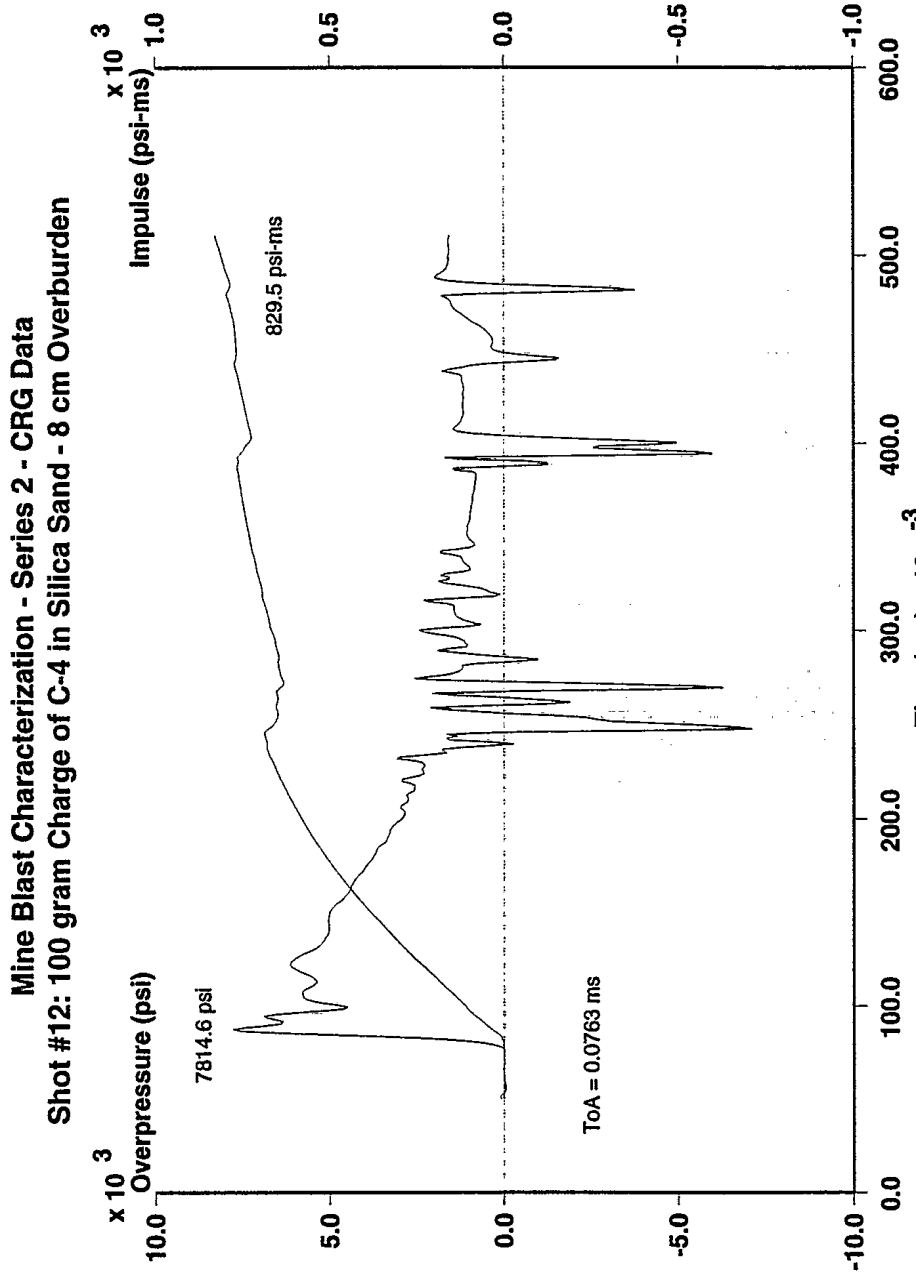

Position 6 (8.23 cm), In Ground Pressure, 2nd Order 100 kHz Butterworth Filter

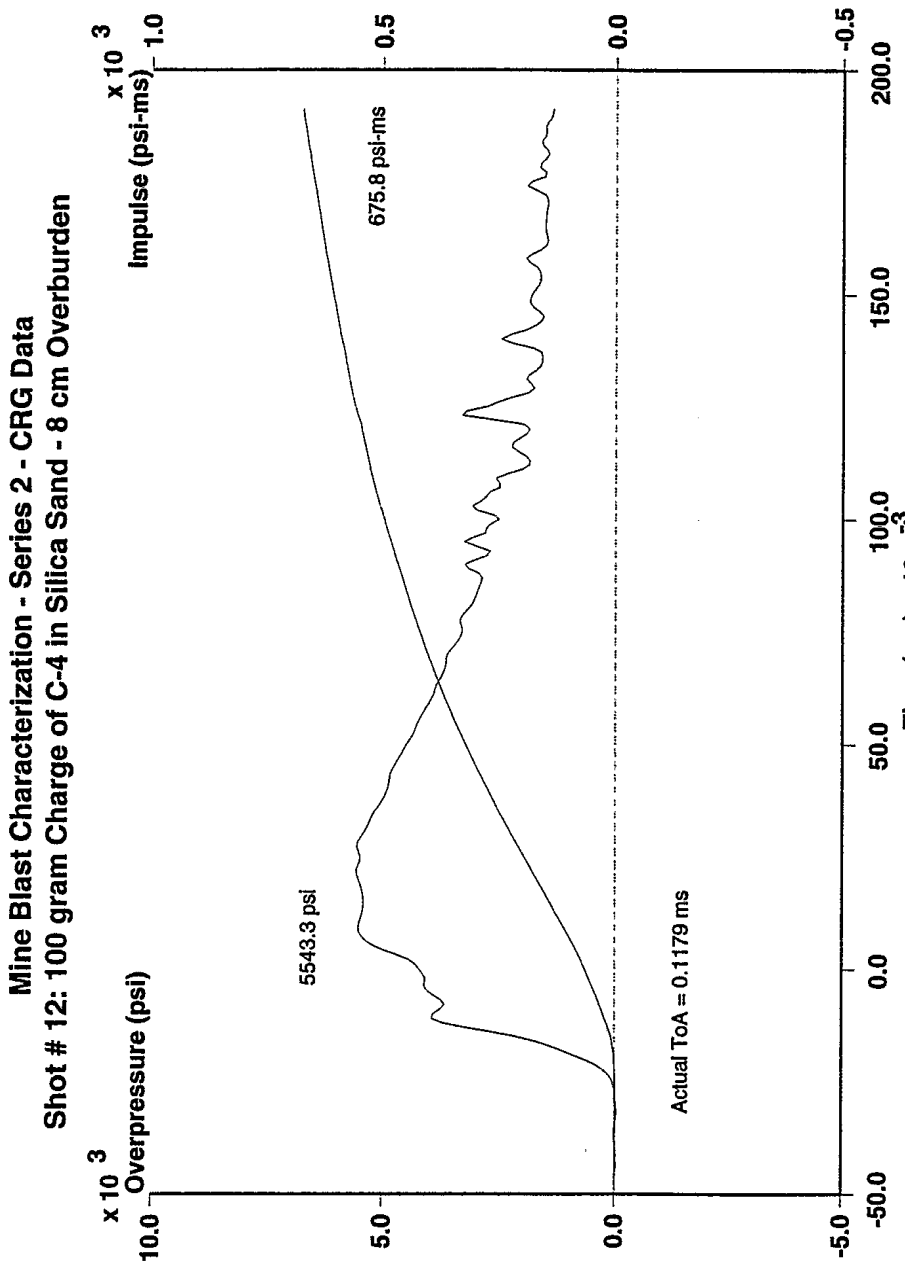

Position 7 (10.73 cm), In Ground Pressure, 2nd Order 100 kHz Butterworth Filter

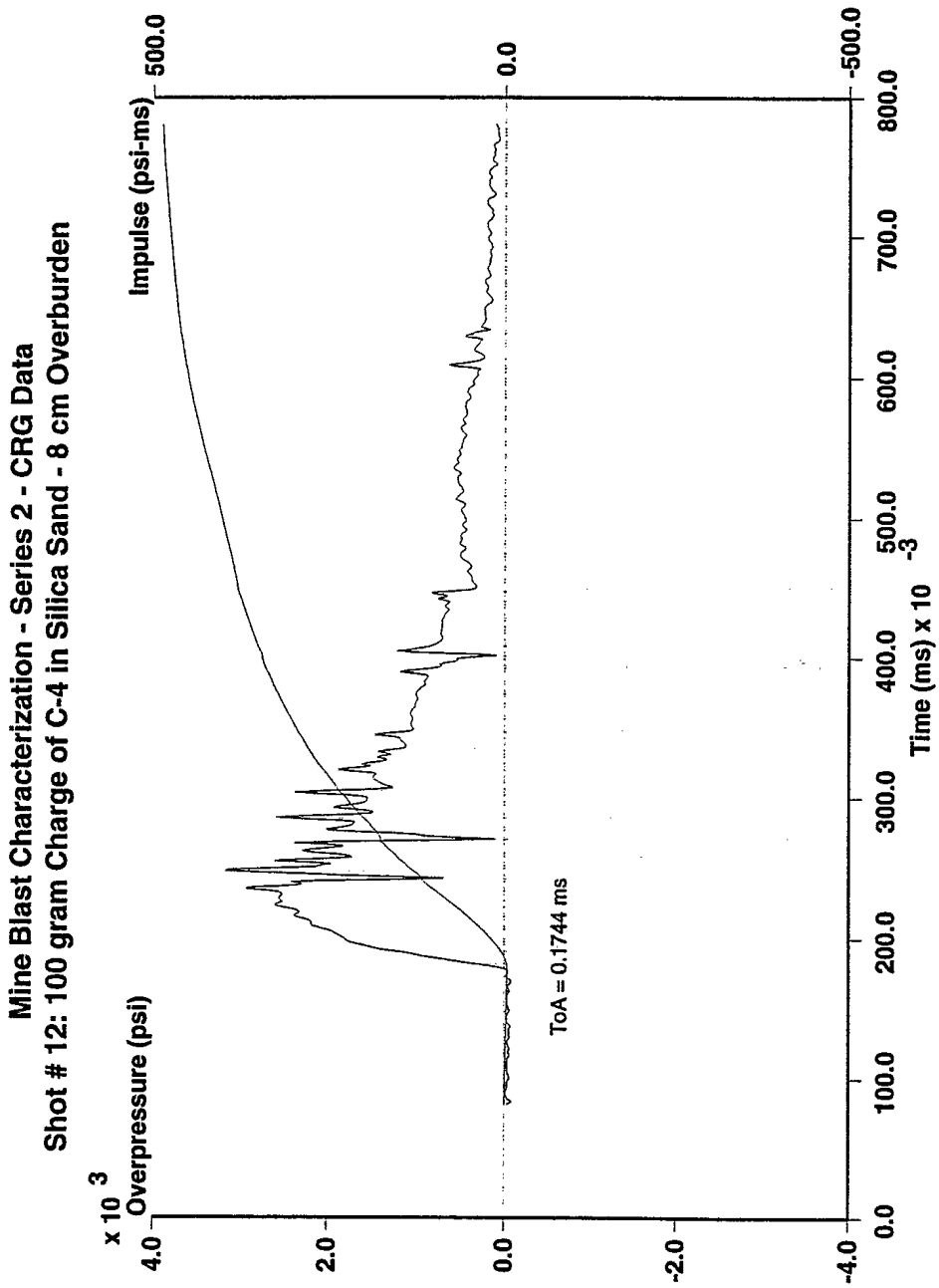

Position 8 (13.23 cm), In Ground Pressure, 2nd Order 100 kHz Butterworth Filter

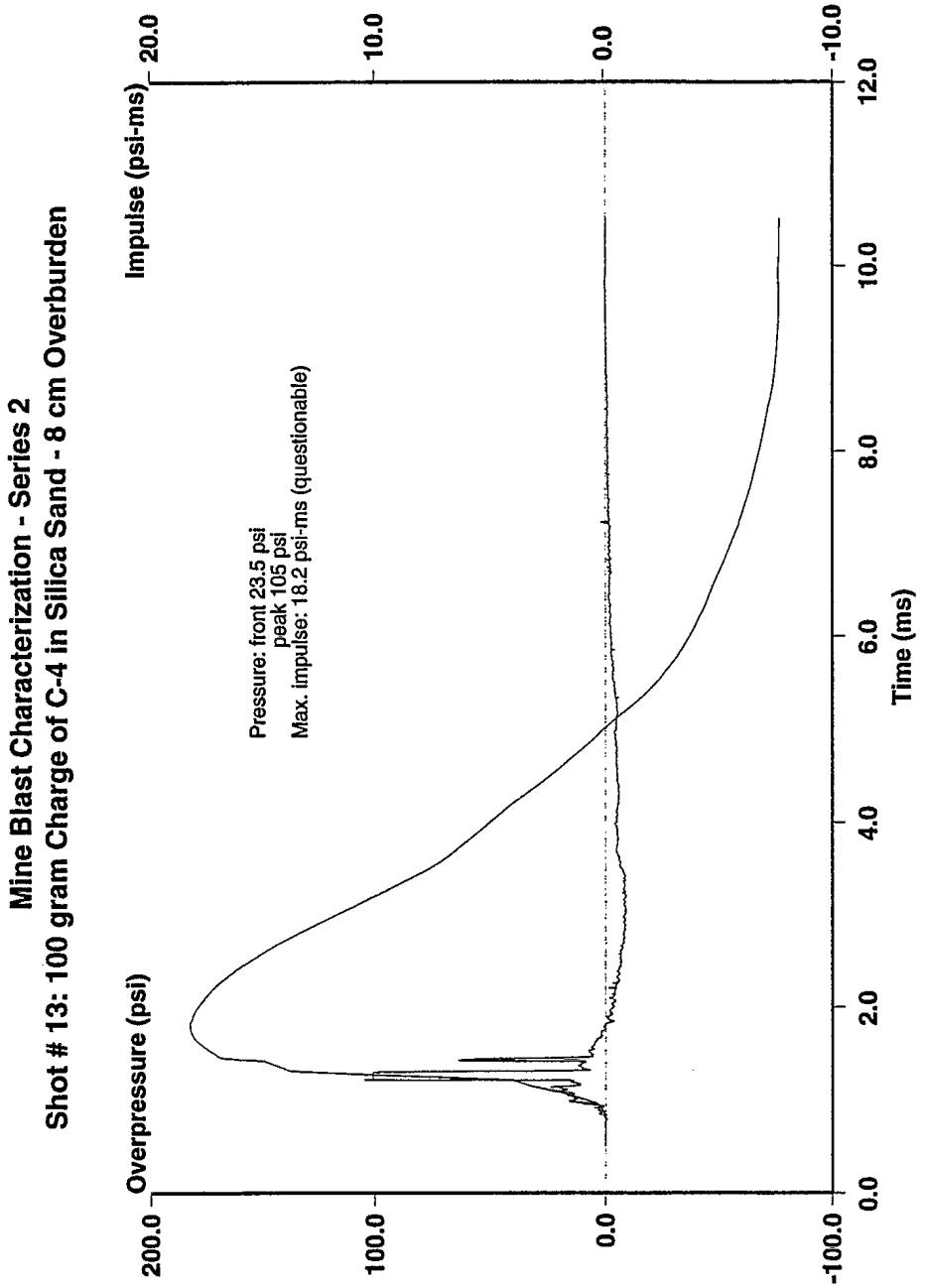

Position 1 (38 cm), Air Shock, 2nd Order 100 kHz Butterworth Filter

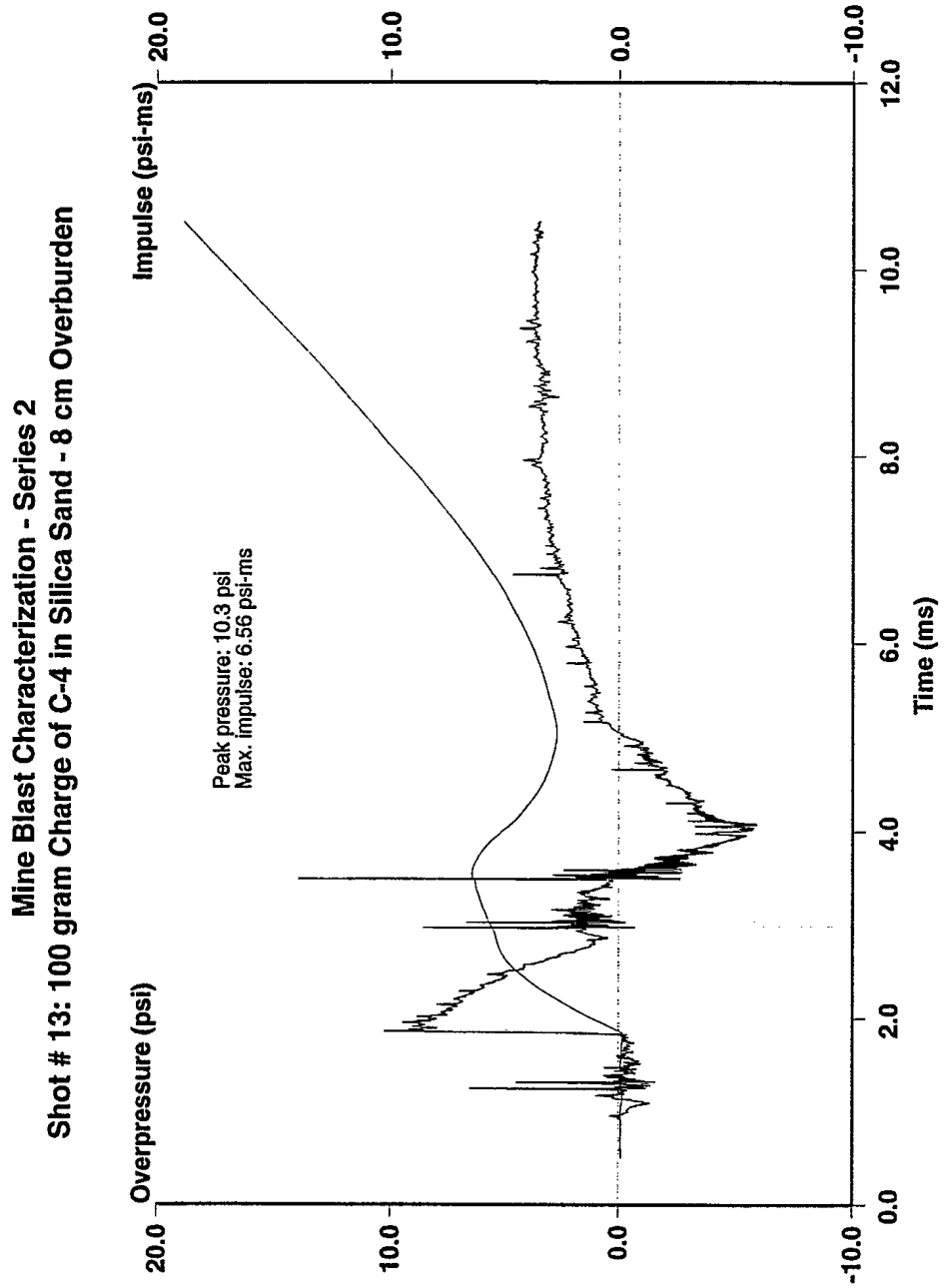

Position 2 (78 cm), Air Shock, 2nd Order 100 kHz Butterworth Filter

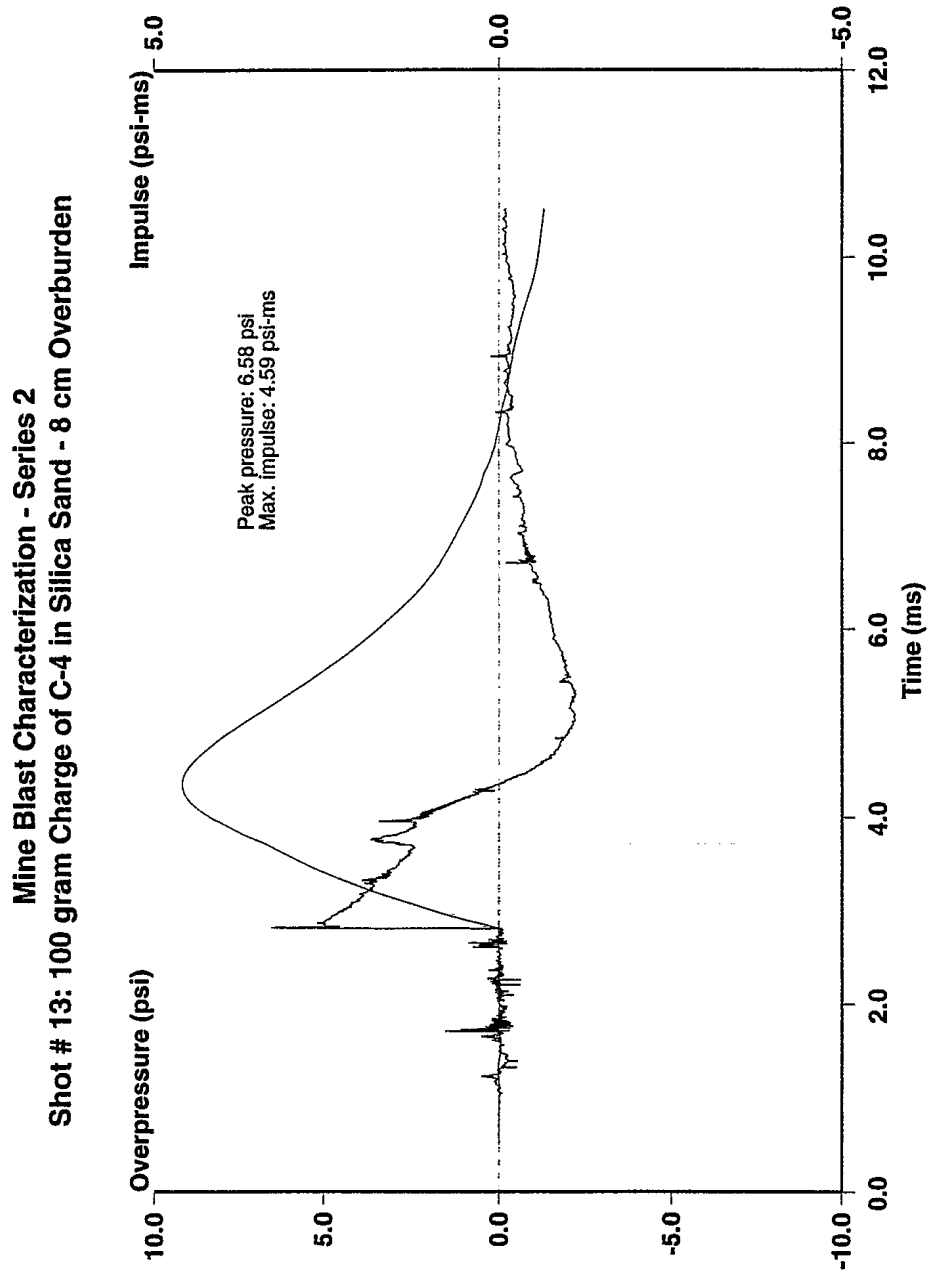

Position 3 (118 cm), Air Shock, 2nd Order 100 kHz Butterworth Filter

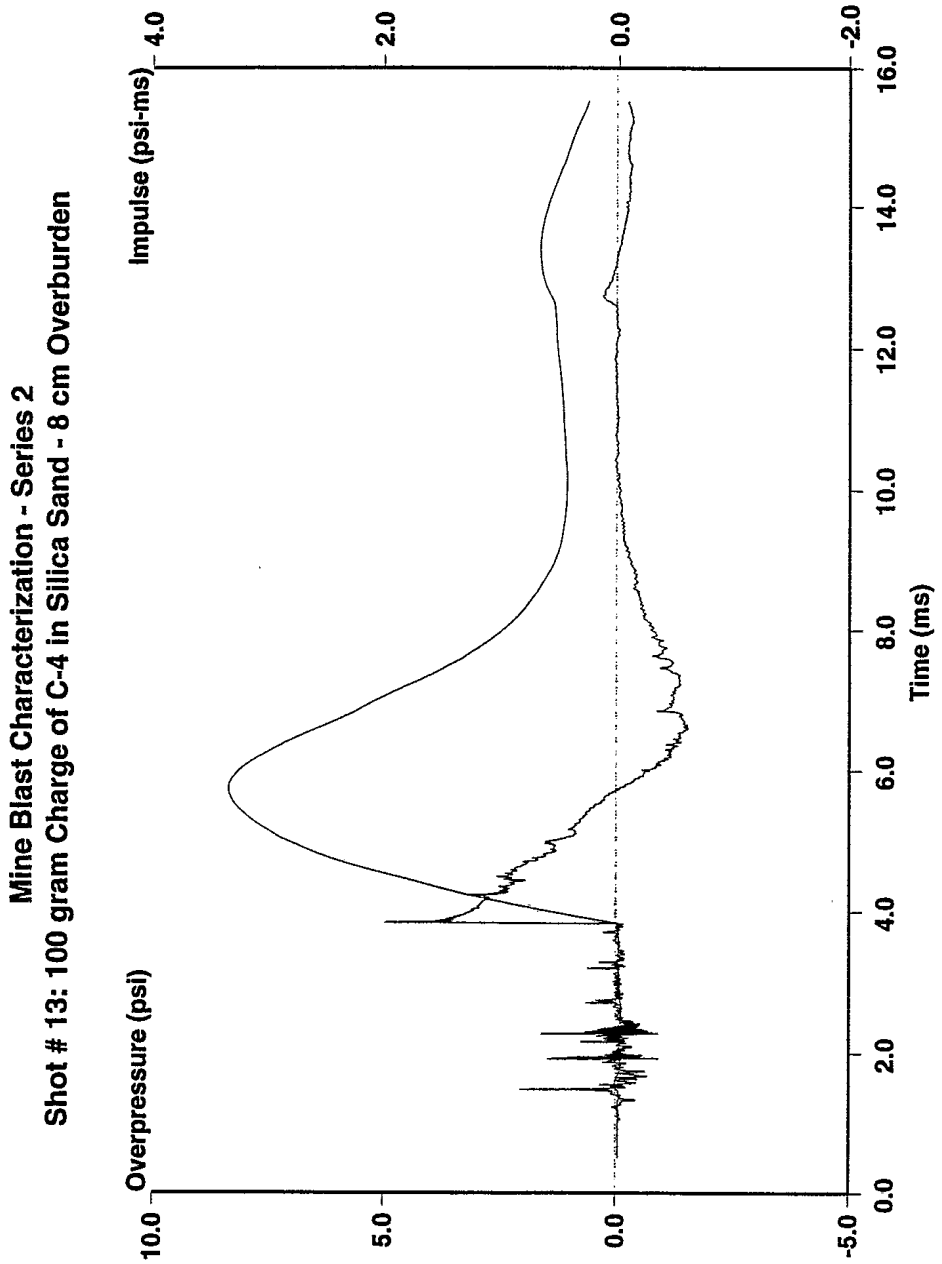
Mine Blast Characterization - Series 2
Shot # 13: 100 gram Charge of C-4 in Silica Sand - 8 cm Overburden
Overpressure (psi)
10.0
5.0
0.0
-5.0
Impulse (psi-ms)
4.0
2.0
0.0
-2.0
0.0
2.0
4.0
6.0
8.0
10.0
12.0
14.0
16.0
Time (ms)
Position 4 (158 cm), Air Shock, 2nd Order 100 kHz Butterworth Filter

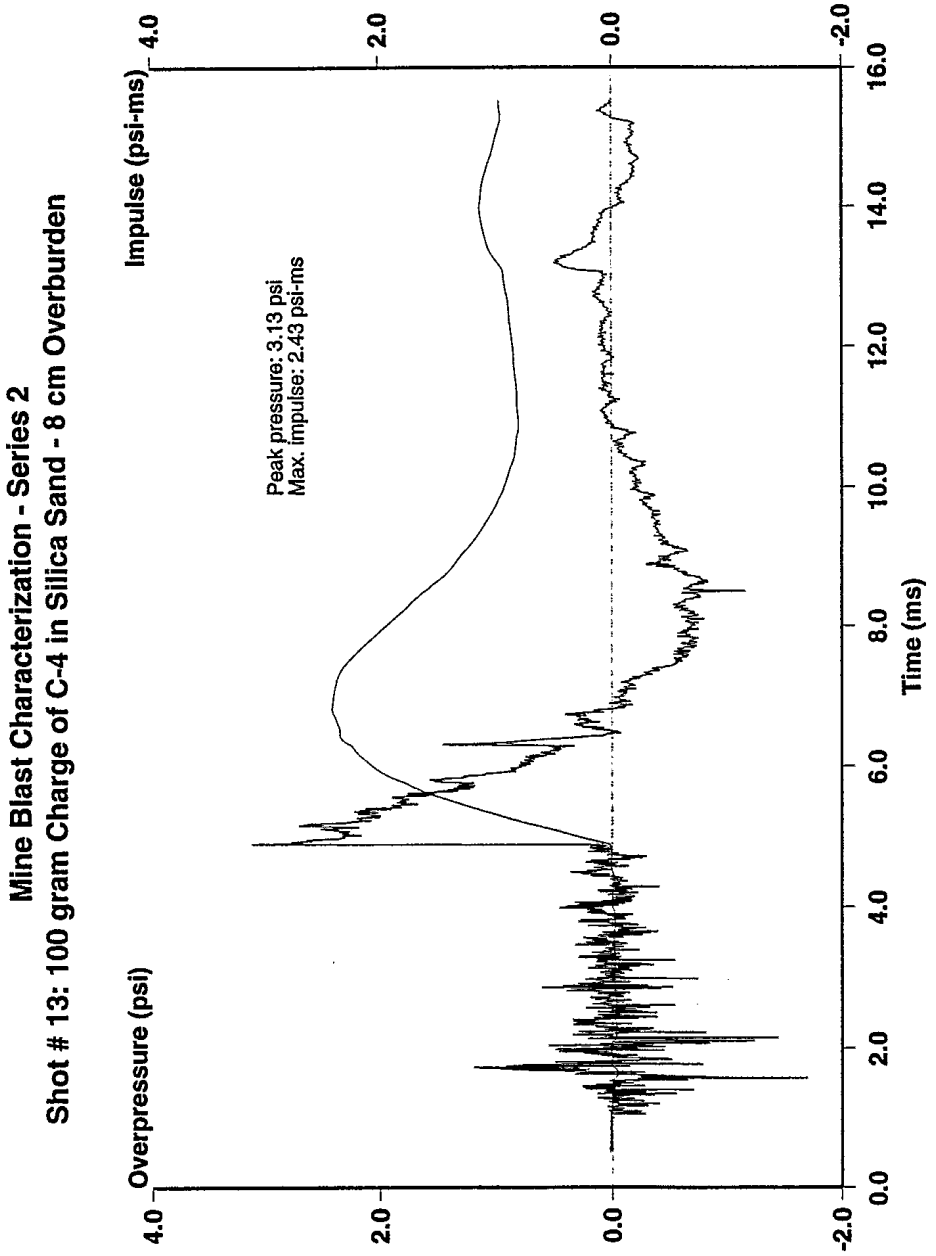

Position 5 (198 cm), Air Shock, 2nd Order 100 kHz Butterworth Filter

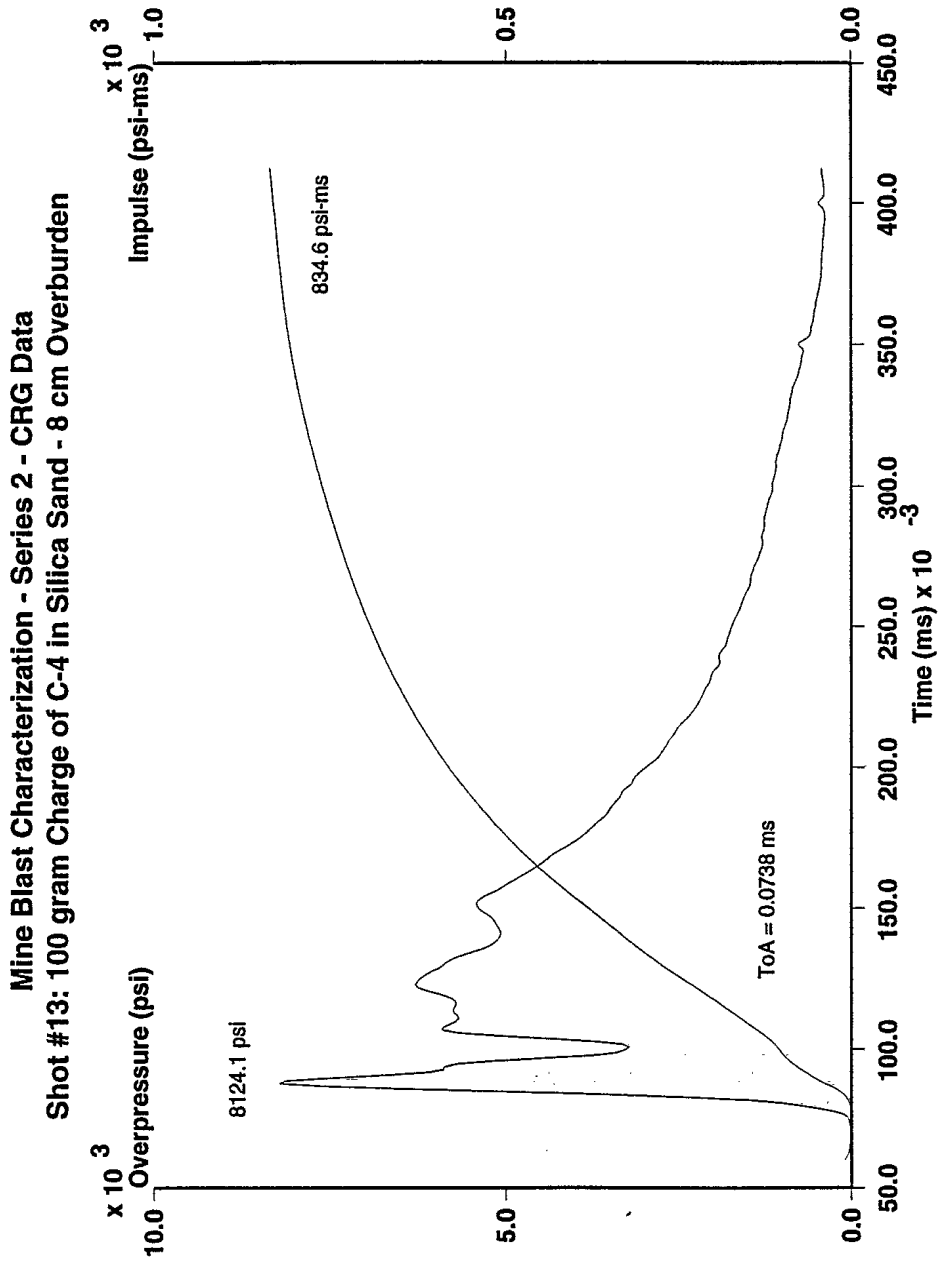

Position 6 (8.23 cm), In Ground Pressure, 2nd Order 100 kHz Butterworth Filter

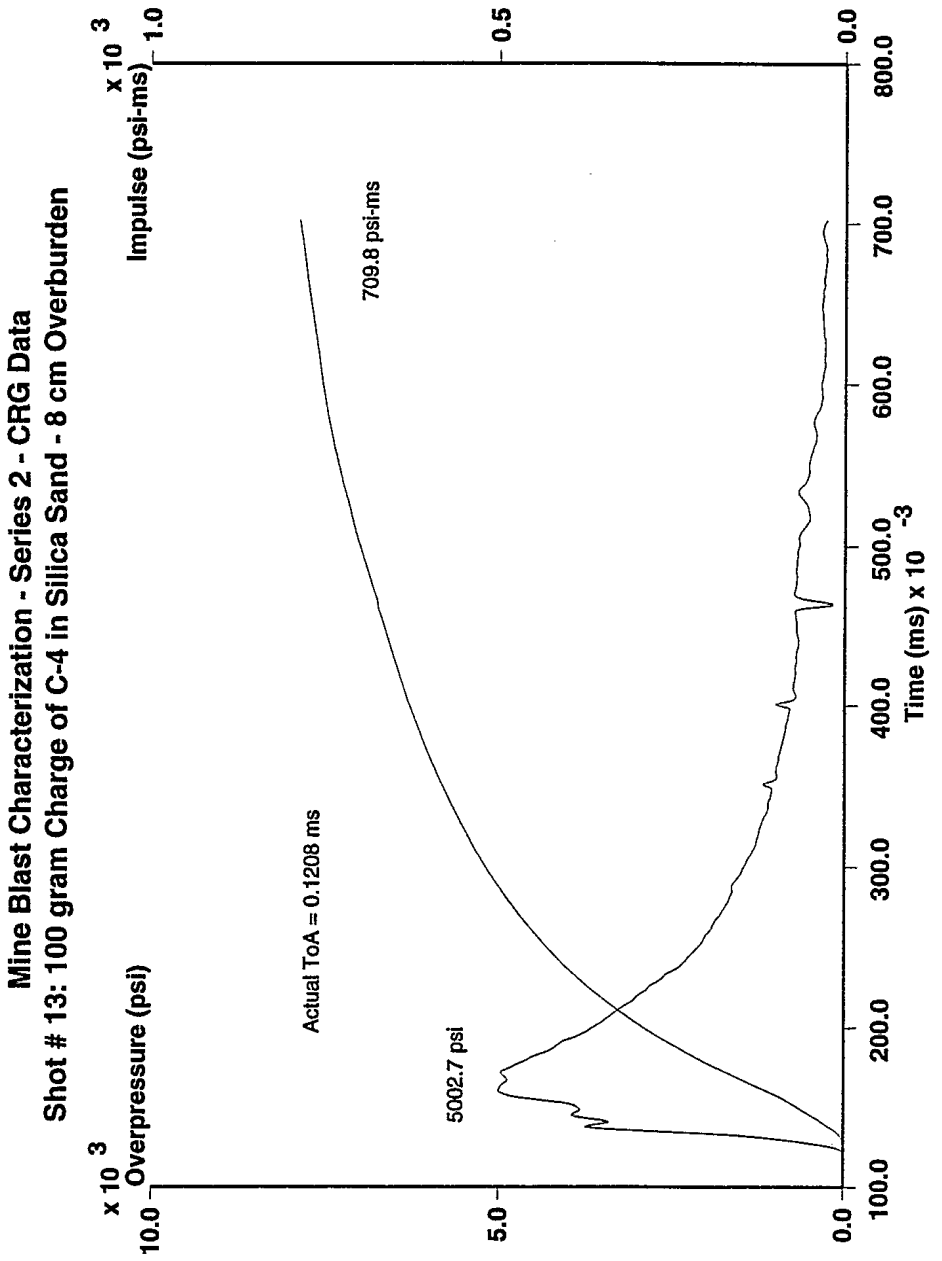

Position 7 (10.73 cm), In Ground Pressure, 2nd Order 100 kHz Butterworth Filter

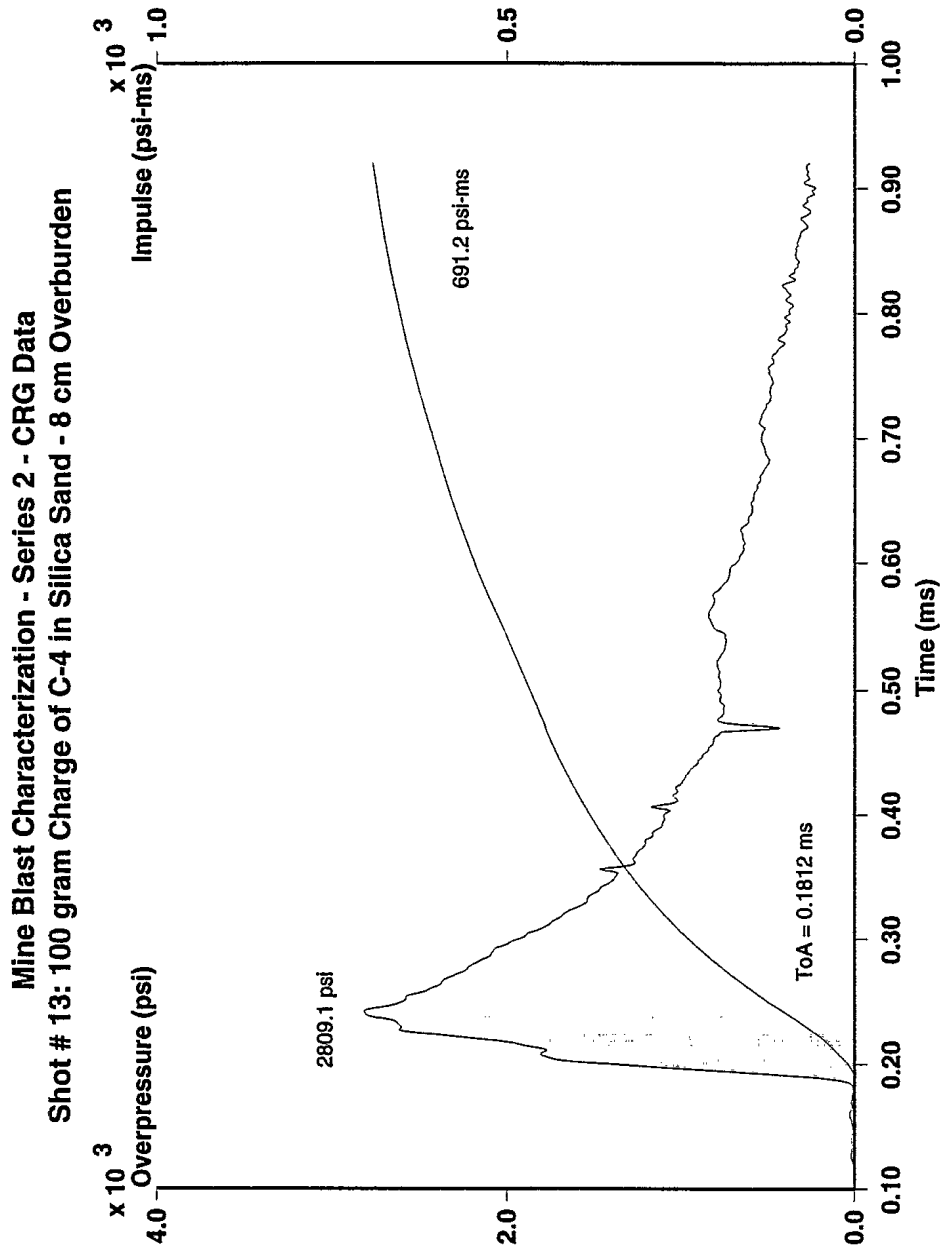

Position 8 (13.23 cm), In Ground Pressure, 2nd Order 100 kHz Butterworth Filter

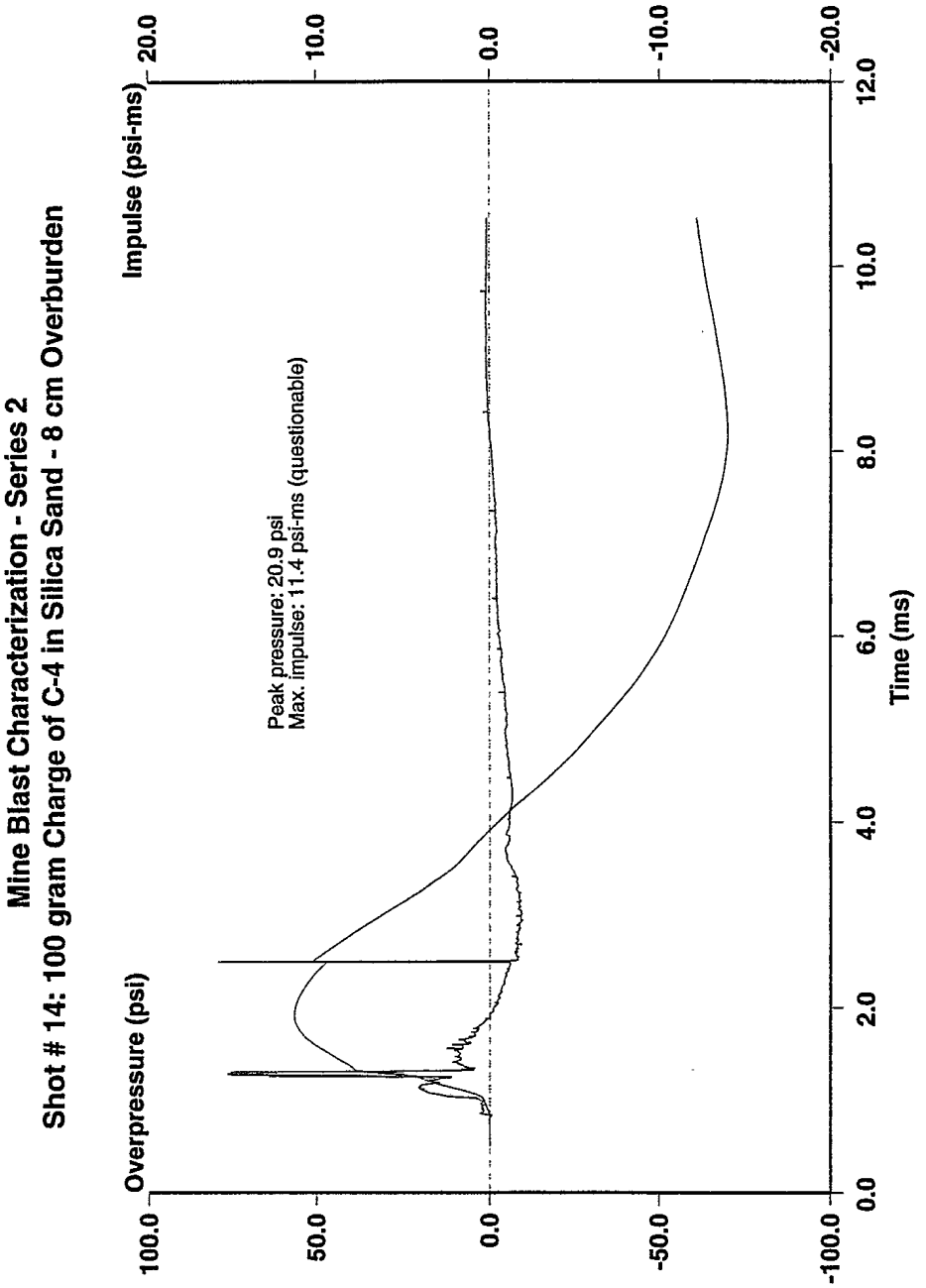

Position 1 (38 cm), Air Shock, 2nd Order 100 kHz Butterworth Filter

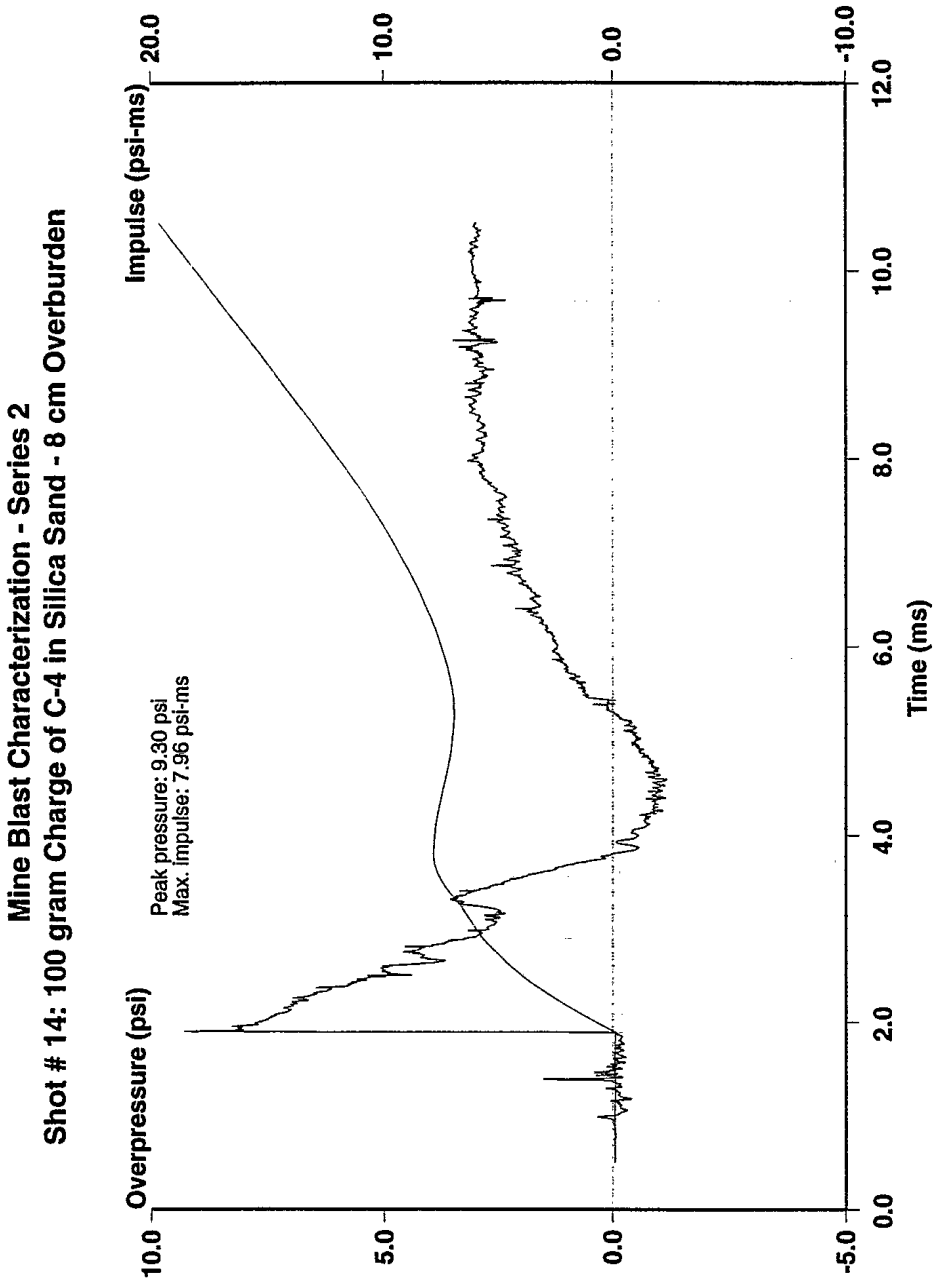

Position 2 (78 cm), Air Shock, 2nd Order 100 kHz Butterworth Filter

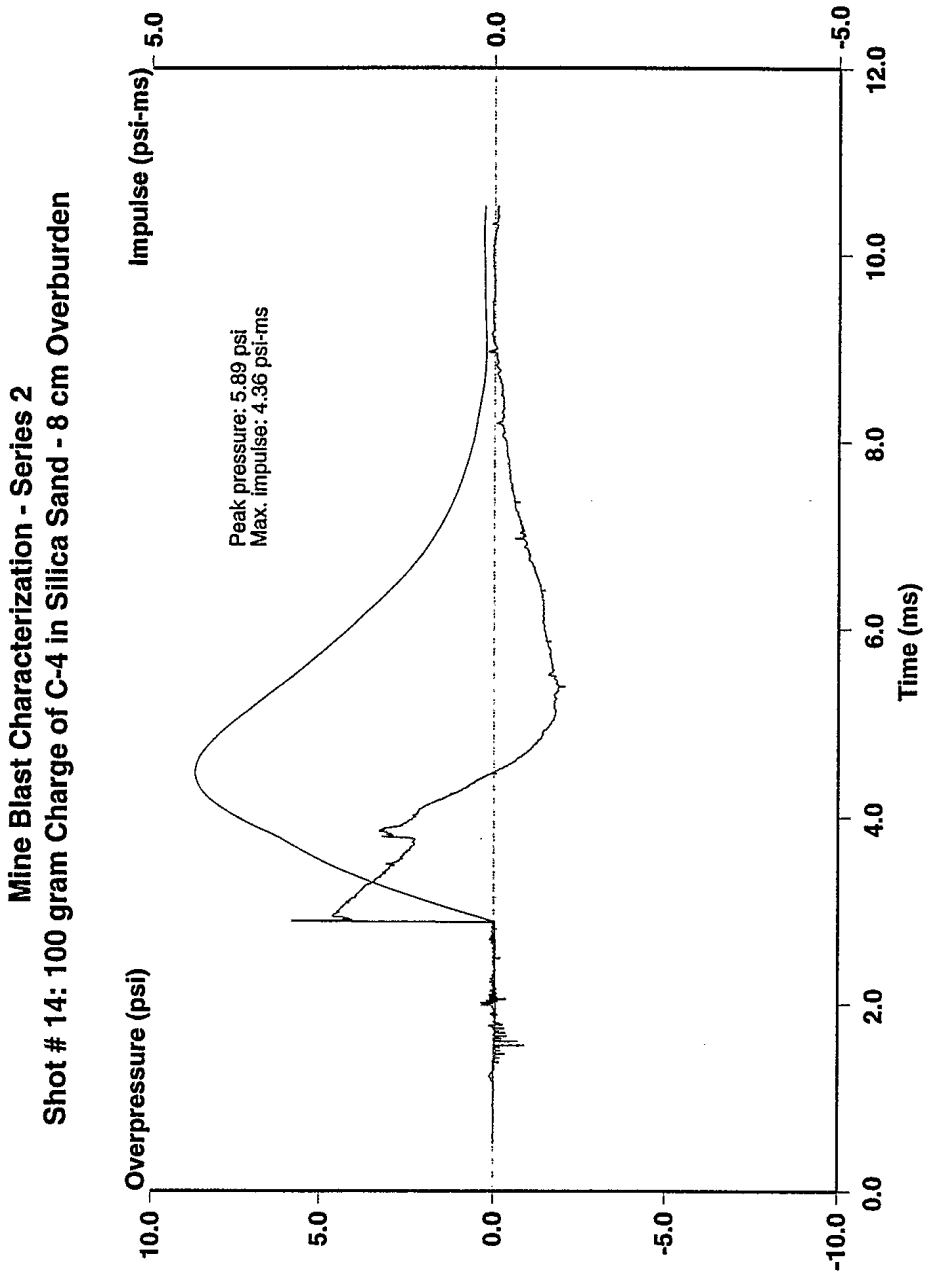

Position 3 (118 cm), Air Shock, 2nd Order 100 kHz Butterworth Filter

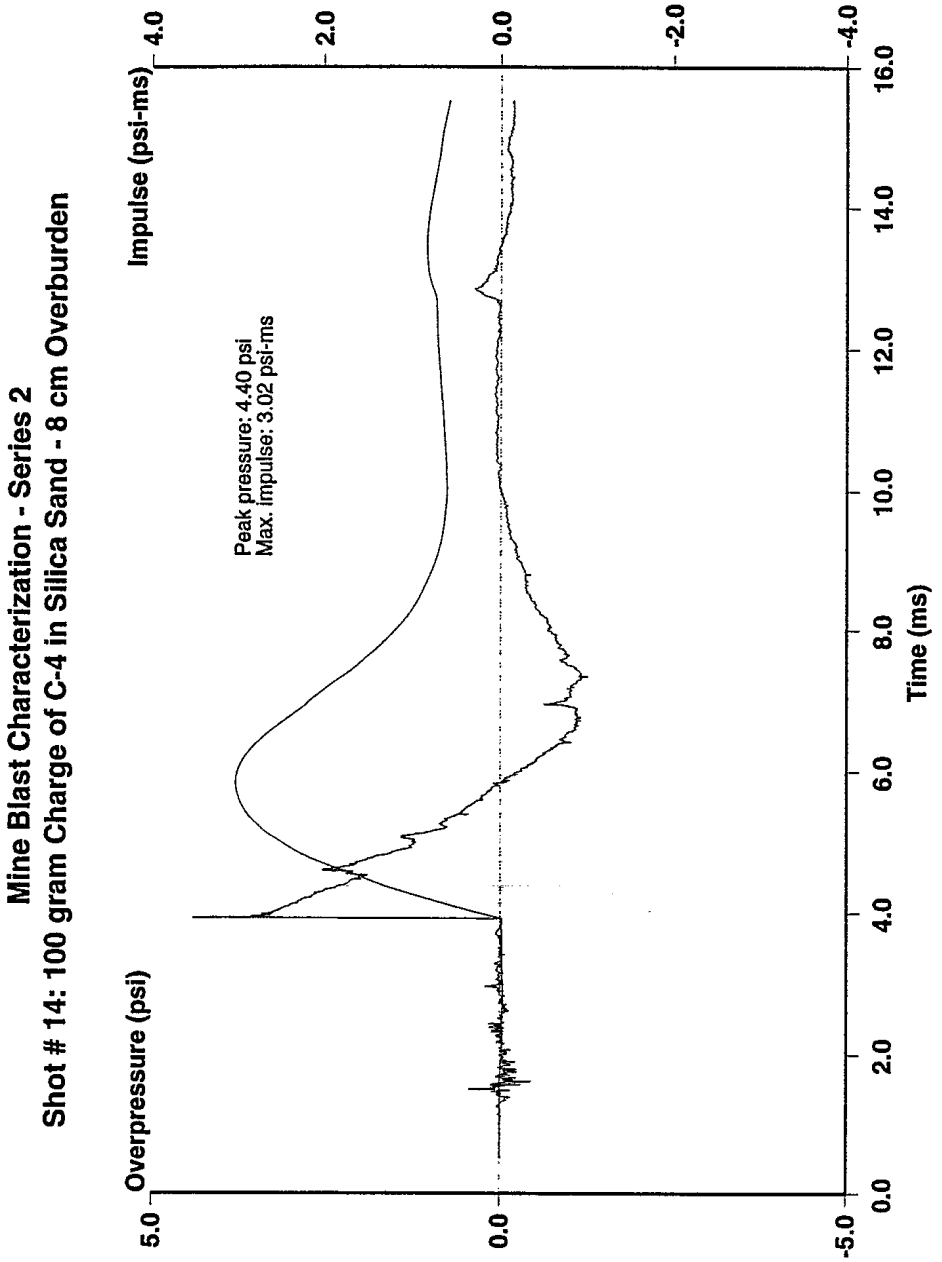

Position 4 (158 cm), Air Shock, 2nd Order 100 kHz Butterworth Filter

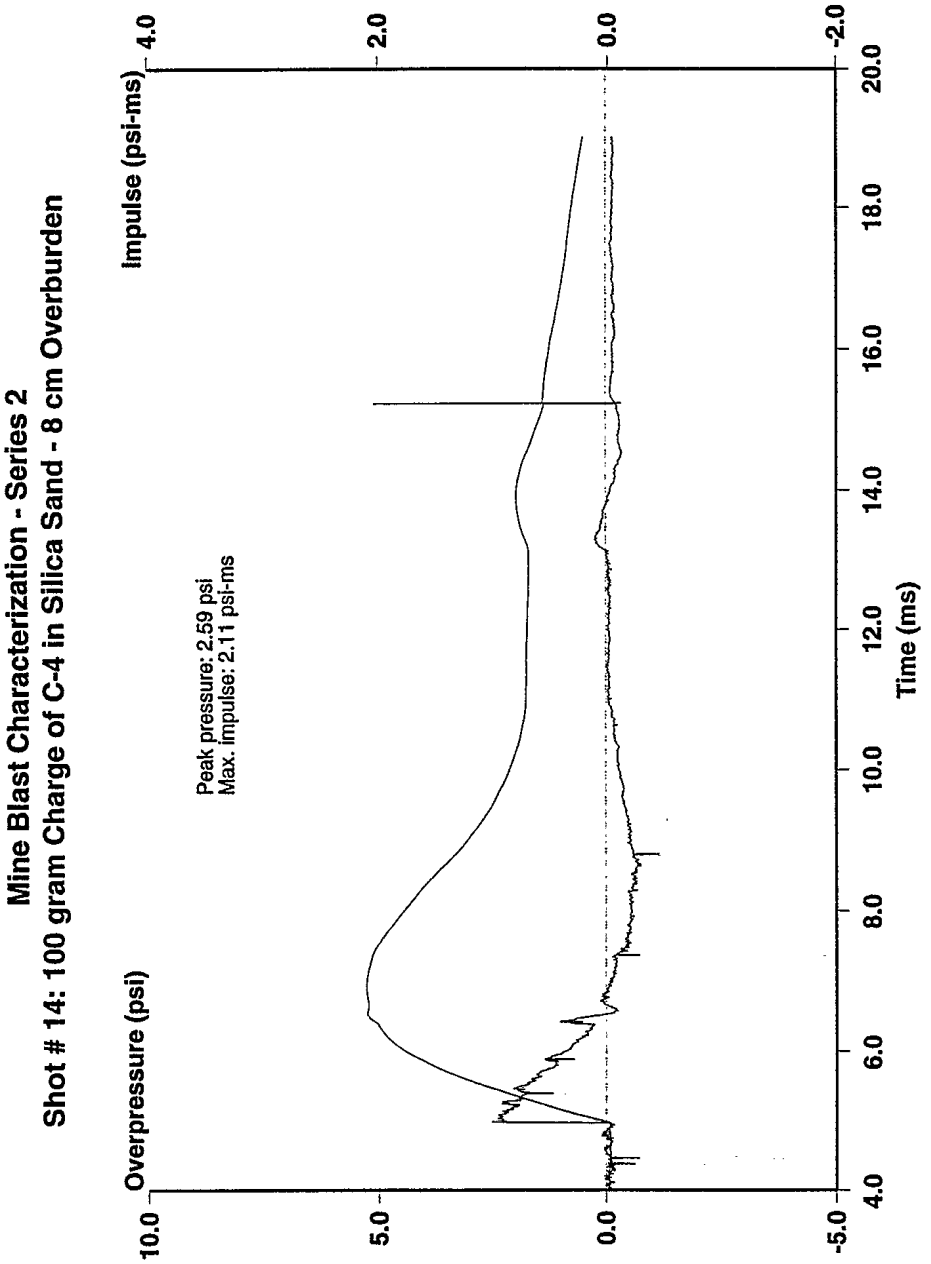

Position 5 (198 cm), Air Shock, 2nd Order 100 kHz Butterworth Filter

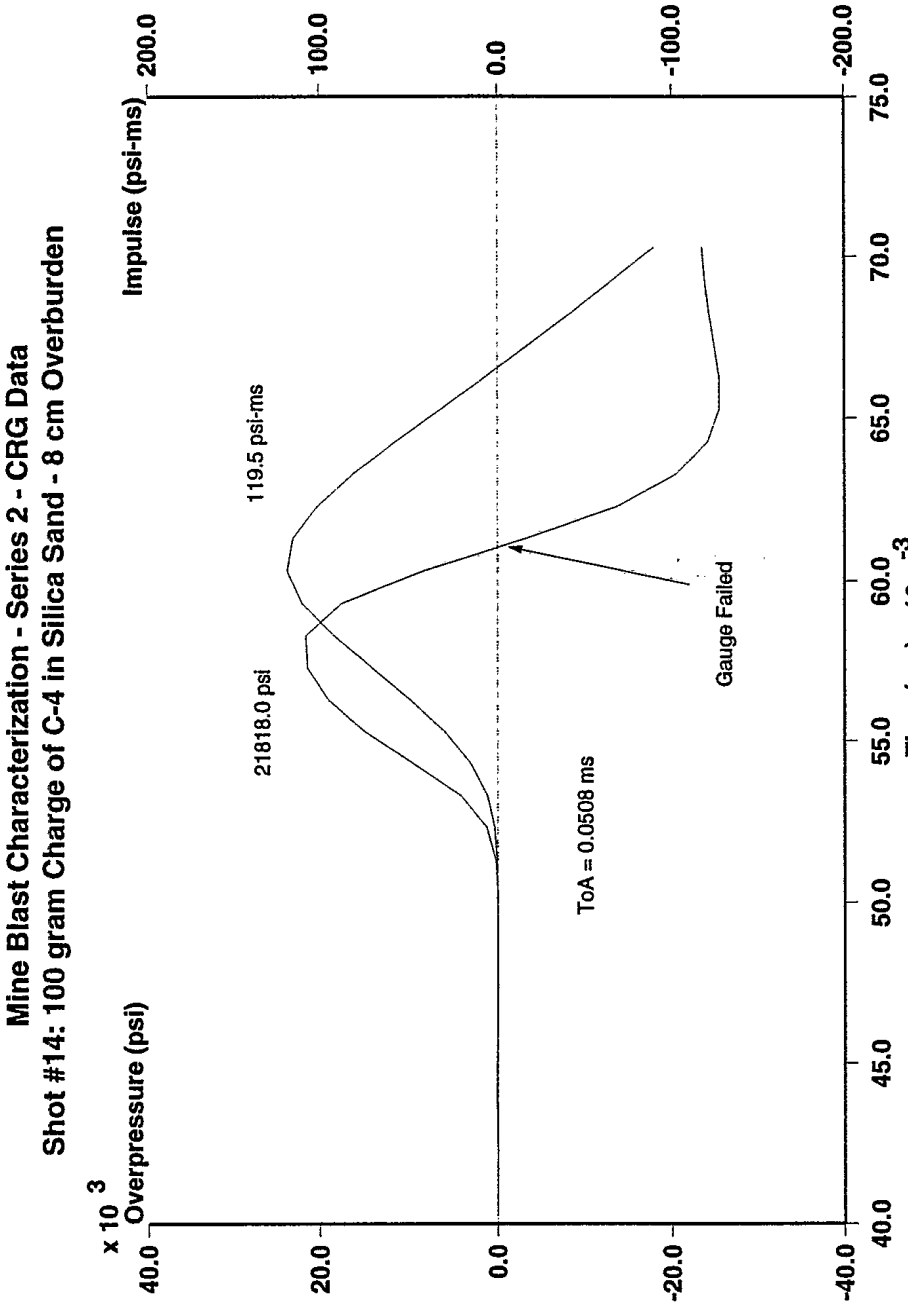

Position 6 (6.23 cm), In Ground Pressure, 2nd Order 100 kHz Butterworth Filter

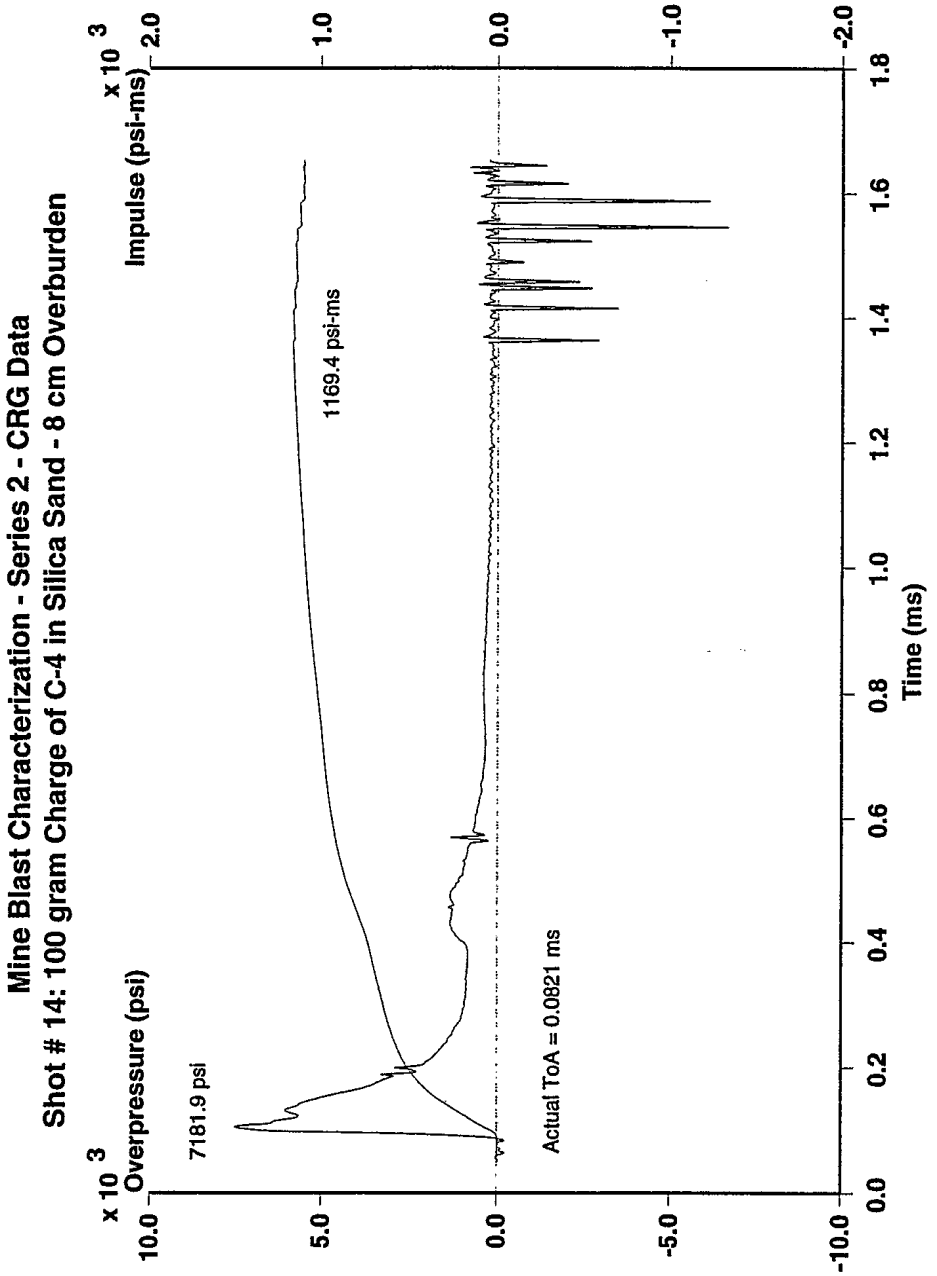

Position 7 (8.73 cm), In Ground Pressure, 2nd Order 100 kHz Butterworth Filter

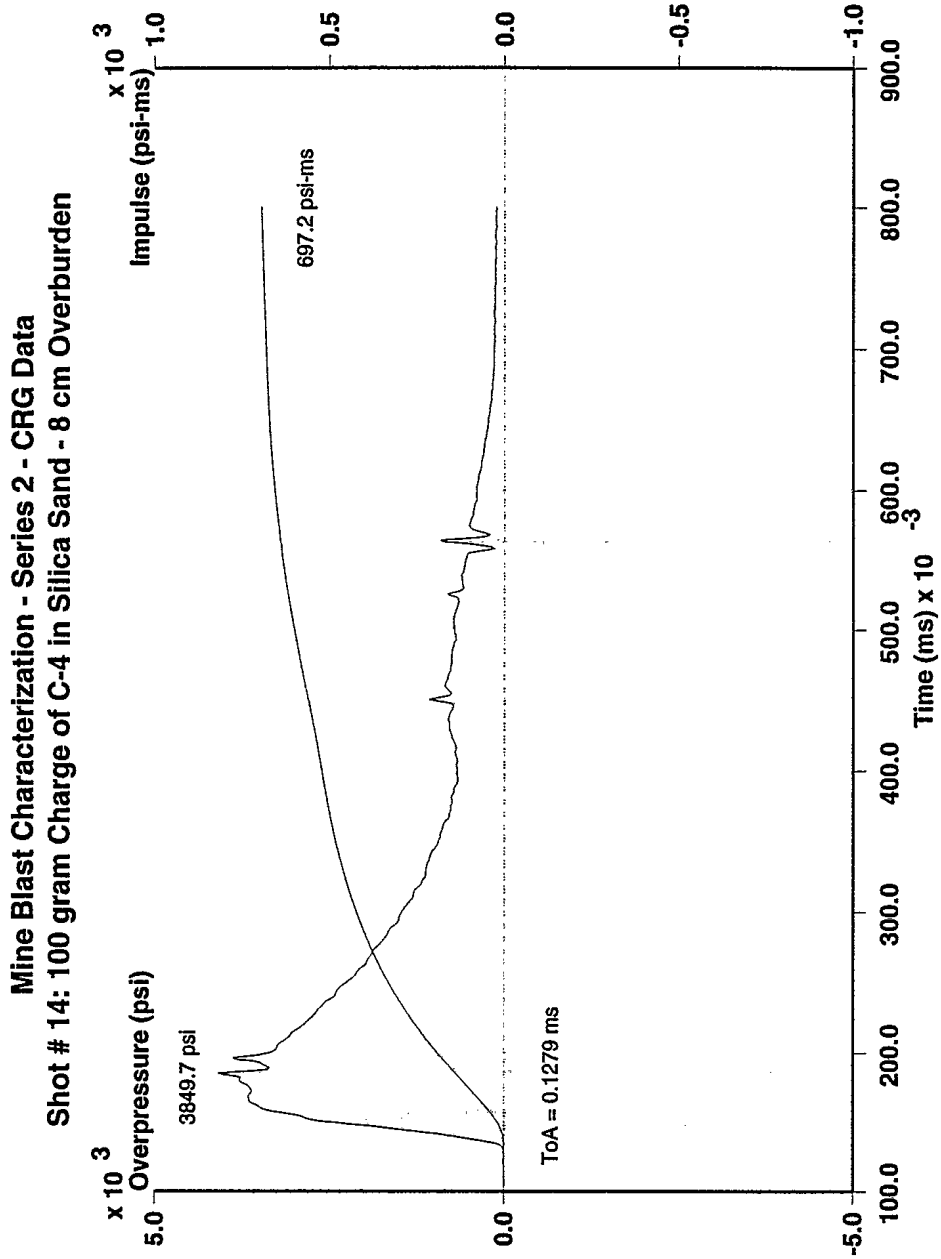

Position 8 (11.23 cm), In Ground Pressure, 2nd Order 100 kHz Butterworth Filter

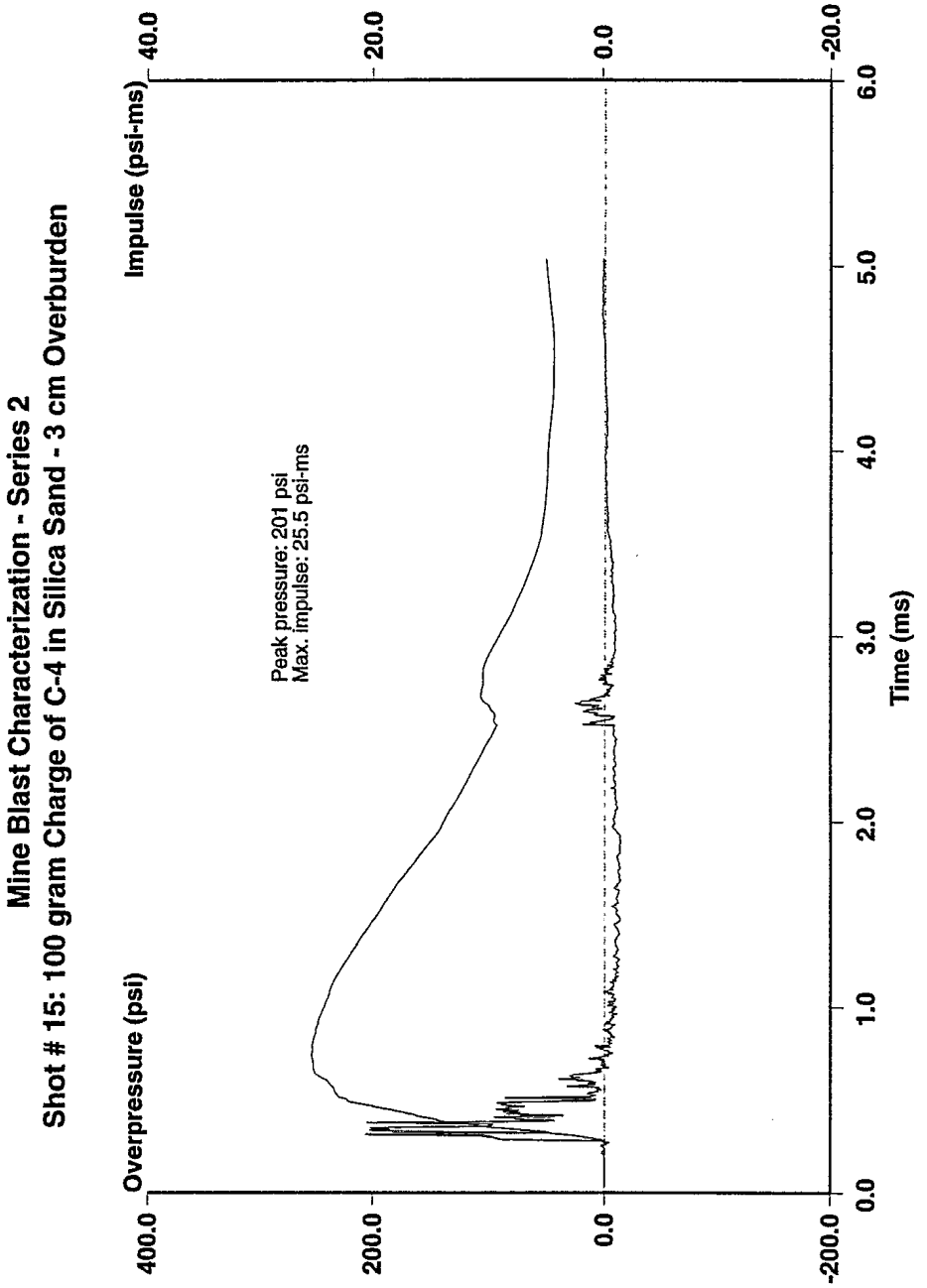

Position 1 (33 cm), Air Shock, 2nd Order 100 kHz Butterworth Filter

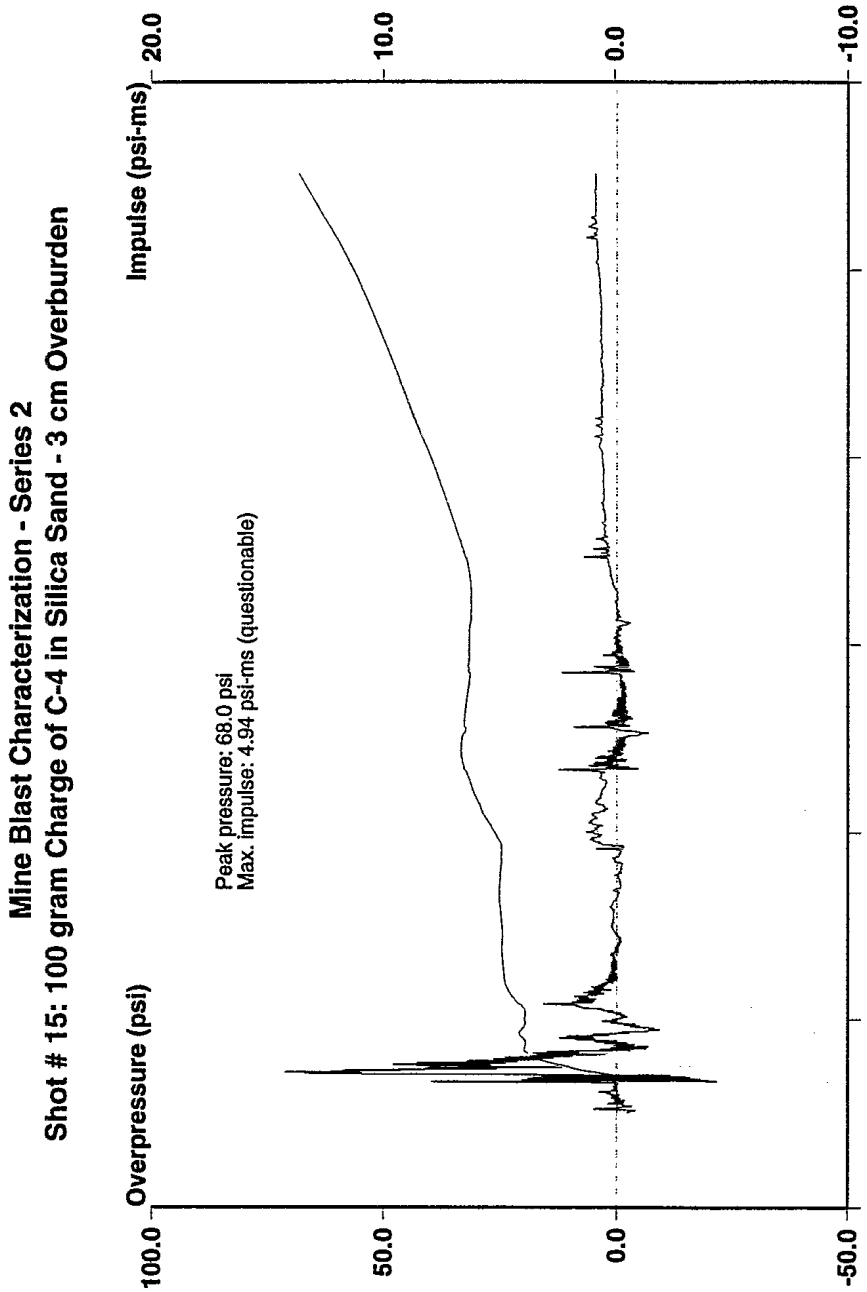

Position 2 (73 cm), Air Shock, 2nd Order 100 kHz Butterworth Filter

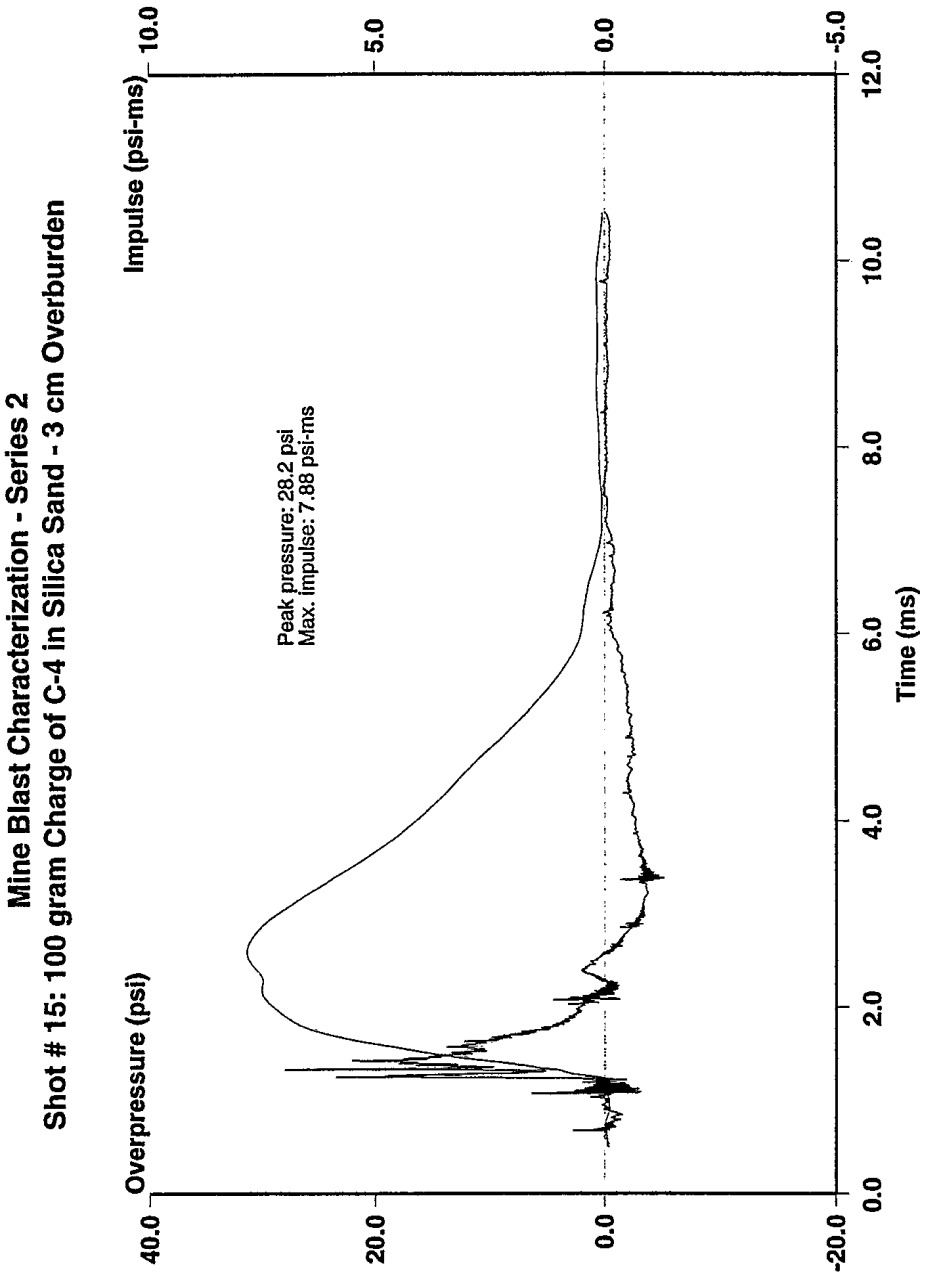

Position 3 (113 cm), Air Shock, 2nd Order 100 kHz Butterworth Filter

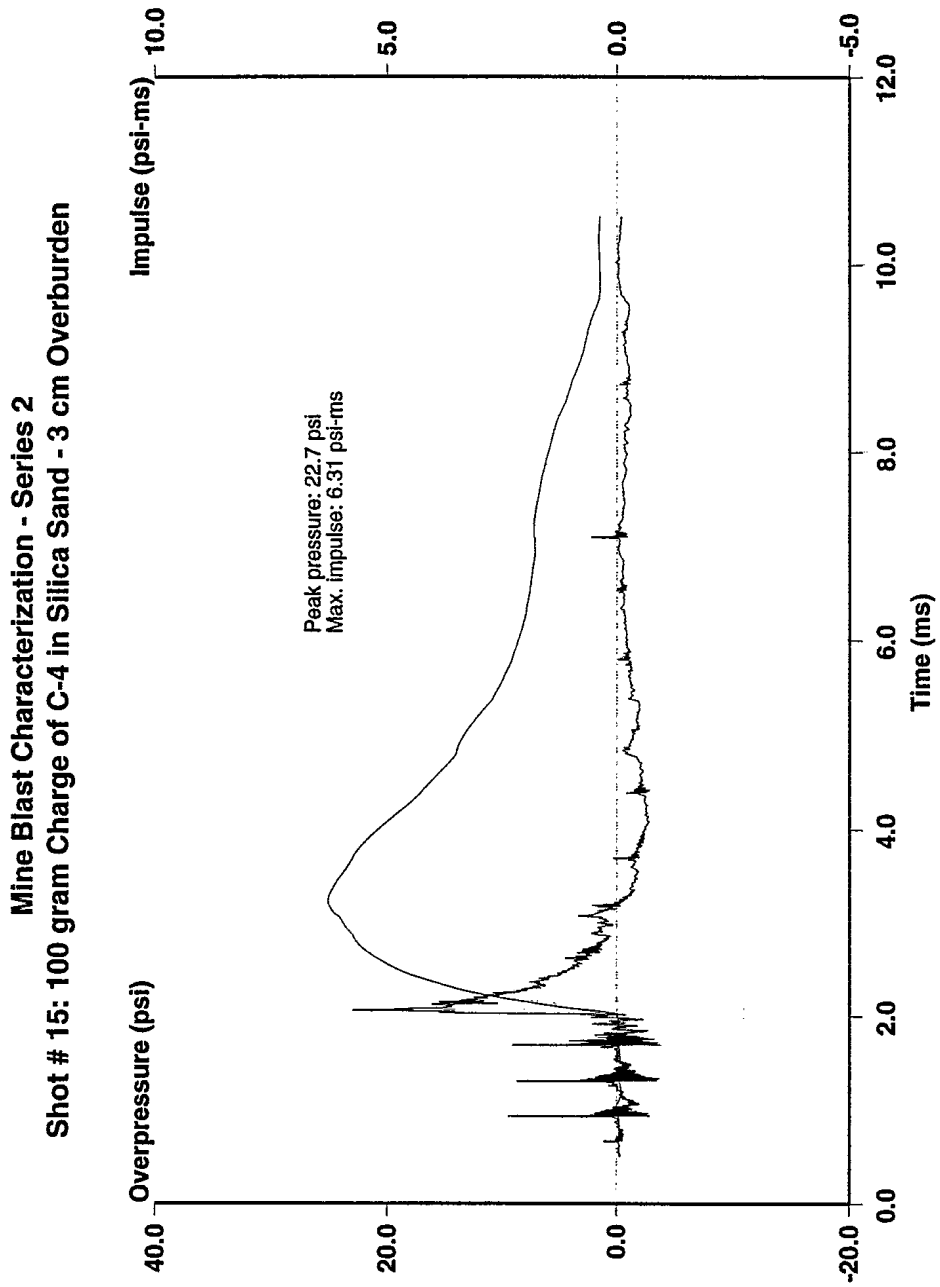

Position 4 (153 cm), Air Shock, 2nd Order 100 kHz Butterworth Filter

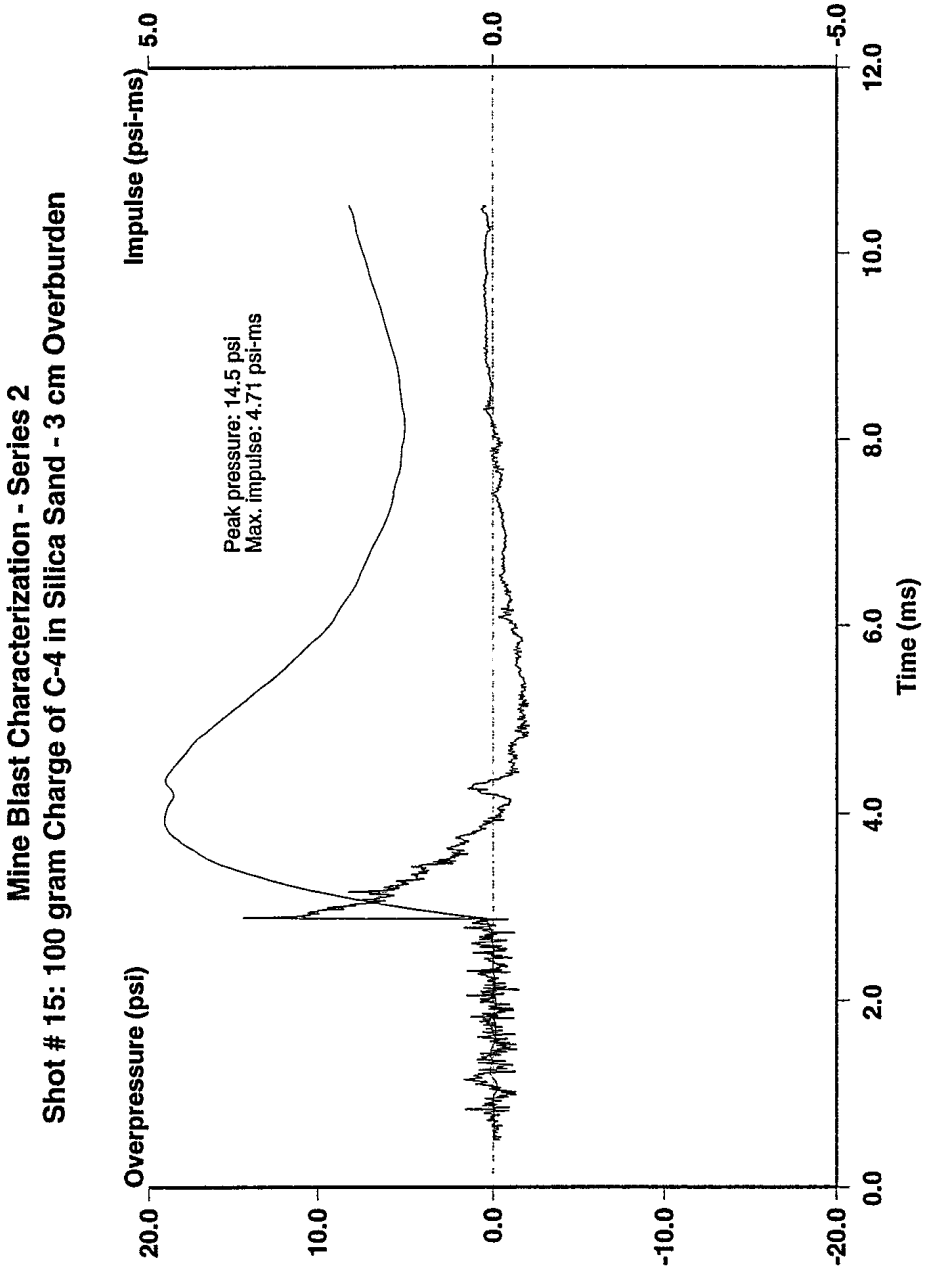

Position 5 (193 cm), Air Shock, 2nd Order 100 kHz Butterworth Filter

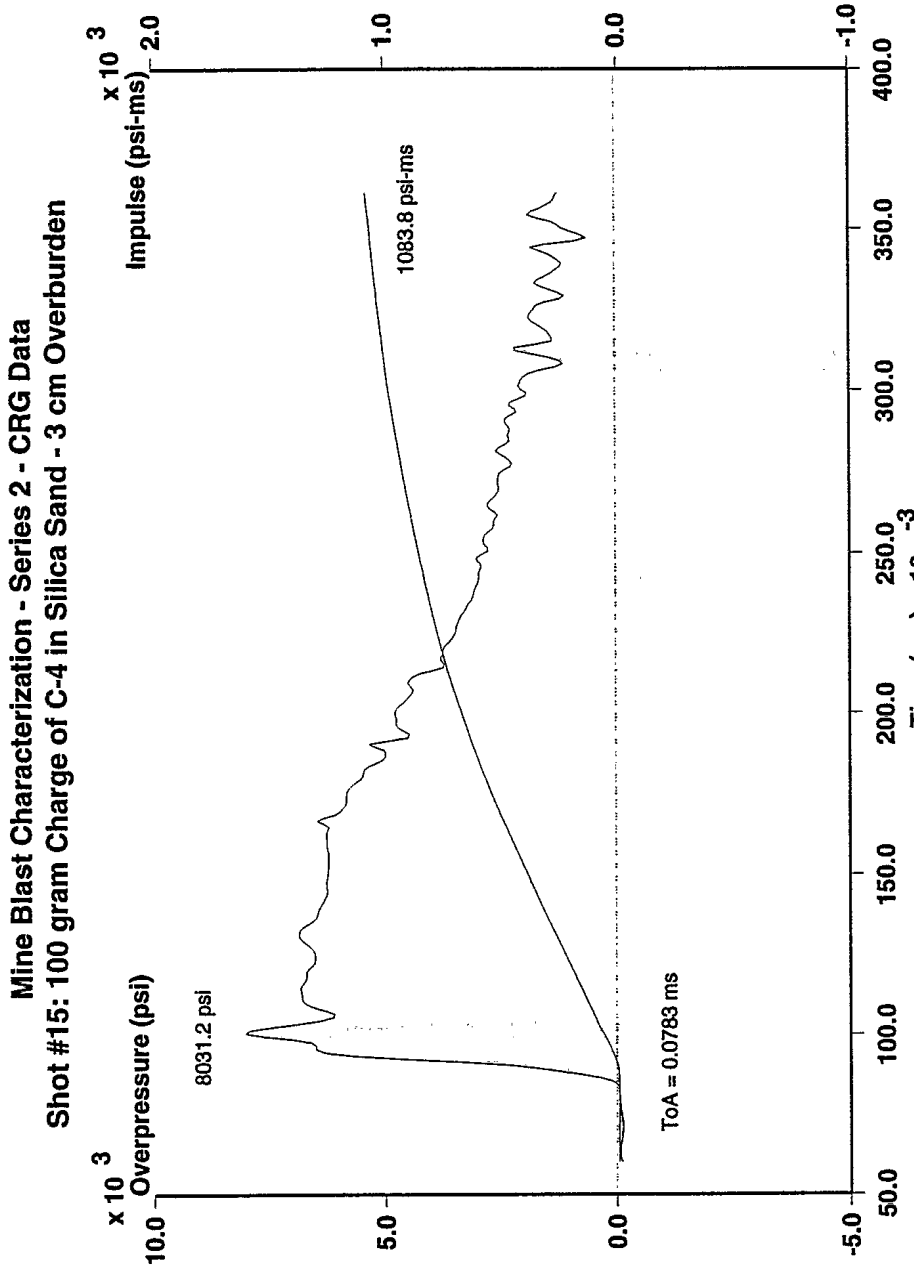

Position 6 (8.23 cm), In Ground Pressure, 2nd Order 100 kHz Butterworth Filter

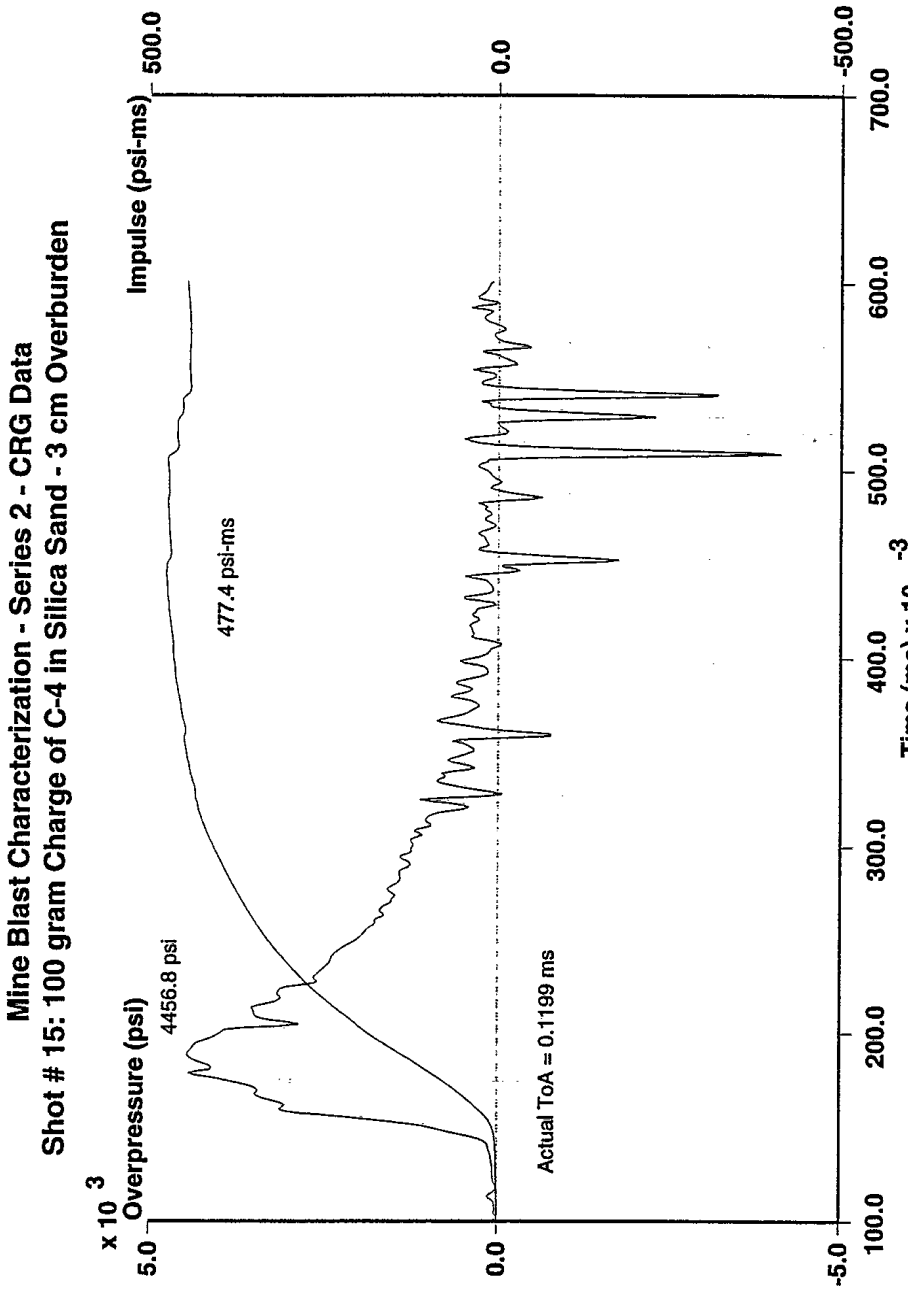

Position 7 (10.73 cm), In Ground Pressure, 2nd Order 100 kHz Butterworth Filter

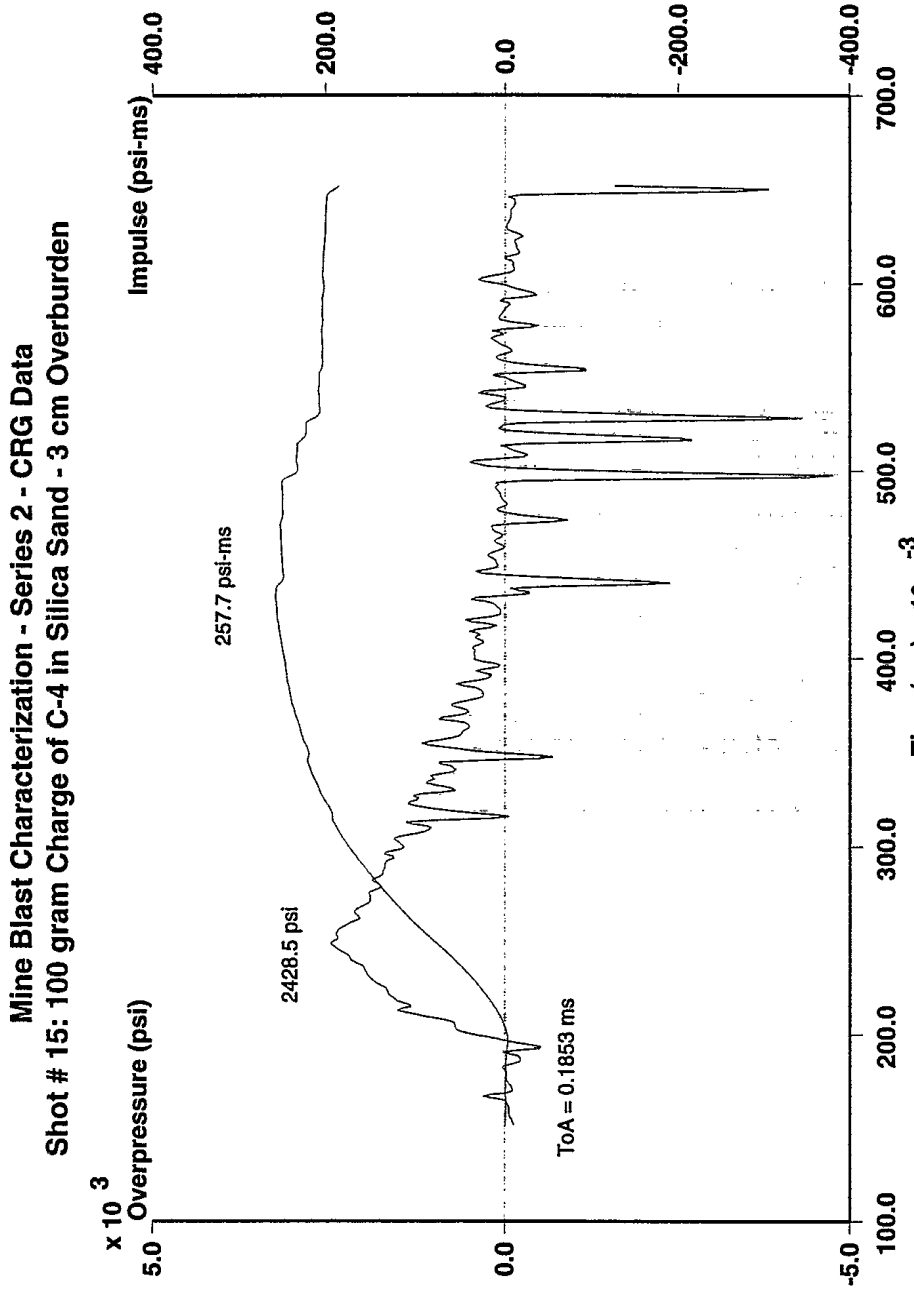

Position 8 (13.23 cm), In Ground Pressure, 2nd Order 100 kHz Butterworth Filter

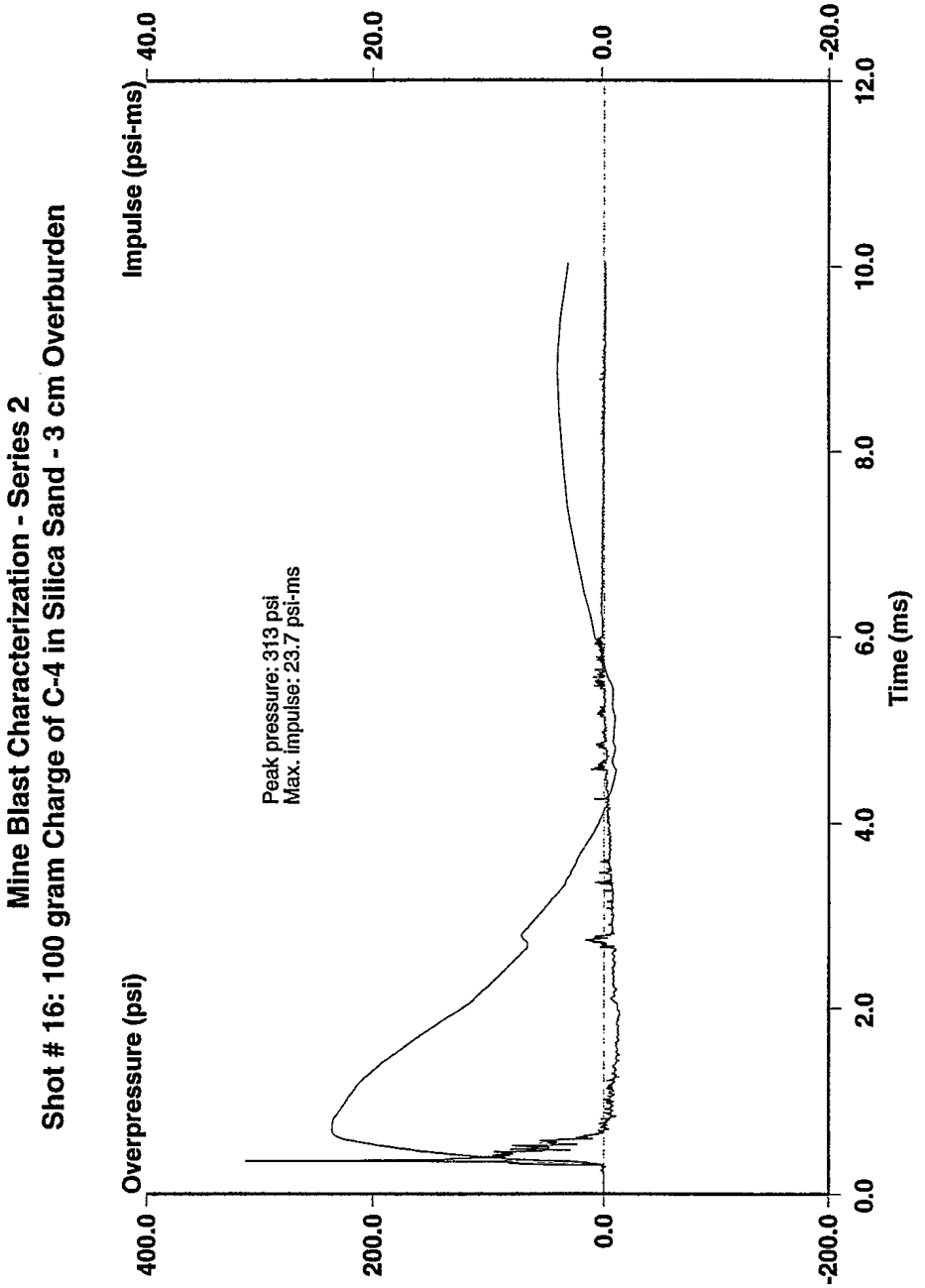

Position 1 (33 cm), Air Shock, 2nd Order 100 kHz Butterworth Filter

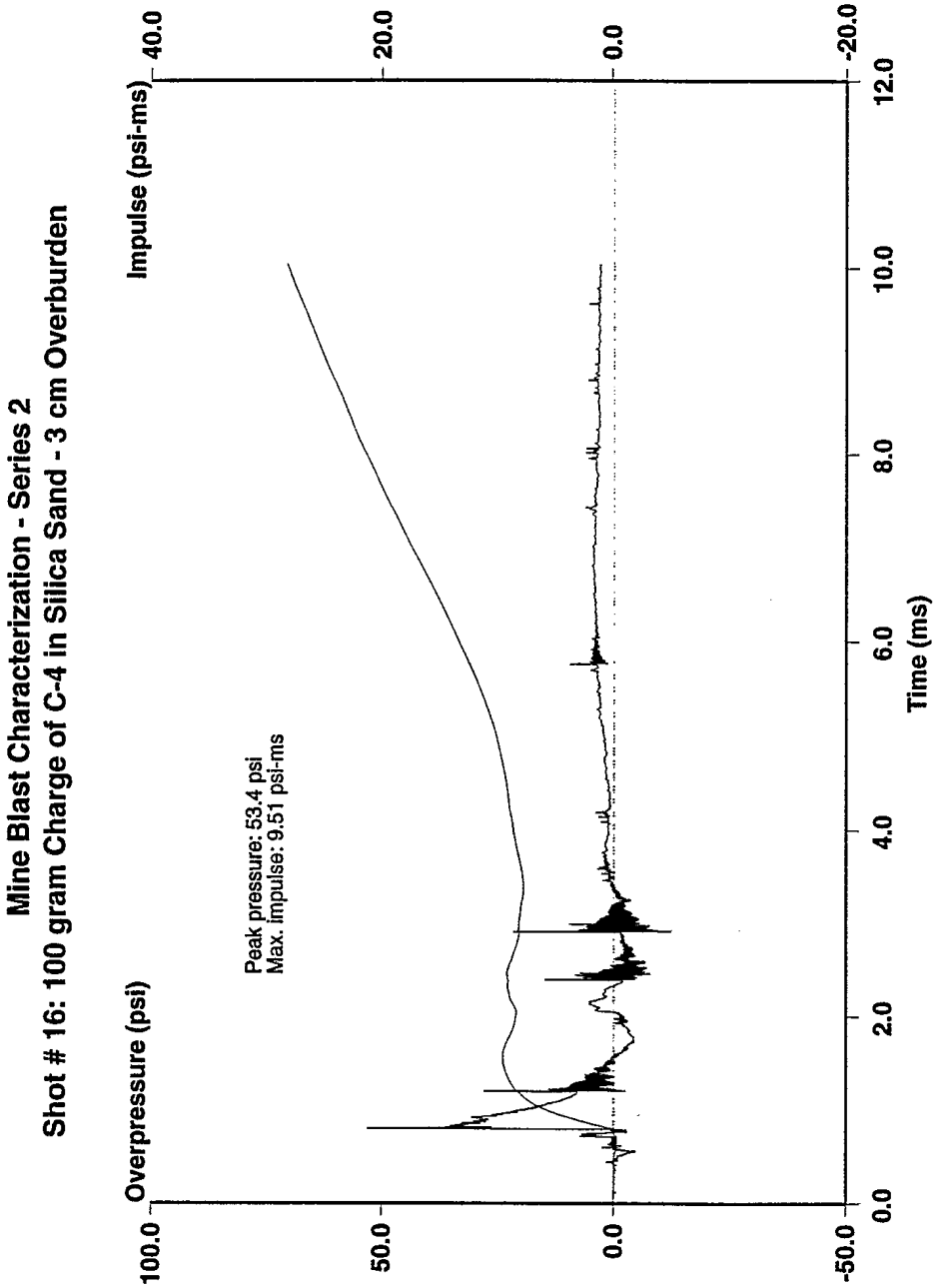
Mine Blast Characterization - Series 2
Shot # 16: 100 gram Charge of C-4 in Silica Sand - 3 cm Overburden
Overpressure (psi)
Impulse (psi-ms)
Time (ms)
Peak pressure: 53.4 psi
Max. impulse: 9.51 psi-ms
100.0
50.0
0.0
-50.0
40.0
20.0
0.0
-20.0
0.0
2.0
4.0
6.0
8.0
10.0
12.0
Position 2 (73 cm), Air Shock, 2nd Order 100 kHz Butterworth Filter

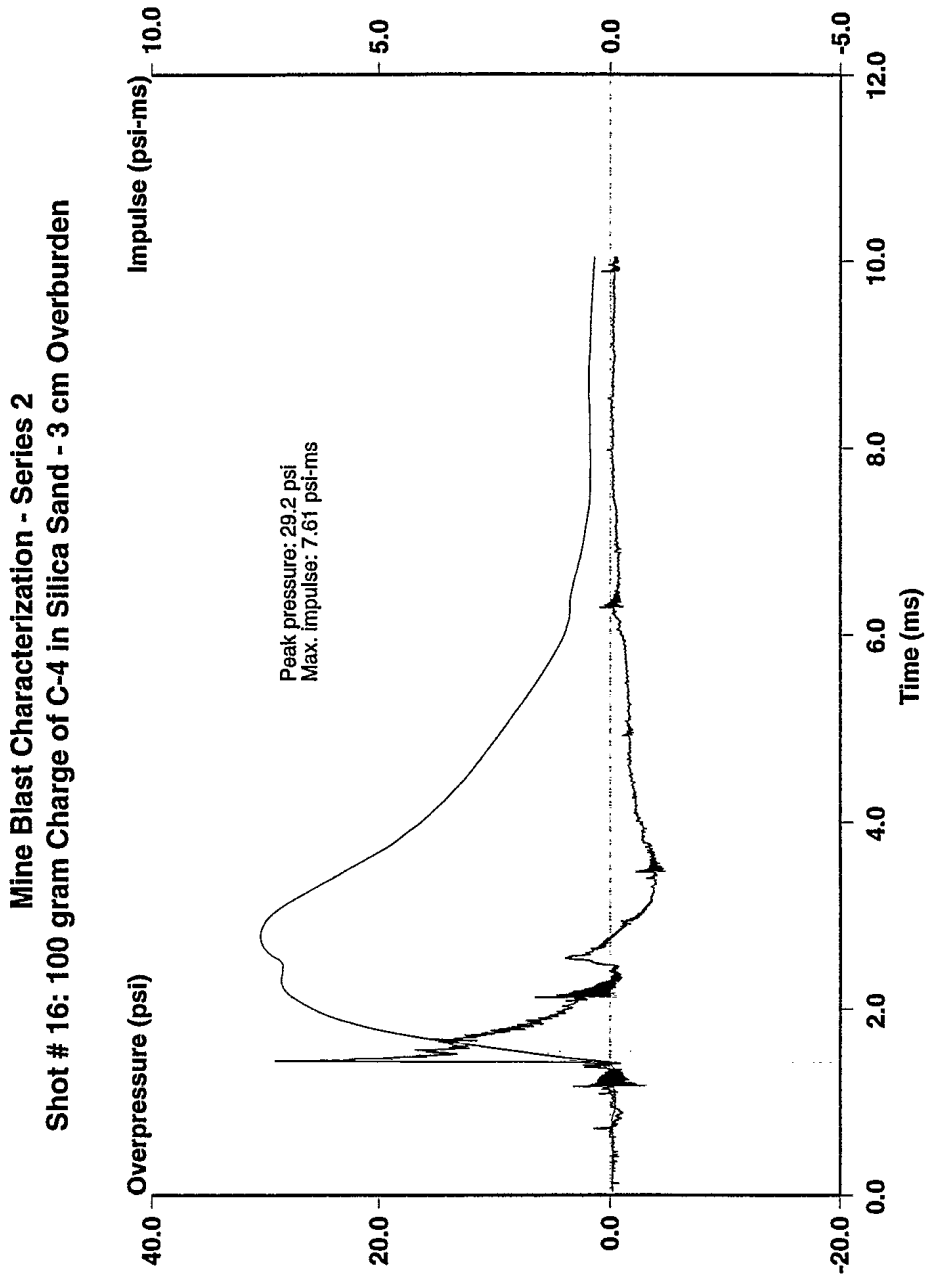

Position 3 (113 cm), Air Shock, 2nd Order 100 kHz Butterworth Filter

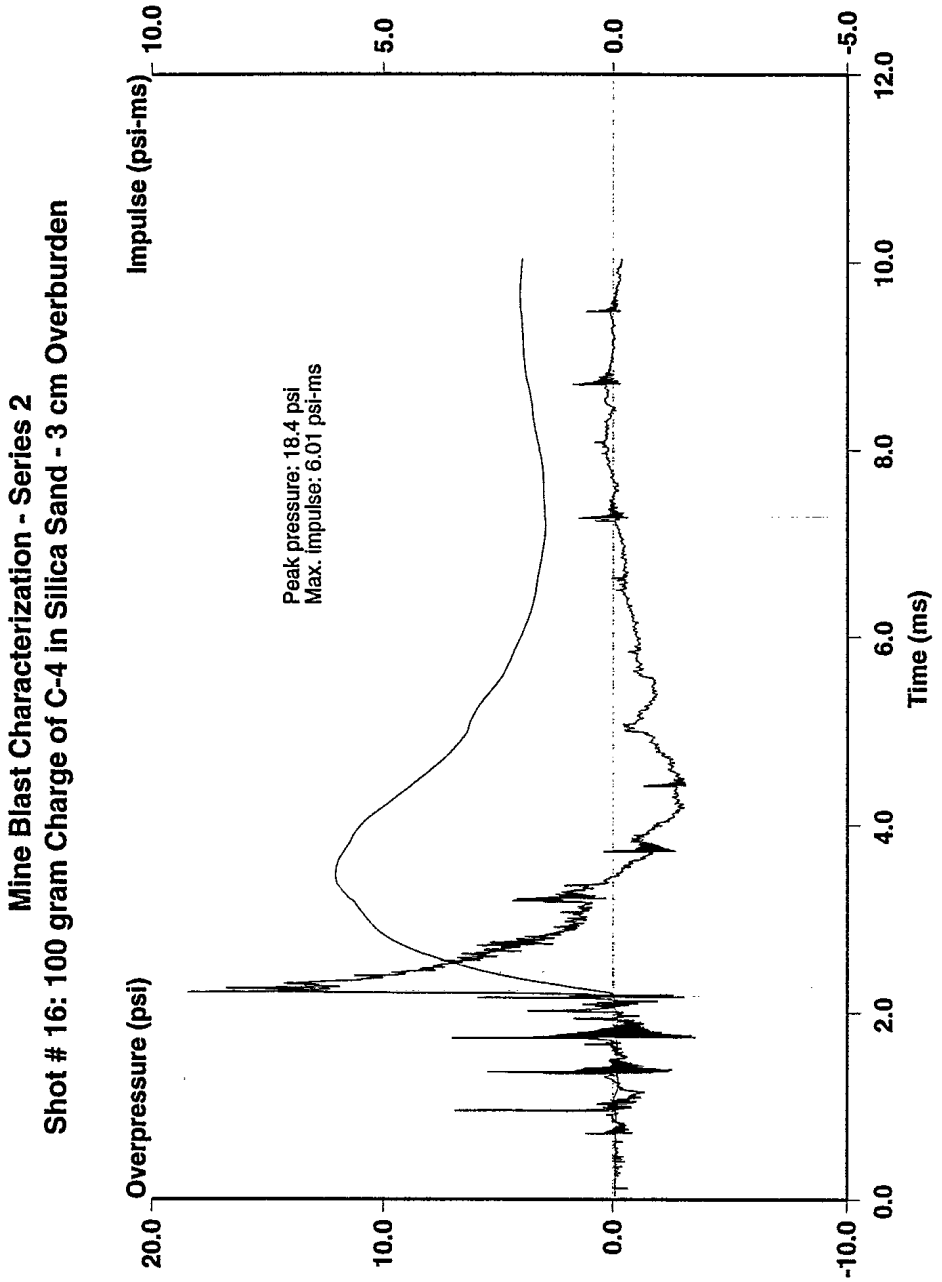

Position 4 (153 cm), Air Shock, 2nd Order 100 kHz Butterworth Filter

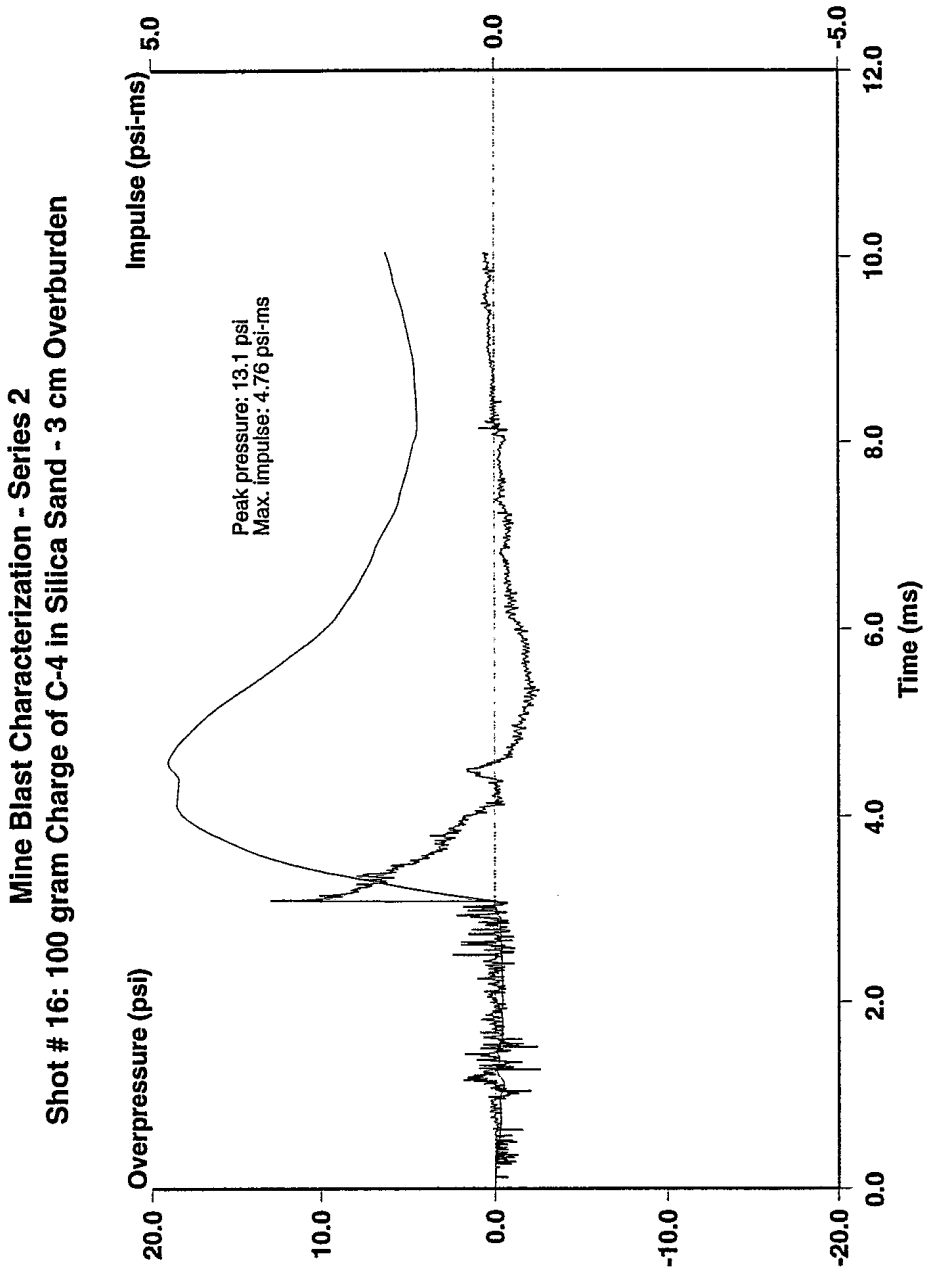

Position 5 (193 cm), Air Shock, 2nd Order 100 kHz Butterworth Filter

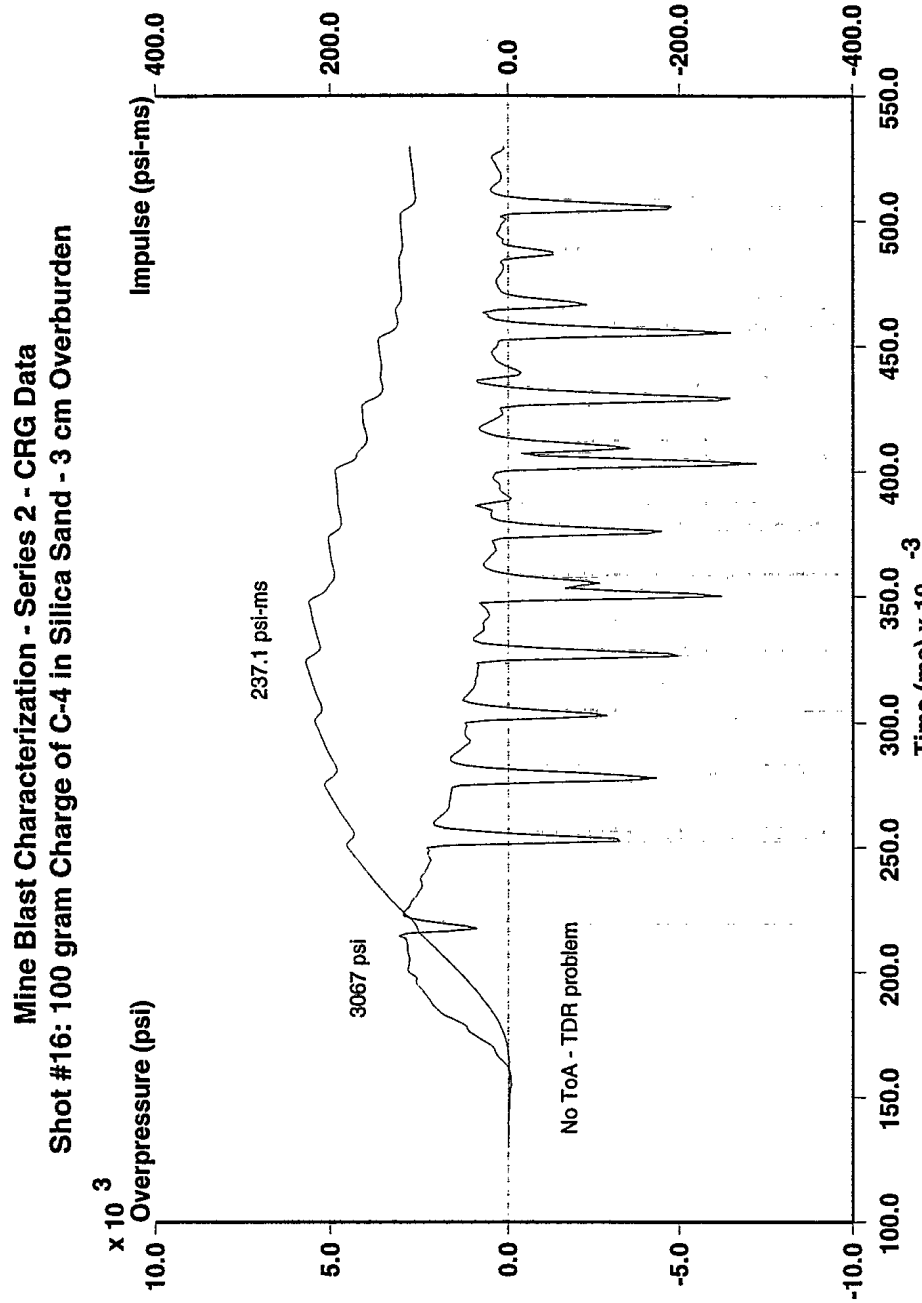

Position 6 (8.23 cm), In Ground Pressure, 2nd Order 100 kHz Butterworth Filter

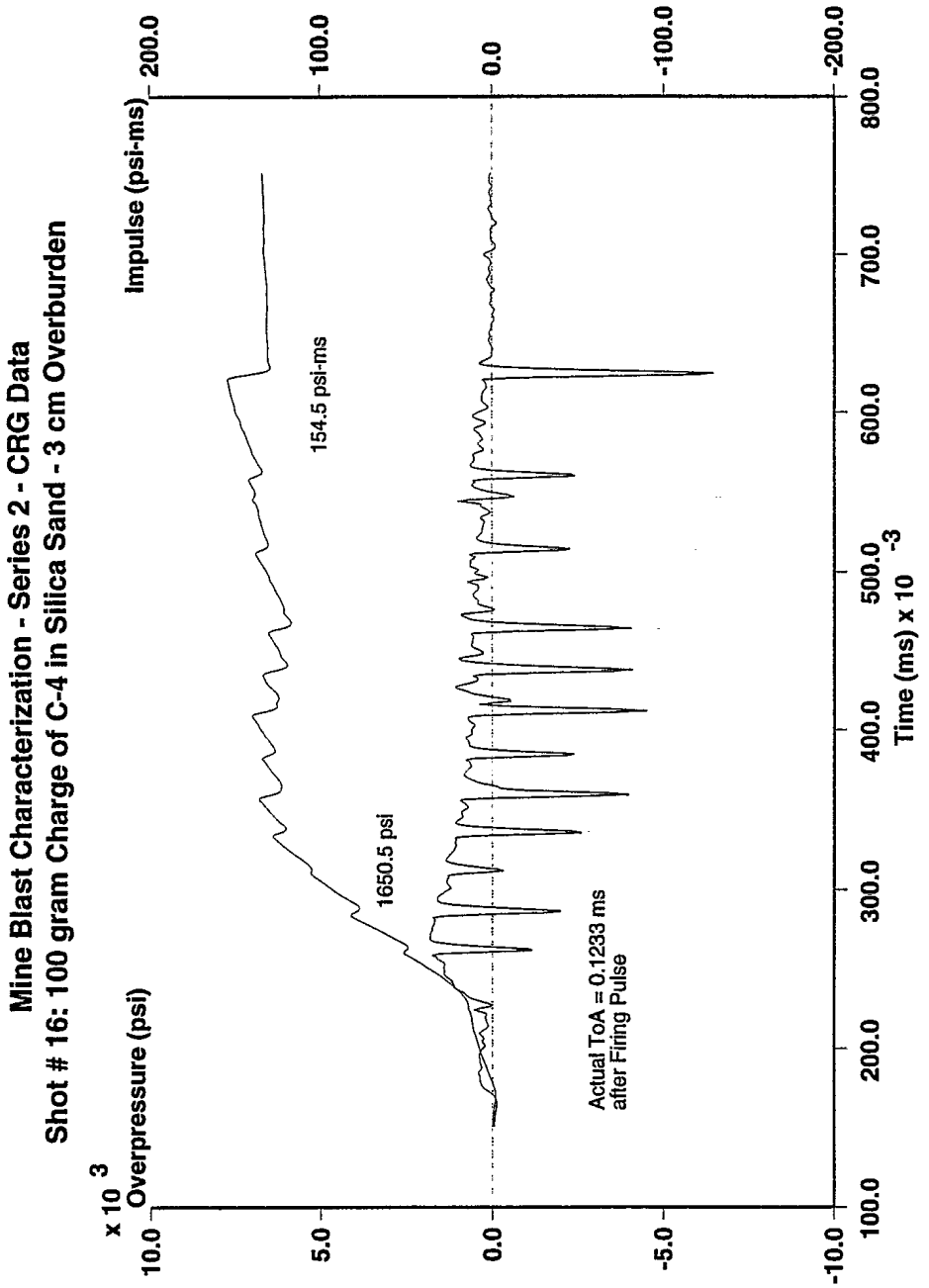

Position 7 (10.73 cm), In Ground Pressure, 2nd Order 100 kHz Butterworth Filter

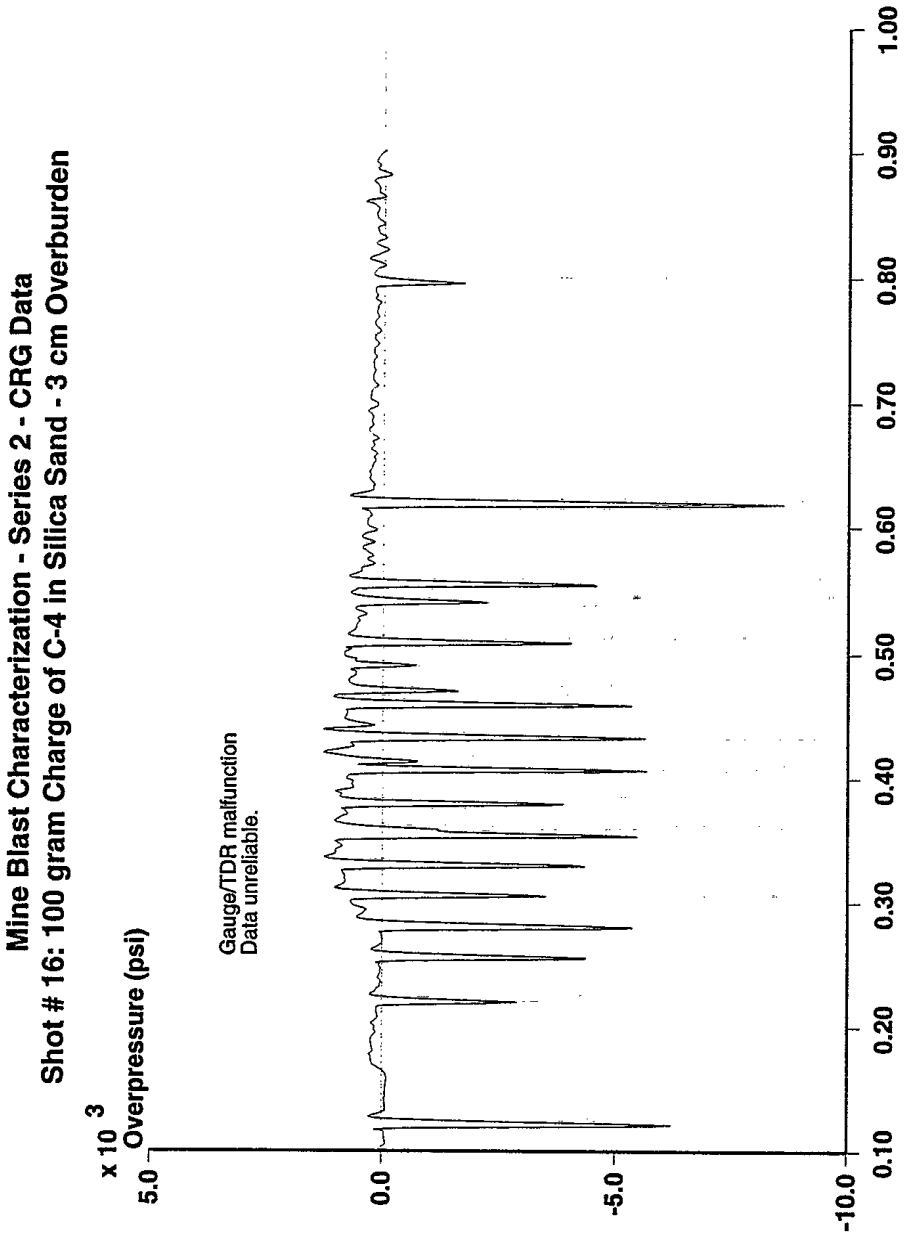
Mine Blast Characterization - Series 2 - CRG Data
Shot # 16: 100 gram Charge of C-4 in Silica Sand - 3 cm Overburden
x 10 3
Overpressure (psi)
5.0
0.0
-5.0
-10.0
Gauge/TDR malfunction
Data unreliable.
0.10
0.20
0.30
0.40
0.50
0.60
0.70
0.80
0.90
1.00
Time (ms)
Position 8 (13.23 cm), In Ground Pressure, 2nd Order 100 kHz Butterworth Filter

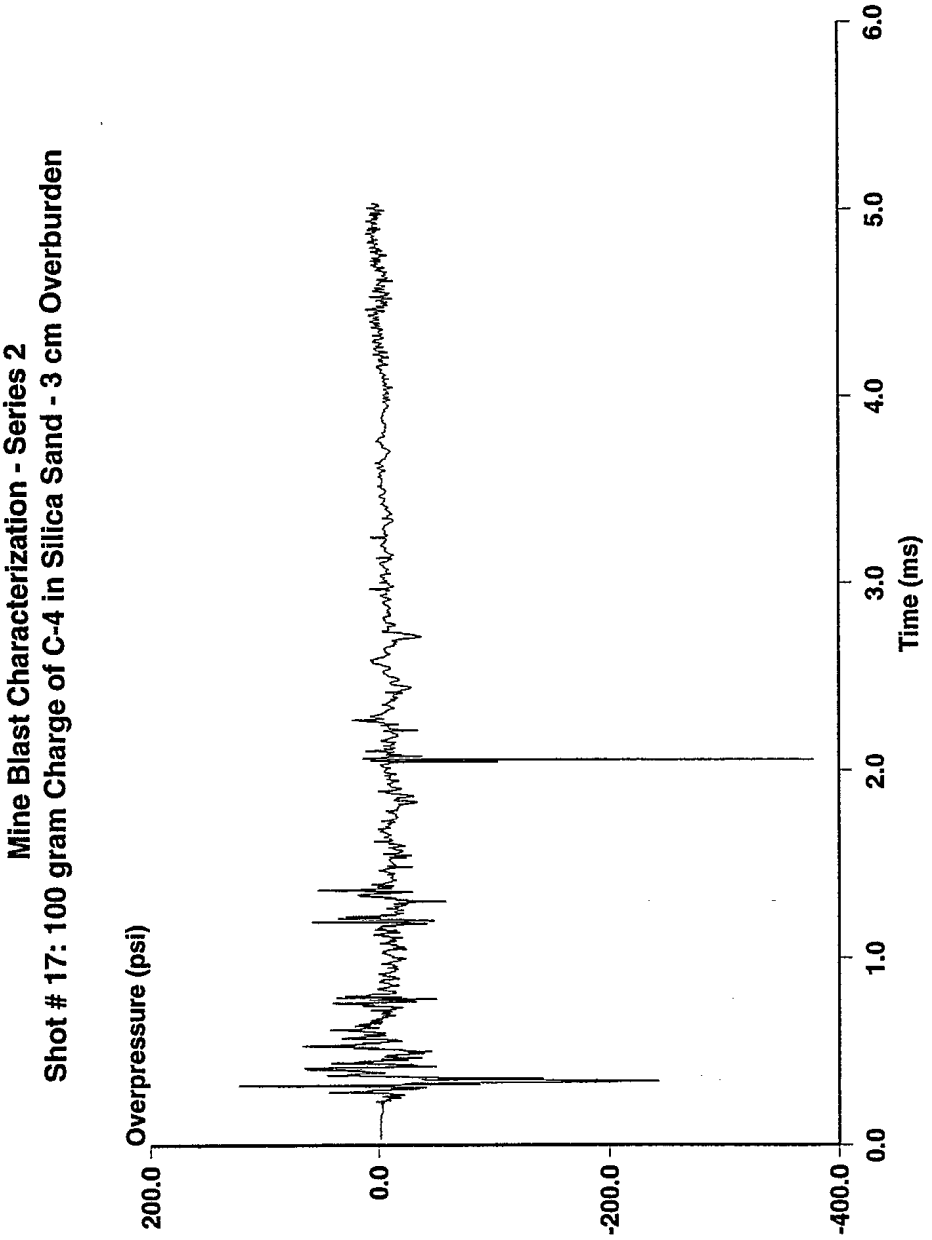
Mine Blast Characterization - Series 2
Shot # 17: 100 gram Charge of C-4 in Silica Sand - 3 cm Overburden
Overpressure (psi)
200.0
0.0
-200.0
-400.0
0.0
1.0
2.0
3.0
4.0
5.0
6.0
Time (ms)
Position 1 (33 cm), Air Shock, 2nd Order 100 kHz Butterworth Filter

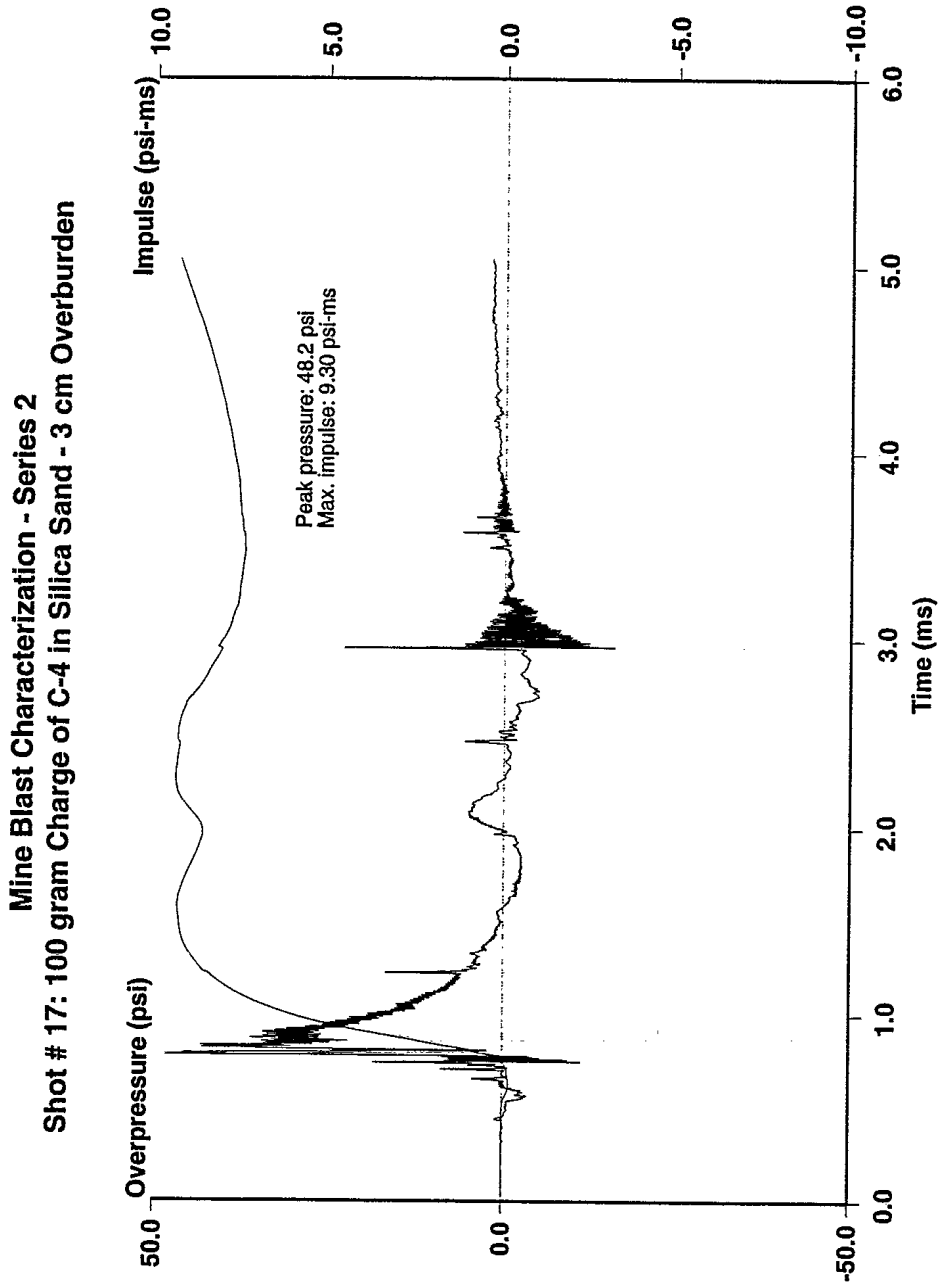

Position 2 (73 cm), Air Shock, 2nd Order 100 kHz Butterworth Filter

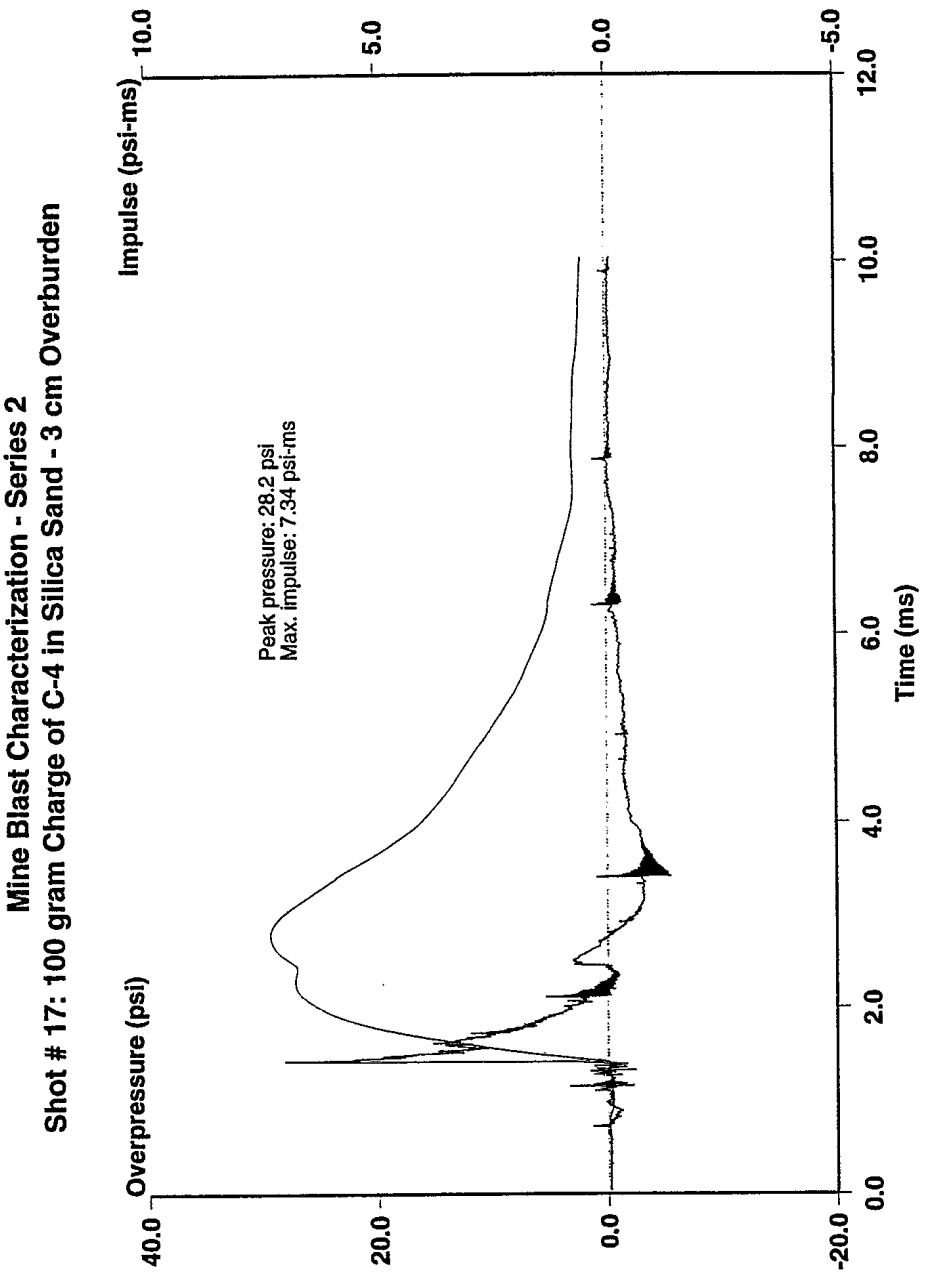

Position 3 (113 cm), Air Shock, 2nd Order 100 kHz Butterworth Filter

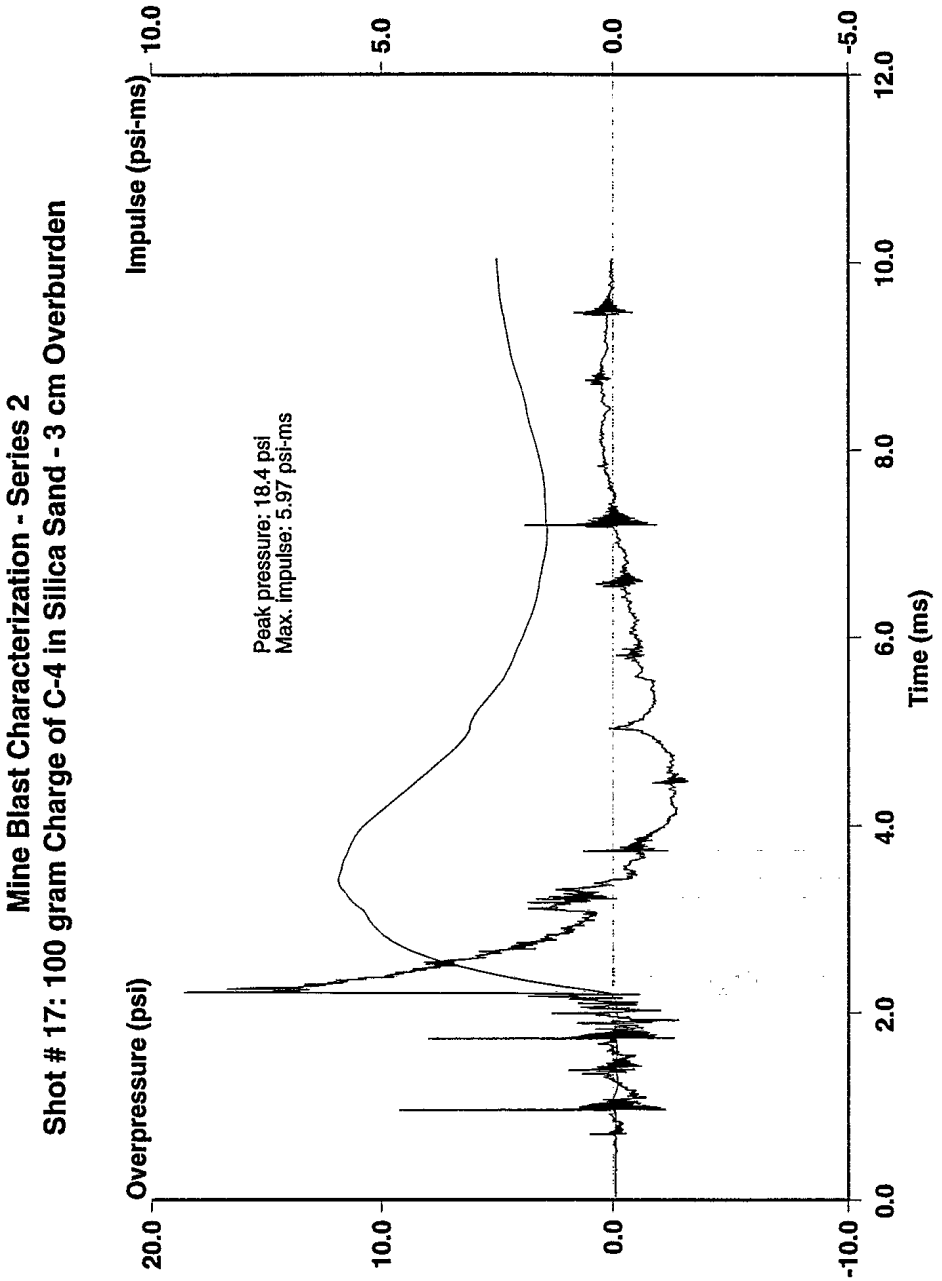

Position 4 (153 cm), Air Shock, 2nd Order 100 kHz Butterworth Filter

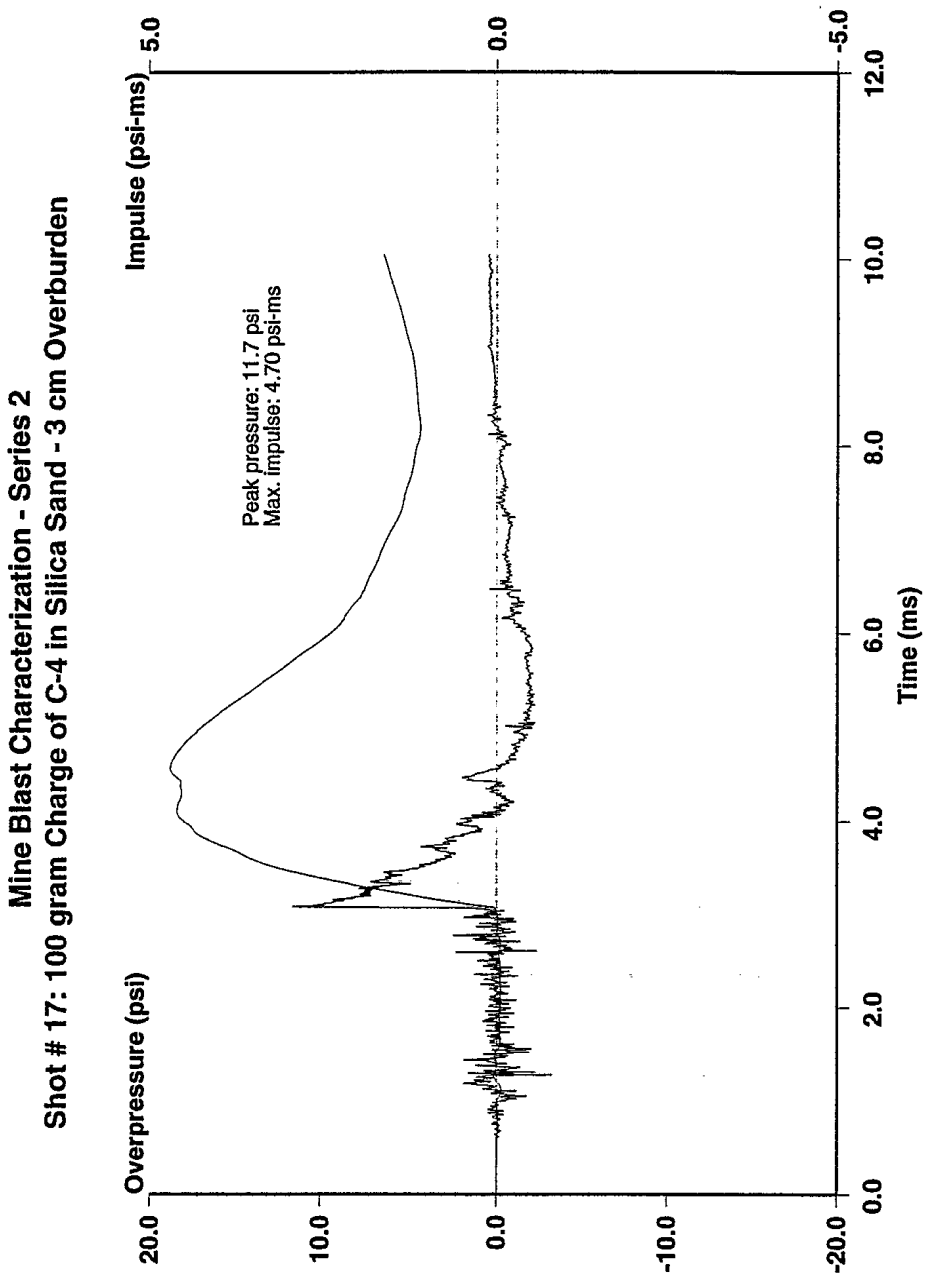

Position 5 (193 cm), Air Shock, 2nd Order 100 kHz Butterworth Filter

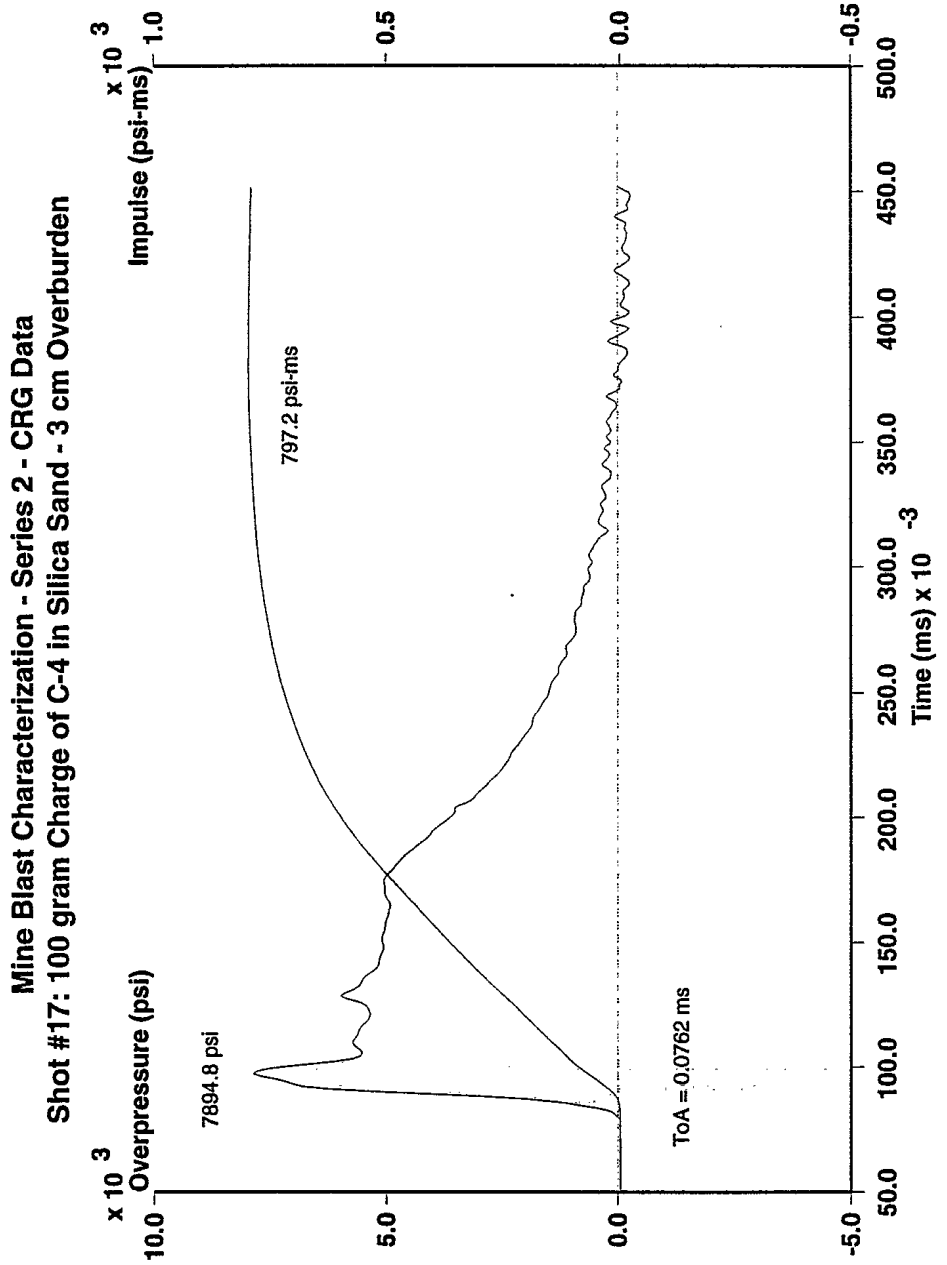

Position 6 (8.23 cm), In Ground Pressure, 2nd Order 100 kHz Butterworth Filter

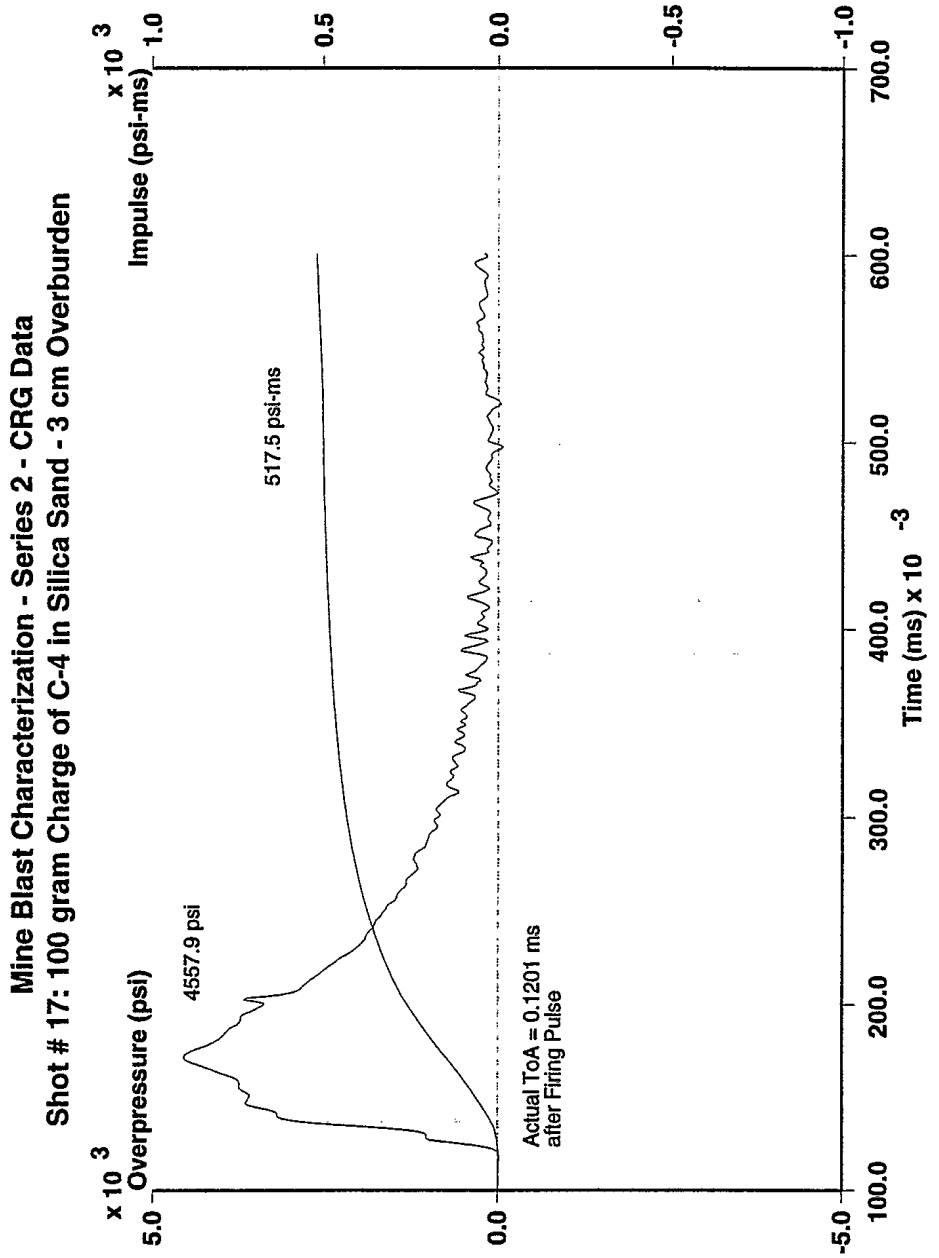

Position 7 (10.73 cm), In Ground Pressure, 2nd Order 100 kHz Butterworth Filter

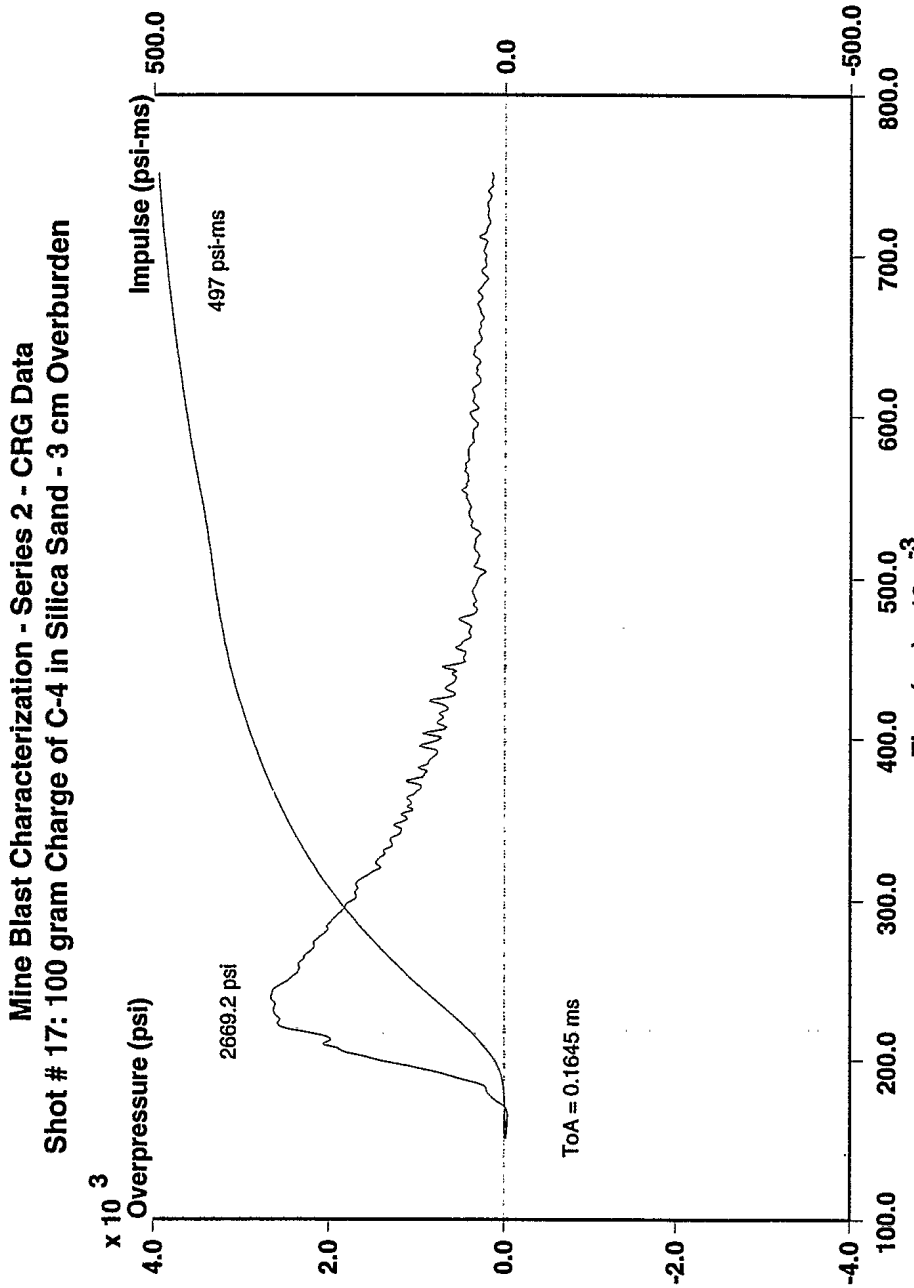

Position 8 (13.23 cm), In Ground Pressure, 2nd Order 100 kHz Butterworth Filter

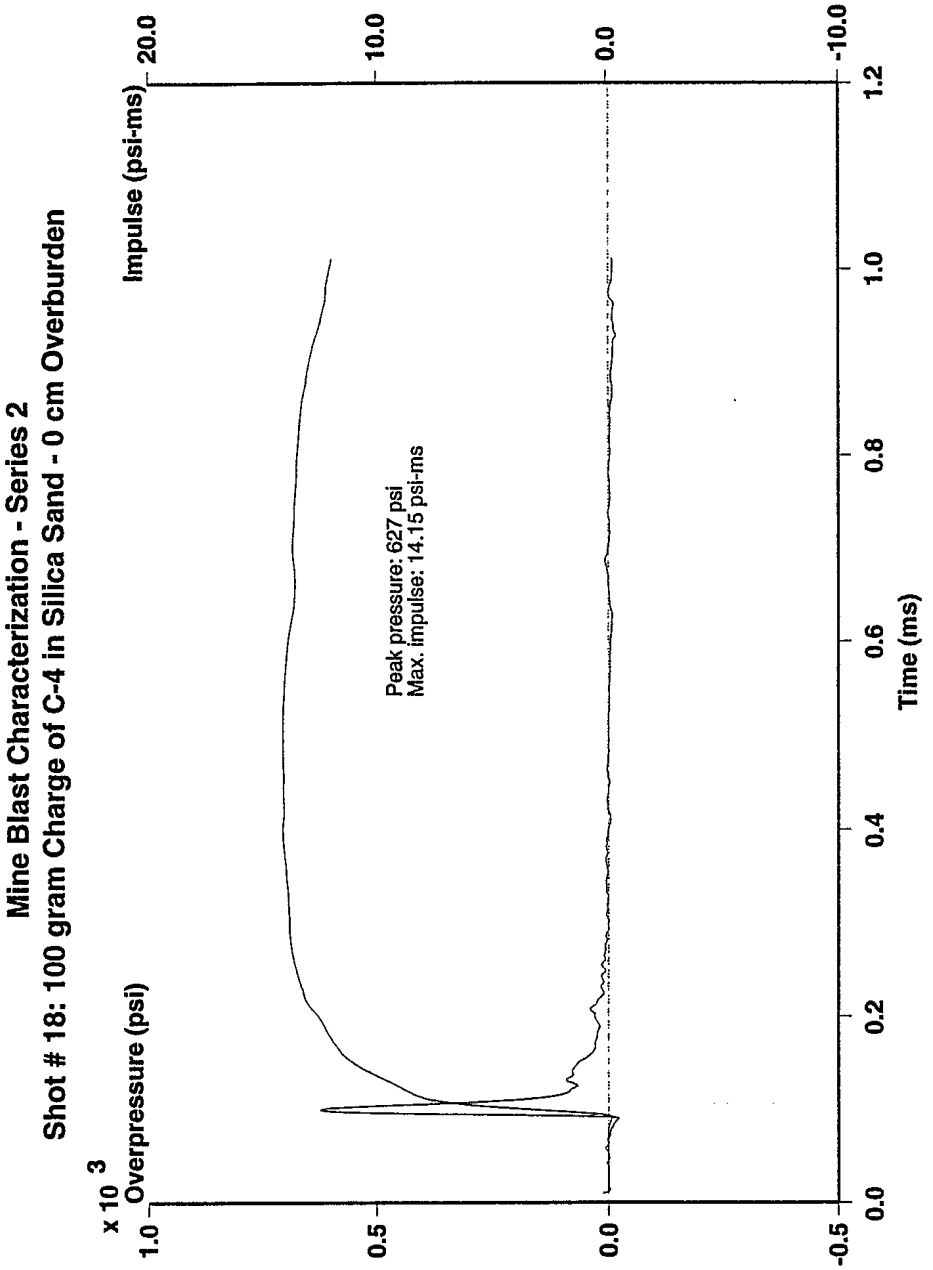

Position 1 (30 cm), Air Shock, 2nd Order 100 kHz Butterworth Filter

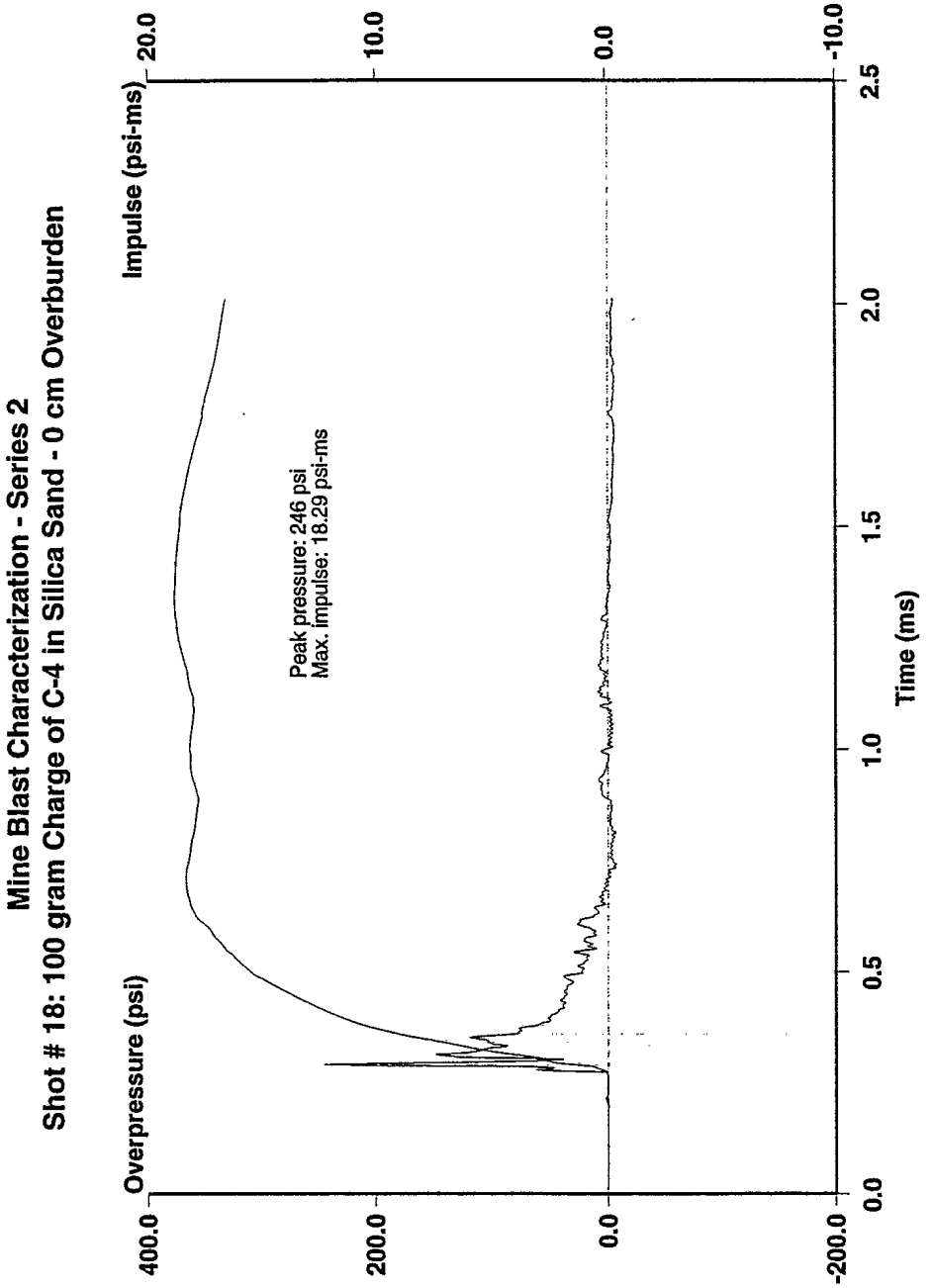
Mine Blast Characterization - Series 2
Shot # 18: 100 gram Charge of C-4 in Silica Sand - 0 cm Overburden
Overpressure (psi)
Impulse (psi-ms)
Time (ms)
Peak pressure: 246 psi
Max. impulse: 18.29 psi-ms
400.0
200.0
0.0
-200.0
20.0
10.0
0.0
-10.0
0.0
0.5
1.0
1.5
2.0
2.5
Position 2 (70 cm), Air Shock, 2nd Order 100 kHz Butterworth Filter

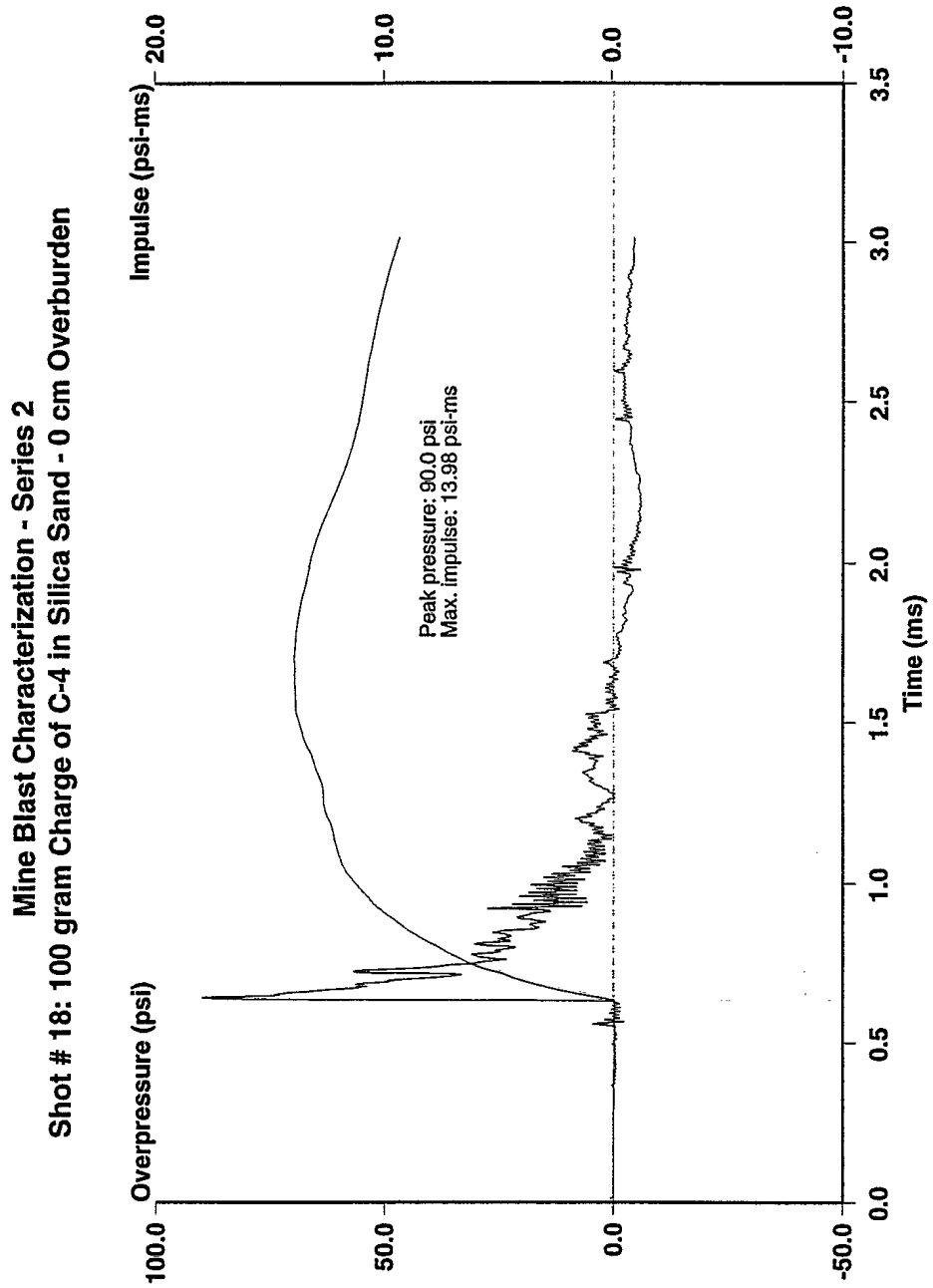

Position 3 (110 cm), Air Shock, 2nd Order 100 kHz Butterworth Filter

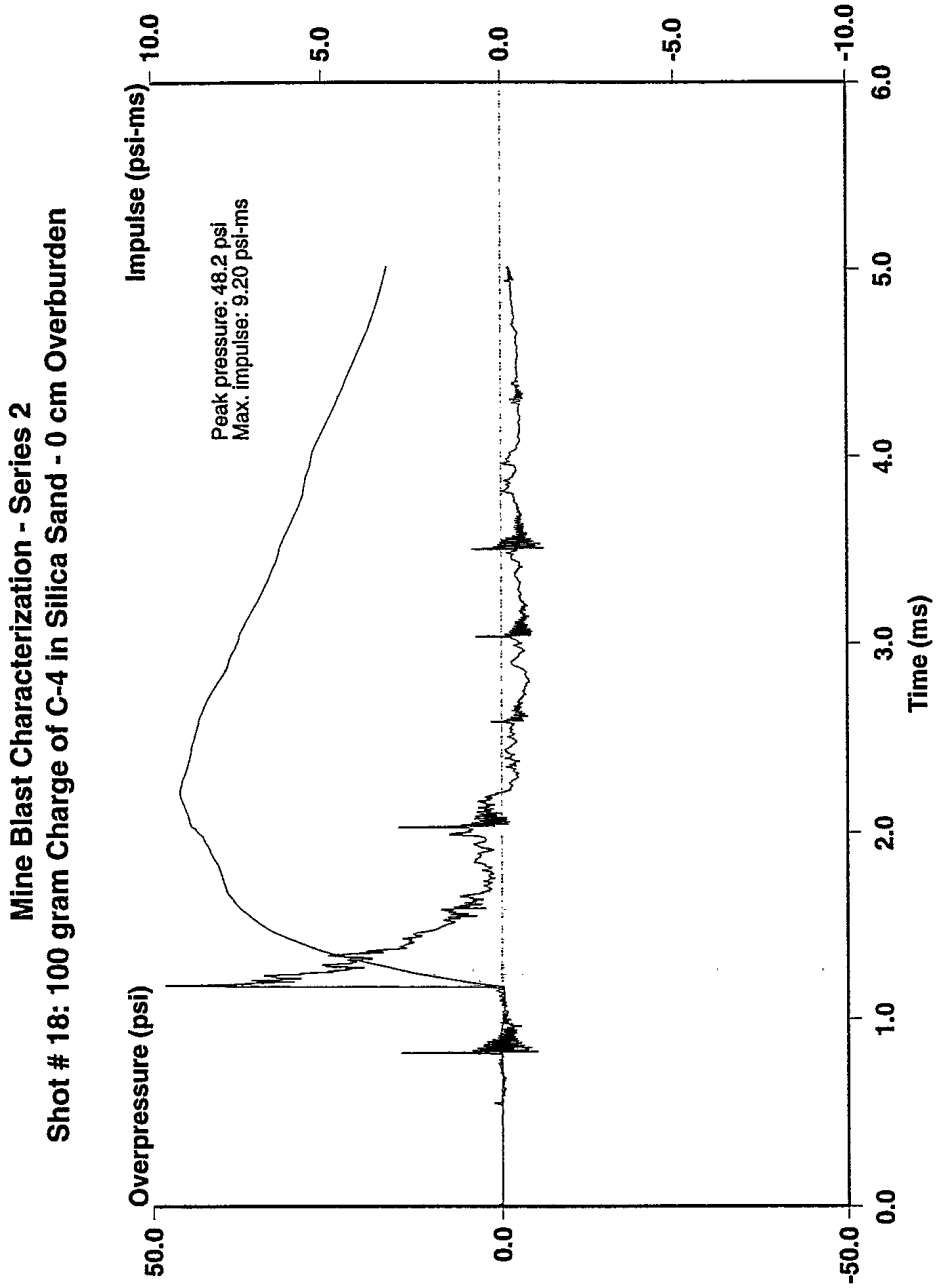
Mine Blast Characterization - Series 2
Shot # 18: 100 gram Charge of C-4 in Silica Sand - 0 cm Overburden
Impulse (psi-ms)
10.0
5.0
0.0
-5.0
-10.0
Peak pressure: 48.2 psi
Max. impulse: 9.20 psi-ms
Overpressure (psi)
50.0
0.0
-50.0
0.0
1.0
2.0
3.0
4.0
5.0
6.0
Time (ms)
Position 4 (150 cm), Air Shock, 2nd Order 100 kHz Butterworth Filter

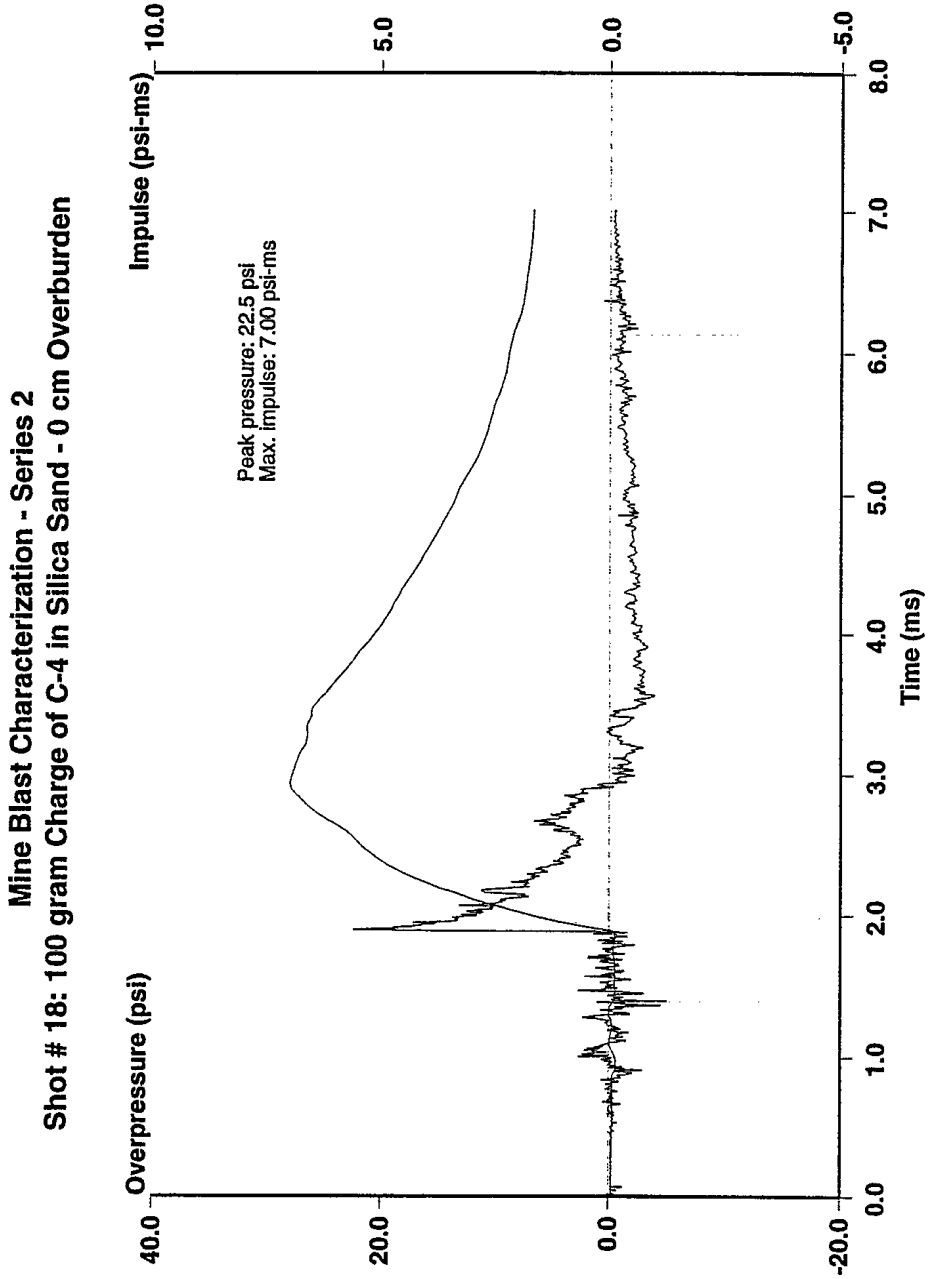

Position 5 (190 cm), Air Shock, 2nd Order 100 kHz Butterworth Filter

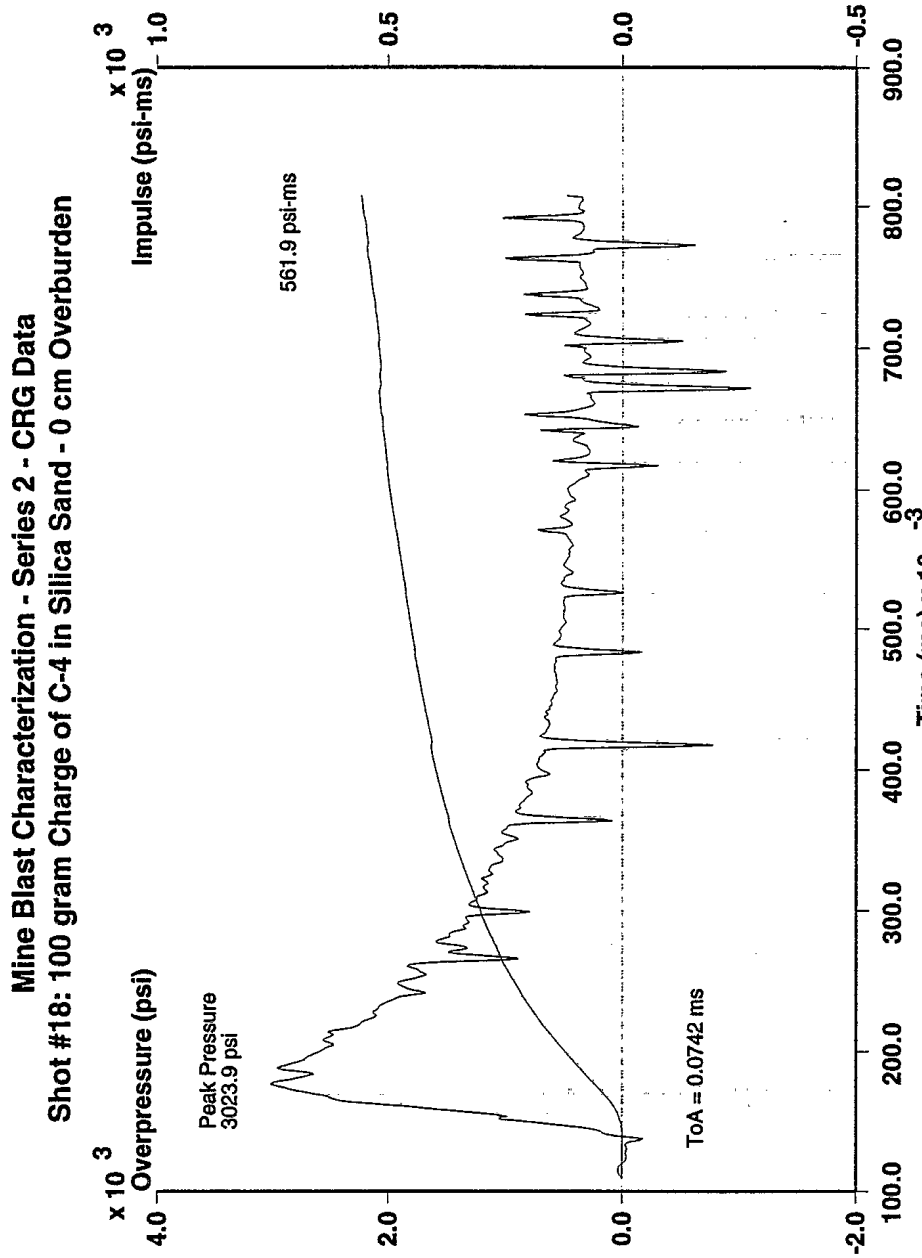

Position 6 (8.23 cm), In Ground Pressure, 2nd Order 100 kHz Butterworth Filter

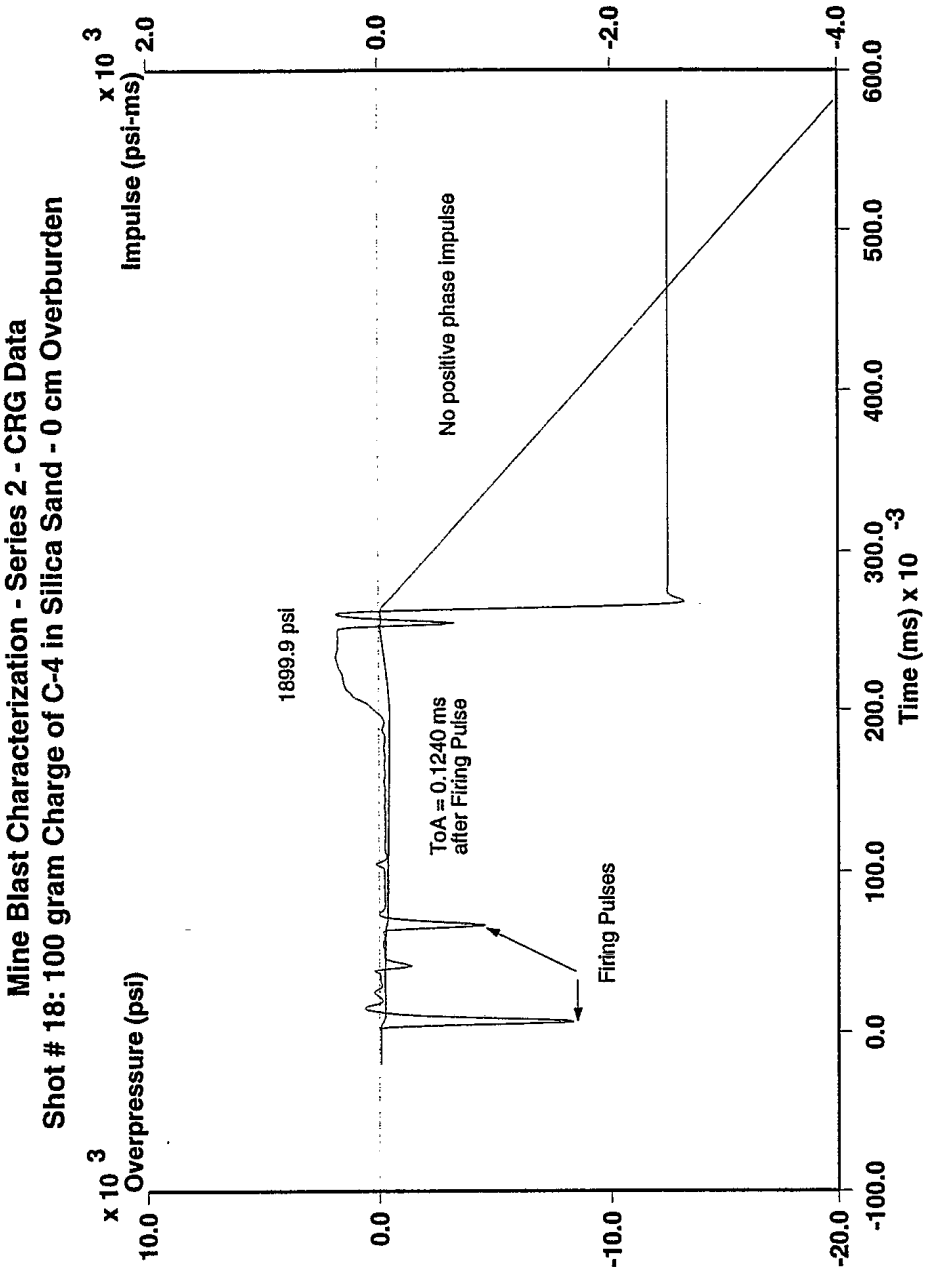

Position 7 (10.73 cm), In Ground Pressure, 2nd Order 100 kHz Butterworth Filter

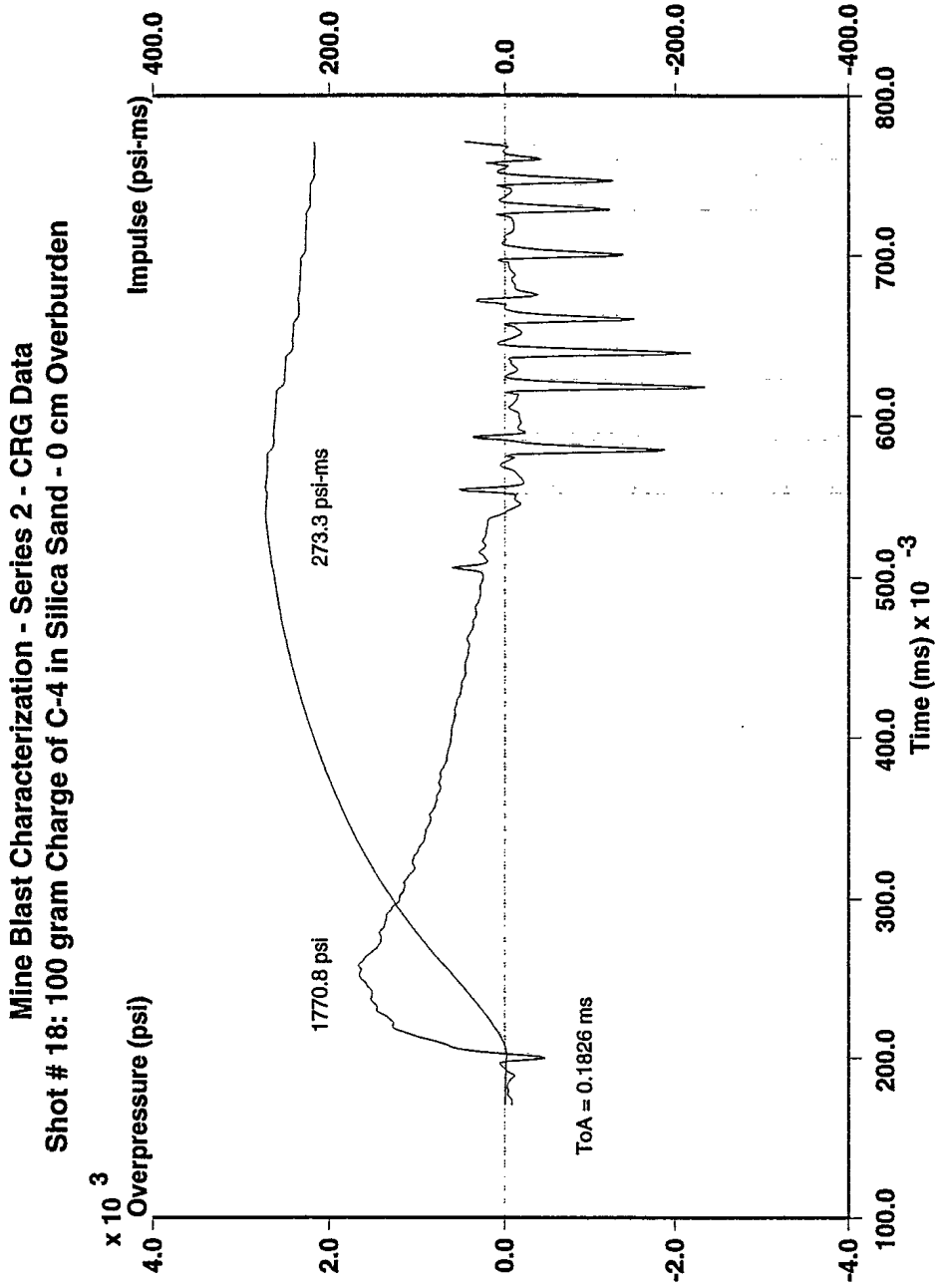

Position 8 (13.23 cm), In Ground Pressure, 2nd Order 100 kHz Butterworth Filter

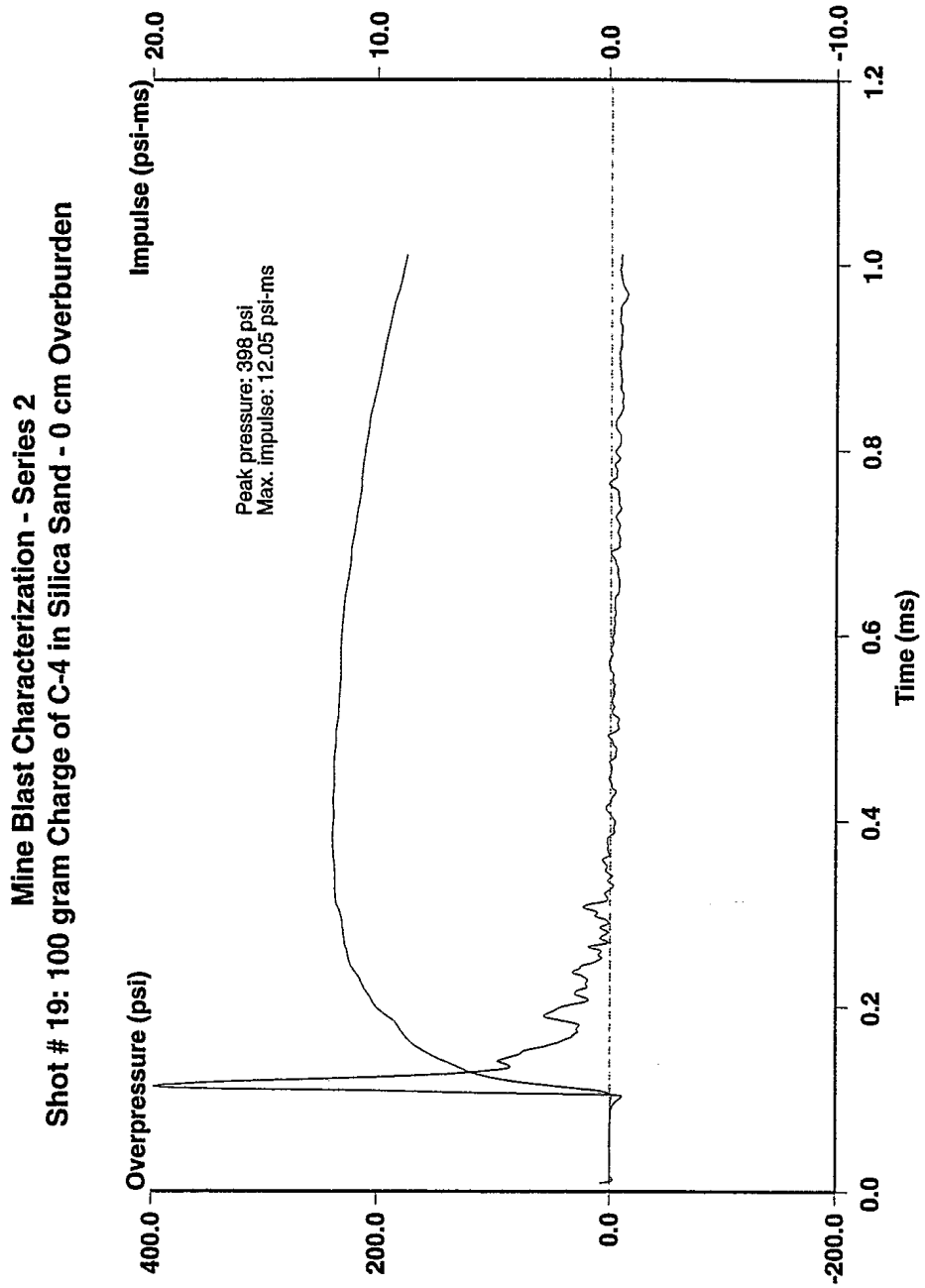

Position 1 (30 cm), Air Shock, 2nd Order 100 kHz Butterworth Filter

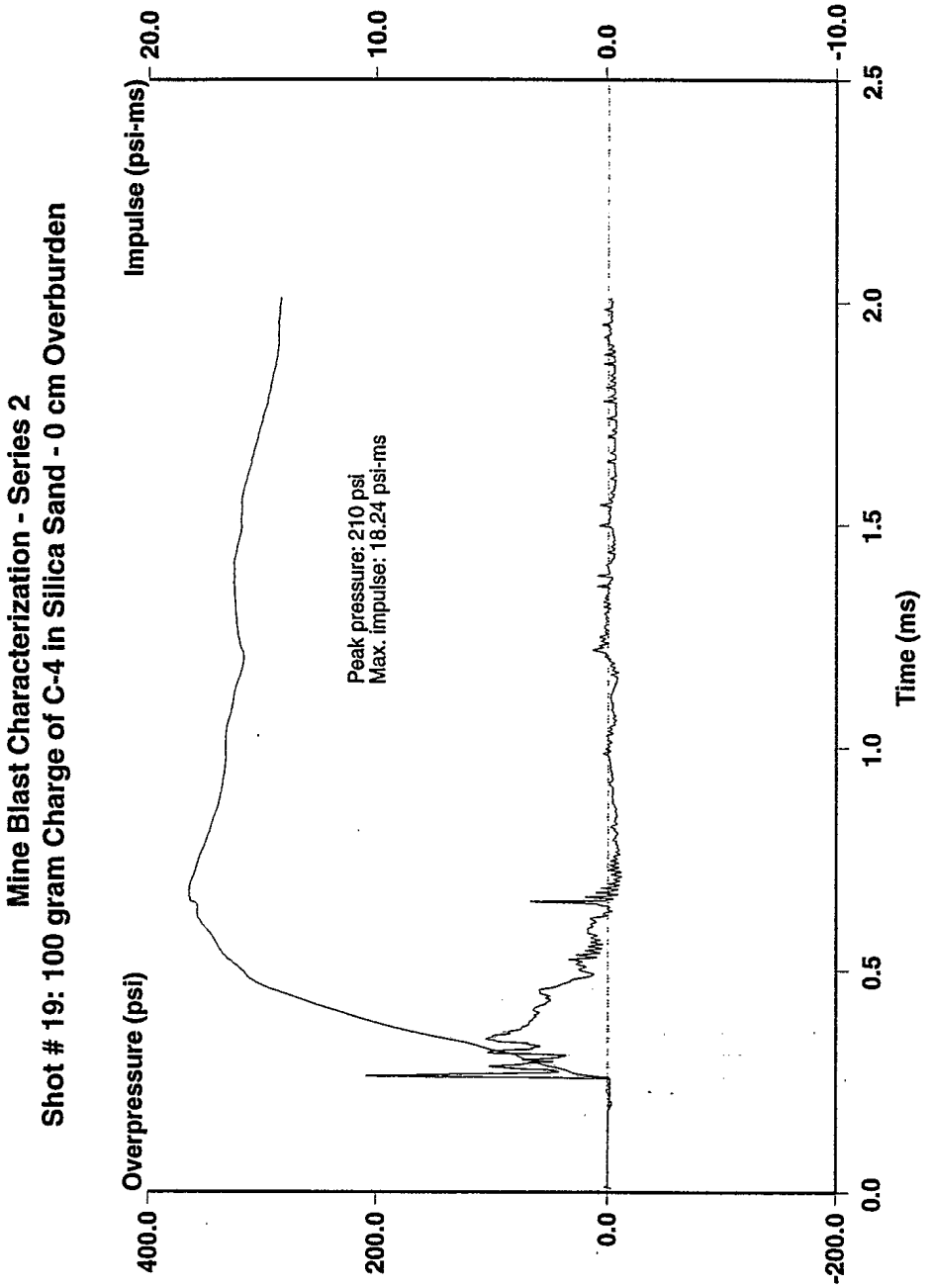

Position 2 (70 cm), Air Shock, 2nd Order 100 kHz Butterworth Filter

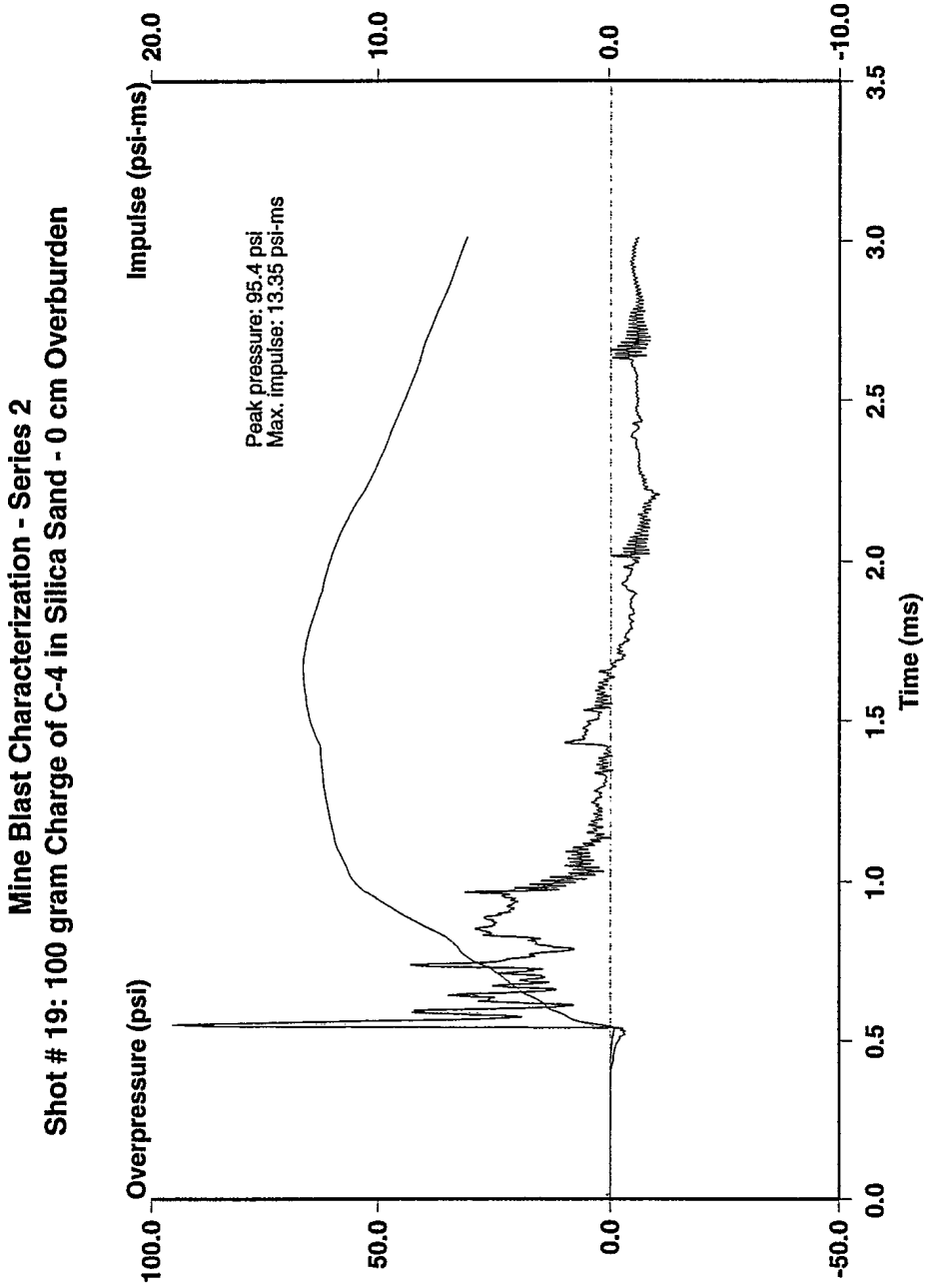

Position 3 (110 cm), Air Shock, 2nd Order 100 kHz Butterworth Filter

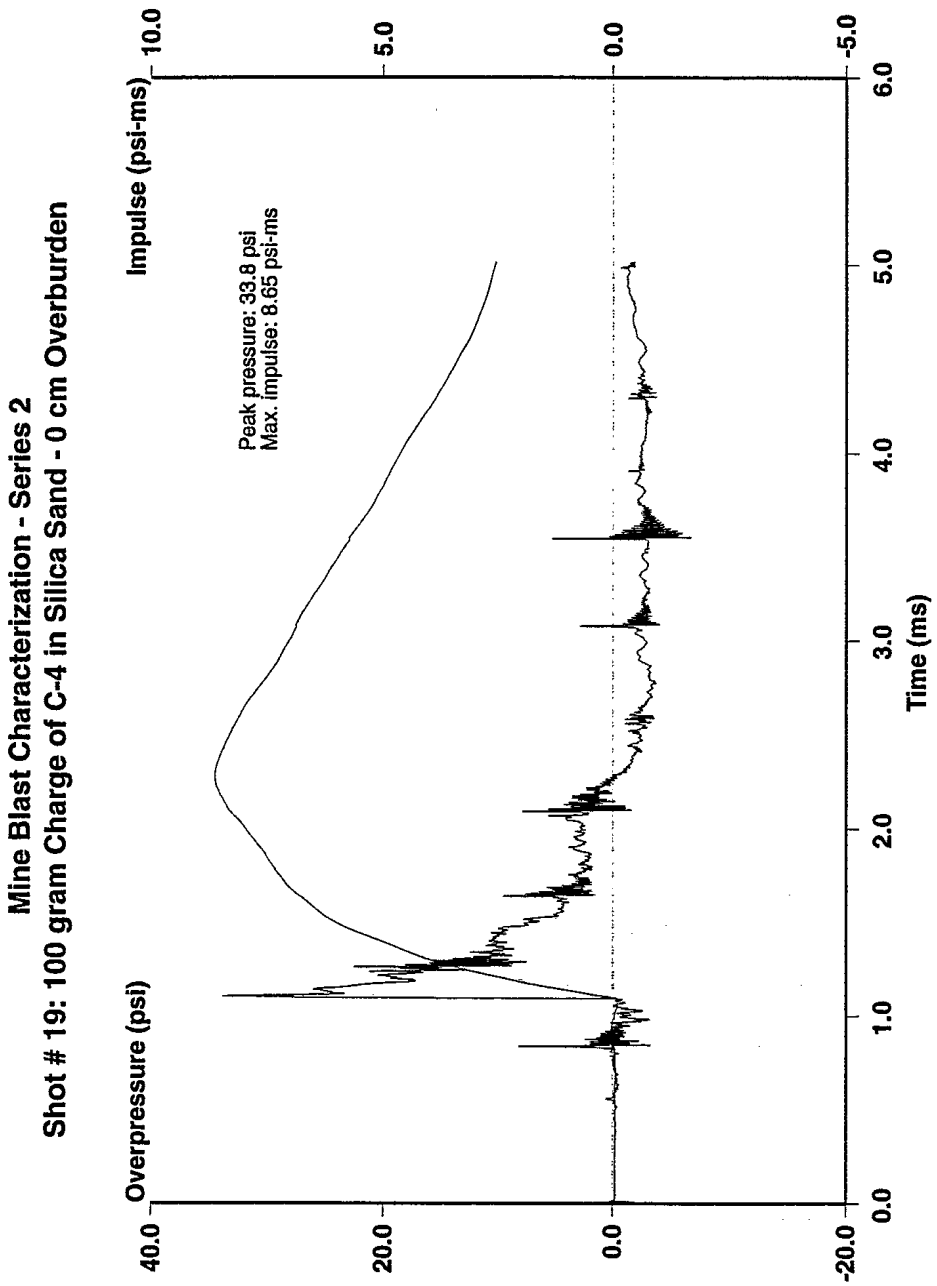

Position 4 (150 cm), Air Shock, 2nd Order 100 kHz Butterworth Filter

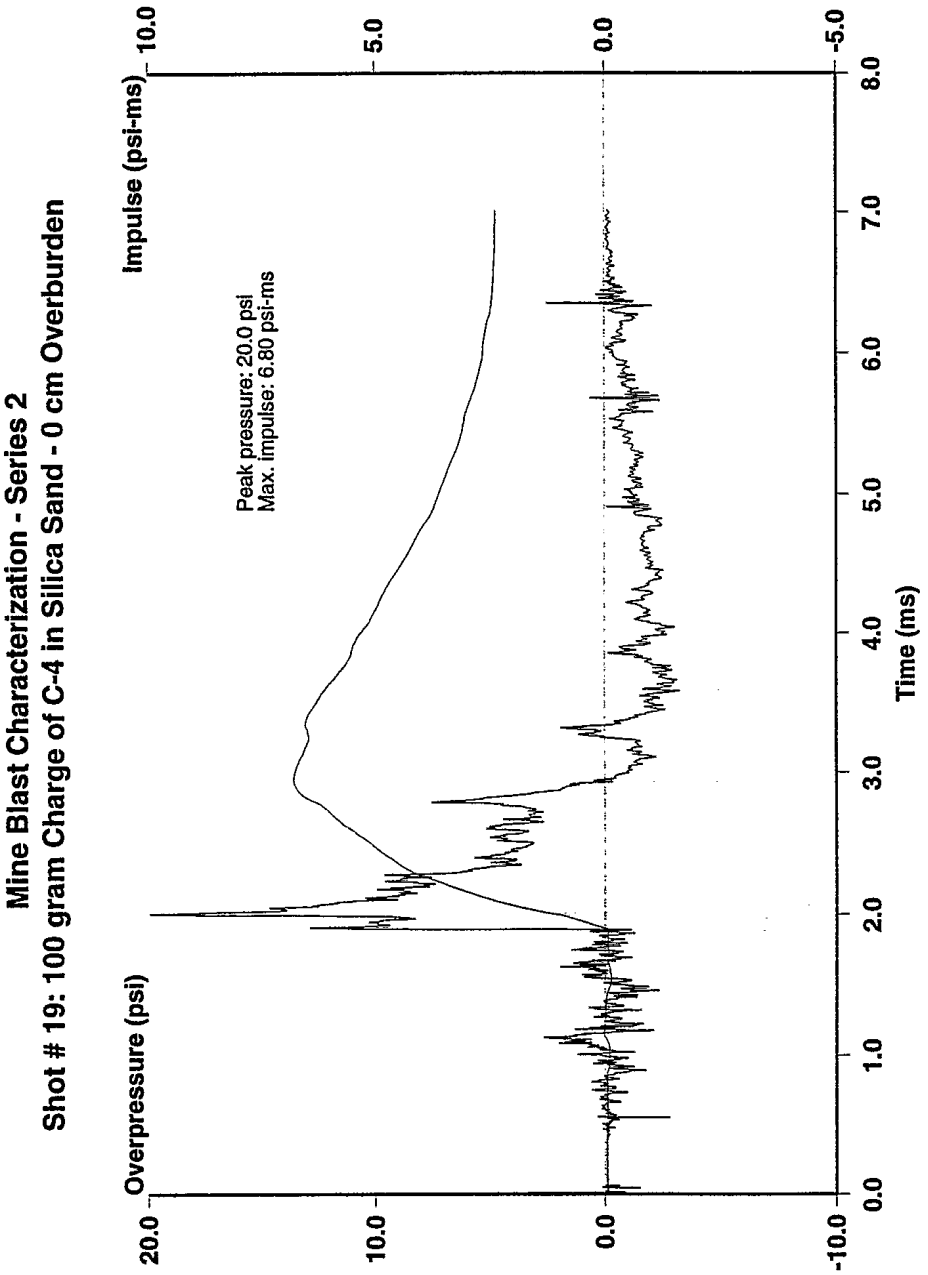

Position 5 (190 cm), Air Shock, 2nd Order 100 kHz Butterworth Filter

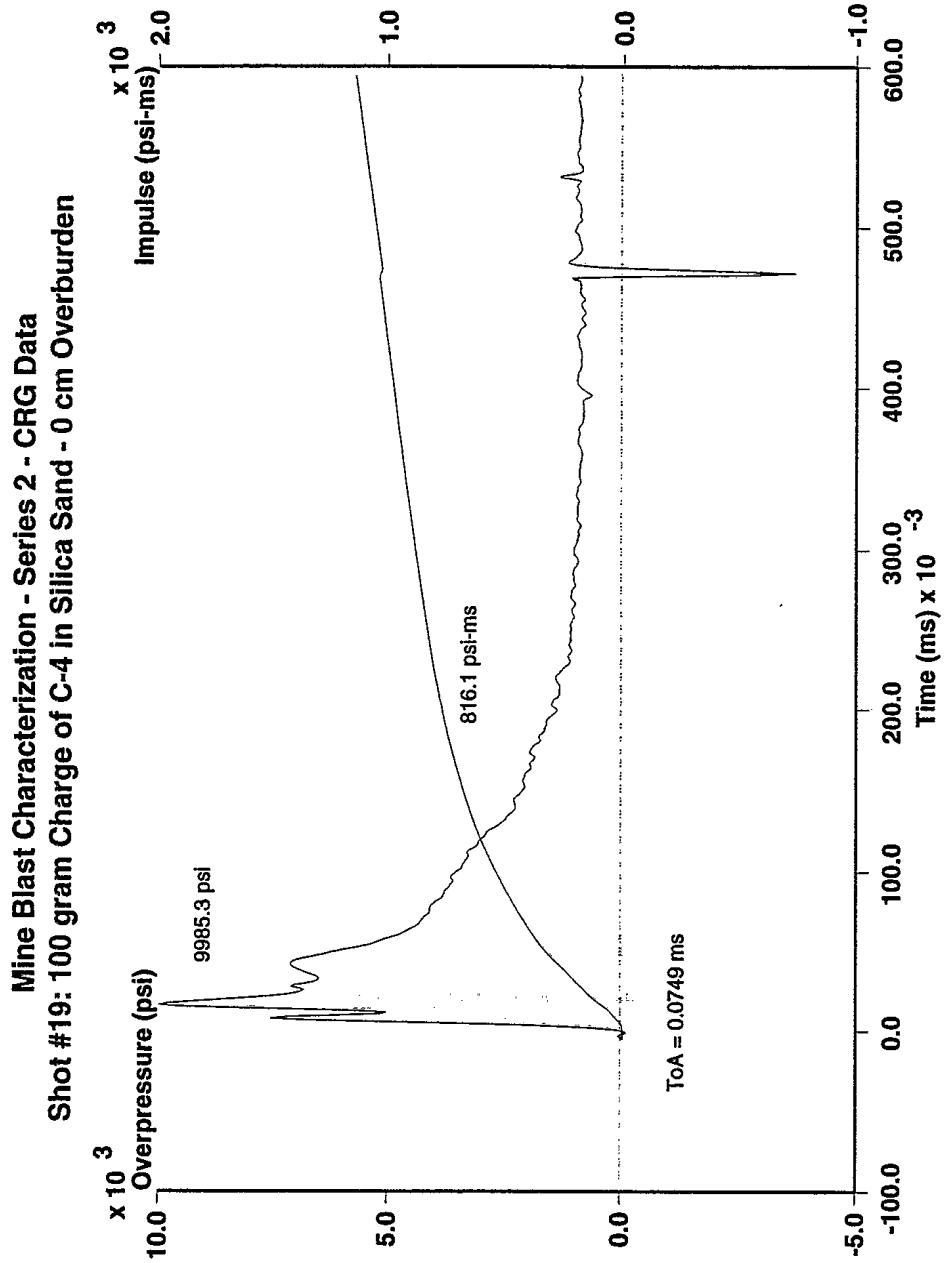

Position 6 (8.23 cm), In Ground Pressure, 2nd Order 100 kHz Butterworth Filter

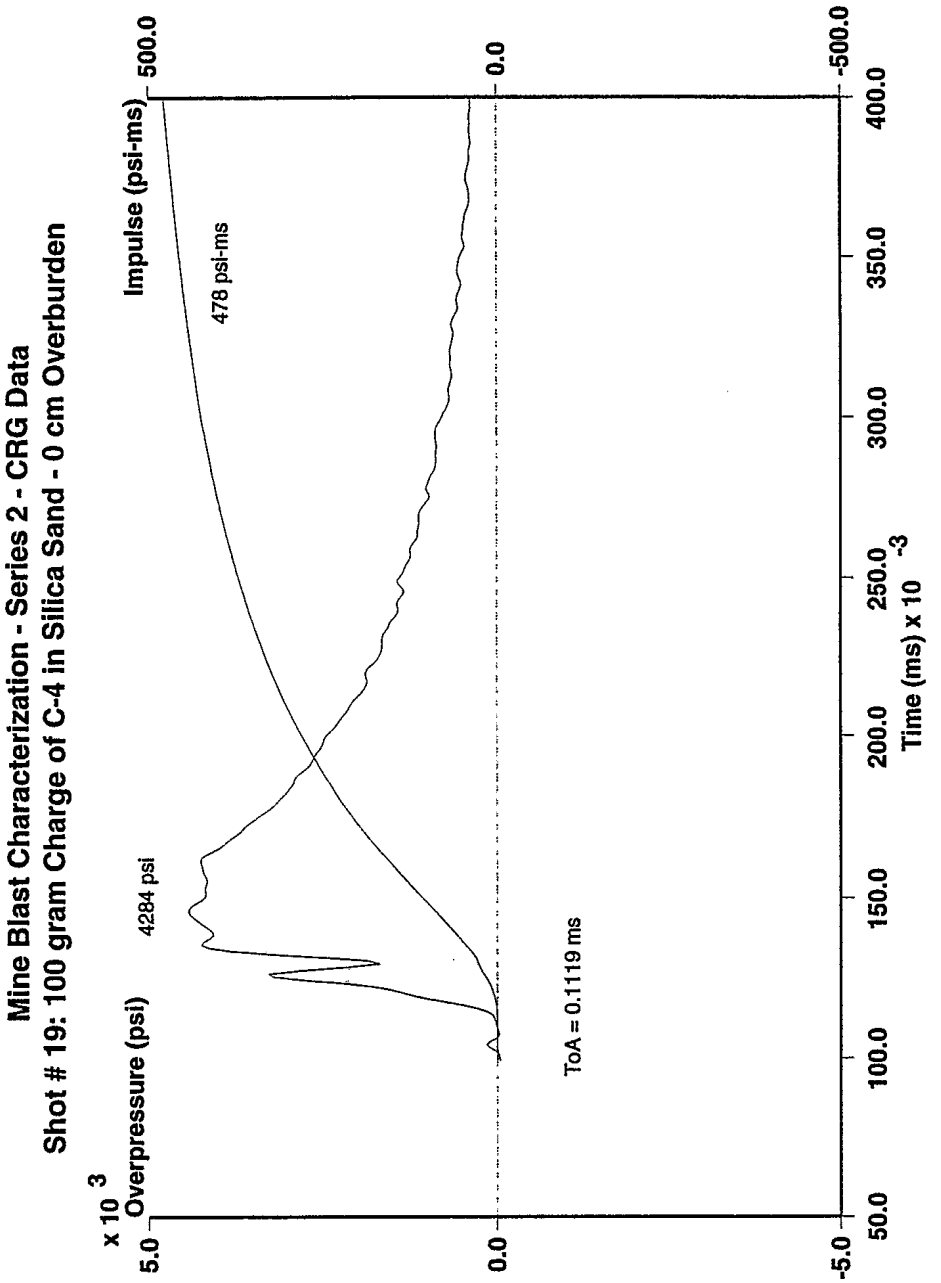

Position 7 (10.73 cm), In Ground Pressure, 2nd Order 100 kHz Butterworth Filter

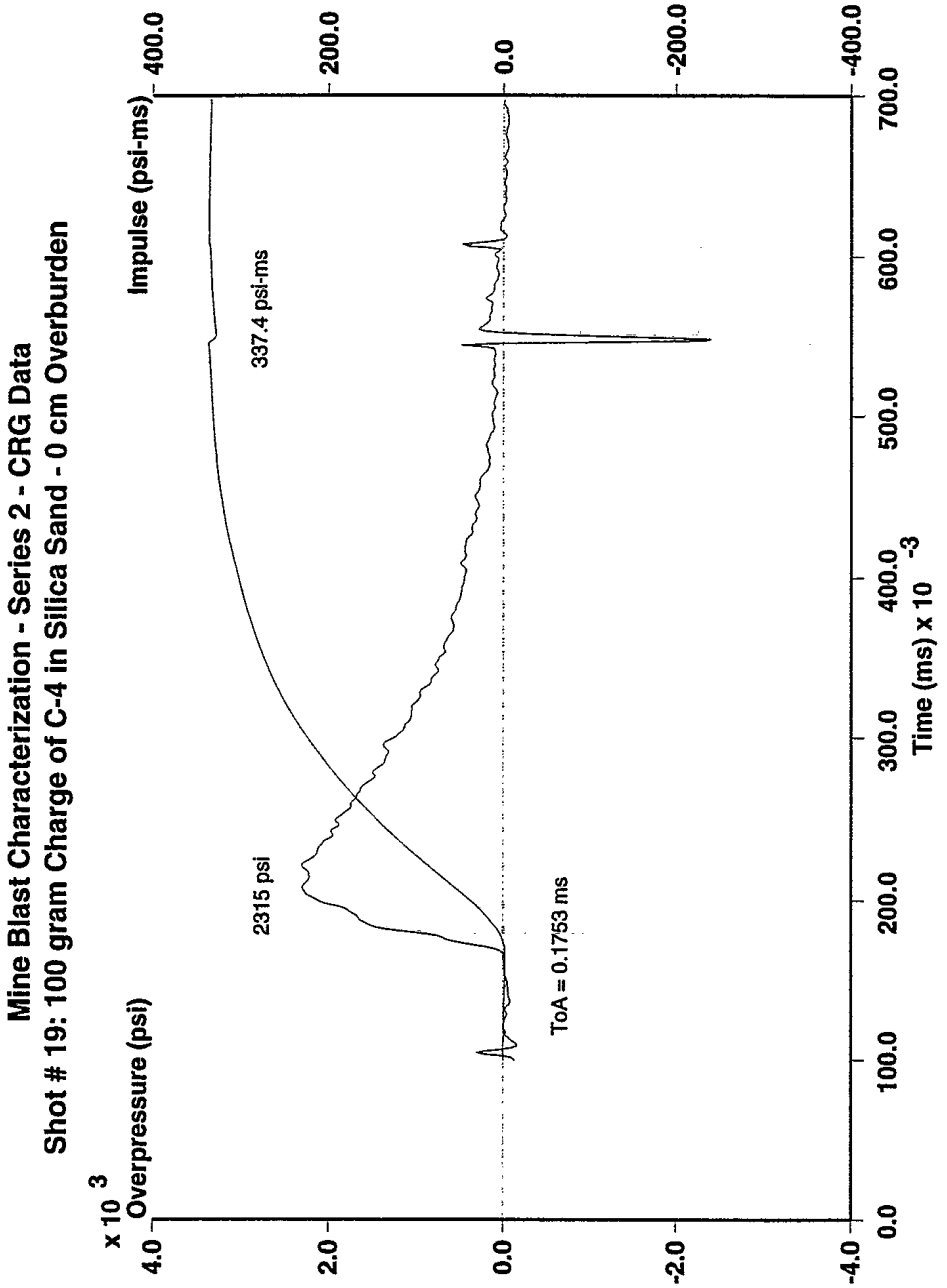

Position 8 (13.23 cm), In Ground Pressure, 2nd Order 100 kHz Butterworth Filter

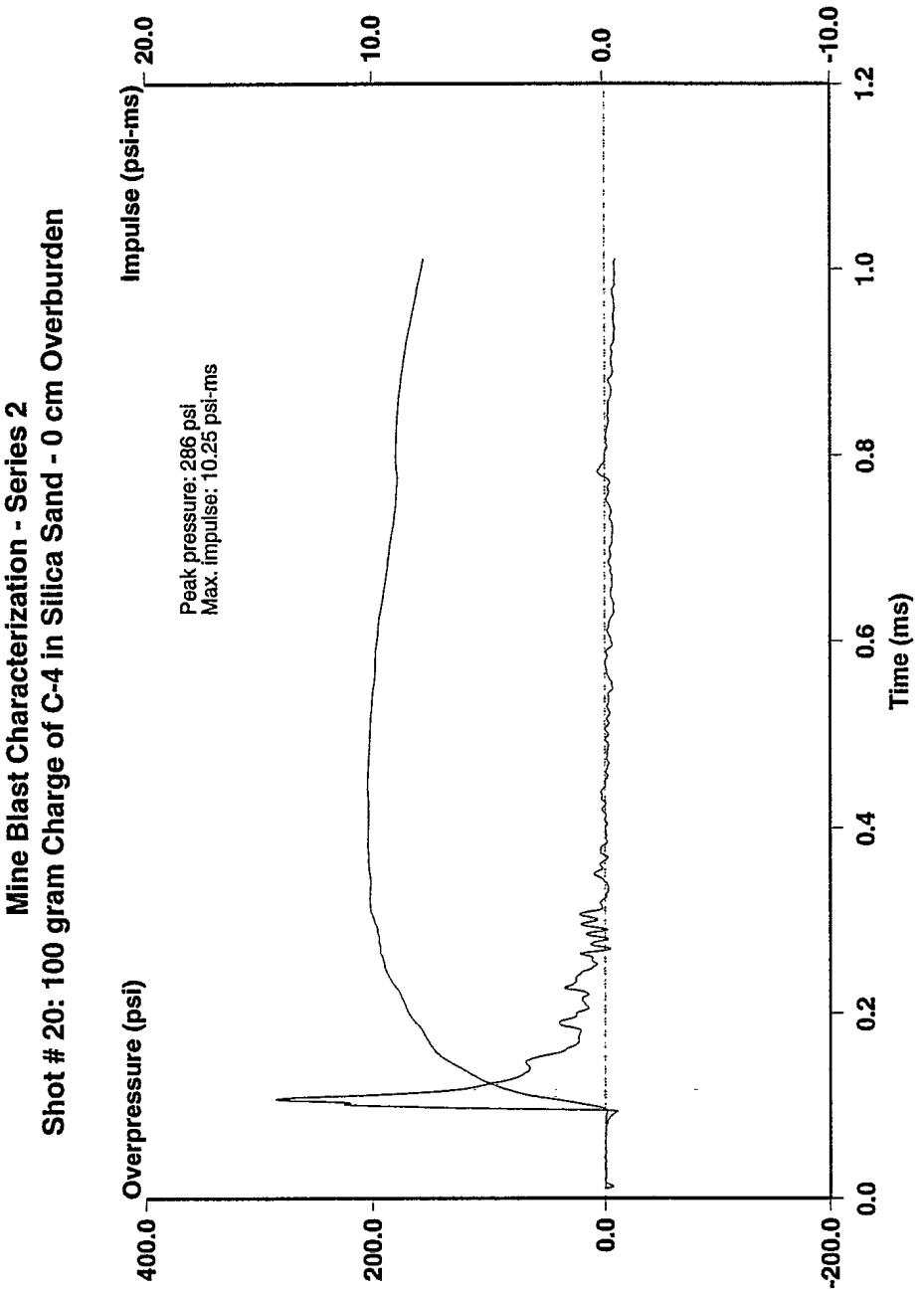
Mine Blast Characterization - Series 2
Shot # 20: 100 gram Charge of C-4 in Silica Sand - 0 cm Overburden
Overpressure (psi)
400.0
200.0
0.0
-200.0
Impulse (psi-ms)
20.0
10.0
0.0
-10.0
Peak pressure: 286 psi
Max. impulse: 10.25 psi-ms
0.0
0.2
0.4
0.6
0.8
1.0
1.2
Time (ms)
Position 1 (30 cm), Air Shock, 2nd Order 100 kHz Butterworth Filter

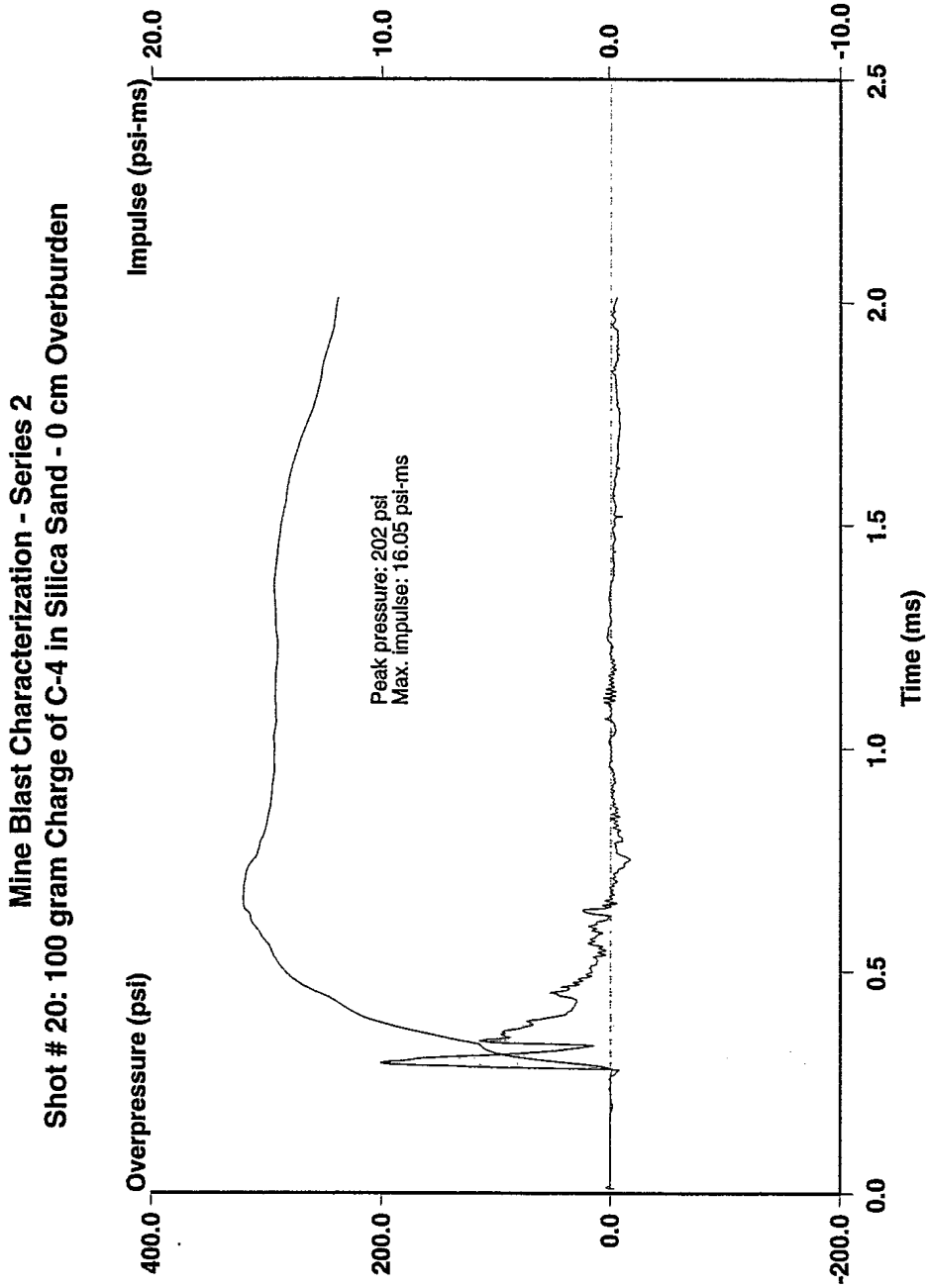
Mine Blast Characterization - Series 2
Shot # 20: 100 gram Charge of C-4 in Silica Sand - 0 cm Overburden
Overpressure (psi)
400.0
200.0
0.0
-200.0
Impulse (psi-ms)
20.0
10.0
0.0
-10.0
Peak pressure: 202 psi
Max. impulse: 16.05 psi-ms
0.0
0.5
1.0
1.5
2.0
2.5
Time (ms)
Position 2 (70 cm), Air Shock, 2nd Order 100 kHz Butterworth Filter

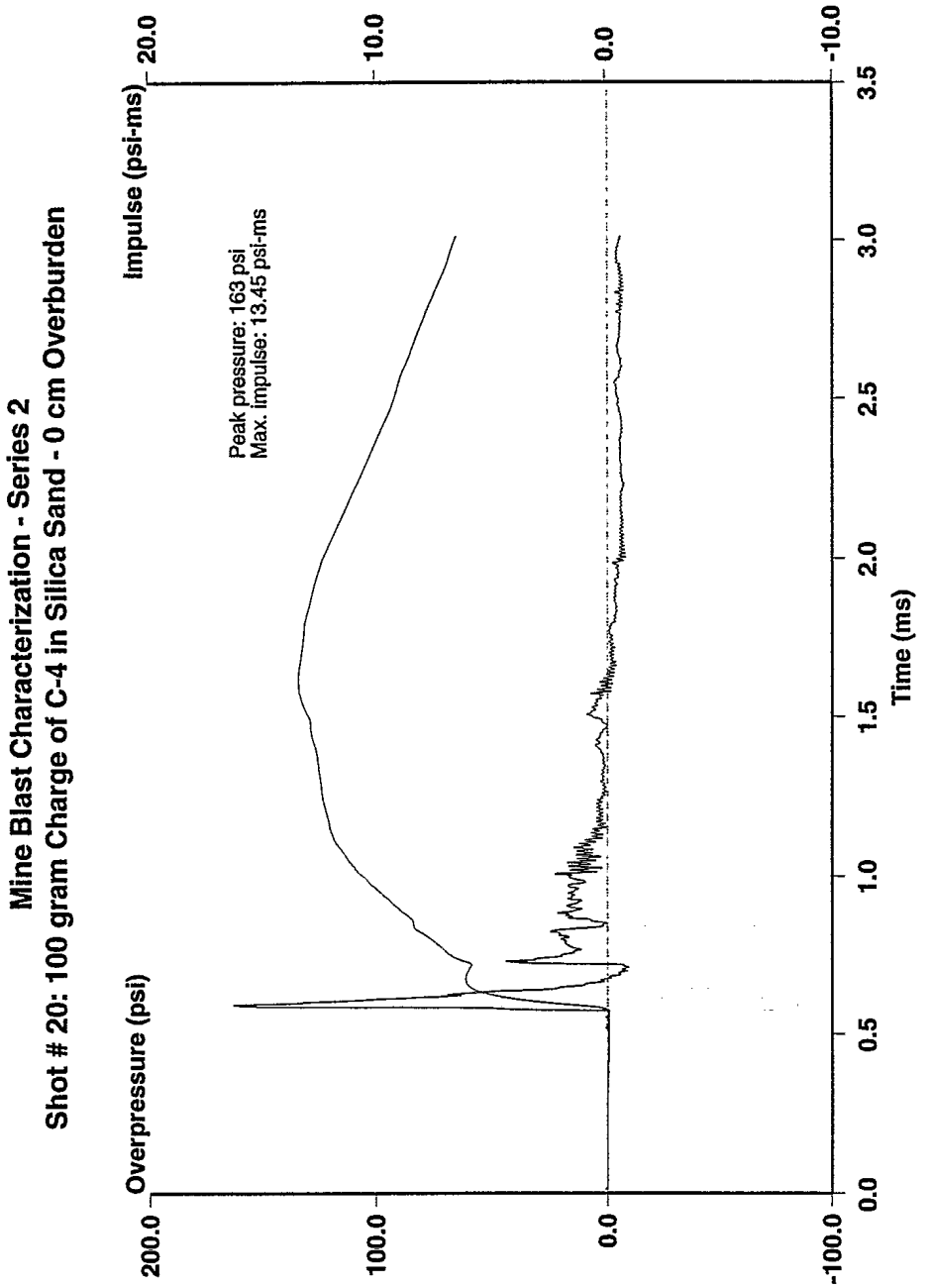

Position 3 (110 cm), Air Shock, 2nd Order 100 kHz Butterworth Filter

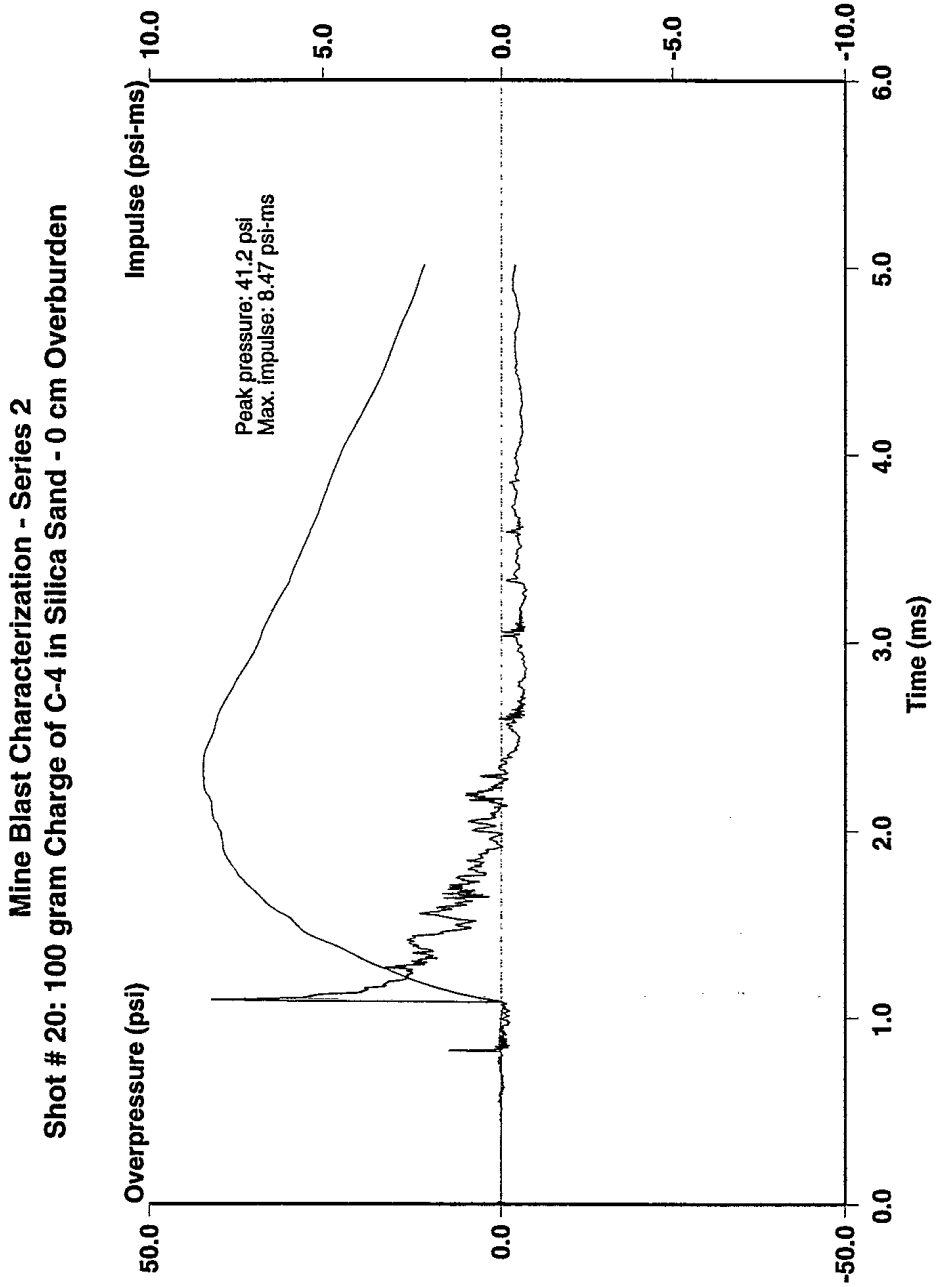

Position 4 (150 cm), Air Shock, 2nd Order 100 kHz Butterworth Filter

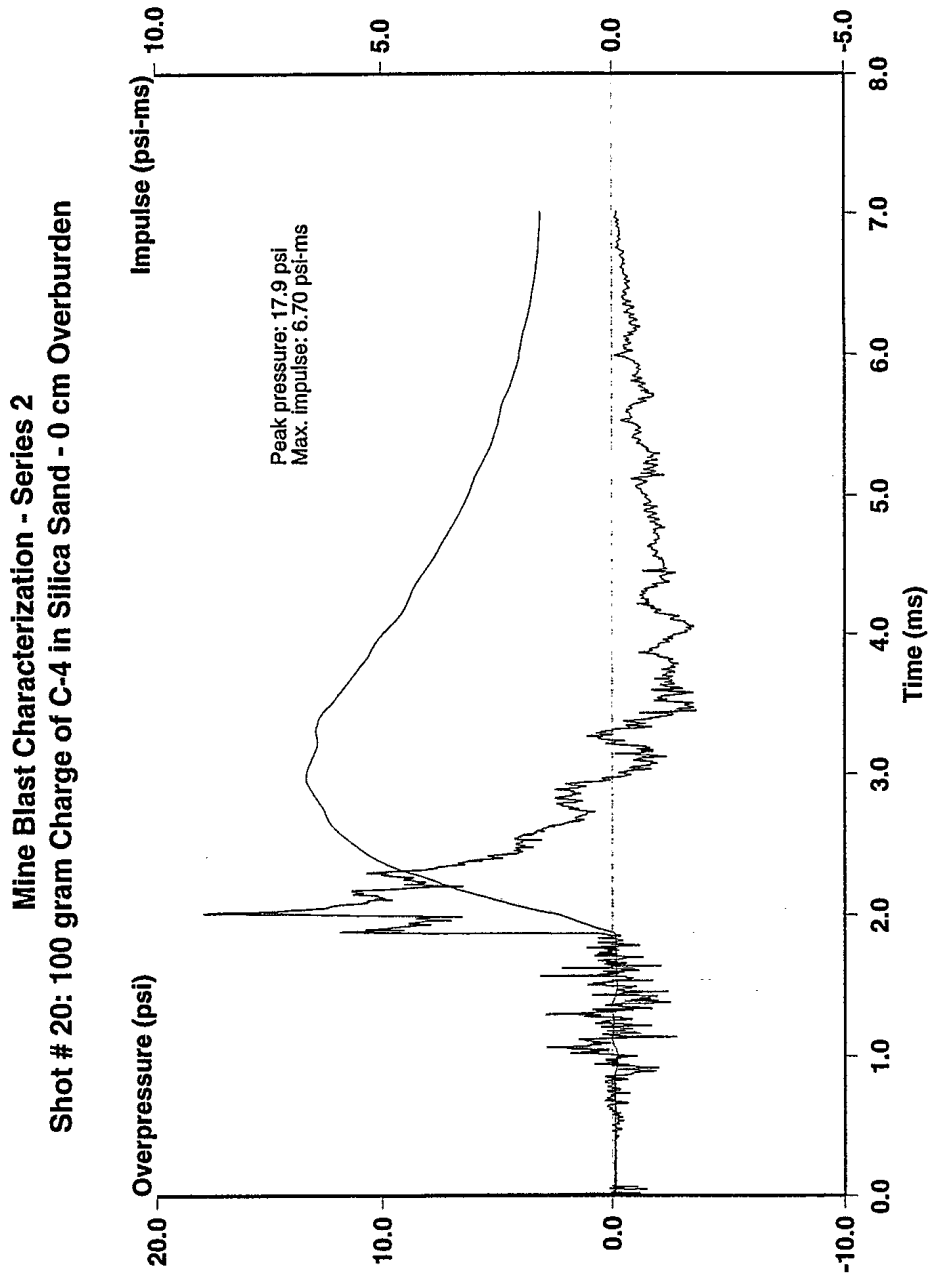

Position 5 (190 cm), Air Shock, 2nd Order 100 kHz Butterworth Filter

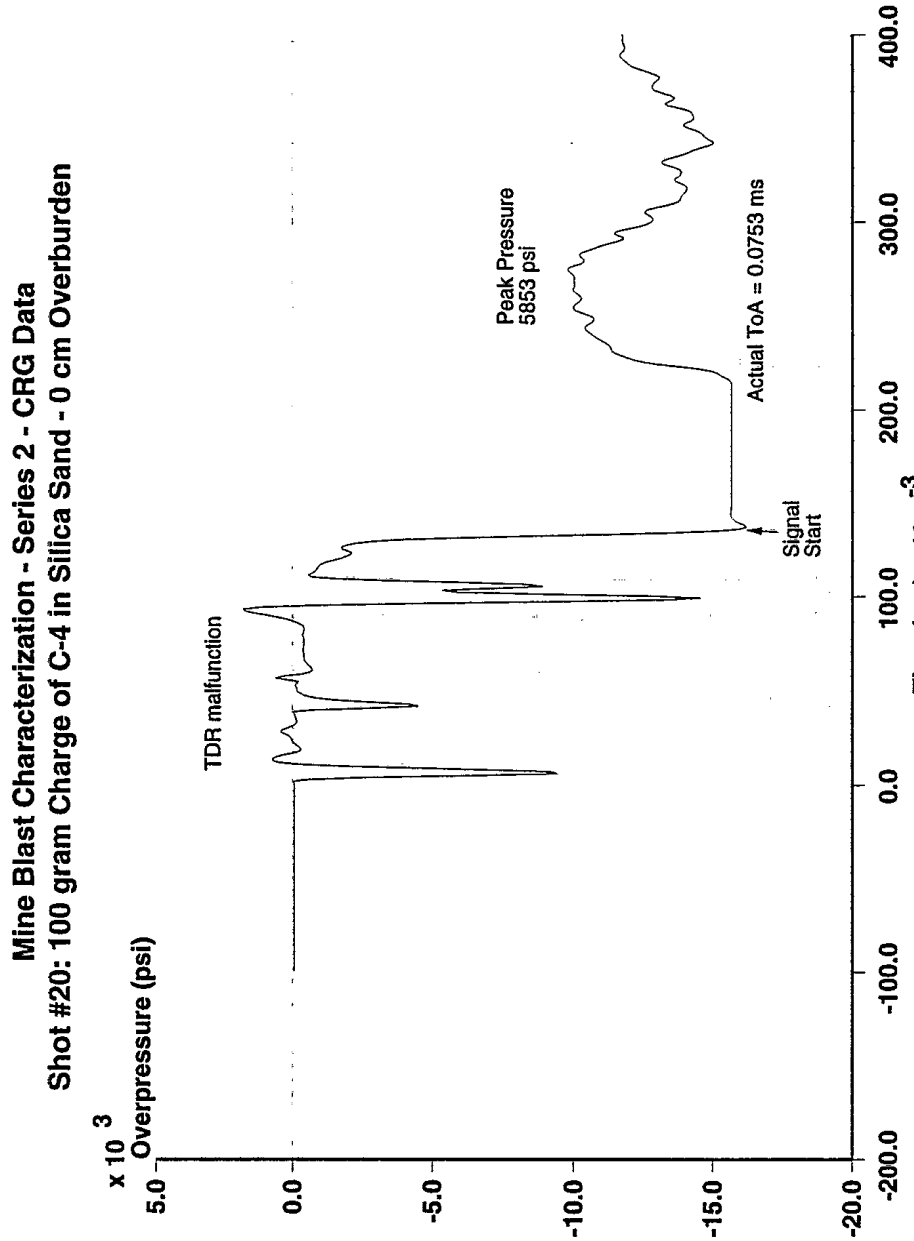

Position 6 (8.23 cm), In Ground Pressure, 2nd Order 100 kHz Butterworth Filter

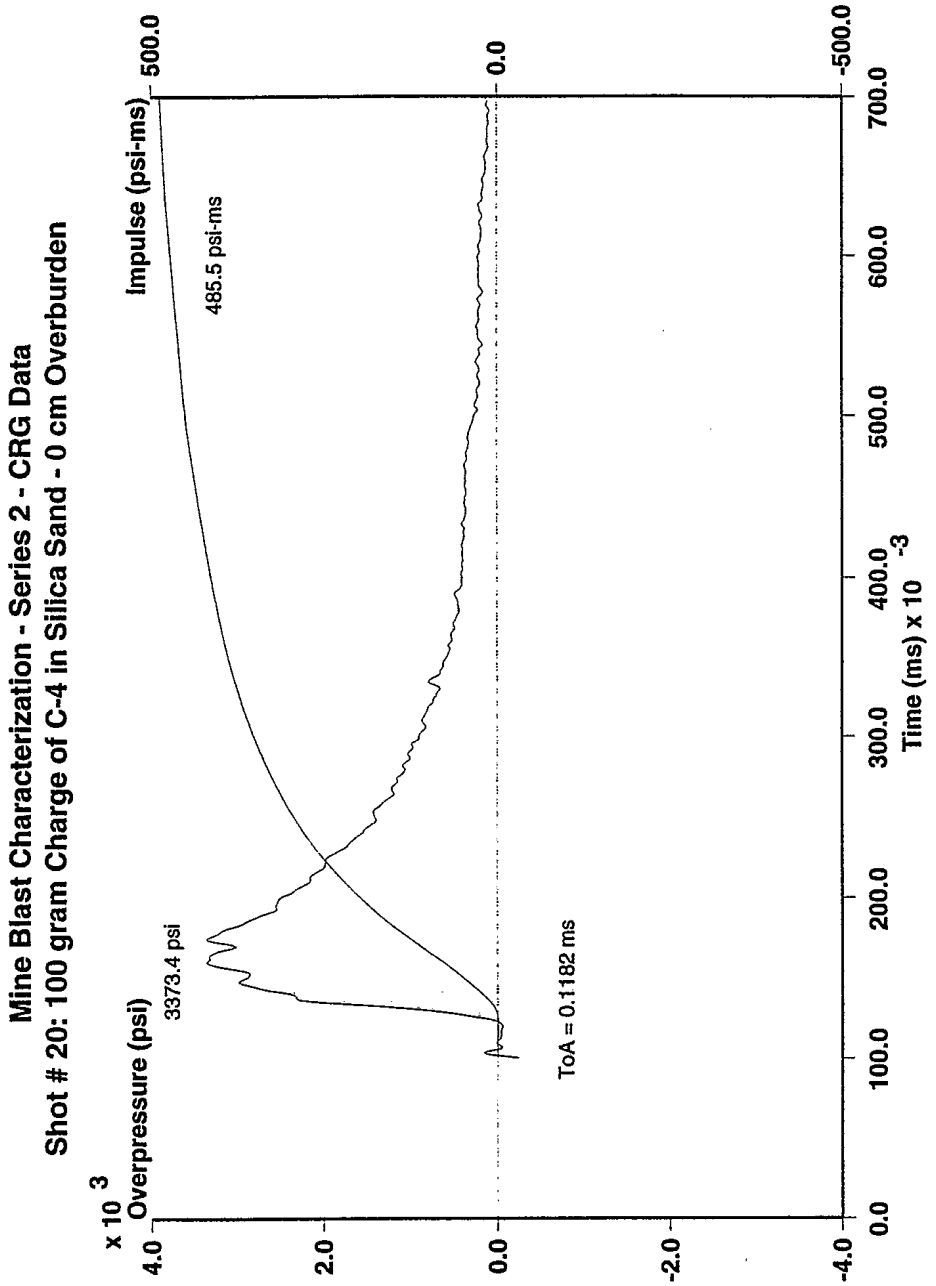

Position 7 (10.73 cm), In Ground Pressure, 2nd Order 100 kHz Butterworth Filter

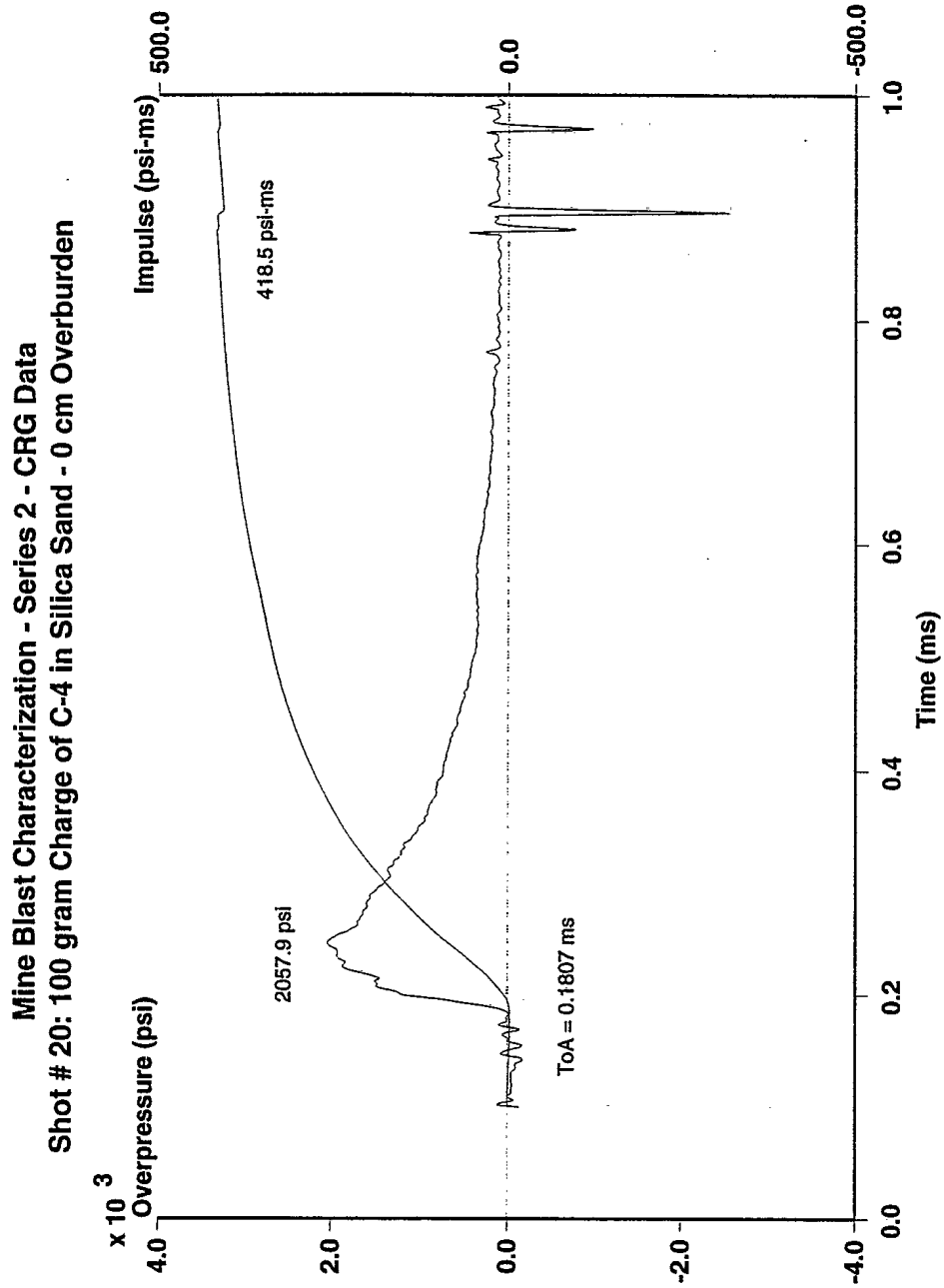

Position 8 (13.23 cm), In Ground Pressure, 2nd Order 100 kHz Butterworth Filter

UNCLASSIFIED
SECURITY CLASSIFICATION OF FORM
(highest classification of Title, Abstract, Keywords)

DOCUMENT CONTROL DATA
(Security classification of title, body of abstract and indexing annotation must be entered when the overall document is classified)

1. ORIGINATOR (the name and address of the organization preparing the document. Organizations for who the document was prepared, e.g. Establishment sponsoring a contractor's report, or tasking agency, are entered in Section 8.)

Defence Research Establishment Suffield

2. SECURITY CLASSIFICATION
(overall security classification of the document, including special warning terms if applicable)

Unclassified

3. TITLE (the complete document title as indicated on the title page. Its classification should be indicated by the appropriate abbreviation (S, C or U) in parentheses after the title).

Detonation of 100-gram anti-personnel mine surrogate charges in sand - A test case for computer code validation

4. AUTHORS (Last name, first name, middle initial. If military, show rank, e.g. Doe, Maj. John E.)

Bergeron, Denis M., Walker, Maj. Robert A., Coffey, Clayton G.

5. DATE OF PUBLICATION (month and year of publication of document)

October 1998

6a. NO. OF PAGES (total containing information, include Annexes, Appendices, etc) 200

6b. NO. OF REFS (total cited in document)

19

7. DESCRIPTIVE NOTES (the category of the document, e.g. technical report, technical note or memorandum. If appropriate, enter the type of report, e.g. interim, progress, summary, annual or final. Give the inclusive dates when a specific reporting period is covered.)

8. SPONSORING ACTIVITY (the name of the department project office or laboratory sponsoring the research and development. Include the address.)

Defence Research Establishment Suffield

9a. PROJECT OR GRANT NO. (If appropriate, the applicable research and development project or grant number under which the document was written. Please specify whether project or grant.)

2hc15 and 2ba12

9b. CONTRACT NO. (If appropriate, the applicable number under which the document was written.)

10a. ORIGINATOR'S DOCUMENT NUMBER (the official document number by which the document is identified by the originating activity. This number must be unique to this document.)

SR 668

10b. OTHER DOCUMENT NOs. (Any other numbers which may be assigned this document either by the originator or by the sponsor.)

11. DOCUMENT AVAILABILITY (any limitations on further dissemination of the document, other than those imposed by security classification)

(X) Unlimited distribution
( ) Distribution limited to defence departments and defence contractors; further distribution only as approved
( ) Distribution limited to defence departments and Canadian defence contractors; further distribution only as approved
( ) Distribution limited to government departments and agencies; further distribution only as approved
( ) Distribution limited to defence departments; further distribution only as approved
( ) Other (please specify):

12. DOCUMENT ANNOUNCEMENT (any limitation to the bibliographic announcement of this document. This will normally corresponded to the Document Availability (11). However, where further distribution (beyond the audience specified in 11) is possible, a wider announcement audience may be selected).

13. ABSTRACT (a brief and factual summary of the document. It may also appear elsewhere in the body of the document itself. It is highly desirable that the abstract of classified documents be unclassified. Each paragraph of the abstract shall begin with an indication of the security classification of the information in the paragraph (unless the document itself is unclassified) represented as (S), (C) or (U). It is not necessary to include here abstracts in both official languages unless the text is bilingual).

This report presents the results from a series of 20 experiments in which 100-gram charges of C4 explosive were buried at various depths in Silica 20 sand and detonated. These experiments were conducted with the goal of studying the basic explosion physics of shallow-buried charges, representative of land mines, and to generate a high-quality data set for the validation of computer codes. The data recorded includes overpressures and shock wave time of arrivals in air and in soil. Above ground gauges 30, 70, 110, 150 and 190 cm above the surface of the sand recorded side-on pressure. In-ground gauges at 7.5, 10.0 and 12.5 cm from the bottom of the charge recorded the passage of the shock in that medium. Flash x-ray exposures captured the early soil deformation while a high-speed camera captured the expansion of the detonation products and late ejecta motion. The data is presented in a format suitable for code validation.

14. KEYWORDS, DESCRIPTORS or IDENTIFIERS (technically meaningful terms or short phrases that characterize a document and could be helpful in cataloguing the document. They should be selected so that no security classification is required. Identifies, such as equipment model designation, trade name, military project code name, geographic location may also be included. If possible keywords should be selected from a published thesaurus, e.g. Thesaurus of Engineering and Scientific Terms (TEST) and that thesaurus-identified. If it is not possible to select indexing terms which are Unclassified, the classification of each should be indicated as with the title.)

Blast Physics

Code Validation

Mine Blast

#509935